

# Exploring temperature and pressure effects on the structure, stability and reactivity of RNAs

**Dissertation**  
zur Erlangung des akademischen Grades  
**Doktor der Naturwissenschaften**  
(Dr. rer. nat.)

eingereicht bei der  
Fakultät für Chemie und Chemische Biologie  
der Technischen Universität Dortmund

vorgelegt von

**Caroline Mello Pimentel Schuabb**  
aus Niterói, Brasilien

Dortmund 2016



# Exploring temperature and pressure effects on the structure, stability and reactivity of RNAs

**Thesis**

For the achievement of the academic degree

**Dr. rer. nat.**

**Submitted to**

The Faculty of Chemistry and Chemical Biology

TU Dortmund University

by

**Caroline Mello Pimentel Schuabb**

From Niterói, Brazil

**Dortmund 2016**





## **Declaration/Erklärung**

The work described in this Dissertation was performed from February 2013 to June 2016 at the Faculty of Chemistry and Chemical Biology, TU Dortmund University under the guidance of Prof. Dr. Roland Winter.

I hereby declare that I performed the work independently and did not use any other but the indicated aids.

Die vorliegende Arbeit wurde in der Zeit von Februar 2013 bis Juni 2016 an der Fakultät für Chemie und Chemische Biologie der Technischen Universität Dortmund unter der Anleitung von Prof. Dr. Roland Winter durchgeführt.

Hiermit versichere ich an Eides statt, dass ich die vorliegende Arbeit selbstständig und nur mit den angegebenen Hilfsmitteln angefertigt habe.

Dortmund 2016

Caroline Mello Pimentel Schuabb



## *Note*

This thesis is based in part on the following publication:

- C. Schuabb, M. Berghaus, C. Rosin, and R. Winter, Exploring the Free Energy and Conformational Landscape of tRNA at High Temperature and Pressure, *ChemPhysChem* (2015) 16, 138-146.

It contains sentences, phrases and figures taken from this publication in agreement with the publisher.



1st Examiner

**Prof. Dr. Roland Winter**

Faculty of Chemistry and Chemical Biology  
Physical Chemistry I  
TU Dortmund University  
Dortmund

2nd Examiner

**Prof. Dr. Heinz Rehage**

Faculty of Chemistry and Chemical Biology  
Physical Chemistry II  
TU Dortmund University  
Dortmund



*"A man should look for what is,  
and not for what he thinks should be"*  
-A. E.





## *Agradecimentos*

Primeiramente, gostaria de expressar o meu mais sincero agradecimento a meu excelente orientador, Prof. Dr. Roland Winter. Sua indispensável orientação, criteriosas discussões e incansável determinação são de extremo valor para mim. Eu sou extremamente agradecida por todo o seu esforço, conselhos, interpretações de resultados, idéias, correções de pôsteres, apresentações e rascunhos de artigo. Tê-lo como orientador foi verdadeiramente uma inestimável experiência.

Agradeço imensamente ao Prof. Dr. Claus Czeslik, pelas inúmeras discussões e todas as suas criteriosas sugestões durante todo o meu doutorado.

Agradeço sinceramente a querida Andrea Kreusel. Desde o começo do processo de minha mudança do Brasil para a Alemanha até os dias atuais sempre pude contar com sua disposição e prestatividade.

Agradeço também a todos os membros, passados e presentes, do grupo PCI pela agradável convivência dentro e fora do ambiente de trabalho. Em especial, gostaria de agradecer a Dr. Salomé Pataráia e Melanie Berghaus pelo nosso trabalho colaborativo, e a Mimi Gao por me auxiliar na versão alemã do sumário deste trabalho.

Agradeço profundamente ao meu pai e a minha mãe. Palavras não podem descrever o quão importante seu cuidado, carinho, amor e incansável dedicação foram essenciais para que eu me tornasse a pessoa que sou hoje. Agradeço do fundo do meu fundo coração por tudo que fizeram e fazem por mim. Amo muito vocês. Um muito obrigada muito especial para toda minha família, pelo essencial apoio e incentivo durante todo esse tempo.

Por último, agradeço especialmente ao meu marido, Vitor. A pessoa com quem divido todos momentos, cada detalhe da minha vida. Agradeço por sempre me apoiar, por escutar com atenção e carinho todos os meus pensamentos, pelos nossos sonhos e por cada passo dado e celebrado juntos, te amo.



## *Acknowledgments*

Firstly, I would like to express my sincere gratitude to my supervisor and excellent mentor, Prof. Dr. Roland Winter. His inestimable guidance, insightful discussions and enthusiastic determination are extremely valuable to me. I am extremely grateful for all his effort, advices, interpretations and for correcting all posters, presentations and drafts of papers. It was an outstanding experience having him as advisor.

I am extremely grateful to Prof. Dr. Claus Czelslik for the numerous discussion and all insightful suggestions throughout my doctorate.

I would like to thank dear Andrea Kreusel. Since the beginning of my moving process from Brazil to Germany till the present day, I could always count on her goodwill and helpfulness.

I also thank all the former and present members of the PCI group for an enjoyable atmosphere, inside and outside the workplace. In particular, Dr. Salomé Pataráia and Melanie Berghaus for our collaborative works, and Mimi Gao for assisting me in the German version of the summary of this work.

I am deeply grateful to my father and my mother. Words cannot describe how important their care, affection, love and tireless dedication have been essential for me to reach this stage of my life. Thank you, from the bottom of my heart, for everything that you have done and still do for me. Love you so much. A very special thanks to all my family, for the essential support and encouragement you gave me all this time.

Finally, I would like to express a more than special thanks to my husband, Vitor. The person with whom I share every moment and detail of my life. Thank you for always supporting me, for listening with attention and affection to all my thoughts, for our dreams and for every celebrated step we make together. I love you.



## Abbreviations

Å	Ångström (1 Å=0.1 nm)
A	Adenine
Cy3	Cyanine 3
Cy5	Cyanine 5
C	Cytosine
DNA	Deoxyribonucleic acid
DSC	Differential scanning calorimetry
EDTA	Ethylenediaminetetraacetic acid
FRET	Förster (fluorescence) resonance energy transfer
FTIR	Fourier transform infrared spectroscopy
G	Guanine
HHP	High hydrostatic pressure
$I_{ratio}$	Intensity ratio
modHpRz	modified hairpin ribozyme
PAGE	Polyacrylamide gel electrophoresis
PDB	Protein data bank
PPC	Pressure perturbation calorimetry
RNA	Ribonucleic acid
mRNA	messenger RNA
tRNA	transfer RNA
rRNA	ribosomal RNA
siRNA	small interference RNA
miRNA	micro RNA
stRNA	small temporal RNA
snoRNA	small nucleolar RNA
tRNA <sup>Phe</sup>	transfer RNA-phenylalanine
sRNAH	small RNA hairpin
SAXS	Small angle X-ray scattering
T	Thymine
TEMED	Tetramethylethylenediamine
Tris	Tris(hydroxymethyl)aminomethane
TRVS	Tobacco ringspot virus
wtHpRz	Wild type hairpin ribozyme
wt%	weight percent
U	Uracil
Y-base	wybutine



## List of figures

### *Chapter 1*

Figure 1. Single strand nucleic acid molecule.

Figure 2. Different coding and non-coding RNA molecules.

Figure 3. Interaction of the tRNA tertiary structure with ions and water molecules.

Figure 4. tRNA<sup>phe</sup> structure.

Figure 5. RNA hairpin tetraloop, gcUUCGgc.

Figure 6. Hairpin ribozyme self-cleavage reaction mechanism.

Figure 7. Hairpin ribozyme secondary structure.

Figure 8. Hairpin ribozyme self-cleavage reaction (schematic).

### *Chapter 2*

Figure 9. Gas membrane diamond anvil cell.

Figure 10. Gas membrane diamond anvil cell during FTIR measurement.

Figure 11. High pressure fluorescence spectroscopy.

Figure 12. Differential scanning calorimetry.

Figure 13. Differential scanning calorimetry (DSC) and pressure perturbation calorimetry (PPC).





### *Chapter 3*

Figure 14. tRNA<sup>Phe</sup> secondary and tertiary structures.

Figure 15. FTIR spectra of tRNA<sup>Phe</sup> at atmospheric pressure and high hydrostatic pressure conditions.

Figure 16. Temperature-dependent FTIR of tRNA<sup>Phe</sup>.

Figure 17. Temperature-dependent FTIR of tRNA<sup>Phe</sup> at different salt conditions.

Figure 18. Differential scanning calorimetry data of tRNA<sup>Phe</sup> in the presence and absence of Mg<sup>2+</sup> ions.

Figure 19. Temperature- and pressure-dependent fluorescence spectra of the tRNA<sup>Phe</sup> Y-base.

Figure 20. Temperature-dependent fluorescence intensity data of the tRNA<sup>Phe</sup>.

Figure 21. Pressure-dependent fluorescence intensity data of the tRNA<sup>Phe</sup>.

Figure 22. Temperature-dependent SAXS analysis of tRNA<sup>Phe</sup> in D<sub>2</sub>O.

Figure 23. Temperature-dependent SAXS analysis of tRNA<sup>Phe</sup> in Tris-HCl buffer.

Figure 24.  $I_{\text{free}}/I_{\text{duplex}}$  analysis of the temperature- and pressure-dependent FTIR data of tRNA<sup>Phe</sup>.

Figure 25. Pressure perturbation calorimetric (PPC) of the tRNA<sup>Phe</sup>.



## ***Chapter 4***

Figure 26. Small RNA hairpin tetraloop, gcUUCGgc.

Figure 27. Theoretically proposed free energy landscape of the small RNA hairpin with the gcUUCGgc sequence.

Figure 28. Theoretically proposed temperature-pressure elliptical-shaped stability phase diagram of the small RNA hairpin tetraloop gcUUCGgc.

Figure 29. Temperature-dependent normalized and second derivative spectra of the small RNA hairpin in the wavenumber region from 1740 to 1600  $\text{cm}^{-1}$ .

Figure 30.  $I_{\text{free}}/I_{\text{duplex}}$  analysis of the temperature-dependent FTIR data of the small RNA hairpin.

Figure 31. Temperature-dependent UV-vis spectra of the small RNA hairpin.

Figure 32. Temperature-dependent UV-vis maximum absorbance at 259 nm of the small RNA hairpin.

Figure 33. Temperature-dependent UV-vis maximum absorbance at 275 nm of the small RNA hairpin.

Figure 34. Temperature-dependent normalized and second derivative spectra of the small RNA hairpin in the wavenumber region from 1600 to 1550  $\text{cm}^{-1}$ .

Figure 35. Temperature-dependent normalized and second derivative spectra of the small RNA hairpin in the wavenumber region from 1530 to 1380  $\text{cm}^{-1}$ .

Figure 36. Pressure-dependent normalized and second derivative spectra of the small RNA hairpin in the wavenumber region from 1740 to 1600  $\text{cm}^{-1}$  at 20 °C.



Figure 37. Pressure-dependent normalized and second derivative spectra of the small RNA hairpin in the wavenumber region from 1740 to 1600  $\text{cm}^{-1}$  at 70 °C.

Figure 38. Pressure-dependent changes of small RNA hairpin free base vibrations of guanine and uracil followed by FTIR.

Figure 39. Pressure-dependent normalized and second derivative spectra of the small RNA hairpin in the wavenumber region from 1600 to 1550  $\text{cm}^{-1}$  at 20 °C.

Figure 40. Pressure-dependent normalized and second derivative spectra of the small RNA hairpin in the wavenumber region from 1600 to 1550  $\text{cm}^{-1}$  at 70 °C.

Figure 41. Pressure-dependent normalized and second derivative spectra of the small RNA hairpin in the wavenumber region from 1540 to 1380  $\text{cm}^{-1}$  at 20 °C.

Figure 42. Pressure-dependent normalized and second derivative spectra of the small RNA hairpin in the wavenumber region from 1560 to 1360  $\text{cm}^{-1}$  at 70 °C.

Figure 43. Effect of temperature and pressure on the structure of the small RNA hairpin.

## *Chapter 5*

Figure 44. Hairpin ribozyme secondary and tertiary structures.

Figure 45. Hairpin ribozyme docking and cleavage process.

Figure 46. Hairpin ribozyme nucleotides interaction in the cleavage pocket (ribozyme zipper/docked or active state).

Figure 47. TBE-urea PAGE of the hairpin ribozyme self-cleavage reaction.



Figure 48. Time evolution of the hairpin ribozyme self-cleavage reaction with  $\text{MgCl}_2$  at different pressures.

Figure 49. Time evolution of the hairpin ribozyme self-cleavage reaction with  $[\text{Co}(\text{NH}_3)_6]\text{Cl}_3$  at different pressures.

Figure 50. Time-dependent normalized and second derivative FTIR spectra of the hairpin ribozyme without cations at atmospheric pressure, in the wavenumber region from 1720 to 1580  $\text{cm}^{-1}$ .

Figure 51. Time-dependent normalized and second derivative FTIR spectra of the hairpin ribozyme with  $\text{MgCl}_2$  at atmospheric pressure, in the wavenumber region from 1740 to 1590  $\text{cm}^{-1}$ .

Figure 52. Time-dependent normalized and second derivative FTIR spectra of the hairpin ribozyme with  $[\text{Co}(\text{NH}_3)_6]\text{Cl}_3$  at atmospheric pressure, in the wavenumber region from 1760 to 1600  $\text{cm}^{-1}$ .

Figure 53. Time-dependent normalized and second derivative FTIR spectra of the hairpin ribozyme without cations at atmospheric pressure, in the wavenumber region from 1600 to 1540  $\text{cm}^{-1}$ .

Figure 54. Time-dependent normalized and second derivative FTIR spectra of the hairpin ribozyme with  $\text{MgCl}_2$  at atmospheric pressure, in the wavenumber region from 1600 to 1530  $\text{cm}^{-1}$ .

Figure 55. Time-dependent normalized and second derivative FTIR spectra of the hairpin ribozyme with  $[\text{Co}(\text{NH}_3)_6]\text{Cl}_3$  at atmospheric pressure, in the wavenumber region from 1600 to 1510  $\text{cm}^{-1}$ .





Figure 56. Time-dependent normalized and second derivative FTIR spectra of the hairpin ribozyme without cations at atmospheric pressure, in the wavenumber region from 1550 to 1300  $\text{cm}^{-1}$ .

Figure 57. Time-dependent normalized and second derivative FTIR spectra of the hairpin ribozyme with  $\text{MgCl}_2$  at atmospheric pressure, in the wavenumber region from 1530 to 1360  $\text{cm}^{-1}$ .

Figure 58. Time-dependent normalized and second derivative FTIR spectra of the hairpin ribozyme with  $[\text{Co}(\text{NH}_3)_6]\text{Cl}_3$  at atmospheric pressure, in the wavenumber region from 1520 to 1320  $\text{cm}^{-1}$ .

Figure 59. Time-dependent normalized and second derivative FTIR spectra of the hairpin ribozyme with  $\text{MgCl}_2$  at 50 MPa, in the wavenumber region from 1760 to 1600  $\text{cm}^{-1}$ .

Figure 60. Time-dependent normalized and second derivative FTIR spectra of the hairpin ribozyme with  $\text{MgCl}_2$  at 100 MPa, in the wavenumber region from 1760 to 1600  $\text{cm}^{-1}$ .

Figure 61. Time-dependent normalized and second derivative FTIR spectra of the hairpin ribozyme with  $[\text{Co}(\text{NH}_3)_6]\text{Cl}_3$  at 100 MPa, in the wavenumber region from 1750 to 1600  $\text{cm}^{-1}$ .

Figure 62. Time-dependent normalized and second derivative FTIR spectra of the hairpin ribozyme with  $\text{MgCl}_2$  at 50 MPa, in the wavenumber region from 1600 to 1530  $\text{cm}^{-1}$ .

Figure 63. Time-dependent normalized and second derivative FTIR spectra of the hairpin ribozyme with  $\text{MgCl}_2$  at 100 MPa, in the wavenumber region from 1600 to 1530  $\text{cm}^{-1}$ .

Figure 64. Time-dependent normalized and second derivative FTIR spectra of the hairpin ribozyme with  $[\text{Co}(\text{NH}_3)_6]\text{Cl}_3$  at 100 MPa, in the wavenumber region from 1600 to 1530  $\text{cm}^{-1}$ .



Figure 65. Time-dependent normalized and second derivative FTIR spectra of the hairpin ribozyme with MgCl<sub>2</sub> at 50 MPa, in the wavenumber region from 1550 to 1350 cm<sup>-1</sup>.

Figure 66. Time-dependent normalized and second derivative FTIR spectra of the hairpin ribozyme with MgCl<sub>2</sub> at 100 MPa, in the wavenumber region from 1550 to 1300 cm<sup>-1</sup>.

Figure 67. Time-dependent normalized and second derivative FTIR spectra of the hairpin ribozyme with [Co(NH<sub>3</sub>)<sub>6</sub>]Cl<sub>3</sub> at 100 MPa, in the wavenumber region from 1530 to 1380 cm<sup>-1</sup>.

Figure 68.  $I_{\text{free}}/I_{\text{duplex}}$  analysis of the time - dependent FTIR data of the hairpin ribozyme with MgCl<sub>2</sub> from 0.1 to 100 MPa.

Figure 69.  $I_{\text{free}}/I_{\text{duplex}}$  analysis of the time - dependent FTIR data of the hairpin ribozyme with [Co(NH<sub>3</sub>)<sub>6</sub>]Cl<sub>3</sub> from 0.1 to 100 MPa.

Figure 70.  $I_{\text{free}}/I_{\text{duplex}}$  analysis of the time - dependent FTIR data of the hairpin ribozyme with MgCl<sub>2</sub> and [Co(NH<sub>3</sub>)<sub>6</sub>]Cl<sub>3</sub> from 0.1 to 100 MPa.

## ***Chapter 8***

Figure A1. Temperature-dependent normalized and second derivative spectra of the labeled small RNA hairpin in the wavenumber region from 1740 to 1600 cm<sup>-1</sup>.

Figure A2.  $I_{\text{free}}/I_{\text{duplex}}$  analysis of the temperature - dependent FTIR data of the labeled small RNA hairpin.

Figure A3. Temperature-dependent UV-vis spectra of the labeled small RNA hairpin.

Figure A4. Temperature-dependent UV-vis maximum absorbance at 259 nm of the labeled small RNA hairpin.



Figure A5. Temperature-dependent UV-vis maximum absorbance at 275 nm of the labeled small RNA hairpin.

Figure A6. Temperature-dependent normalized and second derivative spectra of the labeled small RNA hairpin in the wavenumber region from 1600 to 1540  $\text{cm}^{-1}$ .

Figure A7. Temperature-dependent normalized and second derivative spectra of the labeled small RNA hairpin in the wavenumber region from 1550 to 1300  $\text{cm}^{-1}$ .

Figure A8. Pressure-dependent normalized and second derivative spectra of the labeled small RNA hairpin in the wavenumber region from 1740 to 1590  $\text{cm}^{-1}$  at 20 °C.

Figure A9. Pressure-dependent normalized and second derivative spectra of the labeled small RNA hairpin in the wavenumber region from 1720 to 1590  $\text{cm}^{-1}$  at 70 °C.

Figure A10. Pressure-dependent changes of labeled small RNA hairpin free base vibrations of guanine and uracil followed by FTIR.

Figure A11. Pressure-dependent normalized and second derivative spectra of the labeled small RNA hairpin in the wavenumber region from 1600 to 1540  $\text{cm}^{-1}$  at 20 °C.

Figure A12. Pressure-dependent normalized and second derivative spectra of the labeled small RNA hairpin in the wavenumber region from 1600 to 1550  $\text{cm}^{-1}$  at 70 °C

Figure A13. Pressure-dependent normalized and second derivative spectra of the labeled small RNA hairpin in the wavenumber region from 1550 to 1300  $\text{cm}^{-1}$  at 20 °C.

Figure A14. Pressure-dependent normalized and second derivative spectra of the labeled small RNA hairpin in the wavenumber region from 1540 to 1340  $\text{cm}^{-1}$  at 70 °C.



Figure A15. Effect of temperature and pressure on the structure of the labeled small RNA hairpin.

Figure A16. TBE-urea PAGE of the modified hairpin ribozyme's self-cleavage reaction.

Figure A17. Time evolution of the modified hairpin ribozyme self-cleavage reaction with  $[\text{Co}(\text{NH}_3)_6]\text{Cl}_3$  and  $\text{MgCl}_2$  at different pressures.





## List of tables

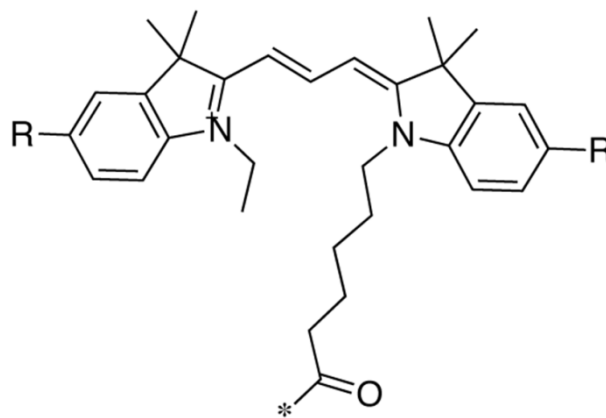
### *Chapter 2*

Table 1. Wavenumbers and spectral assignments of selected infrared bands of nucleic acids from 1800 to 1250  $\text{cm}^{-1}$ .



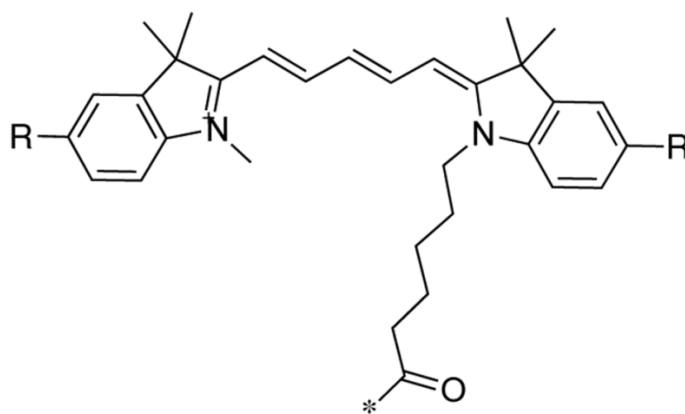
## List of Fluorophores

### Cyanine 3 (Cy 3)



Cy3

### Cyanine 5 (cy 5)



Cy5



# Contents

<b>Declaration/Erklärung</b>	<b>I</b>
<b>Note</b>	<b>II</b>
<b>Examiners</b>	<b>III</b>
<b>Agradecimentos</b>	<b>V</b>
<b>Acknowledgments</b>	<b>VI</b>
<b>Abbreviations</b>	<b>VII</b>
<b>List of figures</b>	<b>VIII</b>
<b>List of tables</b>	<b>XVII</b>
<b>List of fluorophores</b>	<b>XVIII</b>
<b>1. Introduction</b>	<b>1</b>
<b>1.1. Nucleic acids</b>	<b>3</b>
<b>1.2. Ribonucleic acid</b>	<b>4</b>
<b>1.3. Ions and RNA structure</b>	<b>6</b>
<b>1.4. Transfer RNA</b>	<b>8</b>
1.4.1. Brewer's yeast tRNA <sup>Phe</sup> structure	8
1.4.2. tRNA function	10
<b>1.5. Small RNA hairpin</b>	<b>10</b>
<b>1.6. Hairpin ribozyme</b>	<b>12</b>
<b>1.7. High pressure and DNA</b>	<b>15</b>
<b>1.8. High pressure and RNA</b>	<b>16</b>
1.8.1. High pressure and tRNA <sup>Phe</sup>	18
1.8.2. High pressure and small RNA hairpin	19
1.8.3. High pressure and hairpin ribozyme	20
<b>1.9. Aims of this work</b>	<b>21</b>
<b>2. Experimental procedures &amp; biophysical methods</b>	<b>23</b>
<b>2.1. Materials</b>	<b>25</b>
2.1.1. RNA and reagents/instruments and software	25
2.1.2. RNA samples	26
2.1.2.1. General sample handling procedures	26
2.1.2.2. tRNA <sup>Phe</sup>	26
2.1.2.3. Small RNA hairpin	26
2.1.2.4. Hairpin ribozyme	27



<b>2.2. Biophysical methods</b>	<b>28</b>
2.2.1. Fourier transform infrared spectroscopy	28
2.2.1.1. Instrumentation and spectra collection	29
2.2.1.2. FTIR spectroscopy of tRNA <sup>Phe</sup> at ambient and pressure dependent conditions	31
A. Temperature dependent conditions	31
B. Pressure dependent conditions	31
2.2.1.3. FTIR spectroscopy of Small RNA hairpin at ambient and pressure conditions	31
A. Temperature dependent conditions	31
B. Pressure dependent conditions	31
2.2.1.4. FTIR spectroscopy of Hairpin ribozyme at ambient and pressure FTIR conditions	32
A. Time dependent conditions at ambient pressure	32
B. Time dependent conditions at high pressure	32
2.2.1.5. Secondary structure analysis of nucleic acid by infrared spectroscopy	33
A. Nucleic acid infrared band assignment in D <sub>2</sub> O	33
B. Data processing	35
2.2.2. Fluorescence spectroscopy	35
A. tRNA <sup>Phe</sup> temperature dependent fluorescence conditions	36
B. tRNA <sup>Phe</sup> pressure dependent fluorescence conditions	37
2.2.3. Differential scanning calorimetry	37
2.2.4. Pressure perturbation calorimetry	38
2.2.5. UV-vis spectroscopy	40
2.2.6. Hairpin ribozyme kinetic reaction	41
2.2.6.1. Time dependent hairpin ribozyme reaction at ambient pressure	41
2.2.6.2. Time dependent hairpin ribozyme reaction at high pressure	41
2.2.6.3. Polyacrylamide gel electrophoresis	42
<b>3. Exploring the free energy and conformational landscape of tRNA at high temperature and pressure conditions</b>	<b>45</b>
<b>3.1. Background</b>	<b>47</b>
<b>3.2. Experimental details</b>	<b>49</b>
3.2.1. Sample preparation	49
3.2.2. Differential scanning calorimetry and pressure perturbation calorimetry	50
3.2.3. FTIR spectroscopy	50
3.2.4. Fluorescence spectroscopy	51
3.2.5. Small-angle X-ray scattering	52
<b>3.3. Results and discussion</b>	<b>53</b>
<b>3.4. Summary and conclusions</b>	<b>70</b>





<b>4. Exploring temperature and pressure effects on the structure and stability of small RNA hairpin</b>	<b>75</b>
<b>4.1. Background</b>	<b>77</b>
<b>4.2. Experimental details</b>	<b>81</b>
4.2.1. RNA molecule	81
4.2.2. Sample preparation	81
4.2.3. FTIR spectroscopy	82
4.2.3.1. Ambient pressure FTIR	82
4.2.3.2. High pressure FTIR	82
4.2.4. UV-vis spectroscopy	83
<b>4.3. Results and discussion</b>	<b>83</b>
4.3.1. Temperature-dependent analysis of the small RNA hairpin	83
4.3.1.1. Small RNA hairpin in-plane vibrations sensitive to effects of base pairing followed by FTIR	83
4.3.1.2. UV-vis spectroscopy of the small RNA hairpin	87
4.3.1.3. Small RNA hairpin in-plane vibrations sensitive to effects of base stacking followed by FTIR	90
4.3.1.4. Small RNA hairpin base-sugar vibrations followed by FTIR	91
4.3.2. Pressure-dependent analysis of the small RNA hairpin	94
4.3.2.1. Small RNA hairpin in-plane vibrations sensitive to effects of base pairing followed by FTIR	94
4.3.2.2. Small RNA hairpin in-plane vibrations sensitive to effects of base stacking followed by FTIR	99
4.3.2.3. Small RNA hairpin base-sugar vibrations followed by FTIR	103
<b>4.4. Summary and conclusions</b>	<b>106</b>
<b>5. Pressure modulation of hairpin ribozyme structure and self-cleavage reaction</b>	<b>109</b>
<b>5.1. Background</b>	<b>111</b>
<b>5.2. Experimental details</b>	<b>115</b>
5.2.1. RNA molecules	115
5.2.1.1. Wild type hairpin ribozyme	115
5.2.1.2. Modified hairpin ribozyme	116
5.2.2. Sample preparation	116
5.2.3. Fourier transform infrared spectroscopy	116
5.2.3.1. Time dependent kinetics at ambient pressure	116
5.2.3.2. Time dependent kinetics at high pressure	117
5.2.4. Hairpin ribozyme kinetic reaction and PAGE analysis	117
5.2.4.1. Time dependent hairpin ribozyme reaction at ambient pressure	117
5.2.4.2. Time dependent hairpin ribozyme reaction at high pressure	118
5.2.5. PAGE analysis	118
<b>5.3. Results and discussion</b>	<b>119</b>



5.3.1. PAGE analysis of the hairpin ribozyme self-cleavage reaction	119
5.3.2. FTIR analysis of the hairpin ribozyme self-cleavage reaction	123
5.3.2.1. Time-dependent analysis of the hairpin ribozyme at ambient pressure	123
5.3.2.1.1. Hairpin ribozyme in-plane vibrations sensitive to effects of base pairing followed by FTIR	123
A. Hairpin ribozyme without cations	124
B. Hairpin ribozyme with MgCl <sub>2</sub>	126
C. Hairpin ribozyme with [Co(NH <sub>3</sub> ) <sub>6</sub> ]Cl <sub>3</sub>	128
5.3.2.1.2. Hairpin ribozyme in-plane vibrations sensitive to effects of base stacking followed by FTIR	131
A. Hairpin ribozyme without cations	131
B. Hairpin ribozyme with MgCl <sub>2</sub>	133
C. Hairpin ribozyme with [Co(NH <sub>3</sub> ) <sub>6</sub> ]Cl <sub>3</sub>	135
5.3.2.1.3. Hairpin ribozyme base-sugar vibrations followed by FTIR	137
A. Hairpin ribozyme without cations	138
B. Hairpin ribozyme with MgCl <sub>2</sub>	140
C. Hairpin ribozyme with Co(NH <sub>3</sub> ) <sub>6</sub> ]Cl <sub>3</sub>	142
5.3.2.2. Time dependent analysis of the hairpin ribozyme at high hydrostatic pressure	144
5.3.2.2.1. Hairpin ribozyme in-plane vibrations sensitive to effects of base pairing followed by FTIR	145
D. Hairpin ribozyme with MgCl <sub>2</sub> at 50 MPa	145
E. Hairpin ribozyme with MgCl <sub>2</sub> at 100 MPa	147
F. Hairpin ribozyme with Co(NH <sub>3</sub> ) <sub>6</sub> ]Cl <sub>3</sub> at 100 MPa	149
5.3.2.2.2. Hairpin ribozyme in-plane vibrations sensitive to effects of base stacking followed by FTIR	152
D. Hairpin ribozyme with MgCl <sub>2</sub> at 50 MPa	152
E. Hairpin ribozyme with MgCl <sub>2</sub> at 100 MPa	154
F. Hairpin ribozyme with Co(NH <sub>3</sub> ) <sub>6</sub> ]Cl <sub>3</sub> at 100 MPa	156
5.3.2.2.3. Hairpin ribozyme base-sugar vibrations followed by FTIR	157
D. Hairpin ribozyme with MgCl <sub>2</sub> at 50 MPa	158
E. Hairpin ribozyme with MgCl <sub>2</sub> at 100 MPa	161
F. Hairpin ribozyme with Co(NH <sub>3</sub> ) <sub>6</sub> ]Cl <sub>3</sub> at 100 MPa	164
5.3.2.3. <i>I</i> <sub>ratio</sub> analysis of unpaired to paired nucleotides of the hairpin ribozyme self-cleavage reaction	167
5.3.2.3.1. <i>I</i> <sub>ratio</sub> analysis of the ambient and high hydrostatic pressure conditions + MgCl <sub>2</sub>	167
5.3.2.3.2. <i>I</i> <sub>ratio</sub> analysis of the ambient and high hydrostatic pressure conditions + Co(NH <sub>3</sub> ) <sub>6</sub> ]Cl <sub>3</sub>	168



5.3.2.3.3. $I_{\text{ratio}}$ analysis of the ambient and high hydrostatic pressure conditions + $\text{MgCl}_2$ and $\text{Co}(\text{NH}_3)_6\text{Cl}_3$	169
<b>5.4. Summary and conclusions</b>	<b>170</b>
<b>6. Global summary</b>	<b>173</b>
<b>7. Zusammenfassung</b>	<b>183</b>
<b>8. Appendix</b>	<b>193</b>
<b>8.1. Labeled small RNA hairpin</b>	<b>195</b>
8.1.1. Temperature-dependent analysis of the labeled small RNA hairpin	195
8.1.1.1. Labeled small RNA hairpin in-plane base vibrations sensitive to effects of base pairing followed by FTIR	195
8.1.1.2. UV-vis spectroscopy of the labeled small RNA hairpin	198
8.1.1.3. Labeled small RNA hairpin in-plane base vibrations sensitive to effects of base stacking followed by FTIR	201
8.1.1.4. Labeled small RNA hairpin base-sugar vibrations followed by FTIR	203
8.1.2. Pressure-dependent analysis of the labeled small RNA hairpin	206
8.1.2.1. Labeled small RNA hairpin in-plane base vibrations sensitive to effects of base pairing followed by FTIR	206
8.1.2.2. Labeled small RNA hairpin in-plane base vibrations sensitive to effects of base stacking followed by FTIR	210
8.1.2.3. Labeled small RNA hairpin base-sugar vibrations followed by FTIR	214
8.1.3. Summary and conclusions	217
<b>8.2. Modified hairpin ribozyme</b>	<b>219</b>
<b>9. Bibliography</b>	<b>223</b>
<b>10. Publications and presentation</b>	<b>243</b>
<b>11. Curriculum Vitae</b>	<b>247</b>



---

# 1. Introduction





# 1. Introduction

## 1.1. Nucleic acids

Nucleic acids are biopolymers present in all known forms of life, they play an important role in storage of genetic information, gene expression and protein biosynthesis. They are divided into two major categories according to the type of sugar: deoxyribonucleic acid (DNA) and ribonucleic acid (RNA). DNA and RNA are composed of nucleotide bases linked by phosphoric diester bonds, between the 5'-end of phosphate residues and the 3'-OH sugar group of a second nucleotide (Figure 1). The bases can be separated in two groups, according to the aromatic heterocyclic compound of the nitrogenous base, which are pyrimidine or purine rings. The purine bases include guanine (G) and adenine (A), while pyrimidine bases include cytosine (C), thymine (T) and uracil (U). The thymine base is a 5-methyl derivative of uracil, only found in DNA, while in RNA the thymine is substituted by uracil [1].

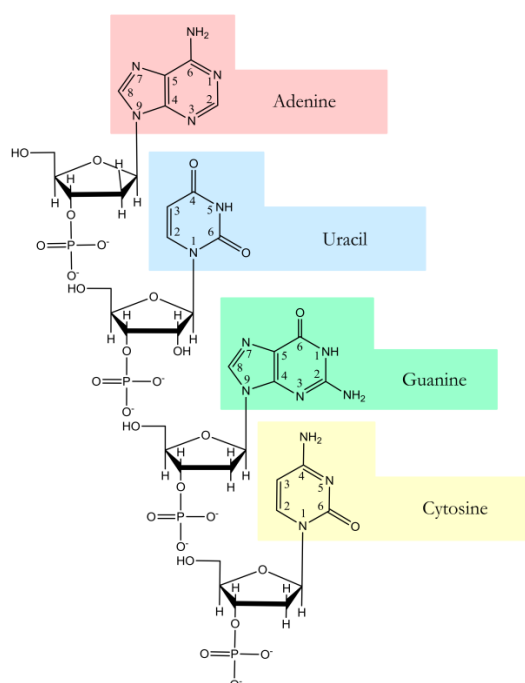


**Figure 1. Single stranded nucleic acid molecule.** It is composed by purine bases, adenine (pink) and guanine (green), and by pyrimidine bases, uracil (blue) and cytosine (yellow). The bases are connected at the backbone by phosphodiester bonds.

## 1.2. Ribonucleic acid

When first studied in the early 1900s, the chemical and biological differences between RNA and DNA were not apparent. In the 1950s, it was clear that DNA was located in the eukaryotic nucleus, but proteins were synthesized in the cytoplasm in the presence of messenger RNA (mRNA) [2,3]. Later, one different class of RNA, the transfer RNA (tRNA), was predicted by Francis Crick [4] as the “adaptor” hypothesis, which was then proved by Mahlon Hoagland and co-workers [5]. It was in 1965 that the 77 nucleotide sequence of yeast alanine-tRNA was found by Robert W. Holley, winning the Nobel Prize in Medicine in 1968 [6]. Around this period the idea of RNA as primordial molecule aroused [7-9], and it was hypothesized by some scientists that RNA molecules could be catalytic, and that early forms of life could have used RNA to carry genetic information and to catalyze biochemical reactions. However, the “RNA world” hypothesis term was first used by Walter Gilbert in 1986 [10].

RNA together with DNA, proteins and carbohydrates constitutes the major macromolecules essential for all known forms of life. It is implicated in many biological non-coding processes as well as genetic coding, *e.g.* gene expression regulation through editing new RNA molecules, and inhibiting gene expression with further destruction of specific RNA molecules. It also plays an active role in response to cellular signaling and protein synthesis [1].

RNA molecules are commonly found as single stranded chain of nucleotides composed of guanine (G), adenine (A), cytosine (C) and uracil (U); but many unusual and modified bases are also found. The base pairs found in RNA usually extend over a few base pairs originated from the folding of the single stranded onto itself creating loops and stems, which generates different types of RNA tertiary structure influencing its function and structure stability. The structural folding is based on canonical interactions as G-C and A-U, but non-canonical interactions as G.U are not uncommon. In addition, RNA molecules with complementary strands, double-stranded RNA, can be found in some viruses as rotaviruses, for example. All RNA in cell is synthesized using DNA as template in a transcription process catalyzed by the RNA polymerase [1]. It is also found in nature some RNA-dependent RNA polymerase, which uses RNA as a template for synthesis, for

example, at the RNA interference pathway and in many RNA viruses [1]. Such as DNA molecules, RNA molecules may have different stem configuration when folded such as A-RNA, the common right-handed double-helical stem with a compact helix, and Z-RNA, the intermediate and unstable left-handed double helical stem with a less compact helix [11]. It was shown in the literature that RNA in the Z-form can be found in cells, but only last a small period of time [12, 13]. However, the conversion of A-RNA into Z-RNA can be achieved through high ionic strength and higher temperatures [14].

Cellular RNA molecules have different functions, sizes, structures and lifespans; therefore, they are divided in two major types known as coding-RNAs, which are represented by messenger RNAs (mRNA), and non-coding RNAs that are classified as transfer RNA (tRNA), ribosomal RNA (rRNA), ribozymes, small interfering RNA (siRNA), microRNA (miRNA), small temporal RNA (stRNA) and small nucleolar RNA (snoRNA) [15]. Besides tRNA and rRNA which are known for participating in the translation process, non-coding RNAs accomplish a variety of functions such as regulation of gene expression at the transcription level, RNA processing and active participation in the translation process, as well as many other functions that are still unknown. Moreover, ribozymes and riboswitches provide biological functions itself, by self-cleaving through a specific nucleophilic attack at the 2'-OH group on the backbone phosphate. Other reactions such as aminoacylation of RNA and RNA polymerization can be catalyzed by small ribozymes [16, 17]. Some coding- and non-coding RNAs structures are represent in Figure 2.



**Figure 2. Different coding and non-coding RNA molecules.** a) Simple single strand mRNA. b) L-shape tertiary structure of tRNA (Image of PDB: 1EHZ [31] created using Pymol Molecular Graphic System, Version 1.8 Schrödinger, LLC). c) Tertiary structure of a hairpin ribozyme at its active state (Image of PDB: 4G6P [164] created using Pymol Molecular Graphic System, Version 1.8 Schrödinger, LLC).

### 1.3. Ions and RNA structure

RNA can fold into different tertiary structures to achieve different complex structures, which makes it a diverse molecule. An important part of this process is the compensation of strong electrostatic repulsion encountered between the closely packed phosphate groups at the backbone. Metal ions, like magnesium, play an important role in reducing backbone repulsion and consequently stabilizing RNA tertiary structure [18-20]. Since the site specific binding of partially dehydrated  $Mg^{2+}$  ions has been demonstrated in the literature [21], a theoretical model, using the nonlinear Poisson-Boltzmann equation, could quantitatively describe that diffusely bound  $Mg^{2+}$  can promote folding by interacting with high electrostatic potential favoring tertiary structure formation [22].

The RNA folding can be described as a consecutive process in which intermediate structure states increase in complexity from secondary to tertiary structure. The RNA folding process is sensitive to the concentration and type of cation available, since the highly negatively charged RNA backbone works against its folding into a more compact structure. Cations will effectively reduce the repulsion between the phosphate groups and promote folding. For example, small concentrations of  $Mg^{2+}$ , in the millimolar range, are

able to stabilize the RNA folded structure more effectively than a monovalent cation at the same concentration. It has been shown in the literature that  $Mg^{2+}$  plays an important role in stabilizing the RNA structure, as for the case of the tRNA tertiary structure. It also indirectly and directly participates in different catalytic reactions of ribozymes, such as the hairpin ribozyme and the hammerhead ribozyme [22-29].

$Mg^{2+}$  and  $K^+$  are the most common ions found *in vivo*, and when in solution these types of ions interact strongly with the water molecules. However, when RNA folds into a more compact structure, bringing the phosphates groups close together, it will increase the retention of cations by the RNA structure. Therefore, the amount of cations retained will depend on the charge density of the RNA, and the way the phosphate groups are spaced. The ion retention will also depend on the ion charge; thus, more monovalent cations are retained than divalent cations. In the presence of DNA and RNA, monovalent ions such as  $Na^+$  and  $K^+$  remain hydrated, and they directly interact with the nucleic acid surface. They create an ion atmosphere, called “diffuse ions”, and the concentration of diffuse ions is directly related to the electrostatic potential of the region. In addition,  $Mg^{2+}$  participates at the ion atmosphere around the nucleic acid molecule, but apparently without any direct contact. The structural stability of RNA increases with increasing concentration of monovalent cations, but it increases dramatically more at higher concentrations of divalent cations such as  $Mg^{2+}$  [22, 30]. The interaction of  $Mg^{2+}$  ions with the RNA structure requires dehydration of the ion atmosphere, and the energy cost of the process tends to be smaller than the ion dehydration energy [23]. The dehydrated  $Mg^{2+}$  will then have strong attraction to the RNAs electrostatic field. How the interaction between ions and RNA occurs has been the subject of many theoretical studies, with the nonlinear Poisson-Boltzmann equation describing both the stoichiometric and energetic linkage between the  $Mg^{2+}$  binding properties and RNA folding. It showed that diffuse ions play a major role in structure stabilization, but  $Mg^{2+}$  can also bind specifically to regions with high electrostatic potential [22].

In summary, the folding of large RNA molecules into a compact native state requires organization and stabilization of electrostatic forces. Coordination of monovalent and divalent cations in hydrated and partially hydrated states, in the RNA structure, have to be

taken into account, because the ions may interact through outer sphere connections and/or inner sphere connections (Figure 3).

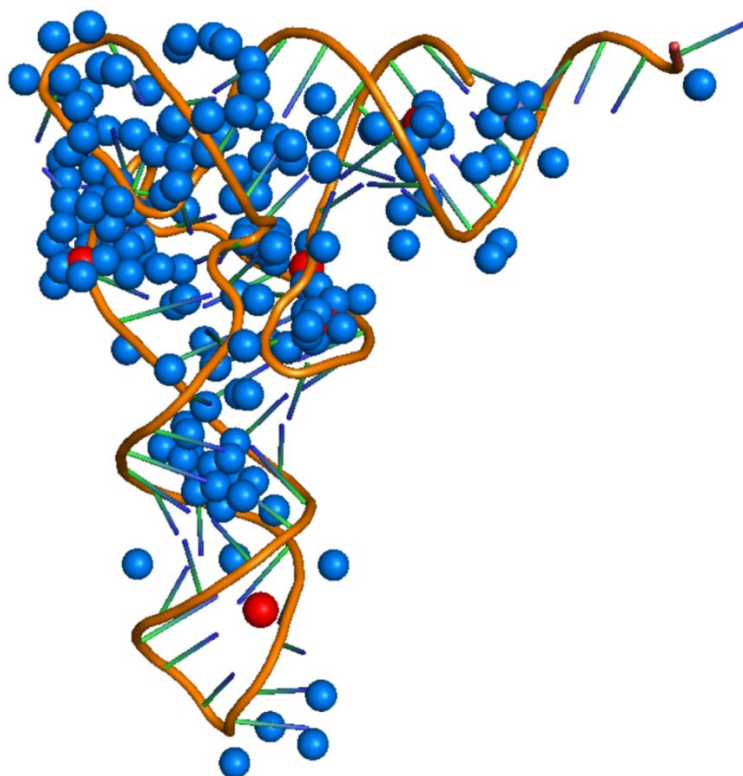


**Figure 3. Interaction of the tRNA tertiary structure with ions and water molecules.** Tertiary structure of tRNA in which the negative charges of the backbone are screened by Mg<sup>2+</sup> ions (red spheres) and water molecules (blue spheres) (Image of PDB: 1EHZ [31] created using Pymol Molecular Graphic System, Version 1.8 Schrödinger, LLC).

## 1.4. Transfer RNA

### 1.4.1. Brewer's yeast tRNA<sup>Phe</sup> structure

tRNAs are non-coding RNAs with the approximately length of 70 to 100 nucleotides. The single-stranded RNA molecule can fold up, by turning upon itself, which creates double-helical segments, resulting in a clover leaf-like secondary structure. Then, the cloverleaf structure folds into a compact L-shaped tertiary structure (Figure 4). The L-shaped structure is held together by an equilibrium of the negatively charged phosphates

at the backbone, stacking interactions between nucleotides, additional hydrogen bonds between polar atoms at different regions of the structure, water molecules and cations as  $Mg^{2+}$  that directly interact with the structure (Figure 4) [1]. The yeast tRNA phenylalanine ( $tRNA^{Phe}$ ) is one of most studied RNA molecules, with a well-established crystal structure, and it is composed of 76 nucleotides with 25.6 kDa [31]. This makes it a great model molecule for structural and functional studies. The literature data [31], Figure 4b, shows six binding sites for  $Mg^{2+}$  ions, which contribute to the structural stability. The modified nucleotide wybutine, also known as Y-base, is located at the anticodon loop where it directly interacts with a magnesium ion (indicated by an arrow in Figure 4a). The Y-base has specific intrinsic fluorescence and is used as a sensitive probe to monitor changes and interactions within the anticodon loop area [31 – 35].

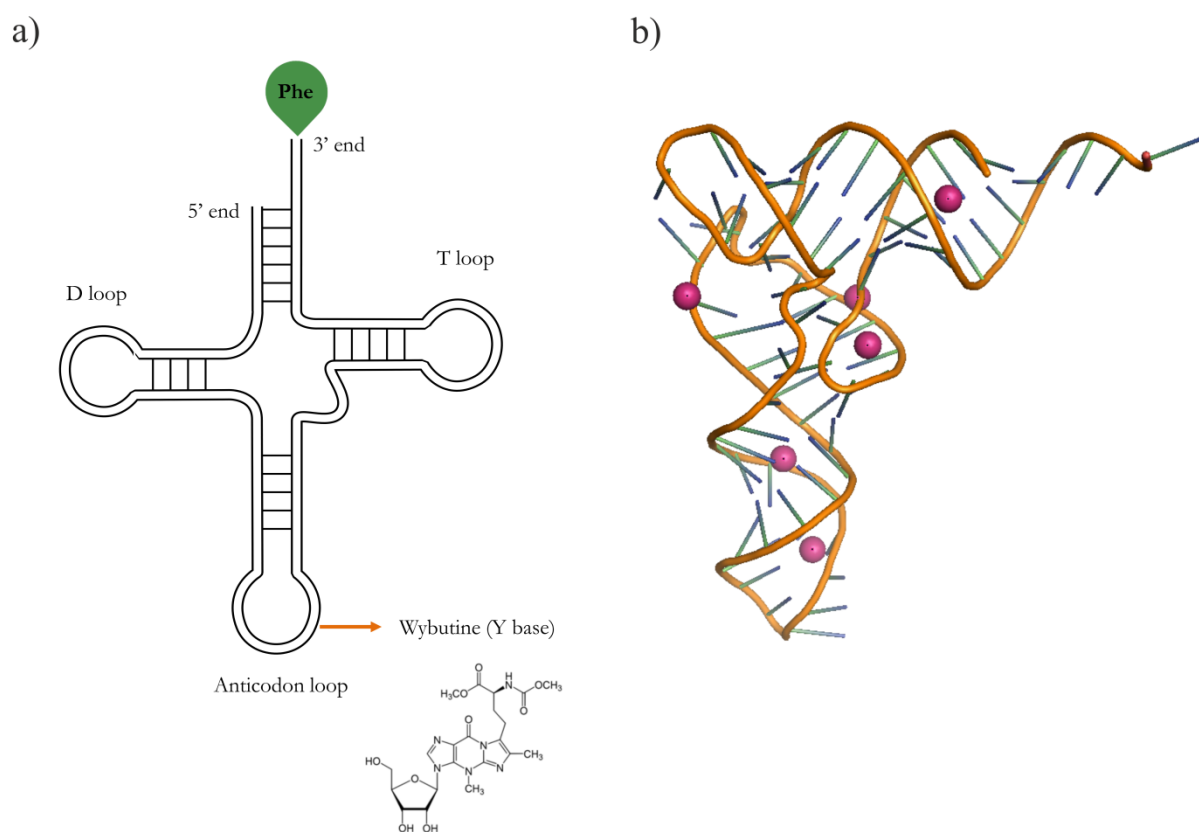


**Figure 4.  $tRNA^{Phe}$  structure.** a) Cloverleaf like secondary structure of tRNA with a phenylalanine ( $tRNA^{Phe}$ ) amino acid attached to the 3'-end. b) L-shaped tertiary structure of yeast- $tRNA^{Phe}$  (Image of PDB: 1EHZ [31] created using Pymol Molecular Graphic System, Version 1.8 Schrödinger, LLC). The  $Mg^{2+}$  ions bonded to the RNA structure are marked as pink spheres.

### **1.4.2. tRNA function**

tRNA is the most abundant small non-coding RNA molecule, representing 4 – 10 % of all cellular RNA, where it actively participates in protein synthesis, together with mRNA and rRNA. After the production and processing of mRNA, by complimentary base pairing with DNA, the information presented at the mRNA sequence is translated into protein. The codons of mRNA, which are a group of three consecutive nucleotides, specify either one amino acid or a stop code to the translation process. However, the codons are not directly recognized. The tRNA works during the translation process as a link between nucleic acids and proteins. The two regions of unpaired nucleotides situated at both ends of the L-shaped structure are crucial for the tRNA activity. One region is the anticodon loop, where three consecutive nucleotides that pair with the mRNA complimentary codon can be found. The other region is a short single stranded area at the 3' end, where the amino acid that matches the mRNA codon is attached. Then, the tRNA delivers the amino acid to the ribosome as it translates the genetic information of an mRNA, producing a corresponding peptide chain. Like other types of RNAs, the tRNA is covalently altered before leaving the nucleus to the cytoplasm. The tRNA also suffers many chemical modifications, since nearly 10 nucleotides in each mature tRNA molecule is an altered version of the nucleotides guanine, cytosine, adenine and uracil. One of these modified nucleotides, inosine for example, can affect the conformation, base pairing of the anticodon and facilitate the recognition of the appropriate mRNA codon by the tRNA molecule [1]. Despite the tRNA generally seen as an adaptor molecule, it has been shown in the literature that tRNA has many other functions, as an unexpected diversity of tRNA-fragments are not merely degradation debris, but have active roles in stress-signalling [36]. In addition, several mitochondrial-related diseases are caused by dysfunction of tRNA, including mutations in tRNA and in the proteins involved with tRNA biogenesis and modifications [37].

### **1.5. Small RNA hairpin**

Hairpin loops are predominant secondary structure elements of different RNA molecules, especially in ribosomes and ribozymes structure [38, 39]. They take part in various



important biological functions, as nucleation sites for RNA folding, sites for tertiary structure interactions and ligand binding [40 – 42]. Among different hairpin loops, the tetraloops are highly common (Figure 5), and they serve as tertiary structure site ordering, and mediate RNA-RNA and RNA-protein interactions [43 – 45]. The tetraloop sequences UNCG (N is related to any nucleotide) and GNRA (N is related to any nucleotide; R is related to purine nucleotides guanine and adenine) are the most common sequences in RNA hairpins. These hairpin sequences have several non-canonical interactions, as wobble base pairs, promoting remarkable thermodynamic stability [46, 47].

The thermodynamic stability of native hairpins tetraloops has been extensively studied. Molecular dynamics, X-ray diffraction and NMR studies of the gcUUCGgc ( $U_{L1}U_{L2}C_{L3}G_{L4}$ ) sequence showed that intramolecular base interactions play a role in stabilization of its structure [48, 49]. These studies showed that the interaction between  $G_{L4}$  and  $U_{L1}$  bases result in the noncanonical G.U trans-wobble base pair. The  $U_{L2}$  base is exposed to the solvent. The  $C_{L3}$  amino group bond to the  $U_{L1}$  2OP1, increases the tetraloop stability. Molecular dynamics studies also showed that at temperatures as high as 1000 K ( $\approx 720$  °C) , extended chain-like conformations are less populated when compared to other more compact intermediate denatured structures [47].

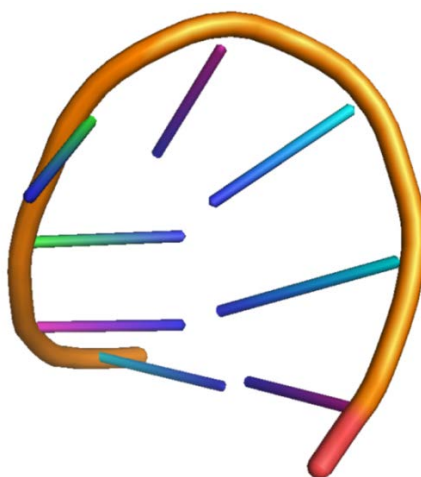


**Figure 5. RNA hairpin tetraloop, gcUUCGgc.** Guanine (blue stick) and cytosine (pink stick) are paired at the stem. There is the wobble base pair of guanine ( $G_{L4}$  - blue stick) and uracil ( $U_{L1}$  - green stick) in the loop. The loop nucleotides cytosine ( $C_{L3}$  - pink stick) is bond to the  $U_{L1}$ , and uracil ( $U_{L2}$  - green stick) is free to the solvent (Image of PDB: 1F7Y [48] created using Pymol Molecular Graphic System, Version 1.8 Schrödinger, LLC).

Experimental and theoretical studies on small RNA hairpin showed that it has a complex energy landscape and a two-state kinetic model cannot describe its normally induced denaturation [47, 50 – 55]. Studies on conformational changes and the stability of hairpin loops can help to understand the thermodynamic stability of RNA structures, as well as its impact on small molecules binding during gene expression.

## **1.6. Hairpin ribozyme**

The hairpin ribozyme, as well as the hammerhead, the hepatitis delta virus (HDV) and the Varkud satellite (VS) ribozymes are part of the small nucleolytic ribozyme group. They are capable of catalyzing a site-specific self-cleavage transesterification reaction at the RNA backbone. The self-cleavage reaction involves the nucleophilic attack of the 2'-hydroxy group on the adjacent phosphorus atom, resulting in a 2', 3'-cyclic phosphate and a 5'-hydroxyl terminus (Figure 6) [56 – 59]. The reaction follows a  $S_N2$  mechanism, in which the reverse reaction (ligation) can also be catalyzed. In this case, a 5'-hydroxyl attacks a cyclic 2', 3'-cyclic phosphate leading to ligation [60]. However, these four ribozymes are structurally unrelated and represent independent evolutionary molecules, but they perform the same cleavage reaction. These ribozymes are all rather small molecules that do not require proteins for activity. For example, the hairpin ribozyme requires about 50 nucleotides to be catalytically active. The widely studied hairpin ribozyme represents an ideal experimental system to study the structure and behavior of catalytic RNAs and will therefore be studied in this thesis [27, 60 – 66].

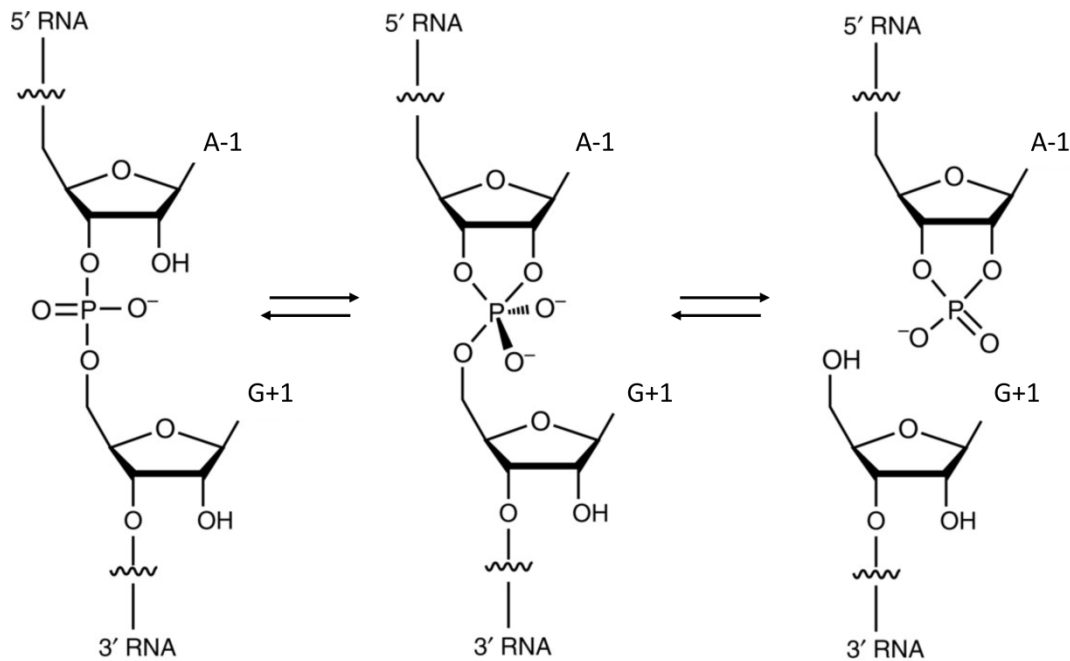


**Figure 6. Hairpin ribozyme self-cleavage reaction mechanism.** The nucleophilic substitution ( $S_N2$  type reaction) occurs between the A-1 and G+1 nucleotides and results in a 2', 3'-cyclic phosphate and a 5'-hydroxyl terminus products.

The hairpin ribozyme derives from the minus strand of the satellite RNA from tobacco ringspot virus (TRVS) and it was the first autocatalytic RNA characterized. These satellite RNAs are single-stranded RNA molecules that replicate via a rolling circle mechanism. This mechanism is important for processing recently produced RNA, which was replicated from a circular positive-strand template. The discovery of such catalytically active RNAs, which simultaneously can store genetic information and act as biocatalyst, greatly supported the "RNA world" hypothesis. This hypothesis suggests that extant life arose from molecular precursors where RNA could not only self-replicate, but also ensure proper metabolism [10]. The minimal two-way junction hairpin ribozyme structure, a derivative from the four-way junction structure, can be separated in two stems, stem A and stem B (Figure 7). The correct folding and interactions between these two domains of the ribozyme are essential to promote catalysis. In the satellite RNA, the stems A and B are part of a four-helix junction ribozyme, but most experiments in the literature were done with the minimal two-helix RNA structure, which is yet catalytically active. The loops present in both stems contain the majority of essential nucleobases and functional groups for catalysis. The close interaction between these loops, also called docking, is

responsible for generating the active conformation of the hairpin ribozyme. Catalysis happens at loop A, between nucleotides A<sub>5</sub> and G<sub>6</sub>. Cations such as Mg<sup>2+</sup> facilitate the docking, however, unlike the hammerhead ribozyme, the hairpin ribozyme does not need cations to perform catalysis. Moreover, the hairpin ribozyme showed to be fully active in the presence of cobalt (III) hexammine, which mimics hydrated Mg<sup>2+</sup>, but cannot make direct coordination with water or RNA ligands [63 – 66].

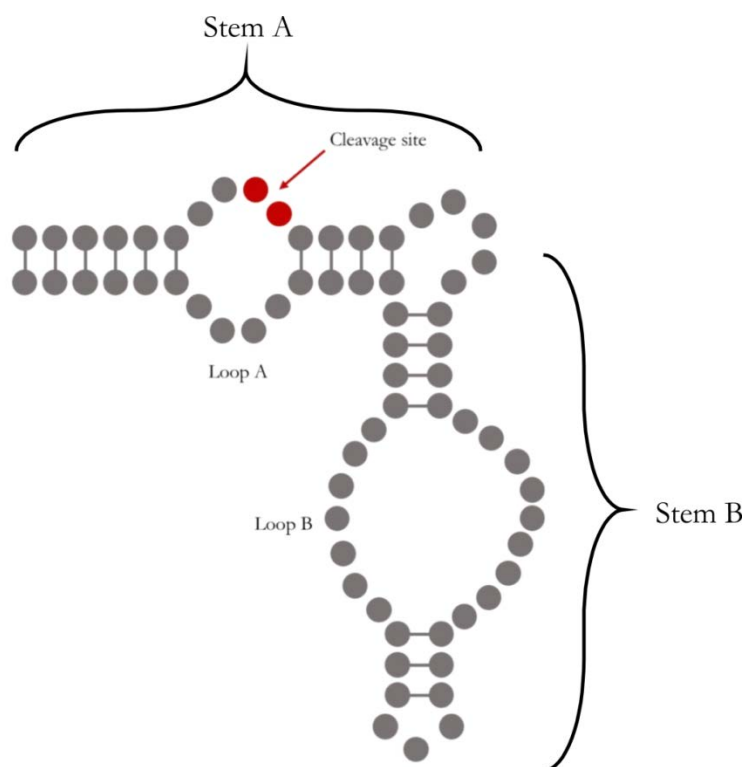


**Figure 7. Hairpin ribozyme's secondary structure.** The structure is based on the minimal two-way junction tobacco ringspot virus satellite hairpin ribozyme. The red arrow marks the cleavage site.

The structure of the hairpin ribozyme rearranges during the docking process, where loops A and B interact. Mutagenesis studies showed that the purine bases G<sub>8</sub>, A<sub>9</sub>, A<sub>10</sub> and A<sub>38</sub> play an active role during catalysis. Analysis of the hairpin ribozyme's crystal structure have shown that the scissile phosphate, G+1 (5'-hydroxyl product), actually adopts the proposed syn conformation and an in line arrangement with A-1 (2'-OH product) which enables the transition state of the S<sub>N</sub>2 transesterification reaction (Figure 8). Docking enables G+1 to make a Watson-Crick pair with C<sub>25</sub>, a hydrogen bond with G<sub>36</sub> and A<sub>38</sub>, which highly stabilizes the cleavage pocket. It has been shown that mutations of G+1, C<sub>25</sub> and A<sub>38</sub> to any other nucleotide abolishes the hairpin ribozyme's activity [27, 28, 65].

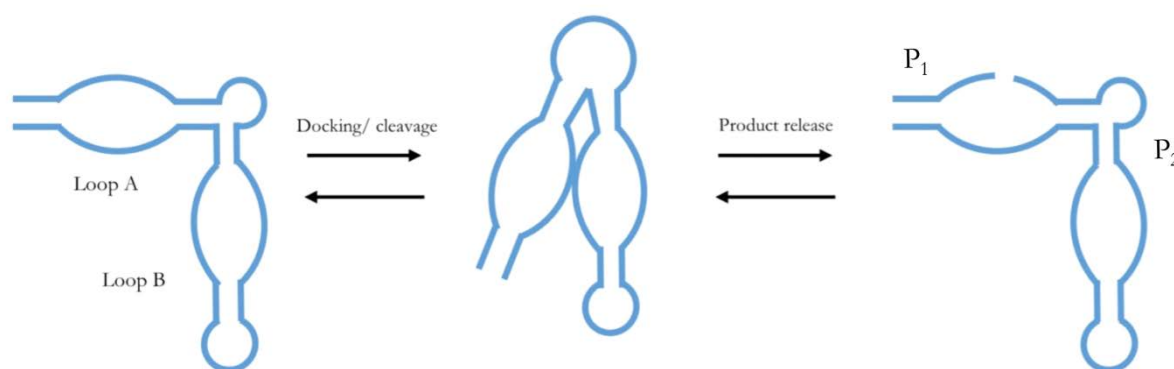


**Figure 8. Hairpin ribozyme self-cleavage reaction (schematic).** The  $S_N2$  transesterification reaction happens between G+1 and A-1 at loop A with active participation of the nucleotides G8 and A38.

The “RNA World” theory suggests that early life arose from simple organisms in which RNA molecules were responsible for storage of genetic information and metabolism. Until today, many organisms have been identified that experience environmental stresses of extreme temperature and/or pressure such as in the deep sea, hydrothermal vents and volcanic environments. Moreover, these environments were proposed to be the birthplace of life or at least similar. Hence, the studies of pressure effects on ribozyme’s activity are of particular interest. On the other hand, pressure is an important physical control parameter in addition to temperature, and it can be used to determine thermodynamic and kinetic parameters which are otherwise inaccessible [67 – 75].

### 1.7. High pressure and DNA

The canonical structure of nucleic acids is a duplex stem stabilized by Watson-Crick base pairing. Various non-canonical structures of nucleic acids have been identified, such as the wobble base pair G.U. Several high-pressure studies were carried out in order to analyze the structural changes and stability of the G-quadruplex [83, 84, 89 – 94]. G-quadruplexes are formed by the stacking of guanine quartets, a four guanine base coplanar arrangement stabilized by Hoogsteen (third strand) base pairing [89]. G-quadruplex can vary in the sequence and in the metal ions bonded to the complex [95], but all G-quadruplex structures have stacking interactions of G-quartet units with a central cavity that binds monovalent cations, such as  $K^+$  or  $Na^+$  [96]. The G-quadruplex

has a more compact conformation than single-stranded DNA/RNA, since it releases water molecules upon folding. Sequences with the potential to G-quadruplex structural arrangements can be found in the genome and appear to be involved in regulation of gene expression [83].

High-pressure analysis of biomolecules such as G-quadruplexes is a useful tool for thermodynamic analysis of its folding/unfolding mechanism. Pressure compresses the molecules and favor lower molecular volume states, but to an extent that depends on the packing and hydration of the biomolecule. The canonical double strand DNA, formed by Watson-crick bonds has in general a negative partial molar volume of melting ( $\Delta V_{tr}$ ), which makes the double strand DNA bonds more stable, in other words, DNA molecules are hardly affected by pressure. However, it was reported in the literature that the poly[d(A-T)] complex have a positive  $\Delta V_{tr}$  and hence melts upon pressurization [83]. On the hand, non-canonical DNA/RNA structures are more sensitive to pressure. G-quadruplex DNA structures have a large and positive  $\Delta V_{tr}$  value, indicating that pressure destabilizes the G-quadruplex structure and it can unfold with increasing pressure. The  $\Delta V_{tr}$  value of G-quadruplex is similar to that of proteins. Literature results suggest that the difference between DNA and G-quadruplex is due to different hydration shells and not from the amount of water molecules taken or released upon pressurization [97 – 99].

It is highly interesting to understand the mechanism by which non-canonical nucleic acid molecules behave under extreme conditions, such as high hydrostatic pressure up to 100 MPa, since these changes can alter gene expression, protein synthesis and nucleic acid-protein interactions in living organisms.

## **1.8. High pressure and RNA**

The “RNA world” hypothesis is based on the idea that before the DNA-proteins system, on which current life is based, RNA or RNA-like molecules were the only one responsible for the genetic information storage and enzymatic activity [76]. However, in the modern world, most ribozymes require protein for efficient catalysis *in vivo*, and the majority of

solely ribozyme active ones have been found only in a few virus-like forms [77]. The discovery of naturally occurring ribozymes, such as self-splicing introns and ribonuclease P, in 1980s established the first reference for the RNA World hypothesis. These studies have demonstrated the evolutionary capabilities of RNA, emphasizing the possibility that life started with RNA. It has also been shown that the catalytic catalogue of RNA is diverse, ranging from riboswitches to autocatalytic ribozymes [77]. RNA replication and activity in early life must fit into a broader thermodynamic and biological context to form the basis of life (Figure 9). However, how were the environmental conditions in the early stages of life developed on Earth?

British and French oceanographers showed that, by the end of the 19<sup>th</sup> century, life can exist in the deepest ocean trenches. Until today, many microorganisms have been found in different natural environments characterized by a wide range of pressure-temperature-composition ( $p$ - $T$ - $x$ ) conditions [78]. The currently knowledge about life at extreme conditions, such as high pressure, derives from studies of deep-sea microorganisms that possess adaptations for growth at pressures roughly in the 10-130 MPa range [79 – 81]. Such pressures are far below those typically used in microorganism survival studies, or used in studies of isolated macromolecular systems. The study of macromolecules adaptation and functionality that are necessary to organisms to growth and reproduce at high hydrostatic pressure can provide valuable information on biochemical and physiological properties, which is necessary to understand the adaptation of life in a pressurized world [77].

There is little known about the effect that both temperature and pressure have on the structural stability of nucleic acids. The tertiary structure of biomolecules is generally stabilized by inter- and intramolecular interactions, which comprises covalent and non-covalent interactions. The non-covalent interactions are weaker and easily perturbed by temperature, but pressure can also perturb molecular interactions, due to the overall system's volume change. Le Châtelier's principle states that application of pressure shifts the system equilibrium toward the smaller volume state. Therefore, properties that depend on hydration and degree of packing of a molecule, like partial molar volume, compressibility and expansibility will establish how high pressure can affect the structure

and also how it can shift the equilibrium between denaturated and native states. The study of the pressure effect upon DNA and RNA, for example, is important to help understand how the genetic expression and regulation system work under pressure. Since pressure affects the partial volume of the biomolecules, it also provides information on the hydration of the molecule. The general high-pressure approach for studying biomolecules ranges from 0.1 MPa to 1000 MPa, where non-covalent bonding in the tertiary structure is affected only [82 – 84]. It has been shown in the literature that structural changes on DNA are very small, and that major changes happen in the hydration layer only, which will influence and alter the way DNA interacts with proteins and the overall transcriptional process [82]. In addition, the binding of proteins and drugs to DNA has been found to be weaker under pressure [85], and pressure reduces the enzymatic activity of RNA polymerase [86, 87]. These informations are very important for understanding how organisms adapt to extreme conditions, such as piezophiles, which only grow optimal in a pressurized environment [88], while other organisms can also grow at atmospheric pressure. Therefore, understanding the effect of pressure on the structure and functionality of molecules such as DNA and RNA can give insight into nucleic acid stability, and how the transcription and translation processes are affected under extreme environmental pressure conditions.

To this end, explanation of mechanistic details involved in the formation and stability of biomolecules, such as proteins and nucleic acids, under extreme environmental conditions, including high hydrostatic pressures (HHP), is of fundamental biological and biotechnological importance.

### **1.8.1. High pressure and tRNA<sup>Phe</sup>**

The tRNA<sup>Phe</sup> is one of the most studied nucleic acid molecules, and it possess elements of the most common structural motifs, such as turns and hairpins. It is responsible for delivering one phenylalanine amino acid in the ribosome during the translation process. Literature studies using FTIR and fluorescence spectroscopy techniques revealed a pressure-induced reorganization of the structure of yeast tRNA<sup>Phe</sup>, and proposed that it was due to changes of the water structure from a tetrahedral to cubic geometric, in the



presence and absence of  $Mg^{2+}$  ions [100]. Pressure also induces the esterification reaction that takes place at the 3' end of tRNA molecules and is responsible to attach one amino acid molecule, in the absence of aminoacyl-tRNA synthetases. It was proposed, using circular dichroism spectroscopy, that the dehydrated state achieved through high pressure is similar to a charged conformation induced by the aminoacyl-tRNA synthetase [101].

Understanding the physical chemistry factors that contributes to the structural stability of the tRNA<sup>Phe</sup> would also help a better prediction of secondary and tertiary structures. Even less is known about how pressure could affect the structure of tRNA and its implications for organisms living under high hydrostatic pressure conditions, such as in the deep sea in which pressures up to 100 MPa are encountered.

### **1.8.2. High pressure and small RNA hairpin**

Small RNA hairpins are one of the most common secondary structures of RNA molecules, and they act as nucleation site for RNA, as ligand binding and as tertiary folding initiation sites. Therefore, to understand the stability of RNA hairpin structures and explore its free energy landscape can help to explain the thermal and pressure stability of different nucleic acid based biological systems [39, 40, 42, 102].

There are few studies in the literature on the effect pressure has on these small hairpin structures. Garcia and Paschek published in 2008 [55] a theoretical study on the folding/unfolding equilibrium thermodynamics of the RNA tetraloop gcUUCGgc. They calculated the free energy of the tetraloop as a function of temperature and pressure. They predicted a pressure and temperature elliptical stability diagram  $\Delta G(p, T)$ , in which the tetraloop would unfold at high hydrostatic pressure. The theoretical study of Miner *et al.* (2016) [103] reported the folding/unfolding thermodynamics and the characterization of the energy landscape of the gcGCAAgc tetraloop in more detail. They showed that the free energy landscape of a folded RNA hairpin tetraloop has many loop ensembles with A-RNA stem. High hydrostatic pressure stabilizes the A-form stem while it destabilizes Z-RNA stem conformations that are also present at ambient pressure.

High hydrostatic pressure experimental studies are of interest in order to confirm these theoretical predictions and provide more information about the small RNA hairpin's structure behavior and stability at extreme pressure conditions.

### 1.8.3. High pressure and hairpin ribozyme

The hairpin ribozyme is a small catalytic RNA isolated from the minus strand of the tobacco ringspot virus satellite RNA. The discovery of ribozymes strengthened the RNA world hypothesis, and the different ribozyme molecules have been extensively studied [27, 59, 60 – 66]. Therefore, studies about the effect of pressure on these molecules are of particular interest, since it would help to understand and to characterize thermodynamic parameters of the hairpin ribozyme and help disentangle its complex dynamics and reaction kinetics. In addition, it can help to understand how such enzymatic mechanism would work in living organisms at extreme conditions, such as the hydrothermal vents, where high pressures are easily encountered and volcanic environments, which are proposed to be similar to the birthplace of life [10].

There are only a few studies in the literature about the pressure effect on the catalytic reaction of hairpin ribozyme. These kinetic studies analyzed the wild-type RNA sequence and a modified RNA sequence of the hairpin ribozyme under high hydrostatic pressure. A positive activation volume ( $\Delta V^\ddagger$ ) of  $34 \pm 5 \text{ ml mol}^{-1}$  was determined, which was associated to a compaction of the ribozyme structure with consequent release/movement of water molecules. Osmotic shock experiments also showed that each RNA molecule released  $78 \pm 4$  water molecules during the docking process [104 – 106].

High pressure can help to determine volume changes associated with the hairpin ribozyme reaction, which can contribute to a better understanding of the conformational changes involved in the self-cleavage mechanism. These studies can also contribute to the RNA world hypothesis, since catalytically active RNAs were found in various living species [105, 107]. Moreover, many organisms live under extreme conditions, and high-pressure analysis of nucleic acid-based molecules may help understand the behavior of such biomolecules in these organisms.

## 1.9. Aims of this work

It is clear that RNA performs multiple vital roles within the cell, such as carrying genetic information, essential participation during protein expression and the catalysis of enzymatic reactions. The study of these biomolecules under extreme conditions, including high hydrostatic pressure, is of fundamental biological and biotechnological importance. Elucidation of the mechanistic details involved in the stability of these biomolecules under extreme conditions, such as the deep sea, hydrothermal vents and volcanic environments, also proposed to be the birthplace of life, is important to understand how piezophilic organisms could adapt and survive where high pressures are easily encountered. To this end, the goals of this study utilizing various biophysical techniques were as follow:

- 1) To elucidate the features and thermodynamic parameters which are essential in determining the temperature and pressure dependent structure of the tRNA<sup>Phe</sup>. The tRNA<sup>Phe</sup> is an important and well established model for RNA function, serving as the ideal platform to start exploring different RNA molecules. Due to the strong ionic-strength dependence of the structure of RNA, the effect of mono- and divalent ions on the temperature and pressure stability of the tRNA was also explored. Temperature- and pressure-dependent studies, using different techniques, were combined in order to reveal the conformational and free energy landscape of four different RNA molecules: the transfer RNA<sup>Phe</sup>, a small RNA hairpin, a wild-type hairpin ribozyme and a modified hairpin ribozyme.
- 2) To investigate the conformational landscape of the small RNA hairpin (gcUUCGgc) as a function of temperature and pressure, and compare with molecular dynamics studies in the literature. Since the small RNA hairpins has the ability to adopt different configurations and it has a high thermodynamic stability, it presents a good model system to study how RNA molecules can adapt to a certain environment of extreme temperature and pressure conditions.
- 3) To study the pressure-induced effects on the self-cleavage reaction of the hairpin ribozyme by following its structural changes. The hairpin ribozyme is one of the major naturally occurring ribozymes, and it was the first autocatalytic RNA

characterized. Ribozymes are RNAs with catalytic properties, which gave support to the RNA world hypothesis. Therefore, it is highly interesting to study this molecule under extreme conditions, since an important step of life evolution might have happened under extreme environmental conditions.

The conformational changes that biomolecules such as nucleic acids undergo at extreme temperature and/or pressure conditions are crucial to the adaptation of biological function in diverse organisms. Therefore, revealing the free energy landscape of these structures, and explore the forces controlling their stability are highly important to understand the thermal and pressure stability of biological systems.

---

## **2. Experimental procedures & biophysical methods**



## 2.1. Materials

### 2.1.1. RNA molecules and reagents

<b>PRODUCT</b>	<b>MANUFACTURER</b>
tRNA <sup>Phe</sup> (R4018)	<b>Sigma-Aldrich, Germany</b>
Small RNA hairpin	<b>IBA Life Science GmbH, Germany</b>
Wild-type hairpin ribozyme	<b>IBA Life Science GmbH, Germany</b>
Labeled wild-type hairpin ribozyme	<b>IBA Life Science GmbH, Germany</b>
Labeled modified hairpin ribozyme	<b>IBA Life Science GmbH, Germany</b>
D <sub>2</sub> O	<b>Sigma-Aldrich, Germany</b>
Trizma®	<b>Sigma-Aldrich, Germany</b>
MgCl <sub>2</sub>	<b>Merck, Germany</b>
[Co(NH <sub>3</sub> ) <sub>6</sub> ]Cl <sub>3</sub>	<b>Sigma-Aldrich, Germany</b>
NaCl	<b>Sigma-Aldrich, Germany</b>
Urea	<b>Sigma-Aldrich, Germany</b>
EDTA	<b>Sigma-Aldrich, Germany</b>
Nuclease-free water	<b>Thermo Fisher Scientific, USA</b> <b>Omega Bio-tek, USA</b>
RNase Away®	<b>Thermo Fisher Scientific, USA</b>
RNase free conical tubes	<b>Ambion®, Thermo Fisher Scientific, USA</b>
RNase free microfuge tubes	<b>Ambion®, Thermo Fisher Scientific, USA</b> <b>Eppendorf, Germany</b>
RNase free tips	<b>Eppendorf, Germany</b>
Whatman disposable syring filter (0.2 µm pore)	<b>GE Healthcare / Life Science, Germany</b>
Syringe	<b>BBraun, Germany</b>
Novex® 15% TBE-urea gel	<b>Thermo Fisher Scientific, USA</b>
SYBR® Gold	<b>Thermo Fisher Scientific, USA</b>
RNA loading buffer (2x)	<b>AMRESCO, USA</b>
Nuclease-free TBE running buffer	<b>Ambion®, Thermo Fisher Scientific, USA</b>

### Instruments and software

<b>INSTRUMENT/SOFTWARE</b>	<b>MANUFACTURER</b>
<b>Magna 550 IR Spectrometer</b>	<b>Thermo Fisher Scientific, USA</b>
<b>Nicolet IR Spectrometer</b>	<b>Thermo Fisher Scientific, USA</b>
<b>ISSK2 Fluorometer</b>	<b>ISS, USA</b>
<b>UV Spectrometer</b>	<b>Shimadzu, Germany</b>
<b>X-cell SureLock™ Mini-cell Electrophoresis System</b>	<b>Thermo Fisher Scientific, USA</b>
<b>AlphaImager®</b>	<b>ProteinSimple, USA</b>
<b>Diacell® VivoDAC</b>	<b>Almax.easyLab, Belgium</b>

<b>GRAMS AI</b>	<b>Thermo Fisher Scientific, USA</b>
<b>Origin 9.0</b>	<b>Origin Labs, USA</b>
<b>ImageJ®</b>	<b>NIH, USA</b>
<b>ChemDraw</b>	<b>Perkin Elmer, USA</b>

## 2.1.2. RNA samples

### 2.1.2.1. General sample handling procedures

All samples, buffer solutions, storage materials and surfaces that would have contact with RNA samples were nuclease free (molecular biology grade) or cleaned with RNase AWAY® reagent, and then rinsed with nuclease free water. All buffers were prepared in nuclease free water or D<sub>2</sub>O and filtered with Whatman® 0.2 µm (cellulose acetate membrane) sterile filter.

### 2.1.2.2. tRNA<sup>Phe</sup>

The phenylalanine transfer RNA (tRNA<sup>Phe</sup>) specific from brewer's yeast purchased from Sigma-Aldrich (Germany) was used without further purification. tRNA<sup>Phe</sup> samples were suspended in a 1 mg mL<sup>-1</sup> nuclease free water solution, and stored at -80 °C. For the techniques applied, different tRNA<sup>Phe</sup> concentrations were lyophilized to remove H<sub>2</sub>O, and then suspended in pure D<sub>2</sub>O or 50 mM TRIS- HCl buffer + 0.1 mM EDTA, pH 7.5, in the presence or absence of 15 mM MgCl<sub>2</sub> and/or 100 mM NaCl. The experiments were carried out multiple times, and different lots of tRNA<sup>Phe</sup> were used. More details about sample conditions will be given in the next sections.

### 2.1.2.3. Small RNA hairpin

The small RNA hairpin (sRNAH non-labeled: 5'-GCUUCGGC-3'; sRNAH labeled: 5'-Cyanine 3 - GCUUCGGC- Cyanine 5 - 3') was synthesized by IBA Life Solutions for Life Science GmbH (Goettingen, Germany), and was received as lyophilized powder. The sRNAH was suspended in a 0.1 mmol µL<sup>-1</sup> nuclease free water solution, and stored at -80 °C. For the techniques applied, different sRNAH concentrations were lyophilized to



remove H<sub>2</sub>O, and then suspended in pure 50 mM TRIS- HCl buffer + 0.1 mM EDTA, pH 7.5. The experiments were carried out multiple times, and different lots of RNA were used. More details about sample conditions will be given in the next sections.

#### 2.1.2.4. Hairpin ribozyme

The different hairpin ribozyme molecules, non-labeled wild-type hairpin ribozyme and fluorescence labeled modified hairpin ribozyme, were synthesized by IBA Life Solutions for Life Science GmbH (Goettingen, Germany), and were received as lyophilized powder. The ribozymes were suspended in a 0.1 nmol  $\mu\text{L}^{-1}$  nuclease free water solution, and stored at - 80 °C.

- Wild-type hairpin ribozyme (wtHpRz)

**5'-AAACAGAGAAGUCAACCAGAGAAACACACGUGUGGUAUAUUAACUGG  
UACCCCGACAGUCCUGUUU-3'**

The wild-type hairpin ribozyme creates a two-way junction hairpin ribozyme that independently folds in a helical domain, which is a simple model system of the original four-way junction tobacco ringspot virus satellite RNA.

- FRET-labeled modified hairpin ribozyme (FRET-modHpRz)

**5'-cyanine 5'-ACGGUGAGAAGGGAGGCAGAGAAACACAC-cyanine 3'-GUCGU  
GGUACAUUACCUGCCACCCCUCCAGUCCACCGU-3'**

The FRET-modHpRz molecule has two fluorescent dyes attached, cyanine 3 phosphoramidite (Cy3) and cyanine 5 phosphoramidite (Cy5) to the loop A and at the loop B, respectively. Their structure is based on two indole rings that are connected by a polymethine chain, Cy3 function as the donor fluorophore and Cy5 as the acceptor for the kinetic FRET studies. The folded (docked) conformation of the HpRz (distance between 3' and 5' ends: ~3 nm) will have a higher FRET signal compared to the undocked state (distance between 3' and 5' ends: ~8 nm).

The FRET-modHpRz sequence is based on the well-resolved crystal structure from Salter et al. (PDB ID: 2OUE) [108]. The experimental data was used to complement molecular dynamics simulation studies done in collaboration with Prof. Dr. Dominik Marx (Ruhr-Universität Bochum). It is a well resolved ribozyme structure (resolution 2.05 Å) in its pre-catalytic form, which especially suits the simulation purpose. The resolved crystal structure contains four different chains including a substrate chain. However, the catalytic reaction is limited by dissociation of the chains. Therefore, a modified hairpin ribozyme sequence was established by taking all the available nucleotides from the crystal structure while adding missing ones via sequence homology based on existing literature [106]. Since only essential nucleobases are required for proper activity, the self-cleavage process is identical in both the wild type and the modified ribozyme [59].

For the techniques applied, different HpRz concentrations were lyophilized to remove H<sub>2</sub>O, and then suspended in pure 50 mM TRIS- HCl buffer + 0.1 mM EDTA, pH 7.5, to half of the final reaction volume. Samples were then subjected to denaturation and renaturation steps (heated up to 90 °C for 1 min and slowly cooled down to 25 °C in 3 °C min<sup>-1</sup> steps) to ensure proper folding of the RNA loops. The cleavage reaction started by addition the second half volume to the mixture, a double concentrated buffer solution of 50 mM TRIS- HCl + 0.1 mM EDTA + 12 mM MgCl<sub>2</sub> or 24 mM Cobalt (III) hexamine + 200 mM NaCl, pH 7.5. Final salt concentrations in the reaction were 6 mM MgCl<sub>2</sub> or 12 mM Cobalt (III) hexamine + 100 mM NaCl. The experiments were carried out multiple times, and different lots of RNA were used. More details about sample conditions will be given in the next sections.

## 2.2. Biophysical methods

### 2.2.1. Fourier-transform infrared spectroscopy

Fourier-transform infrared (FTIR) spectroscopy has proved to be a powerful technique to determine the secondary structure of diverse biomolecules, especially of proteins and DNA, under different conditions of temperature and pressure. IR spectroscopy provides a relatively fast (high time resolution of < μs short measuring time) way to characterize

one molecule's secondary structure features in its native or denatured state. The IR signal is obtained by the molecular vibration absorption of IR light when the frequencies of light and the respective vibrational mode coincide. The frequency of vibration and the probability of absorption depend on the strength and polarity of the vibrating bond, and they are strongly influenced by the inter- and intramolecular environment. The changes in the environment of nucleotides and backbone torsion on the vibration frequency have been extensively analyzed in the present work.

### 2.2.1.1. Instrumentation and spectra collection

Time- and temperature-dependent IR measurements were performed on the Nicolet 5700 FTIR spectrometer equipped with a liquid nitrogen cooled MCT (HgCdTe) detector and a 0.4 mm IR cell with CaF<sub>2</sub> windows, separated by 50 μm polyethylene terephthalate (PET) spacers. The spectrometer was purged continuously with dry air to remove water vapor. Each FTIR spectrum was collected with 256 scans, resolution of 2 cm<sup>-1</sup>, apodised with a Happ–Genzel function, and the data processing step (discussed in the next section) was performed using the GRAMS software as described elsewhere [109 – 111] and then plotted with OriginPro 9.0G software. An external, circulating water thermostat controlled the required temperature in the cell with an accuracy of ± 0.1 °C.

The pressure-dependent FTIR spectra were recorded on the Magna IR 550 spectrometer equipped with a liquid nitrogen cooled MCT (HgCdTe) detector. The infrared light was focused by a spectral bench onto the pinhole of a gas membrane diamond anvil cell (Figure 9 and 10) (Diacell® VivoDAC, Almax.easyLab) with a 50 μm brass spacer. The pressure was controlled by a digital pneumatic controller, PACE Modular Pressure Controller (GE Measurement & Control), attached to a nitrogen cylinder. Fine powdered barium sulphate (BaSO<sub>4</sub>) was used as the pressure calibrant. It was placed in the hole of the brass gasket in the diamond anvil cell and changes in pressure were quantified by the shift of the barium sulphate peak at 983 cm<sup>-1</sup>, related to its stretching vibration [11]. The basic operating principle of a diamond anvil cell is the application of a moderate force on a small area, generating high pressures. Specific details on the use of the high-pressure

diamond anvil cells can be found in the literature [112, 113]. An external, circulating water thermostat controlled the required temperature with an accuracy of  $\pm 0.1$  °C.

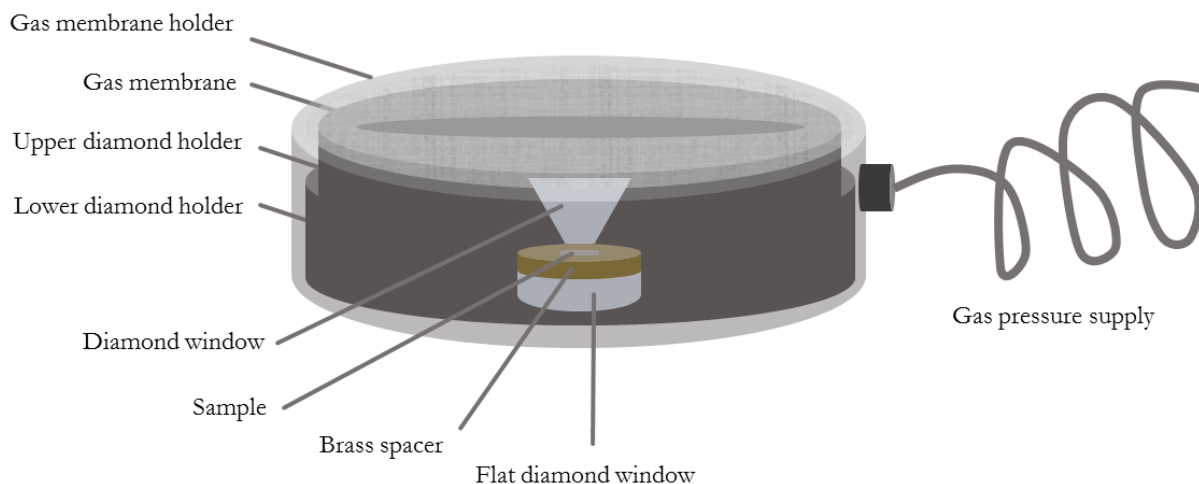


**Figure 9. Gas membrane diamond anvil cell.** Schematic of the gas membrane high-pressure cell Diacell® VivoDAC from Almax.easyLab.

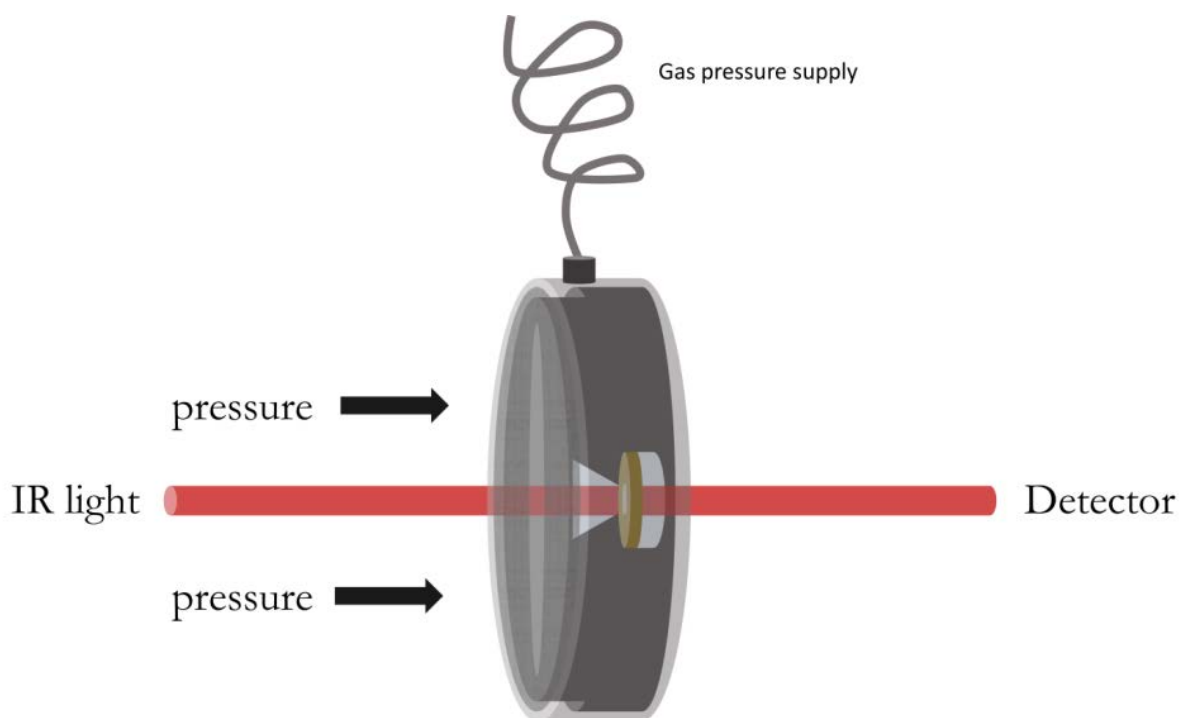


**Figure 10. Gas membrane diamond anvil cell during FTIR measurement.** When the gas pressure is increased, the metal membrane expands, pushing the upper diamond holder part, thereby, increasing the pressure.

### 2.2.1.2. FTIR spectroscopy of tRNA<sup>Phe</sup> ambient and pressure dependent conditions

**A) Temperature dependent conditions:** The tRNA<sup>Phe</sup> samples were lyophilized overnight and then diluted in D<sub>2</sub>O solution with or without 15 mM MgCl<sub>2</sub>, to a final concentration of 0.5 wt % in 50  $\mu$ L volume. The temperature varied from 10 to 80 °C in the FTIR cell. The sample temperatures were equilibrated for 20 minutes before the acquisition of a new IR spectrum.

**B) Pressure dependent conditions:** The tRNA<sup>Phe</sup> samples were lyophilized overnight and then diluted in D<sub>2</sub>O solution with or without 15 mM MgCl<sub>2</sub>, to a final concentration of 4.5 wt % in 6  $\mu$ L volume. The temperature was maintained at 20 °C in the FTIR high-pressure cell, and the pressure varied from 0.1 to 1000 MPa. After each pressure change, the samples were equilibrated for 5 min before the acquisition of a new IR spectrum.

### 2.2.1.3. FTIR spectroscopy of Small RNA hairpin at ambient and pressure conditions

**A) Temperature dependent conditions:** The labeled and non-labeled sRNAH samples were lyophilized overnight and then diluted in 50 mM Tris-HCl buffer + 0.1 mM EDTA, to a final concentration of 0.5 wt% in 50  $\mu$ L volume. The temperature varied from 10 to 80 °C in the FTIR cell. The sample temperatures were equilibrated for 20 minutes before the acquisition of a new IR spectrum.

**B) Pressure dependent conditions:** The labeled and non-labeled sRNAH samples were lyophilized overnight and then diluted in 50 mM Tris-HCl buffer + 0.1 mM EDTA, to a final concentration of 4.5 wt% in 6  $\mu$ L volume. Two different temperatures were used, 20 °C and 70 °C in the FTIR high-pressure cell, and the pressure varied from 0.1 to 400 MPa. After each pressure change, the samples were equilibrated for 5 min before the acquisition of a new IR spectrum.

#### 2.2.1.4. FTIR spectroscopy of Hairpin ribozyme at ambient and pressure conditions

**A) Time dependent conditions at ambient pressure:** The wild-type hairpin ribozyme samples were lyophilized overnight and then diluted in 50 mM Tris-HCl buffer + 0.1 mM EDTA with 6 mM MgCl<sub>2</sub> or 12 mM [Co(NH<sub>3</sub>)<sub>6</sub>]Cl<sub>3</sub> + 100 mM NaCl, to a final concentration of 4.5 wt% in 6 μL volume. The duration of the measurement was 12 hours. The temperature was maintained at 25 °C in the high-pressure FTIR cell. The sample temperatures were equilibrated for 20 minutes before the acquisition of a new IR spectrum. During the hairpin ribozyme kinetic (time dependent) studies, the dead time between cell assembling and first spectrum acquisition should be as little as possible, ranging around ~ 10 minutes. The time dependent measurements were carried out using the high-pressure cell to ensure the same conditions for reaction at the ambient and high pressure analysis.

**B) Time dependent conditions at high pressure:** The wild-type hairpin ribozyme samples were lyophilized overnight and then diluted in 50 mM Tris-HCl buffer + 0.1 mM EDTA with 6 mM MgCl<sub>2</sub> or 12 mM [Co(NH<sub>3</sub>)<sub>6</sub>]Cl<sub>3</sub> + 100 mM NaCl, to a final concentration of 4.5 wt% in 6 μL volume. The duration of the measurement was 12 hours, and the pressure maintained at 50 MPa and 100 MPa. The temperature was maintained at 25 °C in the FTIR cell. After each pressure change, the samples were equilibrated for 5 min before the acquisition of a new IR spectrum. For the hairpin ribozyme kinetic (time dependent) studies, the dead time between high-pressure cell assemble and acquisition of the first spectrum should be as little as possible, being ~ 30 minutes until the desired pressure was reached.

## 2.2.1.5. Secondary structure analysis of nucleic acids by infrared spectroscopy

A) Nucleic acid infrared band assignment in D<sub>2</sub>O

Wavenumber	Assignment	Explanation	Observation
1715 cm <sup>-1</sup>	Triple strand vibrations: G*G - C	C6 = O6 stretch vibrations of guanine in third strand binding	Hoogsteen third strand binding
1689-1678 cm <sup>-1</sup>	Double strand vibrations of guanine	C6 = O6 stretch vibrations of base paired guanine → 1689-1678 cm <sup>-1</sup>	Guanine vibrations shift to lower wavenumbers when unpaired. This band is used to follow the thermal denaturation profile of RNA.
1677-1672 cm <sup>-1</sup>	Double strand vibrations of uracil	C4=O4 stretch vibrations of base paired uracil → 1677-1672 cm <sup>-1</sup>	Uracil vibrations shift to lower wavenumbers when unpaired. This intensity is used to follow the thermal denaturation profile of RNA.
1673-1660 cm <sup>-1</sup>	Free base vibrations of guanine	C6 = O6 stretch vibrations of free guanine → 1673 – 1660 cm <sup>-1</sup>	The intensity of the band decreases upon duplexation. This intensity is also used to follow the thermal denaturation profile of RNA.
1673-1660 cm <sup>-1</sup>	Free base vibrations of uracil	C4 = O4 stretch vibrations of uracil → 1657 – 1653 cm <sup>-1</sup>	The intensity of the band decreases upon duplexation. This intensity is also used to follow the thermal denaturation profile of RNA.
1655-1647 cm <sup>-1</sup>	Free base or base paired vibrations of cytosine	C2 = O2 stretch vibrations of single strand or double strand cytosine	Shift to 1652-1649 cm <sup>-1</sup> and decrease in intensity upon duplexation.
1632-1622 cm <sup>-1</sup>	Free base or base paired vibrations of adenine	C = N and C = C ring vibrations of single strand and double strand adenine	Shifts to 1628-1631 cm <sup>-1</sup> upon duplexation. It is used to follow denaturation of RNA adenine rich regions.
1624-1616 cm <sup>-1</sup>	Free base or base paired vibrations of cytosine	In-plane ring vibrations of single strand or double strand cytosine	
1618-1615 cm <sup>-1</sup>	Free base vibrations of uracil	C = C stretch vibrations of single strand uracil	
1590-1575 cm <sup>-1</sup>	Free base and base paired vibrations of guanine	C = N (C4 = C5, C5 – C6) ring vibration of single or double strand guanine	The intensity of the band decreases upon duplexation. This band can resolve any difference in the denaturation behavior of A- rich and G-rich regions independent from each other.

Wavenumber	Assignment	Explanation	Observation
1568-1564 cm <sup>-1</sup>	Free base and base paired vibrations of guanine	C = N (C6 = O6, C5 – C6) ring vibration of single or double strand guanine	The intensity of the band decreases upon duplexation.
1527-1520 cm <sup>-1</sup>	Free base and base paired vibrations of cytosine	Single strand and double strand in-plane vibrations	Decreases in intensity upon duplexation
1506-1498 cm <sup>-1</sup>	Vibrations of cytosine	In-plane vibrations of cytosine	
1495-1476 cm <sup>-1</sup>	Ring vibrations of adenine and guanine	N7C8H band of adenine and/or guanine	Any interaction at the N7 site of the purine imidazolic ring leads to changes in the position and/or intensity of this band, such as triple helix formation or changes in hydration of the nucleic acid
1464 cm <sup>-1</sup>	Vibration of uracil	Bond stretch of uracil in D <sub>2</sub> O	
1457 – 1453 cm <sup>-1</sup>	Vibrations of adenine in B-form/A-form helices	N1=C6, C6N6 vibrations of adenine in B/A-form	
1438 – 1434 cm <sup>-1</sup>	Vibrations of adenine in Z-form helices	N1=C6, C6N6, C5C6N vibrations of adenine in Z-form	
1425 – 1420 cm <sup>-1</sup>	S-type sugar vibrations of adenine and/or guanine in B-form	C2'-endo (S-type) sugar in B-form helices	
1418 – 1408 cm <sup>-1</sup>	N-type sugar vibrations in A-form helices	C3'-endo (S-type) sugar in A-form helices	
1413 – 1408 cm <sup>-1</sup>	N-type sugar vibrations in Z-form helices	C3'-endo (S-type) sugar in Z-form helices	
1400 cm <sup>-1</sup>	Vibrations of RNA molecules	In-plane C2'OH vibrations in RNA	
1381 – 1369 cm <sup>-1</sup>	Purine bases in anti conformation	C2'/C3'-endo sugar pucker conformation	
1365 – 1360 cm <sup>-1</sup>	Cytidine in anti conformation	C2'/C3'-endo sugar pucker conformation	
1357 – 1352 cm <sup>-1</sup>	Purine bases in syn conformation	C3'-endo sugar pucker conformation	

Table 1. Wavenumbers and spectral assignments of selected infrared bands of nucleic acids from 1800 to 1250 cm<sup>-1</sup>. A = Adenine, C = Cytosine, G = Guanine, U = Uracil [114].



## **B) Data processing:**

Following the spectra collection, a few processing steps were employed, such as background (buffer) subtraction and spectral baseline correction in the required frequency range of interest (for RNA: 1720-1500  $\text{cm}^{-1}$  related to in plane base vibrations sensitive to effects of base pairing and base stacking; 1500-1350  $\text{cm}^{-1}$  base sugar vibrations sensitive to glycosidic bond rotation, backbone and sugar pucker conformation). The spectra were normalized by setting the area to one in these ranges, *e.g.* 1720 to 1600  $\text{cm}^{-1}$ , to allow for a quantitative analysis (curve-fitting, the most common method to resolve overlapping bands in the amide band region of proteins could not be applied to nucleic acid FTIR spectral analysis) of the secondary structure. Second derivative and Fourier self-deconvolution (FSD) analyses were applied to the normalized spectra to identify the overlapping components of different band regions [115]. All the raw spectra were analyzed with a similar set of peaks and parameters. In ambiguous cases (such as the presence of different bands), information from X-ray diffraction of the RNA molecule was taken into account. The band positions were assigned to the secondary structures according to Table 1.

### **2.2.2. Fluorescence spectroscopy**

The excitation of fluorophores occurs by the dissipated electromagnetic radiation of UV light. Fluorescence methods are well known for requiring low concentrations of sample to be detected, if compared with other spectroscopic methods, such as UV-vis or NMR spectroscopy [116, 117].

The fluorescence measurements were carried out with an ISS-K2 fluorimeter (Champaign, Illinois, USA). Excitation light was provided by a xenon lamp through a monochromator, and the emission light collected at 90° passing through another monochromator, and then hitting the detector. Time- and temperature-dependent measurements at ambient pressures were carried out in standard quartz cuvettes (1 cm of optical length). High-pressure fluorescence experiments were carried out using an ISS stainless steel high-pressure vessel coupled to the K2 fluorimeter (Figure 11) [118]. The

maximum pressure of the high-pressure vessel is 3000 bar. Different samples were injected into a round quartz bottle (volume 250  $\mu\text{L}$ ) and sealed with pressure-transmitting Dura Seal film fixed by a rubber O-ring. The cell was placed in the high-pressure vessel, which has three sapphire windows and connected to a manual hydraulic pump and gauge. Water was used as the pressurizing medium. Both ambient and high-pressure cell systems were connected to a water bath for temperature control. For the temperature dependent measurements, the samples were equilibrated for 20 min before taking a new spectrum.

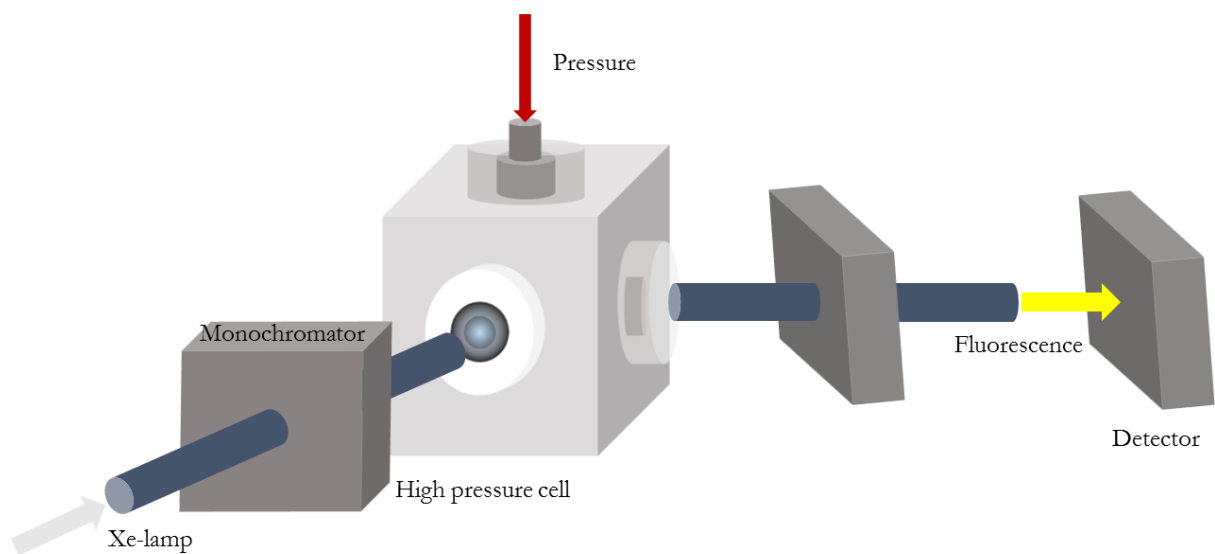


**Figure 11. High pressure fluorescence spectroscopy.** The white light is filtered by a monochromator, and the selected beam reaches the sample. The excited fluorophore will emit fluorescence in all directions. The output at  $90^\circ$  will lead to a second monochromator settled to a specific wavelength of emission that will reach the detector.

### A) tRNA<sup>Phe</sup> temperature dependent fluorescence conditions

The lyophilized tRNA<sup>Phe</sup> was suspended in 275  $\mu\text{L}$  H<sub>2</sub>O solution +/- 15 mM MgCl<sub>2</sub> to a final concentration of 0.04 mM. The samples were excited at 320 nm and the emission spectra of the Y base (wybutine) were recorded between 360 and 560 nm [119]. The ambient-pressure fluorescence measurements were carried out in the standard K2 fluorimeter setup using quartz cuvettes with 275  $\mu\text{L}$  of RNA

sample volume. The temperature ranged from 10 to 80 °C. The fluorescence data were analyzed using OriginPro 9.0G software.

### **B) tRNA<sup>Phe</sup> pressure dependent fluorescence conditions**

The tRNA<sup>Phe</sup> samples were prepared according to section 2.3.1.1. The high-pressure fluorescence measurements were carried out in the ISS high-pressure setup using quartz pressure bottles with 250  $\mu$ L of RNA sample volume [119]. The temperature used was 20 °C. The fluorescence data were analyzed using OriginPro 9.0G software.

### **2.2.3. Differential scanning calorimetry**

Differential scanning calorimetry (DSC) is a thermal analysis technique that tracks how the heat capacity ( $C_p$ ) of a given molecule or material changes by temperature. The  $C_p$  changes of a sample are compared to the  $C_p$  of a reference, buffer or H<sub>2</sub>O. When well-defined structures of macromolecules undergo temperature induced conformational changes, such as unfolding, these changes result in the absorption of heat as a result of redistribution of non-covalent bonds. The differential scanning calorimeters measure this heat uptake, which allows the detection of transitions as melting or phase changes, for example. Through DSC melting transitions, the precise melting temperature ( $T_m$ ) of a molecule and its denaturation enthalpy can be obtained. For example, the unfolding of a protein is an endothermic event, and it is observed as a positive increase of the heat capacity signal. The midpoint of the obtained curve is the melting temperature ( $T_m$ ) and the area under the curve is the enthalpy change ( $\Delta H$ ) of the process.

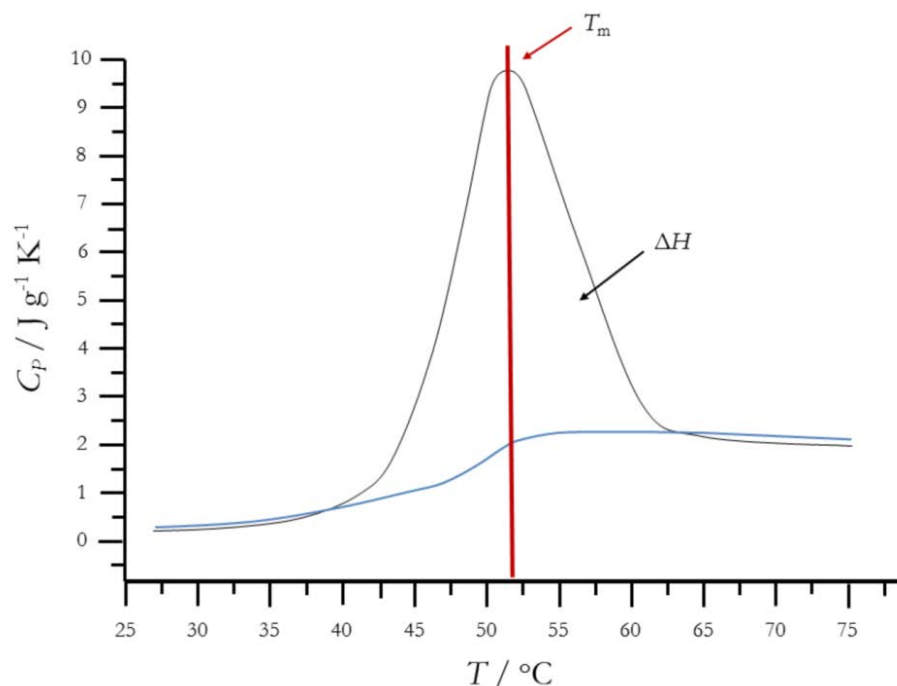


**Figure 12. Differential scanning calorimetry.** Example of a final result obtained with the DSC analysis, *e. g.*, for the unfolding of a protein. It is possible to obtain from the DSC curve the  $T_m$ , at the maximum of the heat capacity, and the  $\Delta H$  through the area under the curve (blue line: baseline).

The DSC measurements were carried out in a VP-DSC micro-calorimeter (Microcal™) (Figure 12). The sample cell was filled with  $0.5 \text{ mg mL}^{-1}$  tRNA<sup>Phe</sup> in D<sub>2</sub>O solution without or with 15 mM MgCl<sub>2</sub>, and the reference cell was filled with D<sub>2</sub>O without or with 15 mM MgCl<sub>2</sub>. The heating rate was  $30^\circ\text{C h}^{-1}$  for the DSC scans and the temperature range from 10 to 90 °C. Data evaluation was performed using Origin for the DSC package supplied with the instrument, and the tRNA<sup>Phe</sup> DSC curves obtained were normalized in relation to the sample concentration and partial specific volume, which is  $0.55 \text{ mL g}^{-1}$  for the tRNA<sup>Phe</sup>, to yield the correct shape of the molar heat capacity peak,  $C_p(T)$  and melting temperature,  $T_m$  [83].

#### 2.2.4. Pressure perturbation calorimetry

The pressure perturbation calorimetry (PPC) method uses as base a DSC calorimeter coupled with a pressure accessory that generates pressure-jumps. It measures the heat ( $Q$ ) resulting from a pressure change ( $\Delta p$ ) on a sample solution. This heat can be used to

derive the thermal volume expansion coefficient,  $\alpha_v$ , as a function of temperature, and in the case of phase transitions, the volume change,  $\Delta V$ , occurring at the phase transition, if the specific volume  $V(T)$  of the molecule is known.

The PPC measurements were performed in the DSC calorimeter using the MicroCal PPC accessory (Figure 13), which applies pressure-jumps between ambient pressure and 0.5 MPa at each temperature. The data were recorded between 10 and 80 °C. At temperatures within the thermal transition region pressure jumps were carried out at intervals of 2 °C. The sample cell was filled with 3 mg mL<sup>-1</sup> tRNA<sup>Phe</sup> D<sub>2</sub>O solution without or with 15mM MgCl<sub>2</sub>, and the reference cell was filled with D<sub>2</sub>O without or with 15 mM MgCl<sub>2</sub>. Control measurements of buffer-versus-buffer, buffer-versus-water and water-versus-water were performed to correct the sample raw data. The instrument software reads the sample and blank data and performs all necessary conversions and corrections to derive the thermal expansion coefficient curve,  $\alpha(T)$ . By integrating the  $\alpha(T)$  curve, the relative volume change of the unfolding transition  $\Delta V/V^{-1}$ , can be obtained [83, 120].

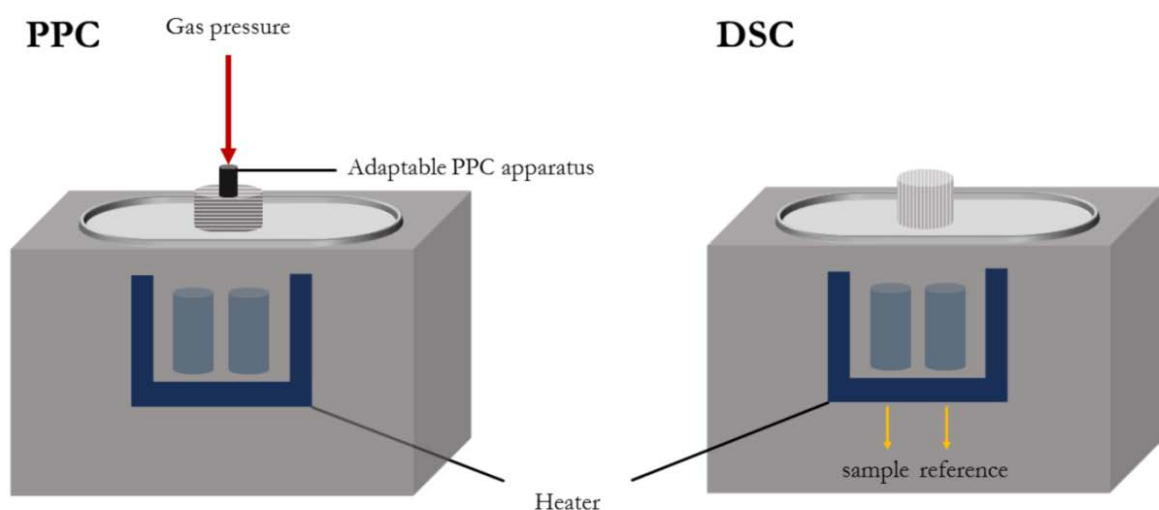


**Figure 13. Differential scanning calorimetry (DSC) and pressure perturbation calorimetry (PPC) (schematic).** The sample and reference are heated together and the heat uptake from the sample during melting is measured. A small PPC apparatus is attached to the sample chamber and pressure-jumps of 0.5 MPa are applied at each temperature, which enables measurement of heat changes at each pressure change.

### 2.2.5. UV-vis spectroscopy

Biological macromolecules, such as proteins and nucleic acids, can absorb light in the UV-visible (UV-vis) region of the spectrum. The absorbance of a sample is linearly dependent on its concentration; therefore, absorption spectroscopy is an appropriate technique for quantitative measurements. The wavelength of absorption and the strength of absorbance of a molecule depend not only on the chemical nature its transition dipole moment but also on the molecular environment of its chromophores. These properties make UV-vis spectroscopy a suitable technique for following studies of ligand-binding reactions, enzyme catalysis and conformational transitions in proteins and nucleic acids. The UV-vis spectroscopic technique is very sensitive, non-destructive and requires small amounts of sample, only.

Nucleic acids have a strong absorbance in the region of 240 – 275 nm. At neutral pH, the absorption maxima range from 275 nm, for guanidine, 270 nm for cytidine, and 260 nm for uracil bases. Therefore, polymeric DNA and RNA show a broad absorbance around 260 nm. When bases are stacked, they are shielded from the solvent and its absorbance is smaller compared to single stranded nucleic acid chains. The RNA denaturation is then followed by an increase in absorbance near 260 nm. The UV-vis spectrum of guanine alone shows absorption maxima around 275 nm [121 – 124].

A UV-1800 UV-vis spectrometer, from Shimadzu, was used to collect absorbance spectra of the small RNA hairpin. An external water bath connected to the cuvette holder kept the temperature constant during all measurements. The ambient pressure measurements were carried out using quartz cuvettes with 300  $\mu$ L of RNA sample volume (Figure 15). The labeled and non-labeled sRNAH samples were lyophilized overnight and then diluted in 50 mM Tris-HCl buffer + 0.1 mM EDTA, to a final concentration of 40  $\mu$ M. The temperature varied from 10 to 80 °C in the cuvette. The sample temperature was equilibrated for 20 minutes before the acquisition of a new spectrum.

## 2.2.6. Hairpin ribozyme kinetic reaction

### 2.2.6.1. Time dependent hairpin ribozyme reaction at ambient pressure

The ambient pressure reactions were carried out in a thermoshaker (cooling thermal shake touch, VWR) with a heating speed of 5 °C min<sup>-1</sup> and cooling rate of 3 °C min<sup>-1</sup> with an accuracy of ± 2%. The lyophilized wild type hairpin ribozyme (wtHpRz) and the labeled-modified hairpin ribozyme (modHpRz) samples were then dissolved in 50 mM Tris-HCl buffer, pH 7.5, with 0.1 mM EDTA, at a final concentration of 28.7 μM. These samples were subjected to denaturation and renaturation. The self-cleavage reaction started by mixing the RNA solution 1:1 with 12 mM MgCl<sub>2</sub> or 24 mM [Co(NH<sub>3</sub>)<sub>6</sub>]Cl<sub>3</sub> + 200 mM NaCl buffer solution. All reactions were conducted at 25 °C, and the time varied from 0 to 360 min. The ribozyme's self-cleavage reaction was stopped by adding 1:1 stopping buffer (7 M urea + 50 mM EDTA, pH 7.5), with further addition of RNA loading buffer 2X (AMRESCO®), and stored in ice. Final aliquots of 10 μL were stored at -80 °C.

### 2.2.6.2. Time dependent hairpin ribozyme reaction at high pressure

The high hydrostatic pressure reactions were carried out in a home-built high-pressure vessel connected to a manual hydraulic pump, using water as pressure-transmitting medium. The temperature was controlled by an external water bath. The lyophilized wtHpRz and the labeled-modHpRz samples were then dissolved in 50 mM Tris-HCl buffer, pH 7.5, with 0.1 mM EDTA, at a final concentration of 28.7 μM. These samples were subjected to denaturation and renaturation. The self-cleavage reaction started by mixing the RNA solution 1:1 with 12 mM MgCl<sub>2</sub> or 24 mM [Co(NH<sub>3</sub>)<sub>6</sub>]Cl<sub>3</sub> + 200 mM NaCl buffer solution in home-built high pressure Teflon bottles, and sealed with pressure-transmitting Dura Seal film fixed by a rubber O-ring. All reactions were conducted at 25 °C. The HpRz samples were maintained at different pressures, 100 MPa, 200 MPa and 300 MPa, from 0 to 360 min. Each data point, at each different time, was measured with a fresh prepared new sample. The ribozyme's self-cleavage reaction was stopped by adding 1:1 stopping buffer (7 M urea + 50 mM EDTA, pH 7.5), with further

addition of RNA loading buffer 2X (AMRESCO®), and stored in ice. Final aliquots of 10  $\mu$ L were stored at -80 °C.

### 2.2.6.3. Polyacrylamide gel electrophoresis

Polyacrylamide gel electrophoresis (PAGE) is a widely used technique for separate biological macromolecules as proteins and nucleic acids. Molecules can be in their native state, to preserve ordered structures, or a chemical denaturant can be added to turn the molecules in an unstructured chain whose mobility depends only on its extended length. The most common denaturant for nucleic acids is urea. It is one of the most used techniques for RNA analysis, since it is applicable for RNA detection, quantification, purification by size and quality assessment. The gels consist of acrylamide, bisacrylamide, denaturant (urea), a free radical source (ammonium persulfate) and a stabilizer (tetramethylethylenediamine – TEMED) that is responsible for catalyzing the acrylamide polymerization. The acrylamide concentration can vary between 5 to 25%, and it influences how the molecules will migrate across the gel, since low acrylamide percentage gels are better to run molecules with high molecular weight. Then, an electrophoretic field is applied across the gel, causing the negatively charged nucleic acid (guaranteed by the sample loading buffer) to migrate across the gel towards the anode. Each biomolecule will have different mobility in the gel, this way small molecules will migrate faster and reach down the gel, while larger molecules will migrate slower and stay on upper areas due to increase resistance within the polymerized gel net.

The reaction products of the hairpin ribozyme were analyzed by denaturing urea polyacrylamide gel electrophoresis (Urea PAGE) using the XCell SureLock® Mini-Cell system (ThermoFisher) with Novex® 15% TBE-Urea gels (ThermoFisher) and TBE running buffer (Ambion®). Cleavage reaction's aliquots of 10  $\mu$ L containing 3.6  $\mu$ M of RNA were applied to the gels. After electrophoresis, the gels were directly stained with SYBR® Gold (Molecular Probes™), and the bands were analyzed by an ultraviolet (UV) transilluminator (AlphaImager Mini, ProteinSimple). The light intensity of each RNA fragment band was quantified using ImageJ software (N.I.H., USA) [125], and the

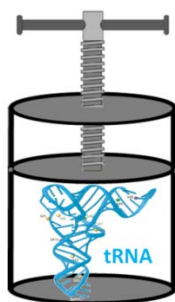


reaction product is presented by the percentage of cleaved RNA over the total RNA amount (cleaved RNA + native RNA).



---

### 3. Exploring the free energy and conformational landscape of tRNA at high temperature and pressure conditions



\* The work of the present study has been published and subsequently reprinted from *ChemPhysChem* (2015) 16, 138-146, Schuabb, C., Berghaus, M., Rosin, C. & Winter, R., “Exploring the free energy and conformational landscape of tRNA at high temperature and pressure conditions” with permission from Wiley & Sons. Copyright John Wiley and Sons.



### **3.1. Background**

Elucidation of the mechanistic details involved in the formation and stability of biomolecules, such as lipid membranes, proteins, and nucleic acids, under extreme environmental conditions, including high hydrostatic pressures (HHP), is of fundamental biological and biotechnological importance [126, 127]. Generally, biopolymers can populate multiple different structural states that each has its own specific or molar volume. Pressure acts to reshuffle the relative populations of these states and favors those with the smaller volume. Thus, a structure-based difference in volume for different conformers underlies the mechanism for pressure-induced conformational changes of proteins and nucleic acids. Moreover, several studies have also revealed that the effects of HHP on biomolecules include changes in hydration and intermolecular interactions, such as hydrogen bonding and hydrophobic interactions [69 - 71, 82, 94, 109, 111, 120, 128 – 130].

Although the effects of pressure on lipid membranes and protein systems have been studied extensively, little is known about the effect of temperature and pressure on the conformation and stability of nucleic acids. In contrast to proteins, intermolecular interactions in nucleic acids (i.e., base pairing and base stacking) are rather strong and are ultimately responsible for driving native folding. The canonical DNA duplex formed with Watson–Crick base pairs generally has been found to have a negative partial molar volume, that is, the volume change upon unfolding (melting),  $\Delta V$ , of DNA is positive, which indicates that applying pressure causes the duplex to be more stable [83, 84, 90, 109].  $\Delta V$  values published for DNA duplexes amount to about 1 to 5 mL mol<sup>-1</sup>, and the  $\Delta V$  value for protein unfolding is typically -30 to -100 mL mol<sup>-1</sup> [89, 109, 113, 126]. Only in special cases, such as poly[d(A-T)], nucleic acid structures have a negative value of  $\Delta V$  and melt upon pressurization. Structural analyses also revealed that the conformation and configuration of the DNA duplexes are not significantly perturbed under high pressure [82, 90]. In contrast to the stabilities of duplexes, which are relatively unaffected by pressure, non-canonical DNA structures, such as G-quadruplex DNA, have been found

to be more sensitive to pressure [89] and the magnitude of the  $\Delta V$  value is similar to magnitudes of  $\Delta V$  measured for proteins.

Even less is known about how pressure affects the formation of RNA structures, though there are indications that RNAs are more pressure sensitive [34, 55, 83, 100, 101, 105, 132]. This would have biological implications for organisms living under high-pressure conditions, such as in the deep sea, in which pressures up to 100 MPa are encountered [126, 127]. For example, the RNA duplex with AU base pairs is slightly destabilized upon pressurization [101] and pressure was found to destabilize tetraloop-receptors [132]. Furthermore, a previous study showed that HHP decreases the cleavage rate of the hairpin ribozyme, which was interpreted as pressure destabilizing formation of a catalytically critical loop–loop tertiary interaction in the ribozyme [105, 133].

RNAs play a key role in translating the genetic information coded in DNA into proteins. Though many physical–chemical factors that contribute to the structural stability of RNAs have been identified, the long-time goal to determine principles that will allow accurate prediction of secondary and three-dimensional structures from sequence has not yet been reached [31]. RNAs fold into complex three-dimensional structures that are critical to their various biological functions. Detailed molecular mechanisms that drive formation of RNA tertiary interactions and how they are affected by temperature and pressure are not yet well understood, however. Herein, the effects of temperature, ion concentration (of mono and divalent ions), and high hydrostatic pressure on the 76-residue yeast phenylalanine transfer RNA, tRNA<sup>Phe</sup>, was examined to determine which features and thermodynamic parameters are essential in maintaining the stability of tRNA under extreme environmental conditions, such as low/high temperature and high pressure. This tRNA has been very well characterized and it possesses elements of the most common structural motifs, such as turns and hairpins. tRNA<sup>Phe</sup> has a cloverleaf-like secondary structure that turns into a L-shape tertiary structure upon folding (Figure 17), and has a modified nucleobase, wybutine or Y-base, which can be used as an intrinsic fluorescence probe that is located in the anticodon loop. The tertiary structure contains various cation-binding sites for divalent ions, such as Mg<sup>2+</sup>, which are required for the

conformational stability of the native RNA [35, 114, 134]. The complex tertiary structure of tRNA is maintained by extensive stacking interactions and base pairing within and between its helical stems, and many of the tertiary base-pairing interactions are non-Watson–Crick associations. Several binding sites have been identified for  $Mg^{2+}$  ions (including the Y-base position), which are important for the molecule's folding and stabilization [31, 35, 114, 133, 135]. How they are affected upon compression is essentially unknown.

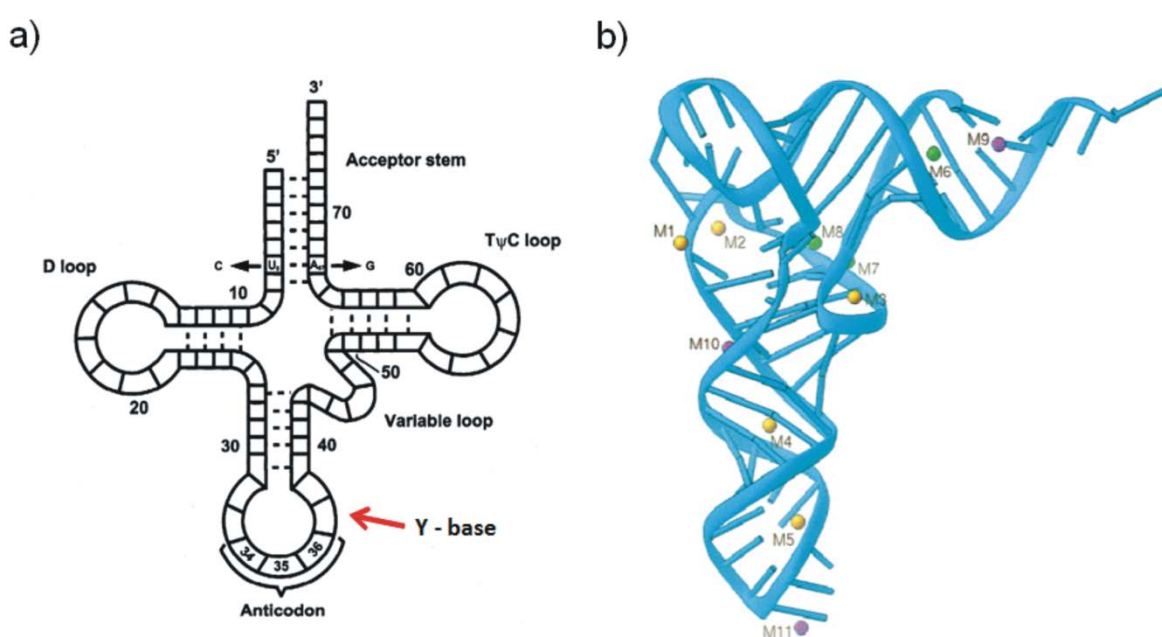


**Figure 14. tRNA<sup>Phe</sup> secondary and tertiary structures.** a) Schematic cloverleaf secondary structure of tRNA<sup>Phe</sup> with the fluorescent wybutine (Y-base) indicated by a red arrow. b) L-shaped tertiary structure of tRNA<sup>Phe</sup> with  $Mg^{2+}$  binding sites indicated by yellow and purple dots (PDB:1EHZ) [31].

## 3.2. Experimental details

### 3.2.1. Sample preparation

Yeast phenylalanine transfer RNA (tRNA<sup>Phe</sup>) was obtained from Sigma–Aldrich (St. Louis, MO) and used without further purification. Nuclease-free water, pipette tips, microfuge tubes, conical tubes, and RNase AWAY reagent were obtained from Ambion

(Life Technologies). All experiments were carried out in D<sub>2</sub>O or 50mM Tris-HCl buffer + 0.1 mM EDTA, pH 7.5, without or with 15 mM MgCl<sub>2</sub> and/or 100 mM NaCl. All samples were lyophilized from solutions in D<sub>2</sub>O and suspended at the different conditions as needed. All items related to sample handling were nuclease-free or cleaned with RNase AWAY reagent (Invitrogen) [34].

### **3.2.2. Differential scanning calorimetry and pressure perturbation calorimetry**

The DSC measurements were carried out by using a VP-DSC microcalorimeter (Microcal). The sample cell was filled with tRNA<sup>Phe</sup> (0.5 mg mL<sup>-1</sup>) in D<sub>2</sub>O without or with 15 mM MgCl<sub>2</sub>, and the reference cell was filled with the respective pure solvent. The heating rate was 30 °C h<sup>-1</sup> for the DSC scans and the chosen temperature range was 10–90 °C. Data evaluation was carried out by using Origin software from the DSC package supplied and the DSC curves obtained were normalized with respect to the sample concentration and partial specific volume of the RNA (0.55 mL g<sup>-1</sup>) to give the apparent molar heat capacity ( $C_p(T)$ ) and melting temperature ( $T_m$ ) [147]. The PPC measurements were carried out in the DSC calorimeter by using the MicroCal PPC accessory as described before (section 2.2.3) [118, 119, 150]. Control measurements of buffer-versus-buffer, buffer-versus-water, and water-versus-water were performed to correct the raw data, which finally led to the apparent coefficient of thermal expansion of the solute ( $\alpha(T)$ ). In case of phase transitions, by integrating the  $\alpha(T)$  curve over the phase-transition region, the relative volume change of the transition ( $\Delta V/V'$ ) could be obtained [118, 119].

### **3.2.3. FTIR Spectroscopy**

The infrared spectra of tRNA<sup>Phe</sup> were recorded and analyzed between 1750 and 1500 cm<sup>-1</sup> that is the region essentially associated with C=O stretching vibrations of paired and free nucleobases and imidazole ring vibrations. Each FTIR spectrum was obtained by recording 256 scans at a spectral resolution of 2 cm<sup>-1</sup>. Spectral evaluation was carried out by using Thermo GRAMS software as described before (section 2.2.1.5), and the experimental data were fitted with Origin- Pro 9.0G software. The ambient-pressure



FTIR measurements were carried out by using a Thermo Nicolet5700 spectrometer with a liquid-nitrogen-cooled MCT detector. The sample chamber was continuously purged with dry air. The sample concentration chosen was 5 mg mL<sup>-1</sup> in a 50 μL sample cell that consisted of 0.4 mm CaF<sub>2</sub> transmission windows and a 0.05 mm spacer. Temperature was controlled by using an external water circuit. The temperature was varied between 10 and 80 °C and the sample was equilibrated for 20 min before acquiring a new spectrum. The pressure-dependent FTIR data were recorded by using a Nicolet Magna550 spectrometer equipped with a liquid-nitrogen-cooled MCT detector. The infrared light was focused onto the pinhole of a gas-membrane-driven diamond anvil cell with a stainless steel spacer (Diacell Vivo DAC, Almax. easyLab) (section 2.2.1.1). Fine BaSO<sub>4</sub> powder was used as an internal pressure calibrant [146, 148, 155]. The chosen tRNA<sup>Phe</sup> concentration was 90 mg mL<sup>-1</sup> in the 5 μL volume of the DAC to give a sufficiently high signal-to-noise ratio. After each pressure change, the sample was equilibrated for 10 min before acquisition of the IR spectrum.

#### **3.2.4. Fluorescence Spectroscopy**

The Y- base fluorescence spectrum of the tRNA<sup>Phe</sup> was recorded by using an ISS K2 fluorimeter (Champaign, Illinois, USA). A solution of 0.04 mM tRNA<sup>Phe</sup> in D<sub>2</sub>O without or with 15 mM MgCl<sub>2</sub> was excited at 320 nm and the emission spectra recorded between 360 - 560 nm [33]. The fluorescence data were analyzed by using OriginPro 9.0G software. The ambient-pressure fluorescence measurements were carried out in quartz cuvettes with a 275 μL sample volume by using the standard fluorometer setup. The temperature was varied between 10 and 80 °C. An external water thermostat bath allowed accurate temperature control. The pressure-dependent measurements were carried out by using the high-pressure cell from ISS equipped with sapphire windows as described before (section 2.2.2), which limited the pressure range to about 240 MPa at ambient temperature. The sample solution inside the pressure cell was separated from the pressurizing medium by using a small quartz bottle (250 μL volume) sealed with a pressure transmitting Dura Seal film. An external water thermostat was connected to the cell and served as a temperature control.

### **3.2.5. Small-angle X-ray scattering**

Temperature-dependent small-angle X-ray scattering (SAXS) data were obtained with a SAXSess mc2 small-angle X-ray scattering instrument from Anton Paar GmbH (Graz, Austria), equipped with a sealed tube X-ray generator Iso-Debyeflex 3003 from GE Inspection Technologies (Ahrensburg, Germany). Cu-K $\alpha$  radiation was used ( $\lambda = 0.154$  nm) and the instrument was operated with 40 kV and 50 mA. Solutions of 0.5 wt% (or 3 wt%) tRNA<sup>Phe</sup> in the absence and presence of 15 mM MgCl<sub>2</sub> were prepared in D<sub>2</sub>O as well as in 50 mM Tris-HCl buffer, 0.1 mM EDTA, pH 7.5. The exposure time of the sample to the X-rays was 30 min per measurement. The data were collected for q-values between 0.12 and 4.00 nm<sup>-1</sup> (q, momentum transfer). The measurements covered a temperature range from 5 to 90 °C in steps of 5 °C.

The sample was measured in the slit configuration using a 1 mm quartz capillary ( $\mu$ -cell) suitable for the TCS 120 temperature-controlled sample holder unit from Anton Paar (Graz, Austria). While recording the temperature-dependent scattering data, temperature was adjusted by the TCS control unit for TCS sample stages from Anton Paar (Graz, Austria). Detection was performed via 2D-imaging plates, which were read out using the Storage Phosphor System Cyclone Plus by Perkin Elmer (Waltham, Massachusetts). The latter was operated by the software Optiquant. The 2D images obtained were transformed to an intensity profile,  $I(q)$ , using the software 2D-SAXSquant. The raw data obtained were normalized to the primary beam intensity and corrected for the background using the pure solvent in SAXSquant 3.1 software provided with the SAXSess mc2 system. Further, the data were desmeared to compensate for instrumental broadening effects ("slit-smearing") using the GNOM software [153]. The latter was also used to calculate the pair-distance distribution functions,  $p(r)$ , using the indirect Fourier transformation method.

### **3.3. Results and discussion**

Conformational transitions of RNA can be detected by using Fourier-transform infrared (FTIR) spectroscopy, at both atmospheric pressure and HHP conditions by using a diamond anvil cell [114, 136, 137]. In the 1800 to 1500  $\text{cm}^{-1}$  wavenumber region, IR bands that originate from nucleobase vibrations appear, which are sensitive to base stacking and base-pairing interactions. The bands mainly originate from in-plane double-bond vibrations, which include C=C, C=N, and C=O stretching. A double strand to single strand transition results in a decrease in the intensity of the IR band at around 1696 to 1684  $\text{cm}^{-1}$  with a concomitant increase in the band at around 1677 to 1653  $\text{cm}^{-1}$ . The former arises due to the C6=O6 stretch of base-paired guanine plus the C2=O2 stretch of uracil. The latter band arises mainly from the stretching vibrations of C6=O6 of free (i.e., non-base paired) guanine, the C2=O2 stretch of free cytosine, and the C4=O4 stretch of free uracil [114, 136].

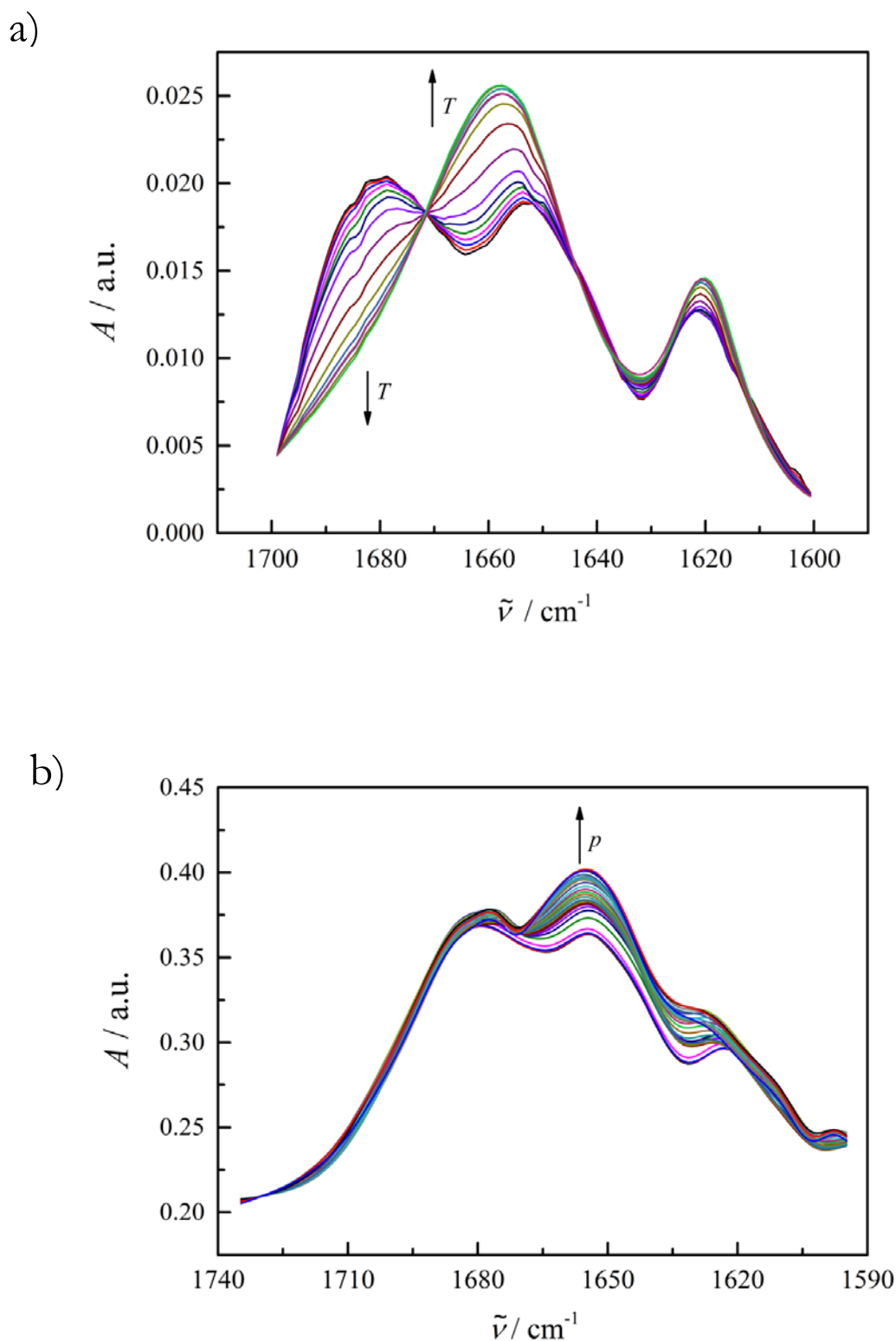


**Figure 15. FTIR spectra of tRNA<sup>Phe</sup> at atmospheric pressure and high hydrostatic pressure conditions.** Examples of a) temperature- and b) pressure-dependent FTIR spectra in the range of 1700–1590 cm<sup>-1</sup> for tRNA<sup>Phe</sup> (5 mg mL<sup>-1</sup>) in pure solvent (D<sub>2</sub>O) from 10 to 80 °C and tRNA<sup>Phe</sup> (90 mg mL<sup>-1</sup>) in 50mM Tris buffer + 0.1 mM EDTA (pH 7.5) from 0.1 to 1000 MPa, respectively. (Selected data)

As representative examples, Figure 15 shows the temperature- and pressure-dependent FTIR spectra of tRNA<sup>Phe</sup> in D<sub>2</sub>O in the wavenumber region from 1740 to 1600 cm<sup>-1</sup>. Thermal unfolding can be easily detected by the decrease in absorbance (*A*) of the IR band at 1686 cm<sup>-1</sup>, which is characteristic of base paired GC vibrations, and the concomitant increase in IR intensity of unpaired nucleic acids at around 1658 cm<sup>-1</sup>.

For better visibility, Figure 16a shows the temperature dependence of this band as difference spectra. Figure 16b depicts the temperature dependence of the 1686 and 1685 cm<sup>-1</sup> bands. In the absence of Mg<sup>2+</sup>, the melting transition extends over a wide temperature range from about 20 to 60 °C, with a midpoint melting temperature (*T*<sub>m</sub>) of ≈ 47 °C. In pure water, the *T*<sub>m</sub> increases from around 47 °C to around 75 °C in the presence of the stabilizing Mg<sup>2+</sup> cations. As expected, corresponding measurements in buffer and NaCl solution in the absence of Mg<sup>2+</sup> ions lead to slightly higher melting temperatures: *T*<sub>m</sub> increases to (54 ± 2) °C in 50 mM Tris-HCl buffer + 0.1 mM EDTA, and to (62 ± 2) °C in 50 mM Tris buffer + 0.1 mM EDTA + 100 mM NaCl (Figure 20). The increase in temperature stability can be attributed to the screening effect of the negative charges along the phosphate–sugar backbone of the tRNA. Conversely, the melting transition in the presence of 15 mM Mg<sup>2+</sup> is hardly affected any further by the addition of other buffer components (50 mM Tris-HCl) and salts (100 mM NaCl). The onset temperature of the melting transition, for example, is 66 to 68 °C for all solvent conditions chosen, that is, 15 mM Mg<sup>2+</sup> ions, 50 mM Tris-HCl buffer + 15 mM MgCl<sub>2</sub>, 50 mM Tris-HCl buffer + 15 mM MgCl<sub>2</sub> + 100 mM NaCl.

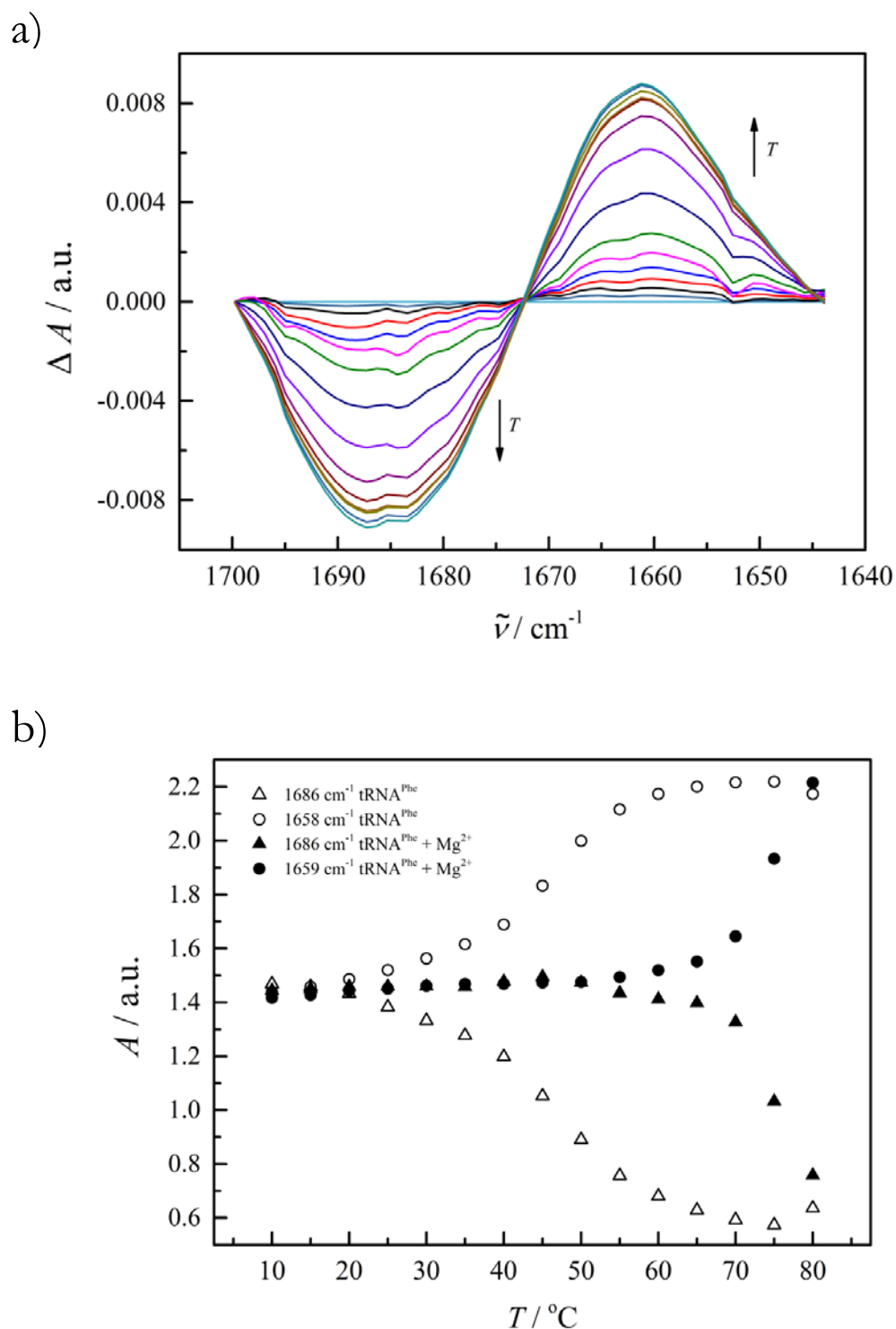


**Figure 16. Temperature-dependent FTIR of tRNA<sup>Phe</sup>.** a) FTIR difference spectra [ $A(T) - A(T=10\text{ }^\circ\text{C})$ ] of tRNA<sup>Phe</sup> (1.1 mM) in D<sub>2</sub>O in the temperature range of 10 - 80 °C. The absorption spectrum at  $T=10\text{ }^\circ\text{C}$  has been subtracted from absorption spectra taken at higher temperatures. b) Intensity decay of the IR band at 1686 cm<sup>-1</sup> (characteristic of basepaired GC vibrations) and of the band at 1658/1659 cm<sup>-1</sup> (characteristic of unpaired bases) as a function of temperature for tRNA<sup>Phe</sup> in pure D<sub>2</sub>O and in the presence of 15 mM Mg<sup>2+</sup>. (Selected data)

As indicated by the much sharper transition, the cooperativity of the melting transition drastically increases in the presence of  $\text{Mg}^{2+}$  cations, that is, the slopes of the base-paired GC vibrations at  $1686\text{ cm}^{-1}$  and of the  $1658/1659\text{ cm}^{-1}$  band characteristic for unpaired G are much steeper (Figure 16). Consistently, the corresponding data for the single-strand vibrations of guanine (at  $\approx 1669\text{ cm}^{-1}$ ) and of adenine (at  $\approx 1621\text{ cm}^{-1}$ ) exhibit the opposite temperature course.

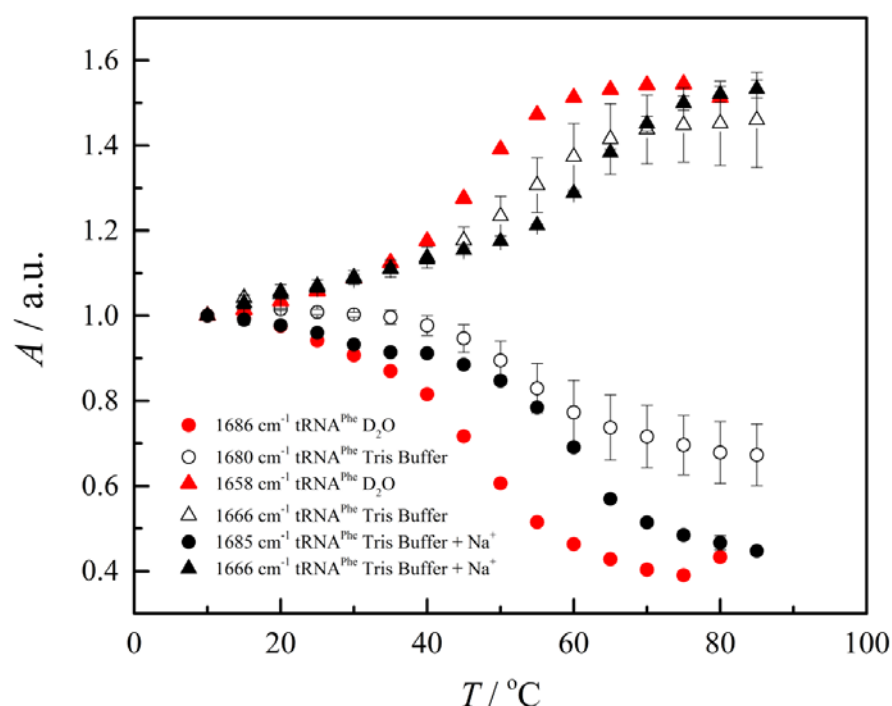


**Figure 17. Temperature-dependent FTIR of tRNA<sup>Phe</sup> at different salt conditions.** Intensity decay of the IR band intensities at  $\approx 1686\text{ cm}^{-1}$  (characteristic of basepaired GC vibrations) and of the band at  $\approx 1558\text{ cm}^{-1}$  (characteristic of unpaired base pairs) as a function of temperature for tRNA<sup>Phe</sup> in pure D<sub>2</sub>O and various buffer solutions (50 mM Tris buffer + 0.1 mM EDTA; 50 mM Tris buffer + 0.1 mM EDTA + 100 mM NaCl) in the absence of 15 mM  $\text{Mg}^{2+}$  from 10 to 85 °C. The error bars cover the scattering of three independent measurements.

A Boltzmann fit to the experimental data (Figure 16) give a  $T_m$  value of  $(47.5 \pm 3)\text{ °C}$  for the rather broad melting transition and a standard van 't Hoff enthalpy change ( $\Delta H$ ) of  $(132 \pm 10)\text{ kJ mol}^{-1}$  in the pure solvent. The value for the corresponding entropy change

( $\Delta S$ ) amounts to approximately  $0.4 \text{ kJ mol}^{-1} \text{ K}^{-1}$ . In the presence of  $\text{Mg}^{2+}$  cations,  $T_m$  increases by more than  $30 \text{ }^\circ\text{C}$ . Owing to the high temperature stability of the  $\text{Mg}^{2+}$ -stabilized  $\text{tRNA}^{\text{Phe}}$ , and thus the missing post-transitional baseline, no accurate thermodynamic values can be obtained in this case. Therefore, additional calorimetric measurements have been carried out. The DSC result present at Figure 18 is in full agreement with the FTIR data, the melting transition of  $\text{tRNA}^{\text{Phe}}$  in pure water extends from  $20$  to  $60 \text{ }^\circ\text{C}$  with a  $T_m$  value of approximately  $45 \text{ }^\circ\text{C}$ , and the melting temperature and cooperativity increase dramatically in the presence of the stabilizing  $\text{Mg}^{2+}$  cations to give a  $T_m$  value of around  $78 \text{ }^\circ\text{C}$  with  $15 \text{ mM MgCl}_2$ . The sharp descending post-melting baseline of the DSC profile of the tRNA in the presence of  $\text{Mg}^{2+}$  ions may be due to heat-induced degradation/aggregation at elevated temperatures. The overall melting enthalpies ( $\Delta H_{\text{cal}}$ ) in the absence and presence of  $\text{Mg}^{2+}$  amount to around  $570$  and  $680 \text{ kJ mol}^{-1}$ . The corresponding  $\Delta S_{\text{cal}}$  values are approximately  $1.8$  and  $1.9 \text{ kJ mol}^{-1} \text{ K}^{-1}$ , respectively. The positive enthalpy and entropy changes upon melting are consistent with disruption of the secondary structure of the molecule. Large differences between van 't Hoff and calorimetric  $\Delta H$  and  $\Delta S$  values in the case of the broad melting transition of  $\text{tRNA}^{\text{Phe}}$  in pure solvent indicates a complex, multistage melting process for the tRNA, which is in agreement with the literature data [136, 138].



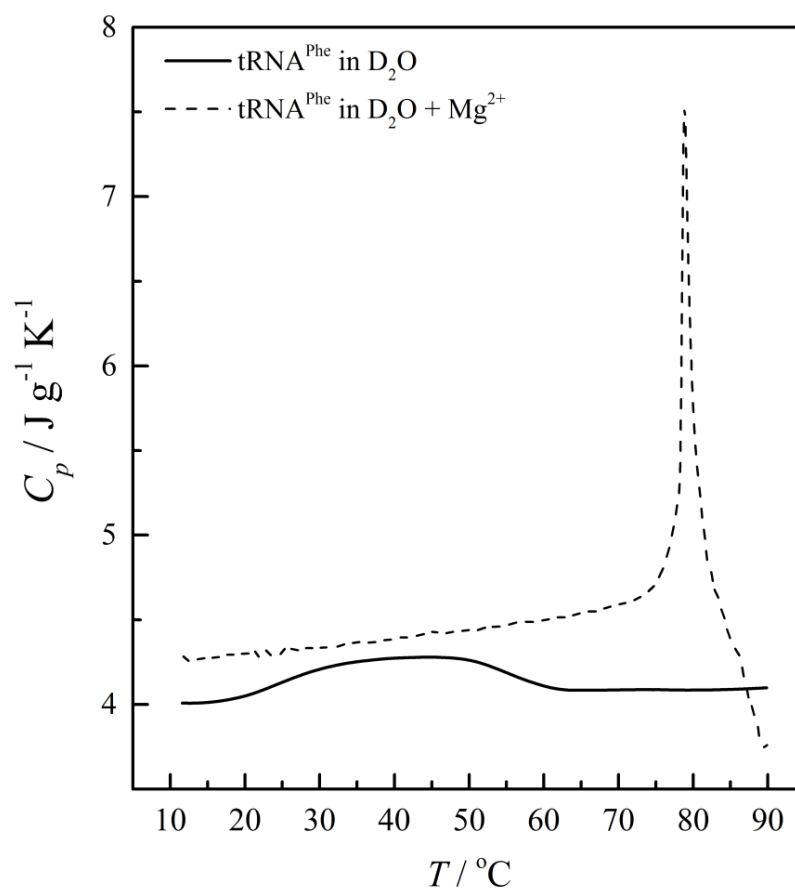


**Figure 18. Differential scanning calorimetry data of tRNA<sup>Phe</sup> in the presence and absence of Mg<sup>2+</sup> ions.** DSC data of tRNA<sup>Phe</sup> (0.5 mg mL<sup>-1</sup>) in D<sub>2</sub>O solution in the absence and presence of 15 mM MgCl<sub>2</sub> from 10 to 90 °C. (Selected data)

Figure 19 shows examples of temperature- and pressure-dependent intrinsic fluorescence spectra of the Y-base, which is located in the anticodon loop of tRNA<sup>Phe</sup>, and the fluorescence intensities ( $I_F$ ) and maxima ( $\lambda_{\text{max}}$ ) in the absence and presence of Mg<sup>2+</sup>.

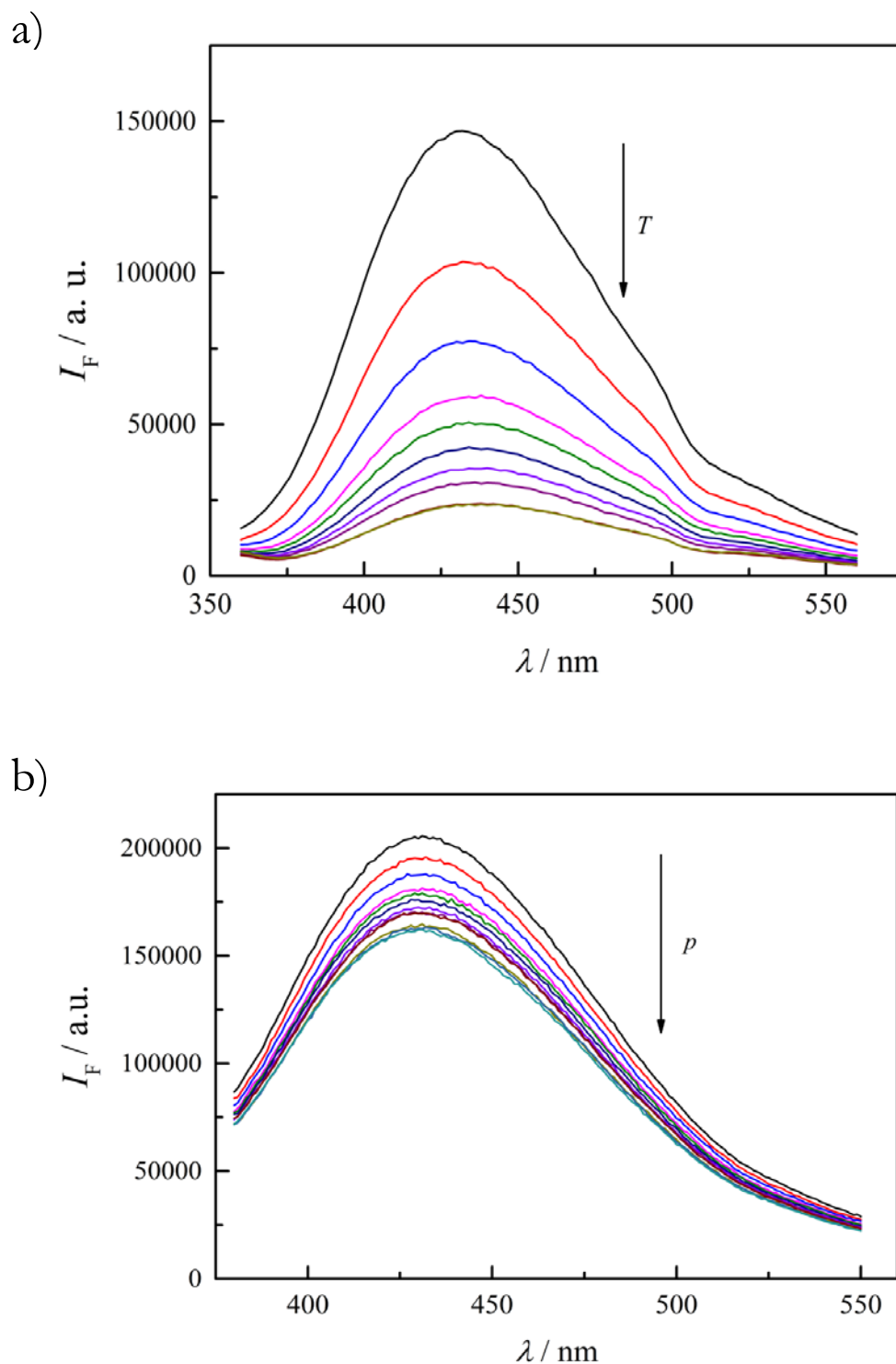
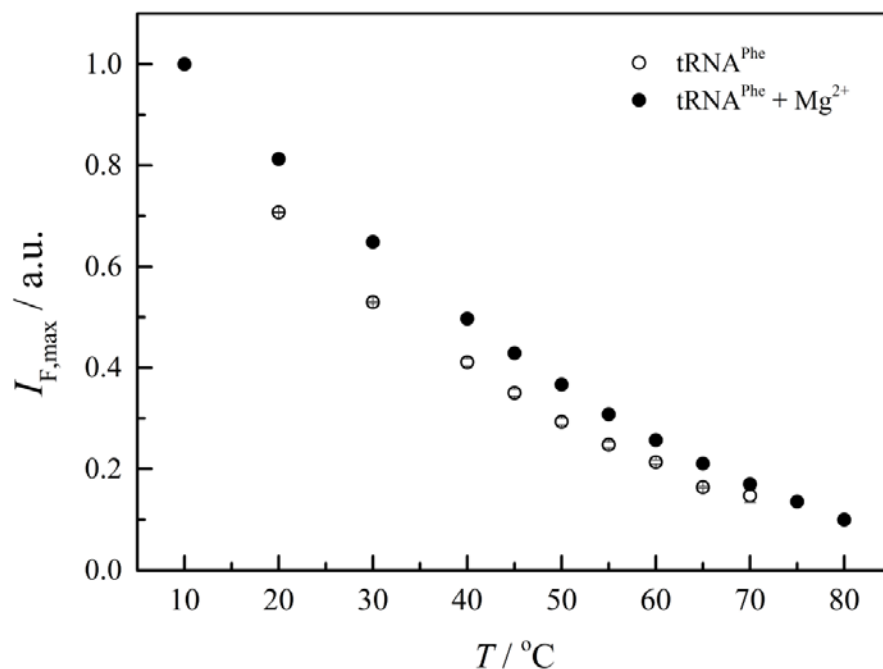


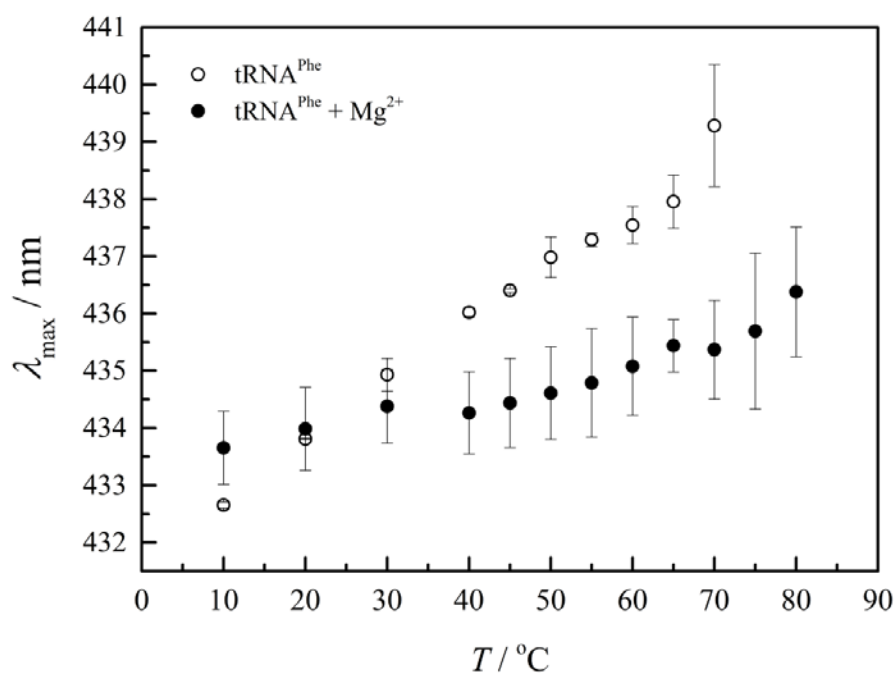
**Figure 19. Temperature- and pressure-dependent fluorescence spectra of the tRNA<sup>Phe</sup> Y-base.** The Y-base (wybutine) is situated at the anticodon loop area and has intrinsic fluorescence, serving as a natural probe to follow modification at this region. a) Temperature-dependent fluorescence spectra of the Y-base of tRNA<sup>Phe</sup> (1.1 mM) in D<sub>2</sub>O from 10 to 80 °C. b) pressure-dependent fluorescence spectra of the Y-base of tRNA<sup>Phe</sup> (1.1 mM) in D<sub>2</sub>O from 0.1 to 250 MPa. (Selected data)

Generally, the fluorescence intensity decreases with increasing temperature, which is due to an increased quenching processes, and conformational changes play an additional role in the interpretation of the fluorescence intensity data at Figure 20a. The Y-base is normally found  $\pi$ -stacked between nucleotide base pairs and largely shielded from the bulk solvent in its  $\text{Mg}^{2+}$ -complexed state. In this stacked-in, largely nonpolar environment, the Y-base fluoresces strongly and the fluorescence intensity has been found to decrease upon  $\text{Mg}^{2+}$  decomplexation [139]. Changes in the maximum of the fluorescence band ( $\lambda_{\text{max}}$ ) are generally indicative of conformational changes, such as those induced by the melting process of base-paired nucleic acids. Figure 20b reveals a more or less continuous increase in the  $\lambda_{\text{max}}$  value of  $\text{tRNA}^{\text{Phe}}$  (redshift) in pure solvent with increasing temperature, which indicates an increasing population of more solvent-exposed Y-bases in the ensemble of conformational substrates with increasing temperature. This observation is in line with the broad transition curves of  $\text{Mg}^{2+}$ -free  $\text{tRNA}^{\text{Phe}}$  as determined by the FTIR and DSC measurements. Complexation of the Y-base by  $\text{Mg}^{2+}$  leads to a small redshift in the fluorescence maximum, in agreement with the literature data [140], and  $\lambda_{\text{max}}$  is not affected much by increased temperature up to the melting temperature owing to a significant shielding of the  $\text{Mg}^{2+}$ -complexed Y-base (Figure 20b).

a)



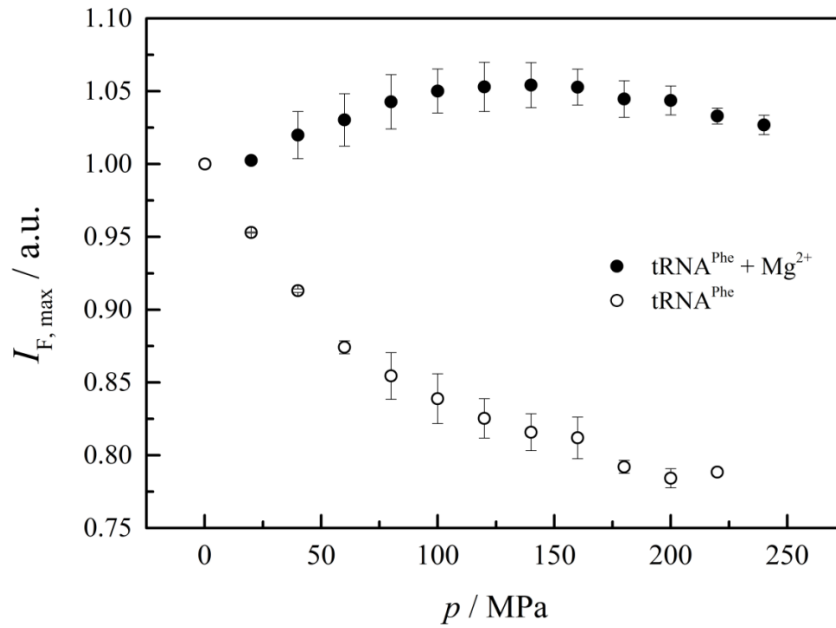
b)



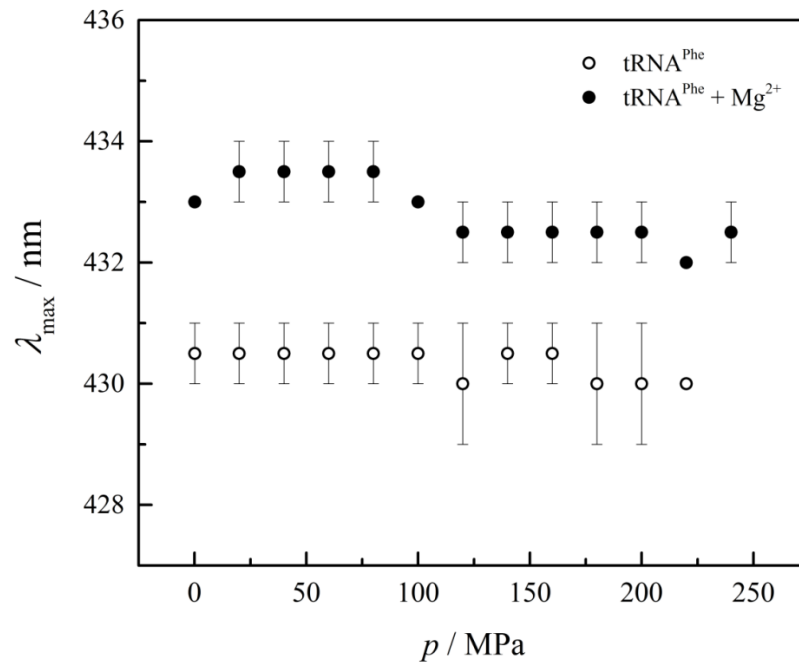
**Figure 20. Temperature-dependent fluorescence intensity data of the tRNA<sup>Phe</sup>.** a) Temperature-dependent changes in the maximum intensity of the normalized fluorescence spectra with 1.1 mM of tRNA<sup>Phe</sup> in D<sub>2</sub>O in the absence and presence of 15 mM Mg<sup>2+</sup>. b) Temperature-dependent changes in the position of its maximum in the absence and presence of 15 mM Mg<sup>2+</sup>. The error bars cover the scattering of three independent measurements.

Figure 21 depicts the pressure-dependent data for the fluorescence intensity and maxima of the Y-base at ambient temperature ( $T = 20\text{ }^{\circ}\text{C}$ ). In contrast with the temperature-dependent results, increasing the pressure up to 250 MPa has a smaller effect on the spectral changes of the Y-base. The fluorescence intensity of tRNA<sup>Phe</sup> in the presence of  $\text{Mg}^{2+}$  is hardly affected by pressure, whereas the  $I_F$  value of the Y-base in the pure solvent decreases slightly with pressure (Figure 21a). The positions of the fluorescence maxima ( $\lambda_{\text{max}}$ ) are rather insensitive to pressure up to 220 MPa, which indicates the absence of significant conformational changes in the anticodon loop from ambient- pressure conditions up to 220 MPa. As the fluorescence intensity of the Y-base is known to decrease drastically upon solvent exposure [140], the data in Figure 21a indicate that pressure leads to a further destabilization of the tertiary structure of tRNA in the area of the Y-base in its  $\text{Mg}^{2+}$ -free state upon mild pressurization. The slight increase in  $I_F$  in the  $\text{Mg}^{2+}$ -complexed state upon compression may result from a further increase in packing density and thus shielding of the Y-base from the surrounding solvent.

a)



b)



**Figure 21. Pressure-dependent fluorescence intensity data of the tRNA<sup>Phe</sup>.** a) Pressure-dependent changes in the normalized fluorescence intensity at  $T = 20$  °C in the absence and presence of 15 mM Mg<sup>2+</sup> from 0.1 to 250 MPa (minor variations in initial  $I_{\max}$  values derive from different spectrometer setups for the temperature- and pressure-dependent studies). b) Pressure-dependent changes in the the position of its maximum at  $T = 20$  °C in the absence and presence of 15 mM Mg<sup>2+</sup> from 0.1 to 250 MPa (minor variations in initial  $I_{\max}$  values derive from different spectrometer setups for the temperature- and pressure-dependent studies). The error bars cover the scattering of three independent measurements.

To reveal corresponding changes in the overall shape of the tRNA<sup>Phe</sup> upon temperature change, small-angle X-ray scattering (SAXS) measurements were also carried out (performed by Melanie Berghaus). As an example, Figure 22 shows the temperature-dependent intensity profiles of tRNA<sup>Phe</sup> in pure solvent (D<sub>2</sub>O) in the absence and presence of Mg<sup>2+</sup>. To gain information about changes in compactness and unfolding of the molecule, the data are also plotted in the Kratky representation (Figure 22, inset). In both cases, a compact form of tRNA<sup>Phe</sup> is observed at low temperatures, as can be seen from the Gaussian shape of the Kratky plots. With increasing temperature, we observed a gradual loss of compactness between 45 and 65 °C for tRNA<sup>Phe</sup> in the absence of Mg<sup>2+</sup>. In the presence of Mg<sup>2+</sup>, the loss of compactness takes place at significantly higher temperatures and within a much smaller temperature range (75–85 °C), in good agreement with the thermodynamic data for tRNA<sup>Phe</sup> unfolding [141] and DSC data (Figure 21).

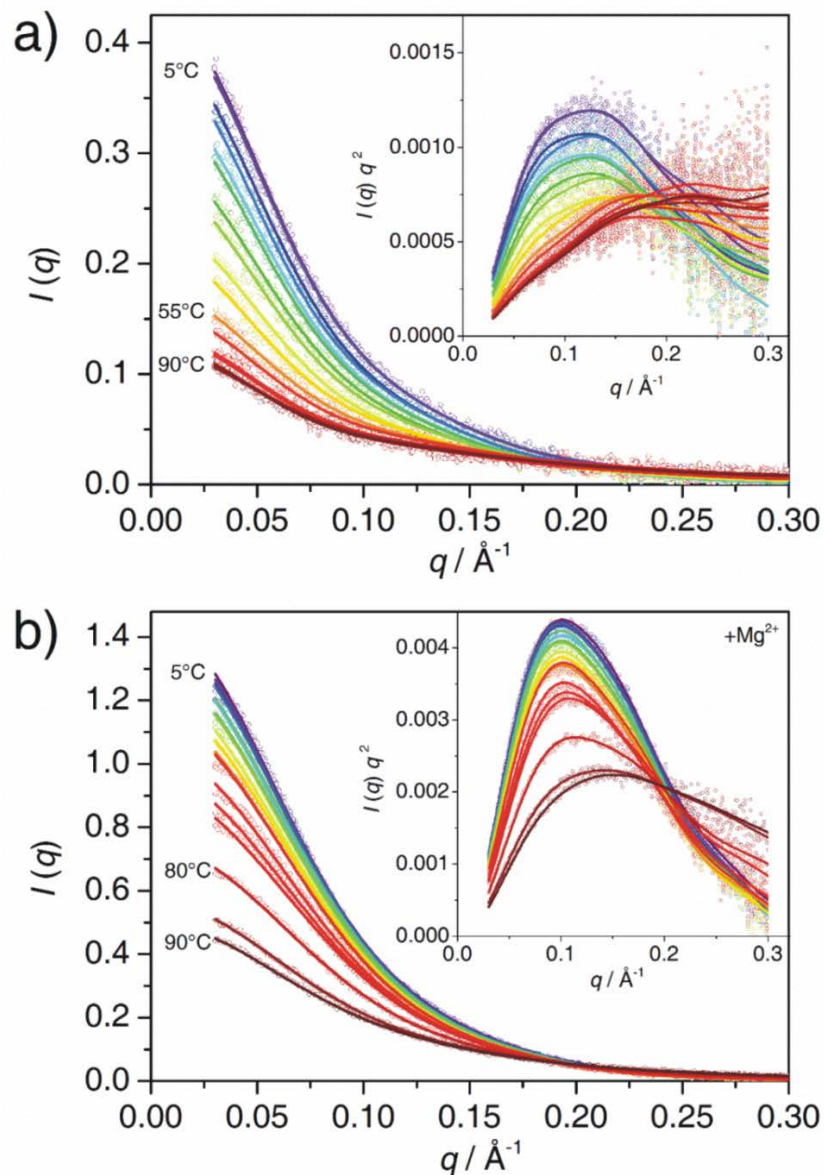


**Figure 22. Temperature-dependent SAXS data and analysis of tRNA<sup>Phe</sup> in D<sub>2</sub>O.** a) tRNA<sup>Phe</sup> in the absence and b) tRNA<sup>Phe</sup> in the presence of 15 mM Mg<sup>2+</sup>. Intensity profiles were recorded in a temperature range from 5 (purple) to 90 °C (dark red) in steps of 5 °C. Solid lines represent fits obtained by using the indirect Fourier transformation method. Concentrations were 0.5 wt% in pure D<sub>2</sub>O and 3 wt% with 15 mM Mg<sup>2+</sup>. Insets: Kratky plots of the respective data (performed by Melanie Berghaus).

Clearly, no complete unfolding is seen here as observed in the presence of urea [142]. Measurements were also carried out in Tris-HCl buffer, which does not lead to significant changes in the temperature-dependent SAXS profiles compared with the data in pure solvent, however (Figure 23).



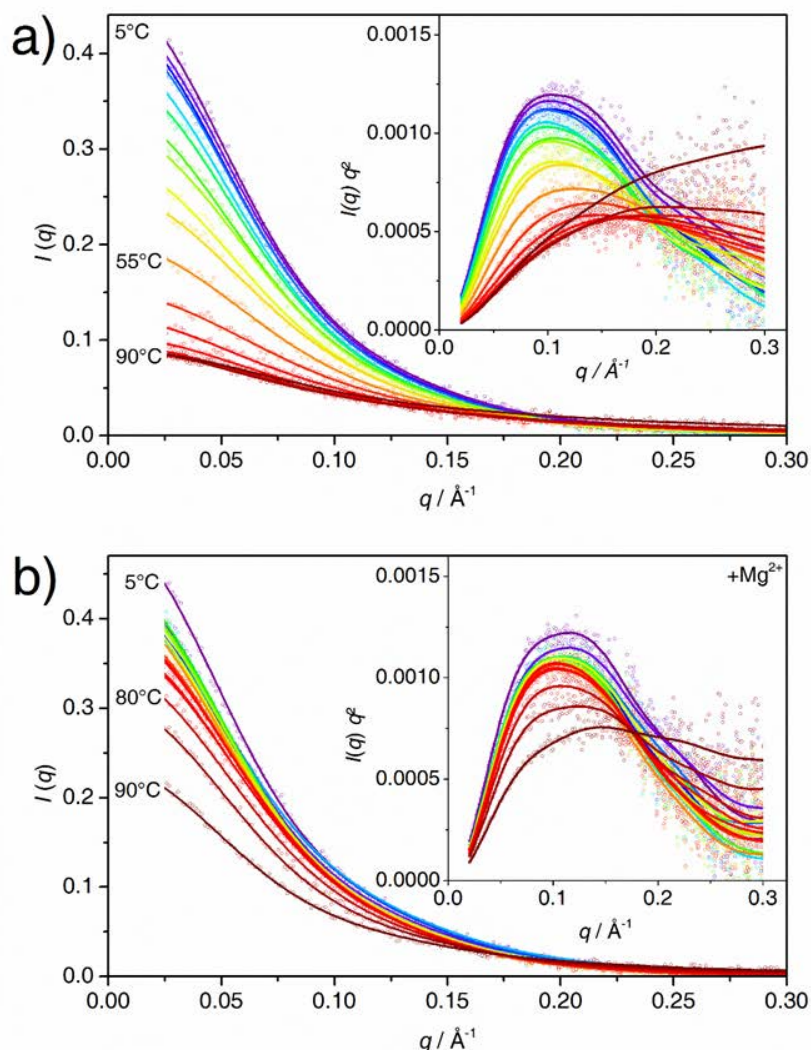


**Figure 23. Temperature-dependent SAXS analysis of tRNA<sup>Phe</sup> in Tris-HCl Buffer.** a) tRNA<sup>Phe</sup> in the absence and b) tRNA<sup>Phe</sup> in the presence of Mg<sup>2+</sup>. Intensity profiles were recorded in a temperature range starting from 5 °C (purple) in steps of 5 °C up to 90 °C (dark red). Open circles represent the corrected original data, the solid lines represent fits obtained using the indirect Fourier transformation method. Concentrations were 0.5 wt% tRNA<sup>Phe</sup>. Inserts: Kratky plots of the respective data (performed by Melanie Berghaus).

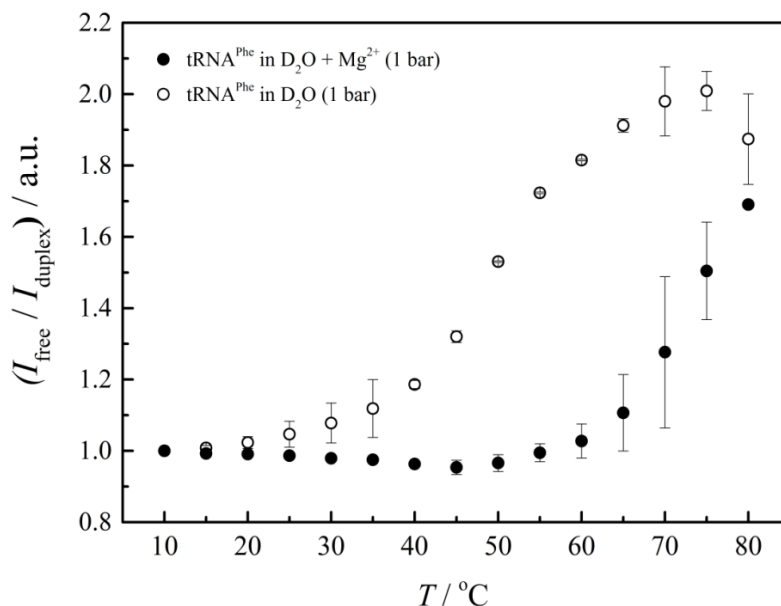
The transition range in Tris-HCl buffer takes place between 50 and 60 °C without Mg<sup>2+</sup> and between 80 and 90 °C with Mg<sup>2+</sup>. Further analysis of the scattering data (Guinier analysis, evaluation of the pair-distance correlation function  $p(r)$ ) indicate that the radius of gyration, which is about 22 Å in the native state, does not change markedly for all

solution conditions upon raising the temperature, that is, the structural changes that take place seem to involve more internal structural rearrangements of the RNA molecule rather than complete unfolding to a random-coil kind of conformation, as often observed for temperature-induced unfolding of proteins [137]. Preliminary pressure-dependent data by using Synchrotron SAXS and a homebuilt pressure cell with diamond windows indicate that the tertiary structure of tRNA<sup>Phe</sup> is highly stable up to 400 MPa in both cases, in the presence and absence of Mg<sup>2+</sup>. Our observations are in good agreement with the FTIR measurements, which reveal only small changes in the secondary structure upon pressurization. However, minor changes in the tertiary structure, which have not been resolved so far by our measurements, cannot be ruled out. The high stability of tRNA<sup>Phe</sup> upon compression may be expected because HHP is known to stabilize helical forms and support the supercoiling of nucleic acids [143].

Figure 15b shows characteristic FTIR spectra of tRNA<sup>Phe</sup> as a function of pressure at ambient temperature ( $T = 20$  °C). The diamond anvil technique, which can be used in the infrared experiments, also allows access to higher pressures ranges up to 1000 MPa. Also here, characteristic changes are clearly visible in the wavenumber region from 1696 to 1684 cm<sup>-1</sup> (double strand) and from 1677 to 1653 cm<sup>-1</sup> (single strand), as discussed. Owing to pressure-induced background changes in the diamond anvil cell and to give a more accurate measure of the conformational changes that occur, the conformational changes in tRNA<sup>Phe</sup> have been determined in terms of the ratio of unpaired to duplexed GC pairs ( $I_{\text{free}}/I_{\text{duplex}}$ ) obtained from the infrared spectra recorded at around 1658 and 1686 cm<sup>-1</sup>, respectively. Figure 24 shows the results for tRNA<sup>Phe</sup> in the absence and presence of Mg<sup>2+</sup> as a function of temperature (a) and pressure (b) (for  $T = 20$  °C). As can be clearly seen, the pressure-dependent changes are rather small, but still significant. At most, an increase of 15 % of unpaired bases is observed upon compression up to 1000 MPa. For  $T = 20$  °C, the  $I_{\text{free}}/I_{\text{duplex}}$  ratio increases slightly up to about 200 and 350 MPa for tRNA<sup>Phe</sup> in the absence and presence of Mg<sup>2+</sup>, respectively. Upon further compression, constant  $I_{\text{free}}/I_{\text{duplex}}$  values are observed up to approximately 600 MPa, which is again followed by a small increase in the number of unpaired base pairs and thus reveals a more phasic pressure effect on the structure of tRNA<sup>Phe</sup> upon pressurization.

For the higher temperature of 45 °C, the effect of pressure on the ratio of unpaired to paired base pairs is similar, but of a few percent only, that is, almost negligible.

a)



b)

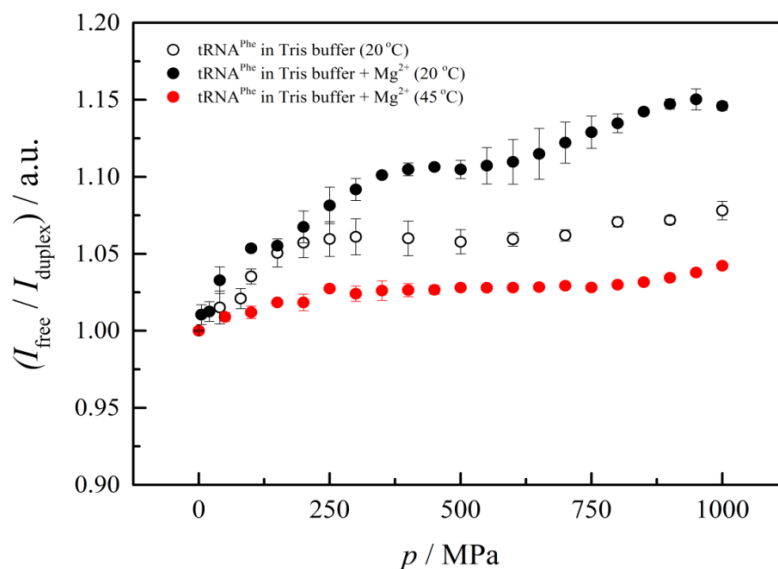


**Figure 24.**  $I_{\text{free}}/I_{\text{duplex}}$  analysis of the temperature- and pressure-dependent FTIR data of tRNA<sup>Phe</sup>.

a) Temperature-dependence of the ratio of unpaired to duplexed GC pairs ( $I_{\text{free}}/I_{\text{duplex}}$ ) as obtained from the infrared spectra recorded at  $\approx 1658 \text{ cm}^{-1}$  and  $\approx 1686 \text{ cm}^{-1}$ , respectively, for tRNA<sup>Phe</sup> in the +/- of 15 mM Mg<sup>2+</sup> from 10 to 80 °C. b) pressure-dependence of the ratio of unpaired to duplexed GC pairs ( $I_{\text{free}}/I_{\text{duplex}}$ ) as obtained from the infrared spectra recorded at  $\approx 1658 \text{ cm}^{-1}$  and  $\approx 1686 \text{ cm}^{-1}$ , respectively, for tRNA<sup>Phe</sup> in the absence and presence of 15 mM Mg<sup>2+</sup>. The error bars cover the scattering of three independent measurements.

The PPC data, do not reveal significant changes in the temperature-dependent expansivity data at  $T_m$  that would indicate a significant volume change upon RNA melting (Figure 25). Which is in agreement with the pressure dependent FTIR where changes are rather small.

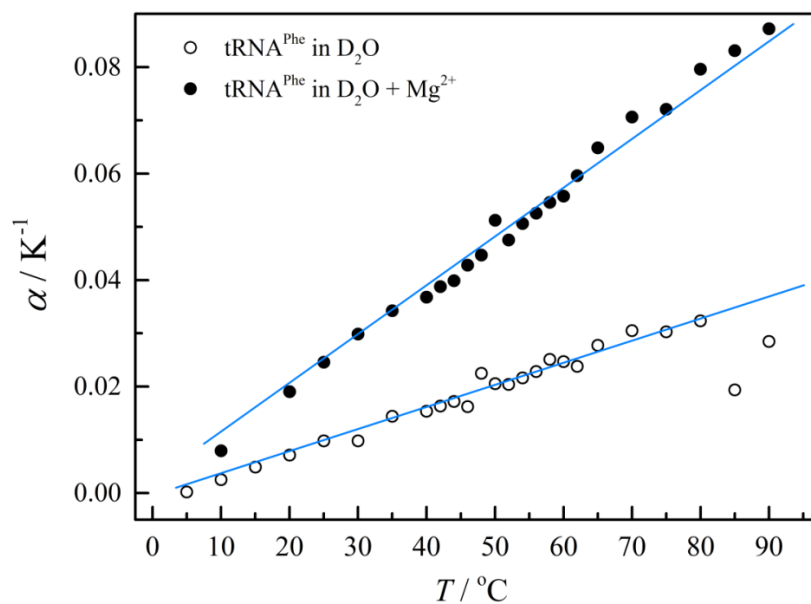


**Figure 25. Pressure perturbation calorimetric (PPC) of the tRNA<sup>Phe</sup>.** The PPC data present the scan of 1 mg mL<sup>-1</sup> of tRNA<sup>Phe</sup> in D<sub>2</sub>O solution in the absence and presence of 15 mM MgCl<sub>2</sub>. The time interval between pressure pulses has been 600 s, and the pressure-jump amplitude was +/- 5 bar (lines are guide to the eyes, only). The larger expansibility of the Mg<sup>2+</sup>-liganded tRNA<sup>Phe</sup> is probably due to a significantly larger hydration shell. No significant volume change upon melting is observed. (Selected data)

### 3.4. Summary and conclusions

A combined temperature- and pressure-dependent study was carried out to explore the conformational and free energy landscape of yeast tRNA<sup>Phe</sup>, an important model for RNA function. The goal was to elucidate the features and thermodynamic parameters that are essential in determining its stability, with the aim of also revealing its structural properties under extreme environmental conditions, such as low/high temperatures and high hydrostatic pressures. Owing to the strong ionic-strength dependence of the structure of nucleic acids, the effect of mono- and divalent ions on the temperature and

pressure stability of the tRNA was also explored. To this end, FTIR and fluorescence spectroscopy, SAXS, and calorimetric methods were applied.

It has been shown that the native structure of tRNA<sup>Phe</sup> is disrupted upon removal of Mg<sup>2+</sup>, which leads to a markedly different temperature and pressure stability of the RNA. Addition of Mg<sup>2+</sup> stabilizes the compact structure of the RNA against temperature, which thus increases the melting temperature of the RNA by about 30 °C and concomitantly increases the cooperativity of the melting transition. Mg<sup>2+</sup> ions stabilize the tertiary structure in such a way that the entire structure melts essentially by a two-state transition, in accordance with the literature data [144]. The increase in the temperature stability can be attributed to an effective screening of the negative charges along the phosphate–sugar backbone of the tRNA. As expected, monovalent ions have a smaller effect (Figure 16), also in agreement with the literature data [145]. According to the SAXS data, the structural changes that take place upon melting seem to involve essentially internal structural rearrangements of the tRNA molecule, rather than a complete disruption of the tertiary structure.

Compared with the pronounced temperature effect, the pressure-dependent changes in the secondary structure of tRNA<sup>Phe</sup> are rather small, however. A maximum increase of only about 15% unpaired bases is observed upon pressurization up to 1000 MPa. Interestingly, a more phasic pressure effect on the structure of tRNA<sup>Phe</sup> was observed in both the Mg<sup>2+</sup>-free and the Mg<sup>2+</sup>-complexed state, which indicates that different regions of the tRNA<sup>Phe</sup> possess different pressure stabilities. Remarkably, at high pressure, the stability is slightly decreased in the Mg<sup>2+</sup>-complexed state, probably owing to the creation of small voids in the compact native structure of tRNA. The fluorescence data of the Y-base, which is located in the anticodon loop of tRNA<sup>Phe</sup>, indicate that pressure-induced melting of the base pairs takes place in other regions of the tRNA structure first (Figure 21a). It can be speculated that structural changes in the hydrating solvent, that is, water, contribute to the pressure-induced changes observed. These changes would only be expected to appear at pressures above about 200 MPa, the pressure at which the structural changes of water start to take place by a steady increase in the number of

nearest neighbors, from approximately 4 to 6.5 at 500 MPa, which can be attributed to the penetration of non-hydrogen-bonded water molecules into the first shell [146]. To reveal the underlying contributions in detail, it would be helpful to carry out molecular dynamics simulations in future work.

Duplex dissociation of nucleic acids is typically accompanied by a significant increase in solvent exposure and subsequent hydration of internal groups and a concomitant release of counterions to the bulk [147]. Whereas the overall volume change upon DNA melting ( $\Delta V$ ) has often been found to be small and positive [109, 147], the spectroscopic data indicate that upon compression, the overall volume change of tRNA<sup>Phe</sup> is very small and slightly negative. This finding is in line with PPC data (Figure 25), which do not reveal significant changes in the temperature-dependent expansivity data at  $T_m$  that would indicate a significant volume change upon RNA melting, seen at Figure 25. Owing to the generally observed marked temperature dependence of  $\Delta V$  [148], small negative values of  $\Delta V$  at lower temperatures and high pressures could still be envisioned, however. The decrease in volumetric effects at the higher temperatures would also explain the smaller pressure effect on Mg<sup>2+</sup>-complexed tRNA<sup>Phe</sup> at 45 °C.

Generally, pressure stabilizes aromatic stacking and has little effect on the hydrogen-bonding interactions that stabilize biomolecular structures. In contrast, pressure generally disrupts charge–charge interactions and favors full hydration of individual charged groups [126]. This effect arises from electrostriction of the water molecules around the individual ions, which causes these water molecules to have a higher density (smaller volume) than in bulk water. Other factors that can contribute to the observed  $\Delta V$  value include differences in hydration of different conformational states and differences in the void volumes of these states. Void volumes arise from solvent-free cavities caused by imperfect packing of groups in the molecule. The different pressure stabilities of DNA and tRNA might be due to a significant void volume contribution to  $\Delta V$  in the case of the less efficiently packed tRNA. In the case of DNA,  $\Delta V$  is essentially determined by hydration changes upon melting [144]. In this way, RNA folding and unfolding differ fundamentally from protein folding and also from DNA melting. The pressure stability of

tRNA<sup>Phe</sup> seems to be similar to that of non-canonical DNA structures, such as G-quadruplex DNA, which have also been found to be susceptible to pressure [89]. We must keep in mind, however, that the sign and magnitude of  $\Delta V$  values generally appear to depend on the experimental temperature and the specific compositional characteristics of the nucleic acid structure in question [128, 149].

The biological implications of our findings would be that organisms living under high pressure conditions, such as in the deep sea, where pressures up to the 100 MPa (1 kbar) level are encountered [126, 127], would hardly be affected by the minor conformational changes that take place in tRNA up to this pressure.





---

## 4. Exploring temperature and pressure effects on the structure and stability of a small RNA hairpin



## **4.1. Background**

The RNA hairpin structure is formed when a polynucleotide single strand folds back on itself to form intramolecular Watson-Crick base pairs, resulting in a helical stem capped by the loop (Figure 26). The hairpin is the predominant secondary structure of RNAs, and its amount varies depending on the RNA type and function. The amount of nucleotide residues at the hairpin loop also varies depending on the RNA molecule; for example, tRNA hairpin loops contain seven nucleotides while ribosomal hairpin loops contain four nucleotides. These variations may have an impact on RNA's structural, thermodynamic, dynamical and hence functional properties [102]. It has been shown in the literature that 70% of all tetraloops in rRNA are either UNCG or GNRA (N is related to nucleotide and R is related to purines) [156], and they vary between organisms, from UUCG to GCAA for the same hairpin in closely related organisms [157]. Also, these RNA hairpins have significant thermodynamic stability due to the presence of several noncanonical interactions [46, 47]. They serve as nucleation site for RNA folding, ligand binding and tertiary folding initiation. Due to their importance, simplicity and size, small hairpins serve as prototype for folding dynamics and structure stability studies [41, 47, 53, 55, 158, 159].

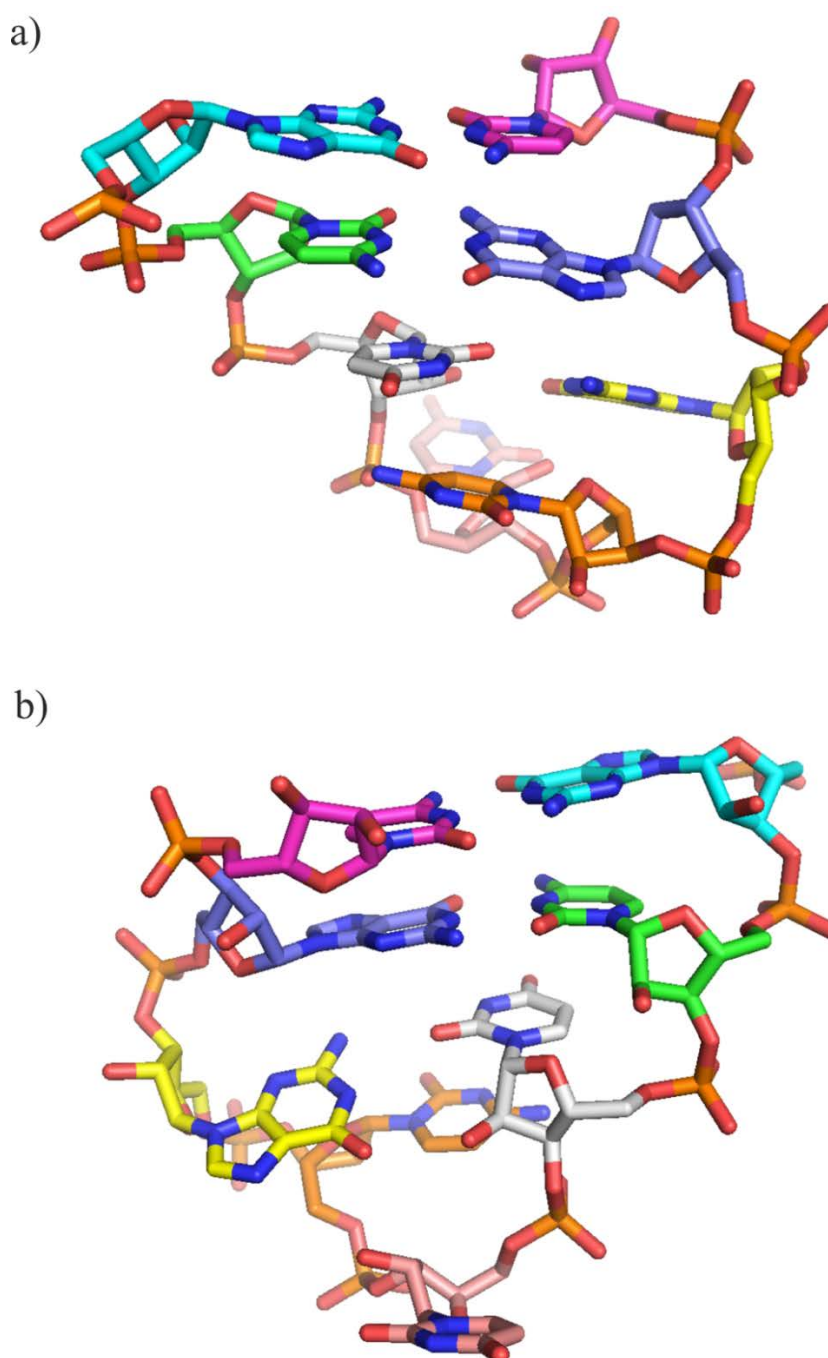


**Figure 26. Small RNA hairpin tetraloop, gcUUCGgc.** (b) is 180° flipped over (a). The nucleotides at the duplex stem can be identified as G<sub>S1</sub> (pink), C<sub>S2</sub> (blue), G<sub>S3</sub> (green) and C<sub>S4</sub> (light blue). The folded sRNAH has a fully formed helix stem. There is a non-canonical hydrogen bond, a G.U trans-wobble interaction, between G<sub>L4</sub> (yellow) and U<sub>L1</sub> (white) bases. U<sub>L2</sub> (light pink) is flipped out and exposed to the solvent. There is also a hydrogen bond between C<sub>L3</sub> (orange) and U<sub>L1</sub> its 2OP1 site, leading to a marked stability of the tetraloop. According to X-ray data, C<sub>L3</sub> would be stacked on U<sub>L1</sub>, however NMR data showed that C<sub>L3</sub> is rotated out of plane in the backbone direction, and does not have an effective stack interaction on top of U<sub>L1</sub> [48, 49] (Image of PDB: 1F7Y [48] created using Pymol Molecular Graphic System, Version 1.8 Schrödinger, LLC).

A molecular dynamics study from D. Chakraborty *et al.* (2014) [47] showed that the energy landscape of small tetraloop hairpins, UUCG and GCAA hairpin loops, is quite complex and that two-state kinetic profiles cannot accurately describe their folding mechanism (Figure 27). They also demonstrated that these structures are highly thermostable, so that even at temperatures as high as 1000 K in their simulations, extended-chain conformations are less populated compared to more compact conformational states. Through variations of counterion concentration coupled with temperature-jump analysis, folding pathways were analyzed and an amount of 86599 transition states was estimated for the UUCG loop and 86599 transition states for the GCAA loop.

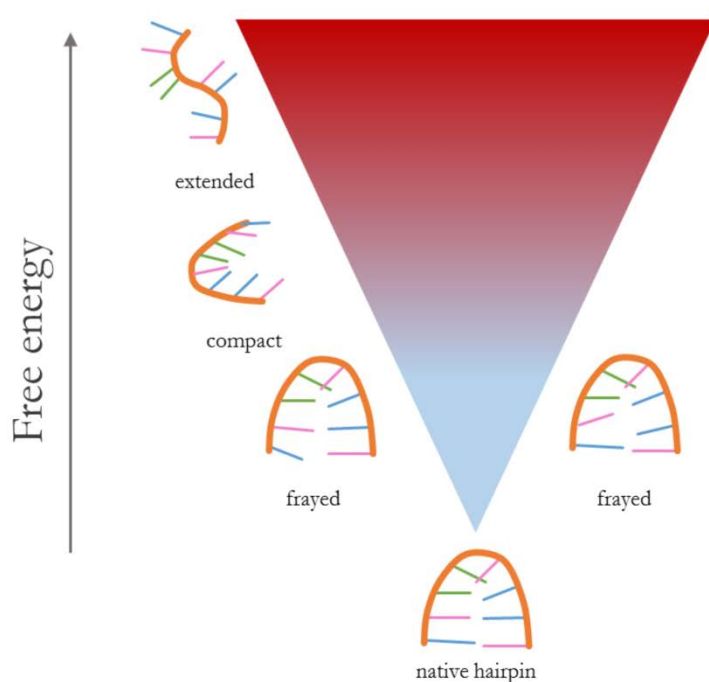


**Figure 27. Theoretically proposed free energy landscape of the small RNA hairpin with the gcUUGCgc sequence.** Representation adapted from the theoretical free energy landscape proposed by D. Chakraborty *et al.* (2014) [47] where denatured compact states are more commonly found than extended states. The different conformations are divided and classified as native, frayed, compact and extended states. The extended states lack any interaction between the nucleotides, compact states lack stem interactions but some loop interactions can be found, frayed states lack one of the stem interactions, and the native state comprises all stem and loop interactions.

The folding/unfolding equilibrium thermodynamics of the RNA tetraloop gcUUCGgc has been theoretically studied by Garcia & Paschek (2008) [55]. In this work, a calculation of the free energy landscape as a function of temperature and pressure was performed, resulting in a temperature-pressure elliptical-shaped stability phase diagram of the small RNA hairpin, which is accompanied by multiple conformational states (Figure 28). Recent molecular dynamics work by Miner *et al.* (2016) [103] characterized the thermodynamics and folding free energy landscape of the RNA tetraloop gcGCAAgc in more detail. They showed that the hairpin structure is primarily dominated by right-handed A-RNA stems with diverse loop conformations. In addition, a left-handed stem Z-RNA, and a compact purine triplet has been found. Each of these structural configurations presented a different stability as a function of temperature and pressure. Under high hydrostatic pressure conditions, the A-RNA conformation is stabilized and its population is therefore increased. On the other hand, the Z-RNA conformation is destabilized and its population decreases. Changes in pressure also modulated the interaction of the RNA molecule with the solvent and ions.

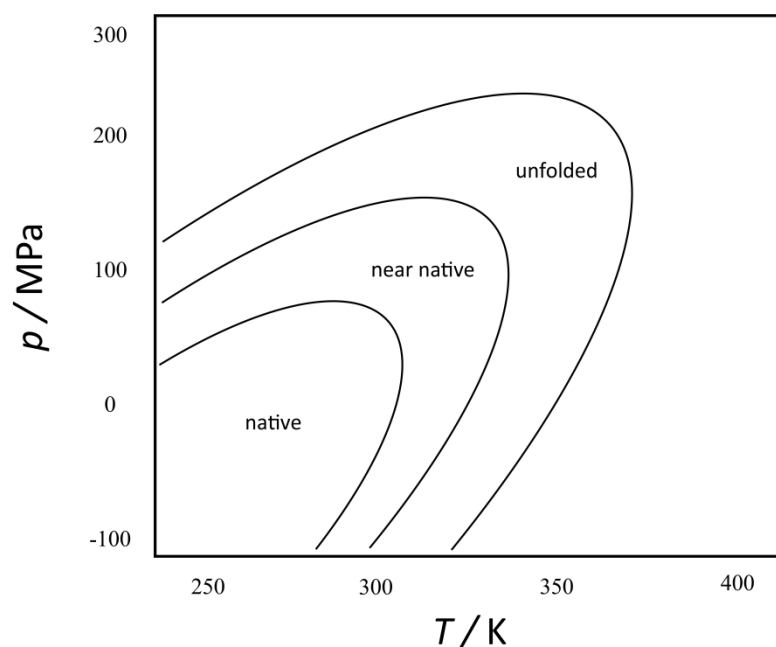


**Figure 28.** Theoretically proposed temperature-pressure elliptical-shaped stability phase diagram of the small RNA hairpin tetraloop gcUUCGgc (adapted from the diagram calculated in the literature [55]). According to this diagram, pressure should destabilize the hairpin structure at lower temperatures, and favor native or native-like conformations of the hairpin at higher temperatures.

The ability of small RNA hairpins to adopt different configurations and its high thermodynamic stability exemplify the ability of RNA molecules to adapt to a certain environment of salt, temperature and pressure conditions. These transformations are crucial for the adaptation of biological function in diverse organisms. Therefore, revealing the free energy landscape of these structures, and explore the forces controlling their stability are highly important to understand the thermal and pressure stability of thermophilic and piezophilic organisms. The question about the adaptation mechanisms of these organisms is still largely unanswered.

## **4.2. Experimental details**

### **4.2.1. RNA molecule**

The small RNA hairpin (sRNAH) molecule used in this study had a 5'-gcUUCGgc-3' sequence. Fluorescent labeled sRNAH molecules were also used, for comparison with results from Förster resonance energy transfer (FRET) measurements performed in a parallel work by Dr. Salomé Pataraiá. The fluorescent dyes were attached to the same molecule, with a final sequence of 5'-Cyanine 3 - GCUUCGGC- Cyanine 5 - 3'. These complimentary UV-vis and FTIR spectroscopy results of the labeled sRNAH are found in the Appendix 8.1.

### **4.2.2. Sample preparation**

The small RNA hairpins (sRNAH non-labeled: 5'-GCUUCGGC-3'; sRNAH labeled: 5'-Cyanine 3 - GCUUCGGC- Cyanine 5 - 3') were synthesized by IBA Life Solutions for Life Science GmbH (Goettingen, Germany), and were received as lyophilized powder. The sRNAH was suspended in a 0.1 mmol  $\mu\text{L}^{-1}$  nuclease free water solution, and stored at -80 °C. For the techniques applied, different sRNAH concentrations were used. The samples were lyophilized to remove H<sub>2</sub>O, and then suspended in pure 50 mM TRIS- HCl buffer + 0.1 mM EDTA, pH 7.5. The experiments were carried out multiple times, and different batches of RNA were used.

### **4.2.3. FTIR spectroscopy**

The infrared spectra of sRNAH were recorded and analyzed between 1750 and 1500  $\text{cm}^{-1}$  that is the region essentially associated with C=O stretching vibrations of paired and free nucleobases and imidazole ring vibrations. Each FTIR spectrum was obtained by recording 256 scans at a spectral resolution of 2  $\text{cm}^{-1}$ . Spectral evaluation was carried out by using Thermo GRAMS software as described in section 2.2.1.5, and the experimental data were fitted with Origin- Pro 9.0G software.

#### **4.2.3.1. Ambient pressure FTIR**

The labeled and non-labeled sRNAH samples were lyophilized overnight and then diluted in 50 mM Tris-HCl buffer + 0.1 mM EDTA, to a final concentration of 0.5 wt % in 50  $\mu\text{L}$  volume. The ambient-pressure FTIR measurements were carried out by using a Thermo Nicolet5700 spectrometer with a liquid-nitrogen-cooled MCT detector. An external water thermostat served as a temperature control. The sample chamber was continuously purged with dry air. The sample concentration chosen was 5  $\text{mg mL}^{-1}$  in a 50  $\mu\text{L}$  sample cell that consisted of 0.4 mm thick  $\text{CaF}_2$  transmission windows and a 0.05 mm spacer.

#### **4.2.3.2. High pressure FTIR**

The labeled and non-labeled sRNAH samples were lyophilized overnight and then diluted in 50 mM Tris-HCl buffer + 0.1 mM EDTA, to a final concentration of 4.5 wt% in 6  $\mu\text{L}$  volume to give a sufficiently high signal-to-noise ratio. The pressure-dependent FTIR data were recorded by using a Nicolet Magna550 spectrometer equipped with a liquid-nitrogen-cooled MCT detector. The infrared light was focused onto the pinhole of a gas-membrane-driven diamond anvil cell with a brass spacer (Diacell Vivo DAC, Almax. easyLab). Fine  $\text{BaSO}_4$  powder was used as an internal pressure calibrant [146, 148, 155]. An external water thermostat served as temperature control. After each pressure change, the sample was equilibrated for 10 min before acquisition of the IR spectrum. Two



different temperatures were used, 20 °C and 70 °C for the FTIR measurements in the gas membrane (VivoDac®) high-pressure cell.

#### **4.2.4. UV-vis spectroscopy**

A UV-1800 UV-vis spectrometer from Shimadzu was used to collect absorbance spectra of the small RNA hairpin. An external water bath connected to the cuvette holder kept the temperature constant during all measurements. The measurements were carried out using standard quartz cuvettes with 300  $\mu\text{L}$  of RNA sample volume. The labeled and non-labeled sRNAH samples were lyophilized overnight and then diluted in 50 mM Tris-HCl buffer + 0.1 mM EDTA, to a final concentration of 40  $\mu\text{M}$  in 300  $\mu\text{L}$  volume. The temperature varied from 10 to 80 °C in the cuvette. The sample temperature was equilibrated for 20 minutes before the acquisition of a new UV spectrum.

### **4.3. Results and discussion**

#### **4.3.1. Temperature-dependent analysis of the small RNA hairpin**

##### **4.3.1.1. Small RNA hairpin in-plane base vibrations sensitive to effects of base pairing followed by FTIR spectroscopy**

Conformational transitions of RNA molecules can be followed by FTIR spectroscopy under varied conditions, such as different temperatures and high hydrostatic pressures. The RNA infrared signal can be divided into two main regions, from 1800 to 1500  $\text{cm}^{-1}$  (related to base pairing and base stacking interaction signals) and from 1500 to 1250  $\text{cm}^{-1}$  (related to glycosidic bond rotation, backbone conformation and sugar pucker). For detailed information on RNA IR band assignment, see Table 1 in section 2.2.1.5. In the 1800 to 1500  $\text{cm}^{-1}$  wavenumber region, the IR bands are originating from nucleobase vibrations which are sensitive to base stacking and base-pairing interactions. The IR bands are related to double or single strand vibrations, which include C=C, C=N, and C=O stretching of free and/or bonded nucleotides. A double strand to single strand

transition results in a decrease in the intensity of the IR band at around 1696 to 1684  $\text{cm}^{-1}$  with a concomitant increase in the band at around 1677 to 1653  $\text{cm}^{-1}$ . The former arises due to the C6=O6 stretch of base-paired guanine plus the C2=O2 stretch of uracil. The latter band arises mainly from the stretching vibrations of C6=O6 of free (i.e., non-base paired) guanine, the C2=O2 stretch of free cytosine, and the C4=O4 stretch of free uracil [114, 136]. For better analysis of the IR bands the 1800 to 1500  $\text{cm}^{-1}$  region can be divided into two areas, from 1720 to 1600  $\text{cm}^{-1}$ , and from 1600 – 1550  $\text{cm}^{-1}$ .

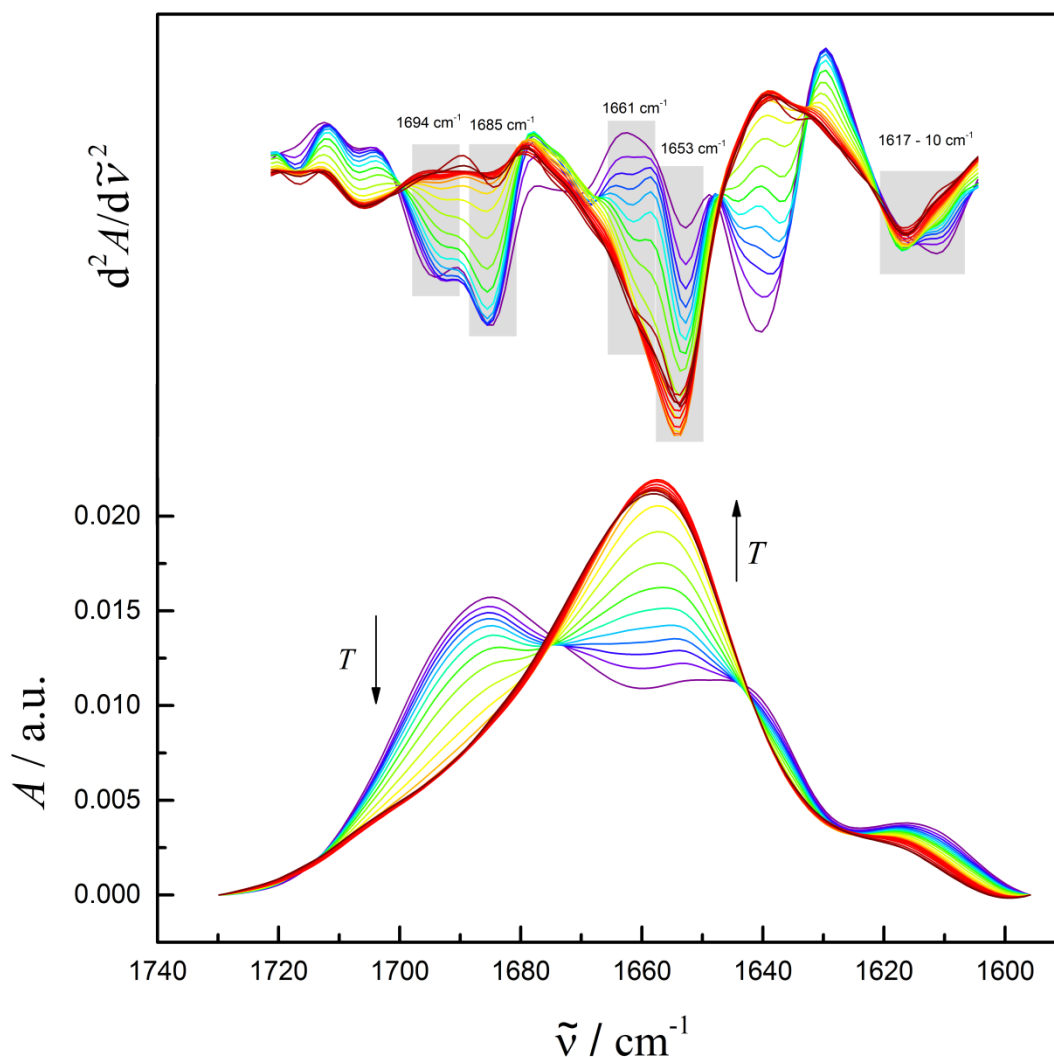


**Figure 29.** Temperature-dependent normalized and second derivative spectra of the small RNA hairpin in the wavenumber region from 1740 to 1600  $\text{cm}^{-1}$ . Second derivative and normalized spectra of 5  $\text{mg mL}^{-1}$  small RNA hairpin in 50 mM Tris-HCl buffer + 0.1 mM EDTA from 10 to 95  $^{\circ}\text{C}$ . In the normalized spectra, the IR band from 1696 to 1684  $\text{cm}^{-1}$ , related to base paired nucleotides, decreases with temperature (indicated by the arrow). The IR band from 1677 to 1653  $\text{cm}^{-1}$ , related to free nucleotides, increases with temperature (indicated by the arrow). The most important bands are indicated by the grey rectangles in the second derivative spectra. The highlighted bands are: 1694  $\text{cm}^{-1}$ , 1685  $\text{cm}^{-1}$ , 1661  $\text{cm}^{-1}$ , 1653  $\text{cm}^{-1}$ , 1617-10  $\text{cm}^{-1}$ . (Selected data)

Figure 29 shows the second derivative and normalized spectra of the temperature-dependent FTIR analysis of the sRNAH in 50 mM Tris-HCl buffer pH 7.5 + 0.1 mM EDTA, from 10 to 95  $^{\circ}\text{C}$ , in the wavenumber region from 1740 to 1600  $\text{cm}^{-1}$ . Thermal

unfolding can be easily detected in the IR spectra by the significant decrease in absorbance ( $A$ ) of the IR band at  $1686\text{ cm}^{-1}$ , which is characteristic of base paired G-C vibrations, and the concomitant significant increase in IR intensity of unpaired nucleic acids at around  $1660\text{ cm}^{-1}$ . It is shown in the second derivative spectra that the IR bands at  $1696\text{ cm}^{-1}$  and  $1685\text{ cm}^{-1}$ , related to base paired vibrations of uracil and guanine, respectively, reveal a constant decrease until total denaturation. There is a concomitant increase of the bands at  $1661\text{ cm}^{-1}$  and  $1653\text{ cm}^{-1}$ , related to free base vibrations of guanine and uracil, respectively. The band intensity displays a strong variation from 30 to  $60\text{ }^{\circ}\text{C}$ , which can be related to total disruption of the Watson-Crick base pairs. The small IR band at  $1610\text{ cm}^{-1}$  shift to  $1617\text{ cm}^{-1}$  during melting, and which can be assigned to free base vibrations of uracil.

The conformational changes in sRNAH have been determined in terms of the ratio of unpaired to paired G-C nucleotides pairs ( $I_{\text{free}}/I_{\text{duplex}}$ ), as seen in Figure 30, obtained from the IR bands of different recorded spectra (Figure 29), at around  $1660$  and  $1686\text{ cm}^{-1}$ , respectively. The sRNAH shows a gradual and significant increase in the intensity ratio with a broad “two-state model” like denaturation melting profile, with the melting transition temperature occurring around  $50\text{ }^{\circ}\text{C}$ . The RNA molecule does achieve a constant  $I_{\text{ratio}}$  plateau from  $70$  to  $95\text{ }^{\circ}\text{C}$ . However, the sRNAH structure might not be fully unfolded as extended chain ensembles. In this temperature range, it may rather comprise various intermediate compact unfolded or coil like structures, as demonstrated in the literature [47]. Molecular dynamics studies have shown that a small RNA molecule, such as the sRNA (gcUUCGgc), is highly stable and can have numerous substates. These states can vary between native structure, frayed structures, compact unfolded/coil like structures, and extended/fully unfolded structures. However, the fully extended state is unpopulated even at a temperature of  $1000\text{ K}$  [47].

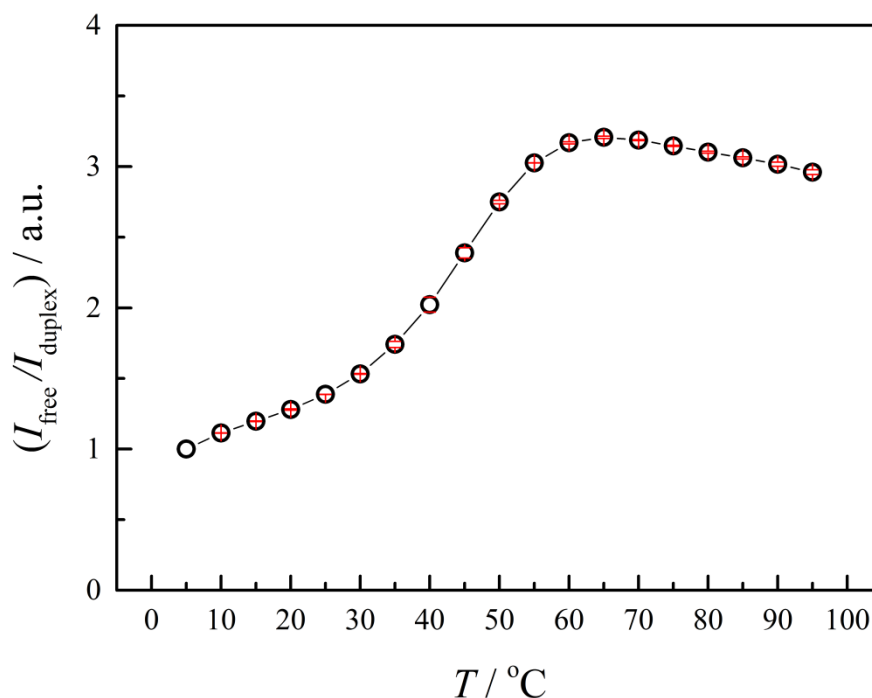


**Figure 30.**  $I_{\text{free}}/I_{\text{duplex}}$  analysis of the temperature-dependent FTIR data of the small RNA hairpin. Temperature-dependence of unpaired to duplexed GC pairs ratio ( $I_{\text{free}}/I_{\text{duplex}}$ ) as obtained from the infrared spectra recorded at  $\approx 1658 \text{ cm}^{-1}$  and  $\approx 1686 \text{ cm}^{-1}$ , respectively, for  $5 \text{ mg mL}^{-1}$  small RNA hairpin in  $50 \text{ mM}$  Tris-HCl buffer +  $0.1 \text{ mM}$  EDTA from  $10$  to  $95 \text{ }^\circ\text{C}$ . The error bars cover the scattering of three independent measurements.

#### 4.3.1.2. UV-vis spectroscopy of the small RNA hairpin

In order to confirm the FTIR melting profile, UV-vis spectroscopy measurements were carried out. Nucleic acids are known to have a strong absorbance in the region of  $240 - 275 \text{ nm}$ . At neutral pH, the UV absorption maxima range from  $275 \text{ nm}$  for guanine,  $270 \text{ nm}$  for cytosine, to  $260 \text{ nm}$  for uracil bases. Consequently, polymeric RNA shows a broad absorbance around  $260 \text{ nm}$ . When nucleotides are stacked, they are shielded from the solvent, and its absorbance is smaller compared to single stranded nucleic acid chains. The RNA denaturation is then followed by an increase in the absorbance around  $260 \text{ nm}$ .

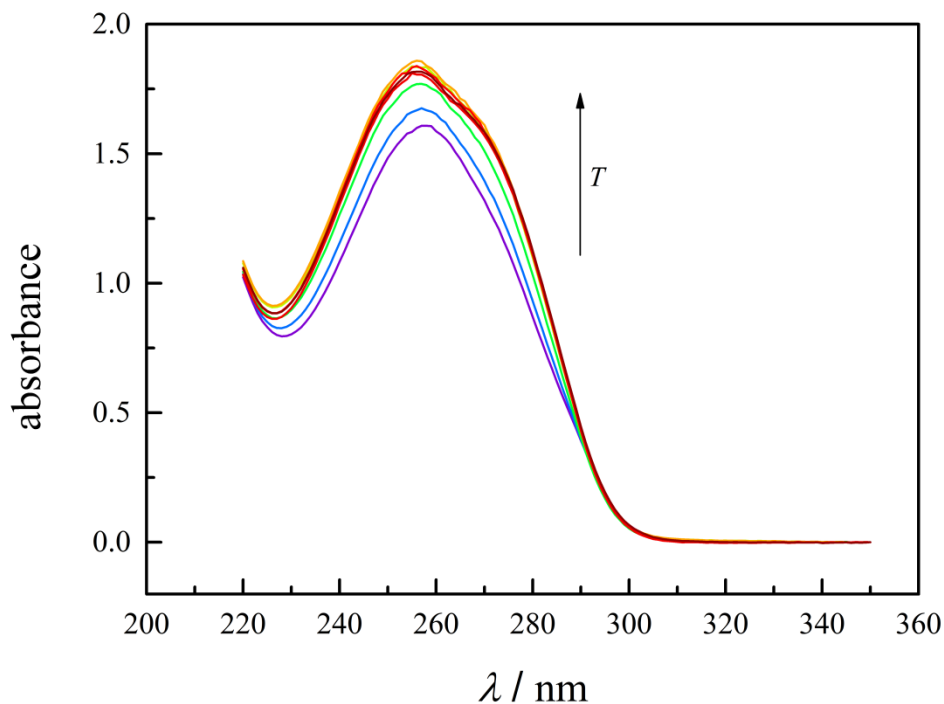


**Figure 31. Temperature-dependent UV-vis spectra of the small RNA hairpin.** UV-vis spectra of 40  $\mu\text{M}$  small RNA hairpin in 50 mM Tris-HCl buffer + 0.1 mM EDTA from 10 to 80  $^{\circ}\text{C}$ . The UV-vis absorbance increases with increasing temperature (indicated by the arrow). (Selected data)

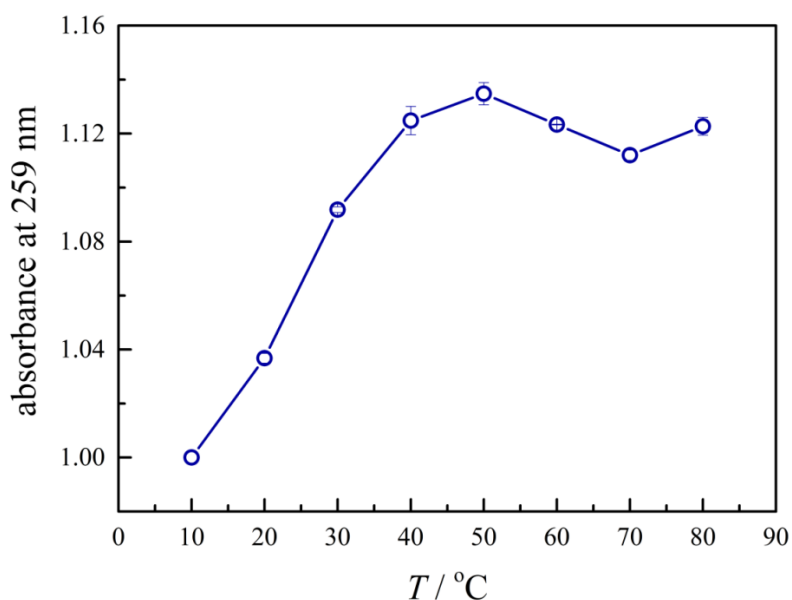


**Figure 32. Temperature-dependent UV-vis maximum absorbance at 259 nm of the small RNA hairpin.** Maximum absorbance at 259 nm, standard marker of polymeric RNA at UV-vis, of 40  $\mu\text{M}$  small RNA hairpin in 50 mM Tris-HCl buffer + 0.1 mM EDTA from 10 to 80  $^{\circ}\text{C}$ . The error bars cover the scattering of three independent measurements.

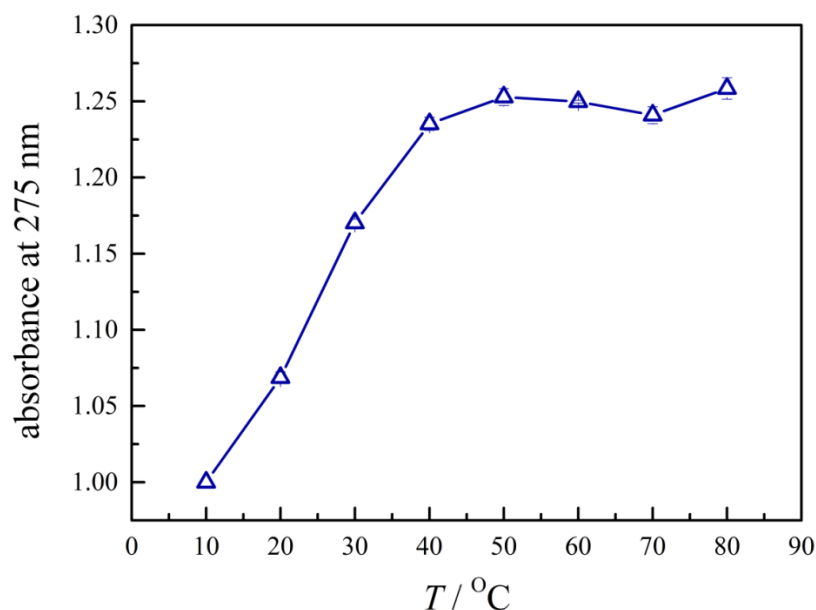


**Figure 33.** Temperature-dependent UV-vis maximum absorbance at 275 nm of the small RNA hairpin. Maximum absorbance at 275 nm, UV absorption maxima for guanine, of 40  $\mu$ M small RNA hairpin in 50 mM Tris-HCl buffer + 0.1 mM EDTA from 10 to 80  $^{\circ}$ C. The error bars cover the scattering of three independent measurements.

The UV-vis spectroscopy results seen in Figures 32 and 33 are in good agreement with the FTIR data. The UV-vis data show a continuous denaturation until 50  $^{\circ}$ C. The UV-vis spectroscopy data suggest that the melting transition cannot be described as a two-state model denaturation profile, but rather a constant increase of the nucleotide free base vibrations until 50  $^{\circ}$ C. It can also be observed that with increase temperature a shoulder appears in the UV-vis spectra (Figure 31) at the wavelength of 275 nm. This UV signal can be related to the absorbance of free guanine, specifically, since the sRNAH stem only has G-C stem connections. The denaturation profile following the signal at 275 nm has the same trend as observed for the main UV signal at 259 nm (Figure 33 and 32 respectively).

### 4.3.1.3. Small RNA hairpin in-plane base vibrations sensitive to effects of base stacking followed by FTIR spectroscopy

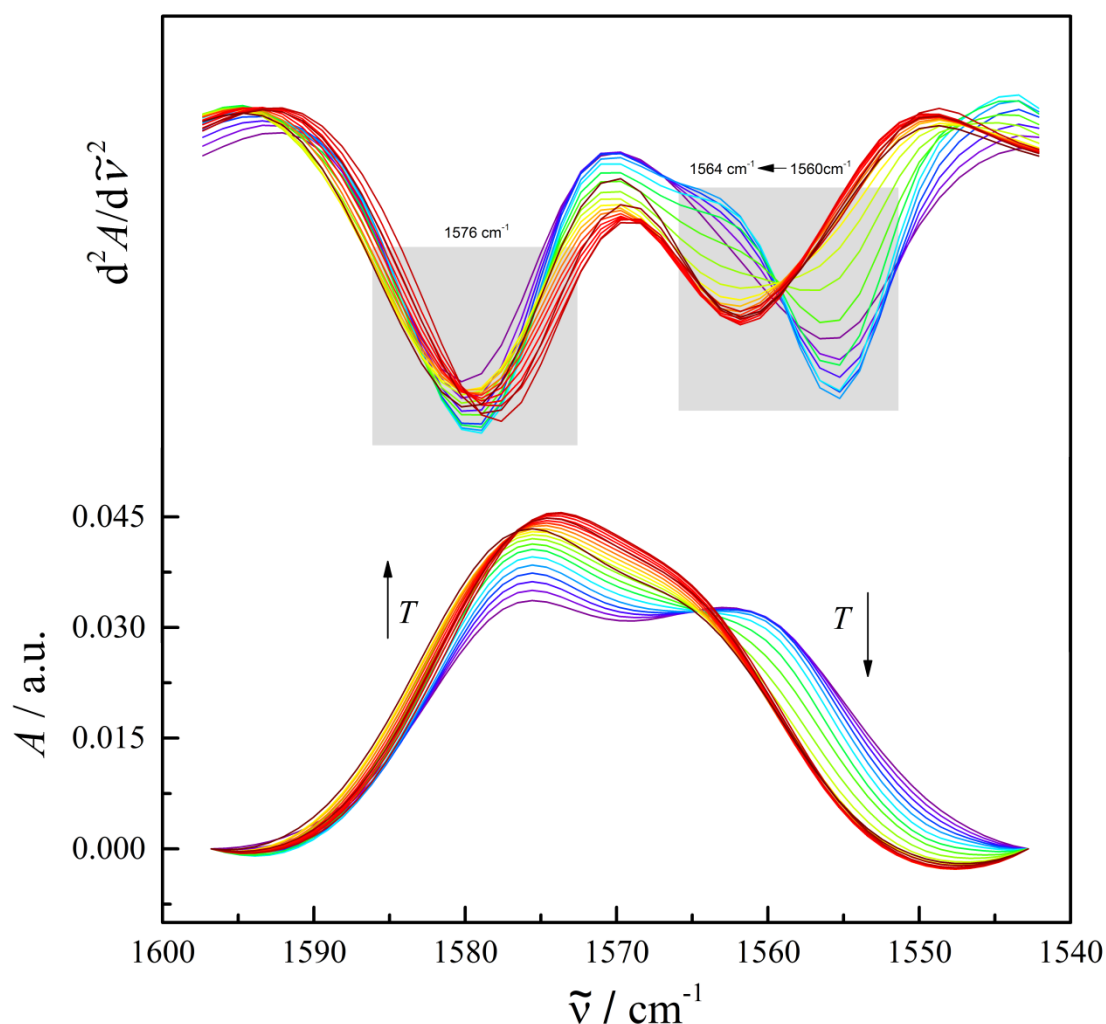


**Figure 34. Temperature-dependent normalized and second derivative spectra of the small RNA hairpin in the wavenumber region from 1600 to 1550  $\text{cm}^{-1}$ .** Second derivative and normalized spectra of 5  $\text{mg mL}^{-1}$  small RNA hairpin in 50  $\text{mM}$  Tris-HCl buffer + 0.1  $\text{mM}$  EDTA from 10 to 95  $^{\circ}\text{C}$ . In the normalized spectra, the IR band at 1590 to 1575  $\text{cm}^{-1}$ , related to ring vibrations of  $\text{C4} = \text{C5}$  and  $\text{C5} - \text{C6}$  of free and base paired guanine, increases with temperature (indicated by the arrow). The IR band at 1568 to 1564  $\text{cm}^{-1}$ , related to ring vibrations of  $\text{C6} = \text{O6}$ ,  $\text{C5} - \text{C6}$  and  $\text{C4} = \text{C5}$  of free and base paired guanine, decreases with temperature (indicated by the arrow). The most important bands are indicated by the grey rectangle in the second derivative spectra. The highlighted bands are: 1576  $\text{cm}^{-1}$ , 1564 - 60  $\text{cm}^{-1}$ . (Selected data)

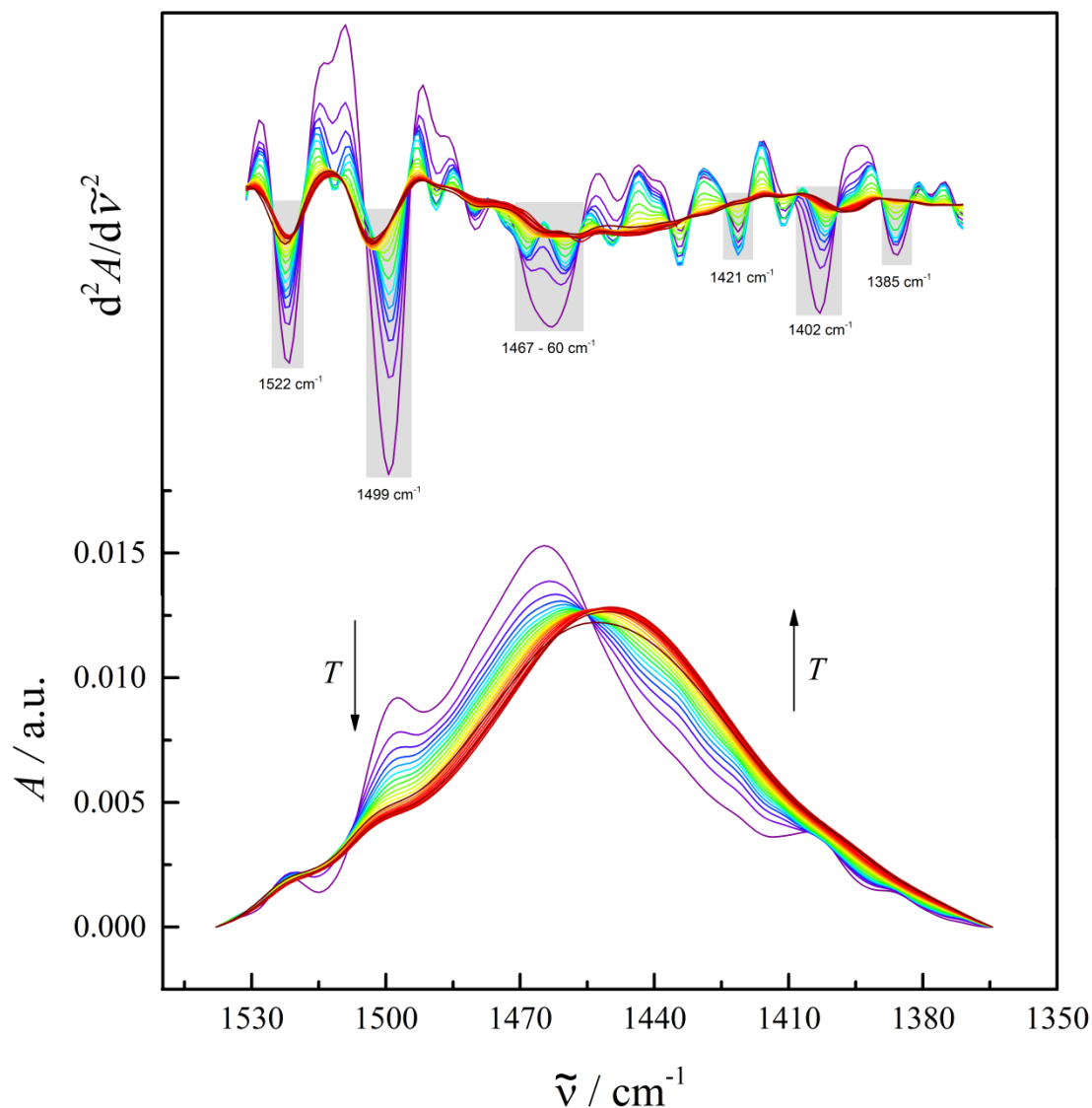


Figure 34 shows the temperature-dependent FTIR spectra of sRNAH in 50 mM Tris-HCl buffer pH 7.5 + 0.1 mM EDTA, from 10 to 95 °C, in the wavenumber region from 1600 to 1550  $\text{cm}^{-1}$ . In this region of the RNA spectra, two IR bands can be observed. One IR band around 1590 to 1575  $\text{cm}^{-1}$  and another IR band around 1568 - 1564  $\text{cm}^{-1}$ . The former band arises from ring vibrations of  $\text{C6} = \text{O6}$ ,  $\text{C5} - \text{C6}$  and  $\text{C4} = \text{C5}$  of free and base paired guanine. The latter band arises from ring vibrations of  $\text{C4} = \text{C5}$  and  $\text{C5} - \text{C6}$  of free and base paired guanine (for a more detailed RNA IR band assignment description, see Table 1 in section 2.2.1.5). The intensity increase of the IR band at 1575  $\text{cm}^{-1}$  follows the denaturation of the sRNAH. Apparently, the IR band at 1560  $\text{cm}^{-1}$  decreases in intensity, however it shifts to higher wavenumbers, as seen in the second derivative spectra. These bands are also assigned in order to follow the behavior of free and base paired guanine of guanine rich regions. Changes in the position of the guanine doublet bands between 1590 – 1564  $\text{cm}^{-1}$  are also related to changes in the environment of the guanine nucleotides [114]. Both bands show pronounced changes in intensity and wavenumber. The increase in intensity confirms loss of structure, and the wavenumber shift indicates that there are some changes in the guanine environment. However, the ring vibrational changes, or stacking interactions, are not as pronounced as the increase of free guanine base pairing vibrations at 1660  $\text{cm}^{-1}$  (Figure 29).

#### 4.3.1.4. Small RNA hairpin base-sugar vibrations followed by FTIR spectroscopy

The base sugar vibrations were also followed by FTIR spectroscopy. The wavenumber area ranges from 1500 to 1250  $\text{cm}^{-1}$  (for a more detailed description of the IR band assignment, see Table 1 in section 2.2.1.5). In this region, the IR bands are originating from base-sugar vibrations which are sensitive to glycosidic bond rotation, backbone and sugar pucker conformations. The IR bands are related to backbone vibrations in A-, B- and Z-forms, sugar pucker in N- or S-type conformations and N7 site vibrations of purines. It is a spectral region where a wide variety of subbands can appear. However, the major IR bands in this spectra region cannot be assigned to the sRNAH, since its minimal sequence does not have, for example, adenine base, which is essential to correlate changes

in backbone conformation. There is no assignment in the literature for guanine, cytosine or uracil in relation to the bands recorded around  $1464\text{ cm}^{-1}$  and  $1440\text{ cm}^{-1}$  by FTIR.



**Figure 35.** Temperature-dependent normalized and second derivative spectra of the small RNA hairpin in the wavenumber region from  $1530$  to  $1380\text{ cm}^{-1}$ . Second derivative and normalized spectra of  $5\text{ mg mL}^{-1}$  small RNA hairpin in  $50\text{ mM}$  Tris-HCl buffer +  $0.1\text{ mM}$  EDTA from  $10$  to  $95\text{ }^{\circ}\text{C}$ . IR bands are originating from base-sugar vibrations that are sensitive to glycosidic bond rotation, backbone and sugar pucker conformations. The IR bands are related to backbone vibrations in A-, B- and Z-forms, sugar pucker in N- or S-type conformations and N7 site vibrations of purines. The most important bands are indicated by the grey rectangle in the second derivative spectra. The highlighted bands are:  $1522\text{ cm}^{-1}$ ,  $1499\text{ cm}^{-1}$ ,  $1476 - 60\text{ cm}^{-1}$ ,  $1421\text{ cm}^{-1}$ ,  $1402\text{ cm}^{-1}$ . (Selected data)

Figure 35 shows the temperature-dependent FTIR spectra of the sRNAH in 50 mM Tris-HCl buffer pH 7.5 + 0.1 mM EDTA, from 10 to 80 °C, in the wavenumber region from 1530 to 1380  $\text{cm}^{-1}$ . The IR band at 1498  $\text{cm}^{-1}$ , which is assigned as in-plane vibrations of cytosine, shows a significant decrease with temperature. This can be related only to the shift from base paired cytosine to free cytosine during denaturation. An IR band can be observed at 1403  $\text{cm}^{-1}$ , which is assigned as RNA vibrations of an in-plane C – O – H deformation mode at the 2' position of the ribose ring [160]. A small IR band at 1421  $\text{cm}^{-1}$  related to purine (guanine) sugar in S-type conformation (sugars at C2'-endo sugar pucker conformation of guanine in B-form) can also be observed. This band shows an increase in intensity during denaturation, indicating that there are environmental changes in the backbone of the sRNAH during melting which favors the B-form upon melting. The sugar pucker conformation is directly related to the backbone conformation.

When the RNA molecule has A- and/or Z-forms, a right-handed more compact helix and a left-handed helix conformation appears, respectively, and the ribose sugar adopts a C3'-endo conformation. It means that the C3 atom of the sugar pucker is above the plane in comparison to the nucleoside. This conformation brings the nucleotides closer, which in turn render the helix more compact than the B- helix. The Z-form has the guanine sugar pucker in C3'-endo conformation, but its cytosine stays in C2'-endo conformation (C2 atom of sugar pucker is above the plane), which makes the Z-form adopt a left-handed helical conformation. The Z-form is an intermediate and less stable backbone conformation that one can find in RNA and DNA. C2'-endo sugar puckers are characteristic of a B-form helix, a less compact right-handed helix typical of the DNA backbone conformation.

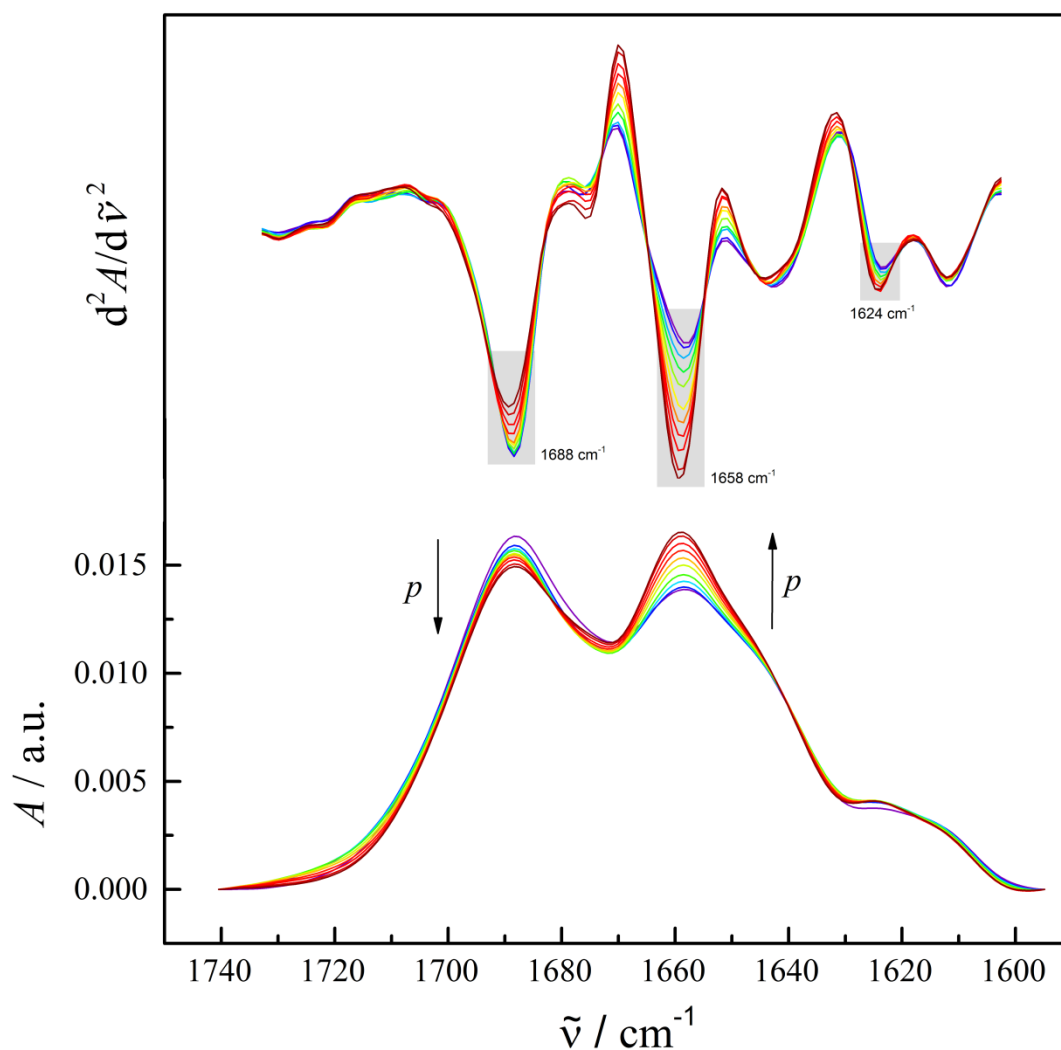
There are distinct changes of secondary structural features seen in the FTIR spectra of the sRNAH upon thermal denaturation. The double helical bonds of the native structure are lost, but apparently, some loop interactions remain. It can also be noted that changes in the intensity of the base pair vibration are more significant than the changes observed for ring stacking vibrations. These temperature-dependent FTIR results suggest that upon

denaturation, the sRNAH adopts a compact unfolded structure rather than a fully unfolded (extended chain) conformation, as suggested by a theoretical study [47].

### **4.3.2. Pressure-dependent FTIR analysis of the small RNA hairpin**

#### **4.3.2.1. Small RNA hairpin in-plane base vibrations sensitive to effects of base pairing followed by FTIR spectroscopy**

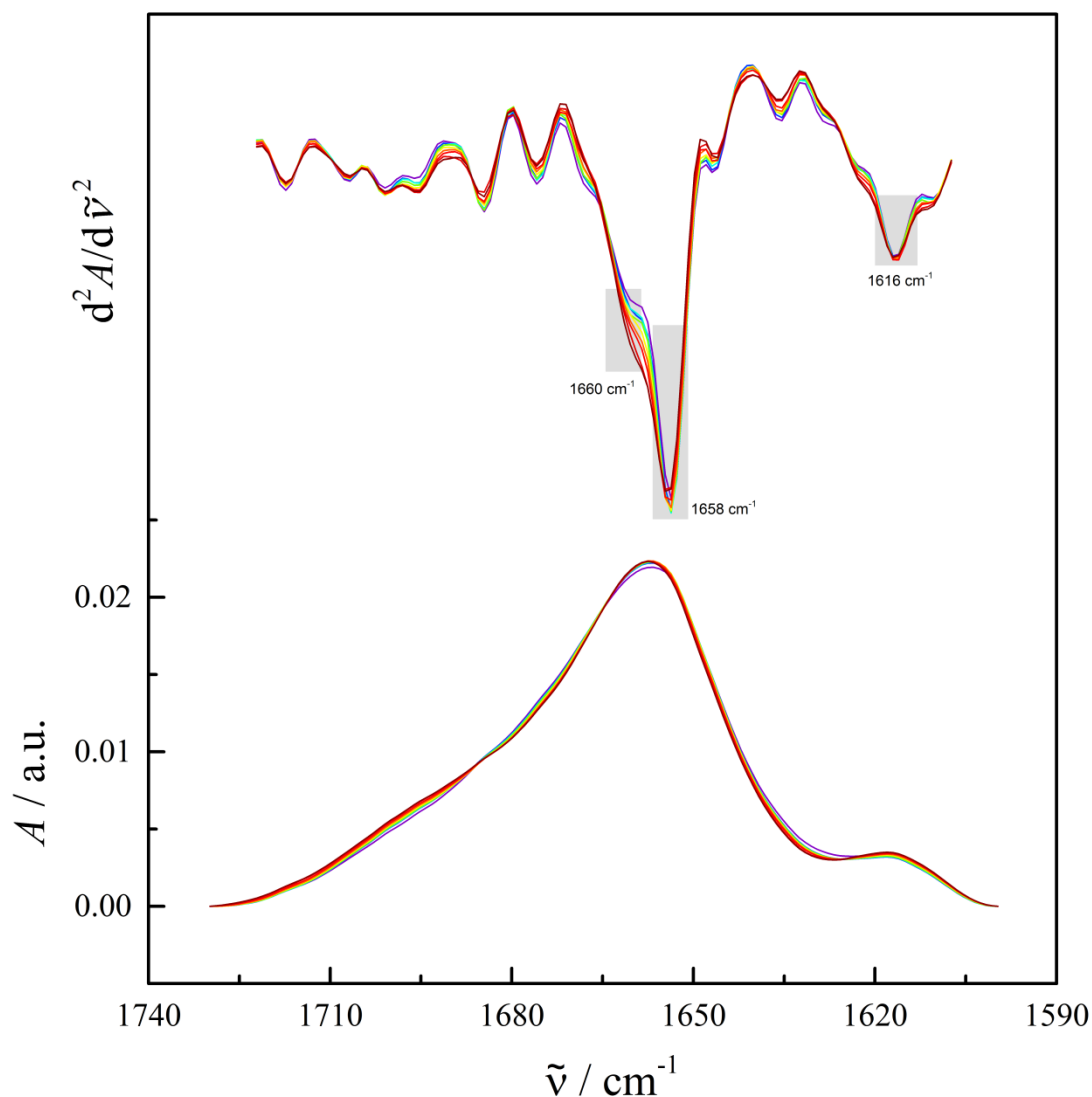
High hydrostatic pressure (HHP) FTIR measurements were also performed for the sRNAH (for experimental details, see section 2.2.1.1 and/or 4.2.3). The HHP pressure measurements were performed for selected temperatures, in order to test the theoretical predictions in which a pressure – temperature ( $p - T$ ) free energy diagram was calculated. According to the diagram, the hairpin structure would be destabilized by high hydrostatic pressure at lower temperature, and that at high temperature the denatured hairpin structure would be stabilized by high hydrostatic pressure [55].



**Figure 36. Pressure-dependent normalized and second derivative spectra of the small RNA hairpin in the wavenumber region from 1740 to 1600  $\text{cm}^{-1}$  at 20  $^{\circ}\text{C}$ .** Second derivative and normalized spectra of 5  $\text{mg mL}^{-1}$  small RNA hairpin in 50  $\text{mM}$  Tris-HCl buffer + 0.1  $\text{mM}$  EDTA from 0.1 to 400 MPa at 20  $^{\circ}\text{C}$ . In the normalized spectra, the IR band from 1696 to 1684  $\text{cm}^{-1}$ , related to base paired nucleotides, decreases with temperature (indicated by the arrow) The IR band from 1677 to 1653  $\text{cm}^{-1}$ , related to free nucleotides, increases with temperature (indicated by the arrow). The most important bands are indicated by the grey rectangle in the second derivative spectra. The highlighted bands are: 1688  $\text{cm}^{-1}$ , 1658  $\text{cm}^{-1}$ , 1661  $\text{cm}^{-1}$ , 1624  $\text{cm}^{-1}$ . (Selected data)

Figure 36 shows the pressure-dependent FTIR spectra of sRNAH in 50  $\text{mM}$  Tris-HCl buffer pH 7.5 + 0.1  $\text{mM}$  EDTA, from 0.1 to 400 MPa at 20  $^{\circ}\text{C}$ , in the wavenumber region from 1740 to 1600  $\text{cm}^{-1}$ . Pressure causes a small decrease in absorbance ( $A$ ) of the

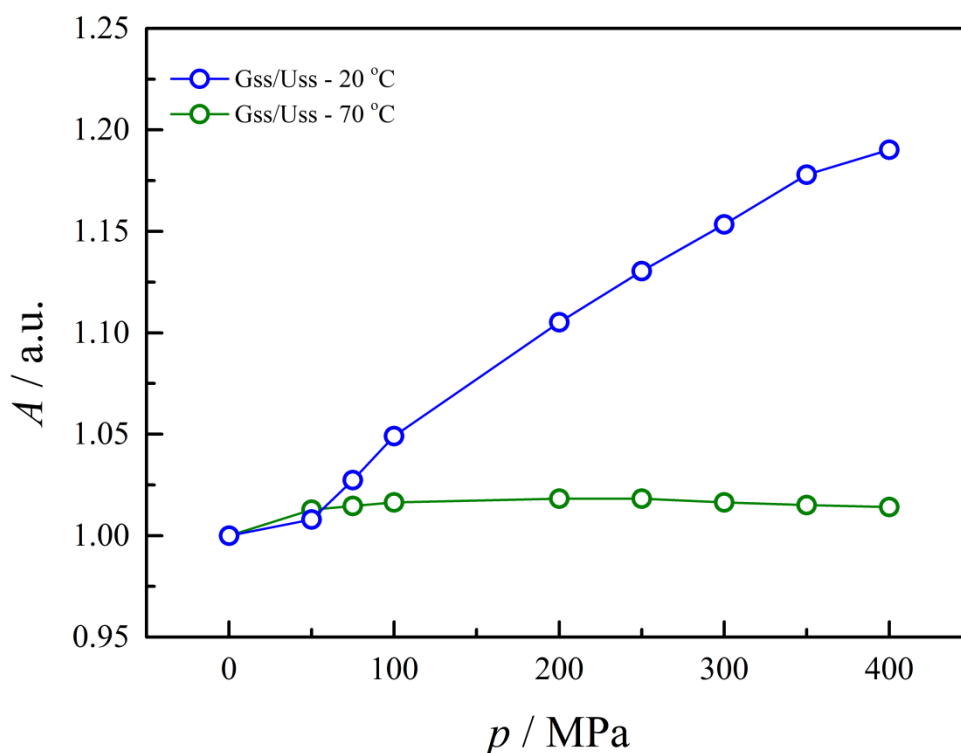
IR band at  $1686\text{ cm}^{-1}$ , which is characteristic of base paired G-C vibrations, and a concomitant increase in IR intensity of unpaired nucleic acids around  $1660\text{ cm}^{-1}$ . It can be seen that the sRNAH structure is destabilized by pressure, which is mainly due to the increase of single strand vibrations of guanine at  $1660\text{ cm}^{-1}$ . However, the structural destabilization is rather small when compared to the temperature dependent FTIR data (Figure 29). The pressure-induced destabilization of the sRNAH structure, at  $20\text{ }^{\circ}\text{C}$ , may be related to variations of non-native intermediate structures, where different base pair arrangements appear. For example, frayed intermediate ensembles vary between only one base pair the stem, the terminal base pair or the closing base pair, as seen in Figure 26 [47, 103]. The FTIR result shows that the hyperstable sRNAH is not completely unfolded by pressure up to  $400\text{ MPa}$ . Pressure apparently induces only small structural rearrangements of the native fold at  $20\text{ }^{\circ}\text{C}$ , probably due to changes in volume and hydration of the RNA molecule.



**Figure 37. Pressure-dependent normalized and second derivative spectra of the small RNA hairpin in the wavenumber region from 1740 to 1600  $\text{cm}^{-1}$  at 70  $^{\circ}\text{C}$ .** Second derivative and normalized spectra of 5  $\text{mg mL}^{-1}$  small RNA hairpin in 50 mM Tris-HCl buffer + 0.1 mM EDTA from 0.1 to 400 MPa at 70  $^{\circ}\text{C}$ . In the normalized spectra, the IR band from 1696 to 1684  $\text{cm}^{-1}$ , related to base paired nucleotides, is not observed after denaturation. The IR band from 1677 to 1653  $\text{cm}^{-1}$ , related to free nucleotides, does not show significant changes under high hydrostatic pressure. The most important bands are indicated by the grey rectangle in the second derivative spectra. The highlighted bands are: 1660  $\text{cm}^{-1}$ , 1658  $\text{cm}^{-1}$ , 1616  $\text{cm}^{-1}$ . (Selected data)

Figure 37 shows the pressure-dependent FTIR spectra of sRNAH in 50 mM Tris-HCl buffer pH 7.5 + 0.1 mM EDTA, from 0.1 to 400 MPa at 70  $^{\circ}\text{C}$ , in the wavenumber

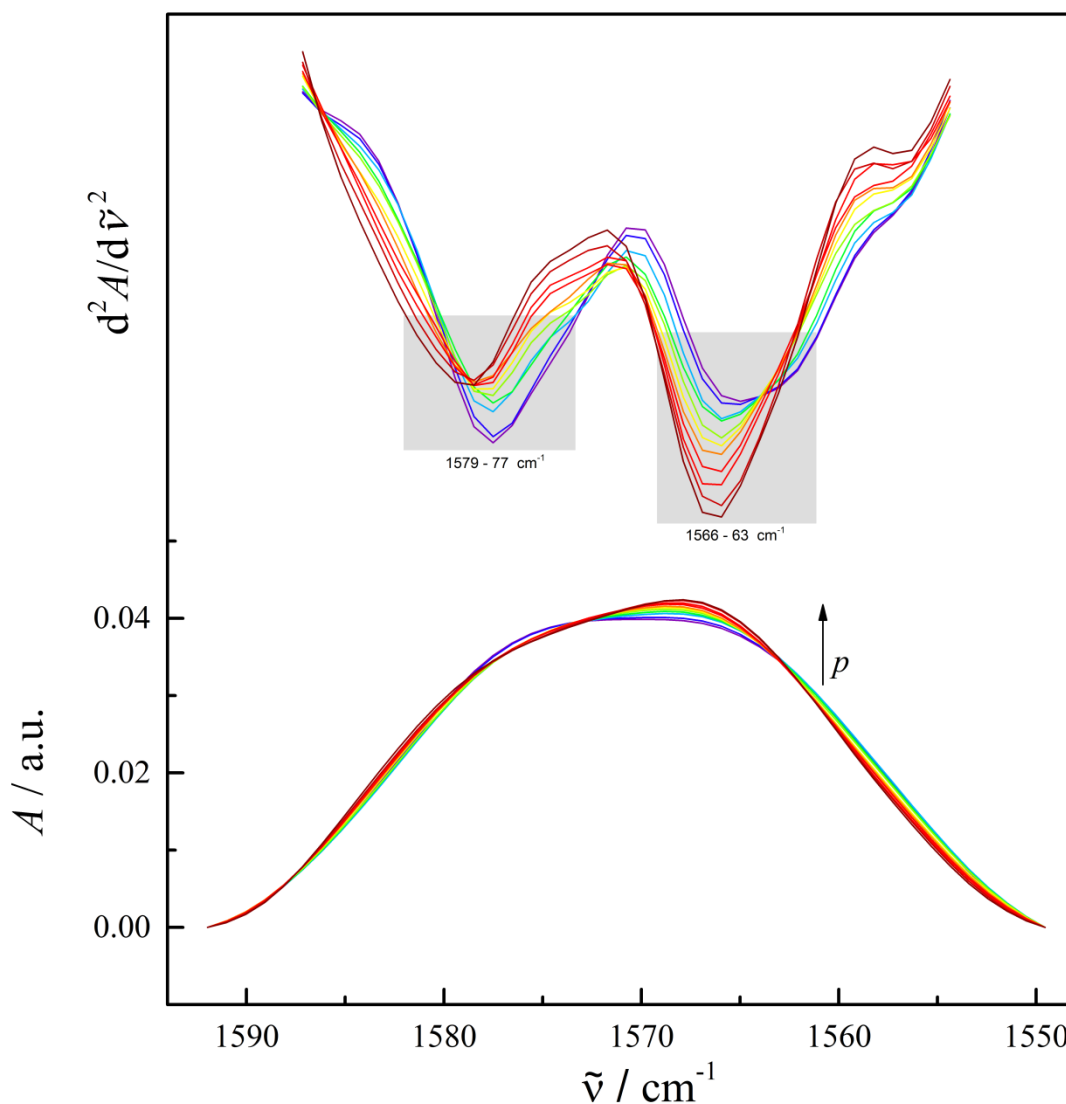
region from 1740 to 1600  $\text{cm}^{-1}$ . Pressure does not cause changes in absorbance ( $A$ ) of the IR band at 1660  $\text{cm}^{-1}$ , characteristic for unpaired guanine bases. Due to thermal denaturation of sRNAH molecule, there is no IR band at 1686  $\text{cm}^{-1}$ , which is characteristic of base paired G-C vibrations. The comparison between the IR band absorbance at 1660  $\text{cm}^{-1}$  of the pressure dependent FTIR measurements at 20 °C and 70 °C is shown in Figure 38 below. It can be seen that pressure does not promote refolding of the native sRNAH structure, since no IR signal for G-C base pairs can be detected. In addition, the compact unfolded structures are not further destabilized by pressure, as the signal of single strand vibrations of guanine at 1660  $\text{cm}^{-1}$  does not change [47, 103].



**Figure 38. Pressure-dependent changes of the small RNA hairpin free base vibrations of guanine and uracil followed by FTIR.** Pressure-dependence change of the intensity of unpaired GC pairs obtained from the infrared spectra recorded at  $\approx 1658 \text{ cm}^{-1}$  for  $5 \text{ mg mL}^{-1}$  small RNA hairpin in  $50 \text{ mM}$  Tris-HCl buffer +  $0.1 \text{ mM}$  EDTA from 0.1 to 400 MPa, at 20 °C and 70 °C.

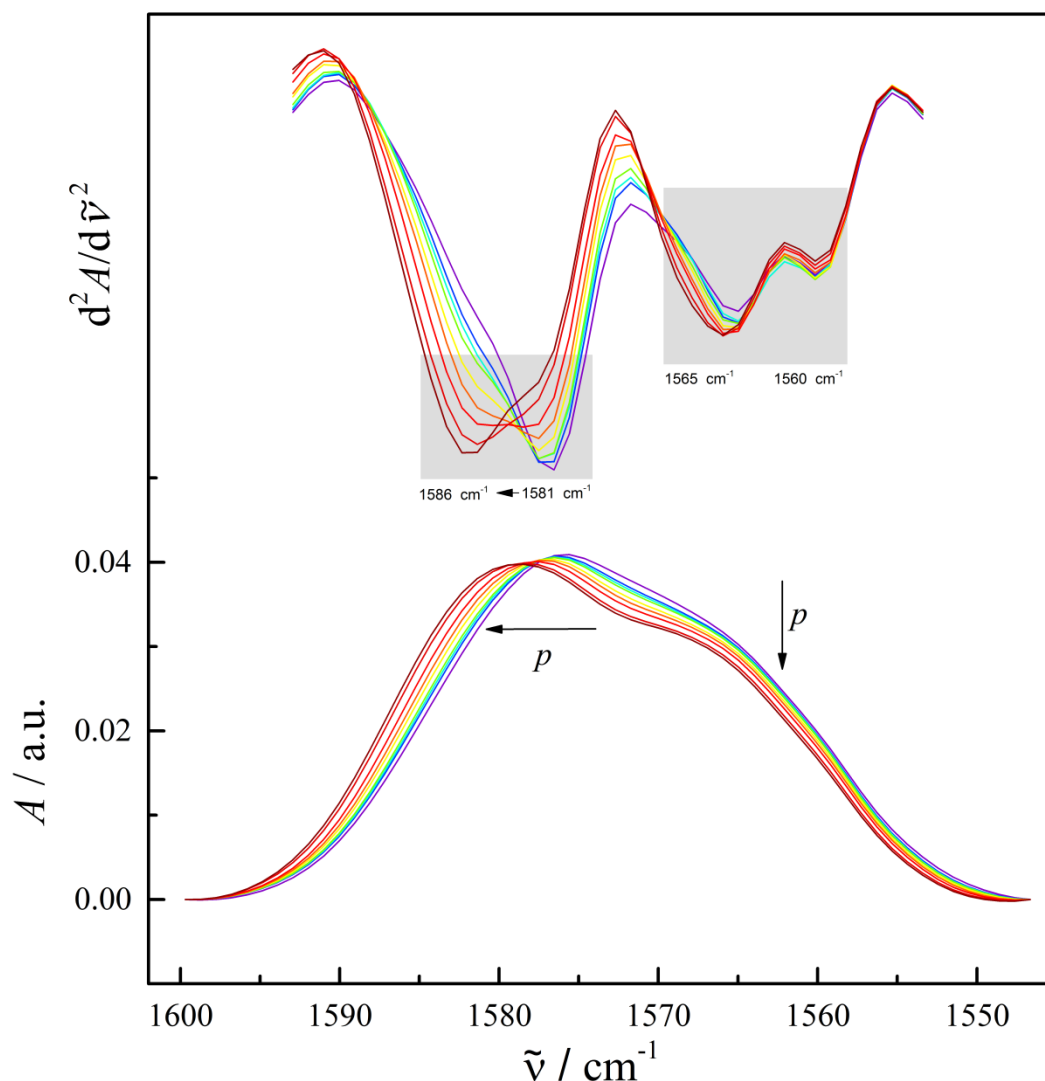


### 4.3.2.2. Small RNA hairpin in-plane base vibrations sensitive to effects of base stacking followed by FTIR spectroscopy



**Figure 39. Pressure-dependent normalized and second derivative spectra of the small RNA hairpin in the wavenumber region from 1600 to 1550  $\text{cm}^{-1}$  at 20 °C.** Second derivative and normalized spectra of 5  $\text{mg mL}^{-1}$  small RNA hairpin in 50 mM Tris-HCl buffer + 0.1 mM EDTA from 0.1 to 400 MPa at 20 °C. In the normalized spectra, the IR band at 1590 to 1575  $\text{cm}^{-1}$  is related to ring vibrations of C4 = C5 and C5 – C6 of free and base paired guanine and does not show significant changes. The IR band at 1568 to 1564  $\text{cm}^{-1}$ , related to ring vibrations of C6 = O6, C5 – C6 and C4 = C5 of free and base paired guanine, shows a small increase in intensity (indicated by the arrow). The most important bands are indicated by the grey rectangle in the second derivative spectra. The highlighted bands are: 1579 - 77  $\text{cm}^{-1}$ , 1566 - 63  $\text{cm}^{-1}$ . (Selected data)

Figure 39 shows the pressure-dependent FTIR spectra of the sRNAH in 50 mM Tris-HCl buffer pH 7.5 + 0.1 mM EDTA, from 0.1 to 400 MPa at 20 °C, in the wavenumber region from 1600 to 1550  $\text{cm}^{-1}$ . The two characteristic IR bands in this region are the bands around 1590 to 1575  $\text{cm}^{-1}$ , and 1568 to 1564  $\text{cm}^{-1}$ . Both of these bands arise from ring vibrations of  $\text{C6} = \text{O6}$ ,  $\text{C5} - \text{C6}$  and  $\text{C4} = \text{C5}$  of free and base paired guanine. Changes in the position of this band are related to environment changes of guanine, and they are also used to follow the behavior of guanine-rich areas. The intensity of both IRs band reduces when guanine forms base pairs (for more detailed RNA IR band assignment, see Table 1 in section 2.2.1.5). It can be observed that the sRNAH displays a very small increase of the IR band around 1566  $\text{cm}^{-1}$ , only. The intensity of the IR band around 1580  $\text{cm}^{-1}$  does not exhibit significant changes with increasing pressure. These results show that the effect of high hydrostatic pressure even up to 400 MPa on the native structure of the sRNAH is rather small, especially when related to guanine ring vibrations.



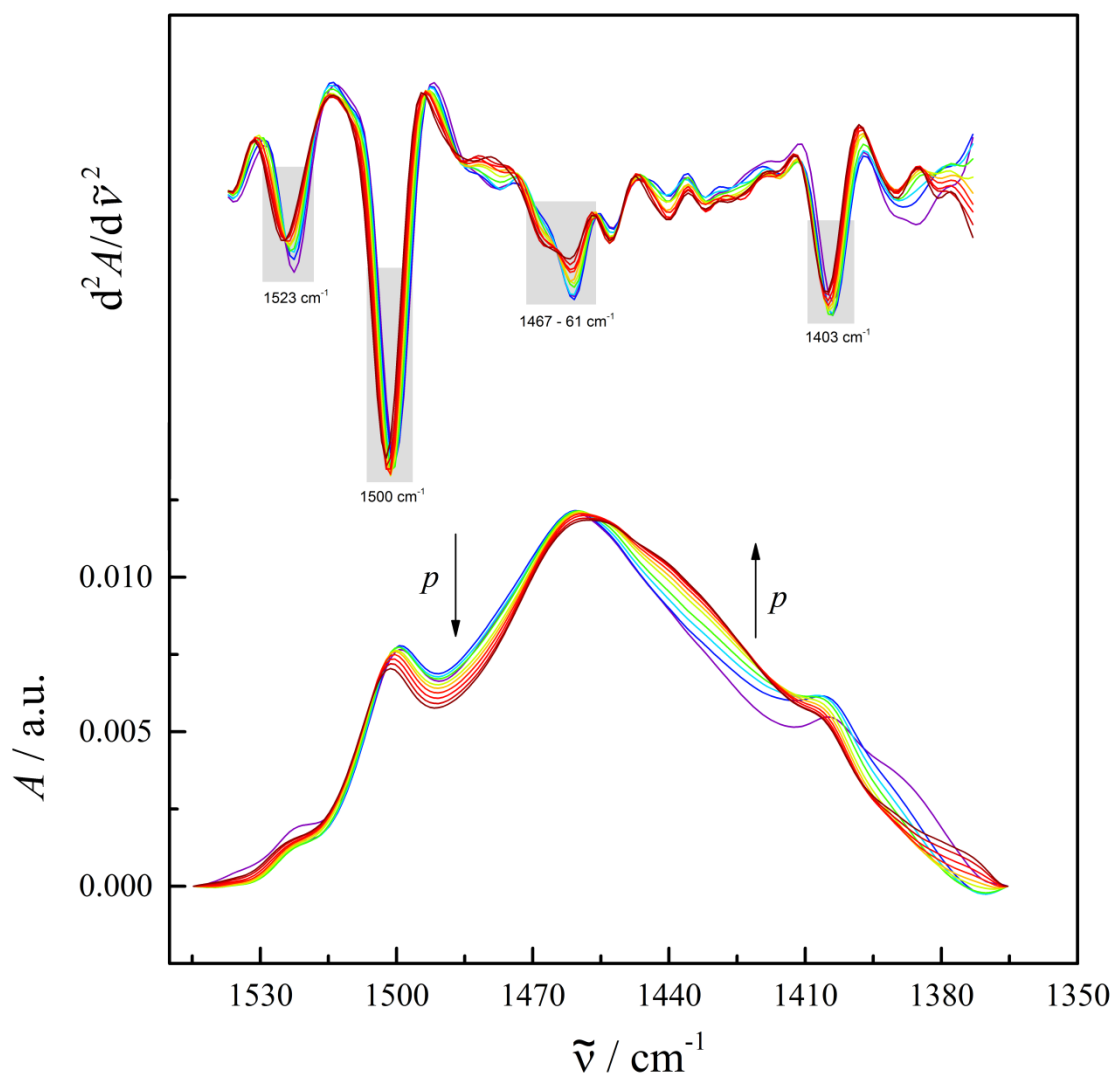
**Figure 40. Pressure-dependent normalized and second derivative spectra of the small RNA hairpin in the wavenumber region from 1600 to 1550  $\text{cm}^{-1}$  at 70  $^{\circ}\text{C}$ .** Second derivative and normalized spectra of 5  $\text{mg mL}^{-1}$  small RNA hairpin in 50  $\text{mM}$  Tris-HCl buffer + 0.1  $\text{mM}$  EDTA from 0.1 to 400 MPa at 70  $^{\circ}\text{C}$ . In the normalized spectra, the IR band at 1590 to 1575  $\text{cm}^{-1}$ , related to ring vibrations of C4 = C5 and C5 – C6 of free and base paired guanine, shows a significant wavenumber shift (indicated by the arrow). The IR band at 1568 to 1564  $\text{cm}^{-1}$ , related to ring vibrations of C6 = O6, C5 – C6 and C4 = C5 of free and base paired guanine, shows a small intensity decrease with increasing pressure (indicated by the arrow). The most important bands are indicated by the grey rectangle in the second derivative spectra. The highlighted bands are: 1586 - 81  $\text{cm}^{-1}$ , 1565 - 60  $\text{cm}^{-1}$ . (Selected data)

Figure 40 shows the pressure-dependent FTIR spectra of the sRNAH in 50  $\text{mM}$  Tris-HCl buffer pH 7.5 + 0.1  $\text{mM}$  EDTA, from 0.1 to 400 MPa at 70  $^{\circ}\text{C}$ , in the wavenumber

region from 1600 to 1550  $\text{cm}^{-1}$ . The two characteristic IR bands of this region are the bands around 1590 to 1575  $\text{cm}^{-1}$ , and 1568 to 1564  $\text{cm}^{-1}$ , respectively. Both of these bands arise from ring vibrations of  $\text{C6} = \text{O6}$ ,  $\text{C5} - \text{C6}$  and  $\text{C4} = \text{C5}$  of free and base paired guanine. Changes in the position of this band are related to the environment of guanine, and they are also used to follow the behavior of guanine-rich areas. The intensity of both IR bands reduce when guanine forms base pairs (for a more detailed RNA IR band assignment, see Table 1 in section 2.2.1.5). It can be observed that the IR band around 1576  $\text{cm}^{-1}$  shifts to higher wavenumber, to  $\sim 1582 \text{ cm}^{-1}$ , but the intensity does not change upon pressurization. The intensity of the IR band around 1565  $\text{cm}^{-1}$  reveals a small decrease with pressure, only. Obviously, high hydrostatic pressure does not have a significant effect on the ring vibrations of guanine of the sRNAH structure after thermal denaturation.

The thermal denaturation results of the sRNAH reveal that, at 70 °C, the structure was largely denatured, probably assuming a compact unfolded state, where some loop connections may still be present. Therefore, pressure has a small effect on the base pairing and base stacking interactions of the sRNAH under these conditions. It might induce some minor structural rearrangements only and does not promote formation of new native stem connections after thermal denaturation.

### 4.3.2.3. Small RNA hairpin base-sugar vibrations followed by FTIR spectroscopy



**Figure 41. Pressure-dependent normalized and second derivative spectra of the small RNA hairpin in the wavenumber region from 1540 to 1380  $\text{cm}^{-1}$  at 20 °C.** Second derivative and normalized spectra of 5  $\text{mg mL}^{-1}$  small RNA hairpin in 50 mM Tris-HCl buffer + 0.1 mM EDTA from 0.1 to 400 MPa at 20 °C. IR bands originate from base-sugar vibrations that are sensitive to glycosidic bond rotation, backbone and sugar pucker conformations. The IR bands are related to backbone vibrations in A-, B- and Z-forms, sugar pucker in N- or S-type conformations and N7 site vibrations of purines. The most important bands are indicated by the grey rectangle in the second derivative spectra. The highlighted bands are: 1523  $\text{cm}^{-1}$ , 1500  $\text{cm}^{-1}$ , 1467 – 61  $\text{cm}^{-1}$ , 1403  $\text{cm}^{-1}$ . (Selected data)

Figure 41 shows the pressure-dependent FTIR spectra of sRNAH in 50 mM Tris-HCl buffer pH 7.5 + 0.1 mM EDTA, from 0.1 to 400 MPa at 20 °C, in the wavenumber

region from 1540 to 1380  $\text{cm}^{-1}$ . The IR band at 1522  $\text{cm}^{-1}$ , which is characteristic of in-plane vibrations of cytosine shows small variations in intensity, only. The IR band at 1500  $\text{cm}^{-1}$ , which is also characteristic of in-plane vibrations of cytosine shows a more significant intensity decrease than the former band. This intensity decrease could be related to small structural rearrangements caused by pressure. The IR bands observed from 1490 to 1420  $\text{cm}^{-1}$  are assigned in the literature to adenine backbone vibrations, and unfortunately cannot be related to this sRNAH structure. An IR band can be observed at 1403  $\text{cm}^{-1}$ , which is assigned to RNA vibrations of the in-plane C – O – H deformation mode at the 2' position of the ribose ring [160]. These observations are in agreement with the others IR bands observed in the IR spectra of sRNAH, revealing that at lower temperatures, pressure has a small destabilizing effect on the sRNAH backbone and sugar pucker conformation only when compared to the thermal denaturation profile.

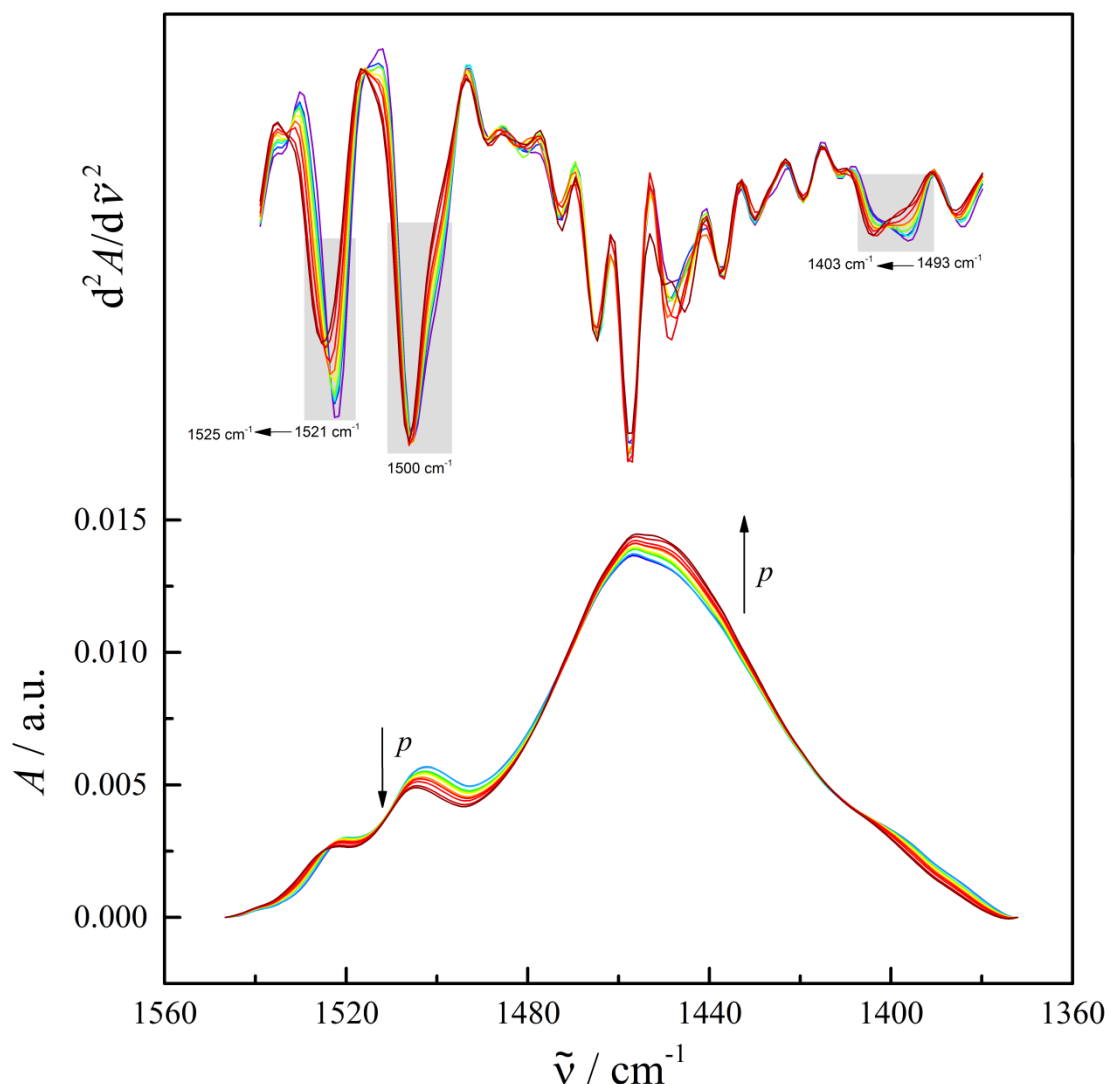


**Figure 42. Pressure-dependent normalized and second derivative spectra of the small RNA hairpin in the wavenumber region from 1560 to 1360  $\text{cm}^{-1}$  at 70  $^{\circ}\text{C}$ .** Second derivative and normalized spectra of 5  $\text{mg mL}^{-1}$  small RNA hairpin in 50  $\text{mM}$  Tris-HCl buffer + 0.1  $\text{mM}$  EDTA from 0.1 to 400 MPa at 70  $^{\circ}\text{C}$ . IR bands originate from base-sugar vibrations that are sensitive to glycosidic bond rotation, backbone and sugar pucker conformations. The IR bands are related to backbone vibrations in A-, B- and Z-forms, sugar pucker in N- or S-type conformations and N7 site vibrations of purines. The most important bands are indicated by the grey rectangle in the second derivative spectra. The highlighted bands are: 1525 - 21  $\text{cm}^{-1}$ , 1500  $\text{cm}^{-1}$ , 1403 - 93  $\text{cm}^{-1}$ . (Selected data)

Figure 42 shows the pressure-dependent FTIR spectra of sRNAH in 50  $\text{mM}$  Tris-HCl buffer pH 7.5 + 0.1  $\text{mM}$  EDTA, from 0.1 to 400 MPa at 70  $^{\circ}\text{C}$ , in the wavenumber region from 1540 to 1380  $\text{cm}^{-1}$ . The IR band at 1522  $\text{cm}^{-1}$ , which is characteristic of in-

plane vibrations of cytosine, shows a small shift to slightly higher wavenumber, only. The IR band at  $1500\text{ cm}^{-1}$ , which is also characteristic of in-plane vibrations of cytosine, has a more significant intensity decrease than the former band. This intensity decrease can be related to the small structural rearrangement caused by pressure, since the sRNAH is probably not fully unfolded. The sRNAH may consist of some unfolded/compact conformational states where small interactions between the nucleotides are still possible. The IR bands observed from  $1490$  to  $1420\text{ cm}^{-1}$  are assigned in the literature to adenine backbone vibrations and cannot be related to this sRNAH structure. An IR band can be observed at  $1400\text{ cm}^{-1}$ , which is assigned to RNA vibrations of the in-plane C – O – H deformation mode at the 2' position of the ribose ring [160].

The pressure-dependent FTIR results show that pressure does not favor the stabilization of more compact conformations and does not promote formation of new native stem connection as proposed by an earlier molecular dynamics study [55]. This theoretical study proposed an elliptical  $p$ ,  $T$ -stability diagram, where the structure of the sRNAH (gcUUCggc) could be denatured at high hydrostatic pressure and low temperature, and high hydrostatic pressure could promote the refolding of its native or near-native structure at high temperatures. In the present results, pressure revealed a small destabilizing effect at lower temperatures, but this seems to be a small fraction when compared to the thermal denaturation scenario. It has been shown in the literature that the free energy landscape of the sRNAH could have a variety of intermediate structures, classified as extended unfolded, compact unfolded, frayed and native [47]. These results together indicate that at high temperature, pressure may induce variations between different unfolded compact states, where many different loop arrangements can be found. At lower temperatures, pressure causes a minor destabilization of the native conformation that could promote a shift between native-like and frayed conformations.

#### **4.4. Summary and conclusions**

The conformational changes of the sRNAH, gcUUCGgc, were experimentally analyzed over a wide range of temperatures and pressures, by UV-vis spectroscopy and FTIR



spectroscopy. The temperature-dependent FTIR results showed that the sRNAH structure might not be fully unfolded, as extended chain ensemble, but it rather populates intermediates states of compact unfolded or coil like structures. In these compact unfolded structures, the double helical bonds of the native structure are lost, but apparently some loop interactions still remain. In the literature, molecular dynamics calculation showed that the small RNA molecule is highly stable and can have around 80,000 transition states, confirmed by the broad melting transition observed for the sRNAH. These states can vary between native structure, frayed structure, compact unfolded/coil like structure, and extended/fully unfolded structure. However, the fully extended state is an unpopulated state, and it can only be achieved under forced melting conditions [47].

The secondary structural features observed for sRNAH, in the pressure-dependent FTIR analysis shows that pressure has a small influence on the sRNAH structure at lower temperature, and it does not promote formation of new native stem connections at higher temperatures, the opposite as proposed by an earlier molecular dynamics study [55]. This theoretical study proposed an elliptical  $p, T$ -stability diagram, where the structure of the small RNA hairpin (gcUUCGgc) could denature at high hydrostatic pressure and low temperature, and high hydrostatic pressure could promote refolding to its native or near-native structure at higher temperatures. We show that pressure has a small destabilizing effect at lower temperatures, but this effect is rather small when compared to the thermal denaturation profile (Figure 43). Pressure can perturb the sRNAH structure and populate intermediate structures.

The formation of the Z-form backbone conformation of the small RNA hairpin is unfavorable, but as an intermediate state, it can occasionally be induced. For example, some conditions such as high salt concentrations can promote its formation. Molecular dynamics studies by Miner *et al.* (2016) [103] showed that high hydrostatic pressure has a stabilizing effect on the A-form, and destabilizes the Z-form of the RNA tetraloop (gcGCAAgc). We show that pressure has a small effect on the sugar pucker conformation of the sRNAH structure at low and high temperatures. These small changes indicate that

pressure causes small rearrangements of A-form RNA, only, but as proposed by theory, pressure did not induce Z-form RNA.

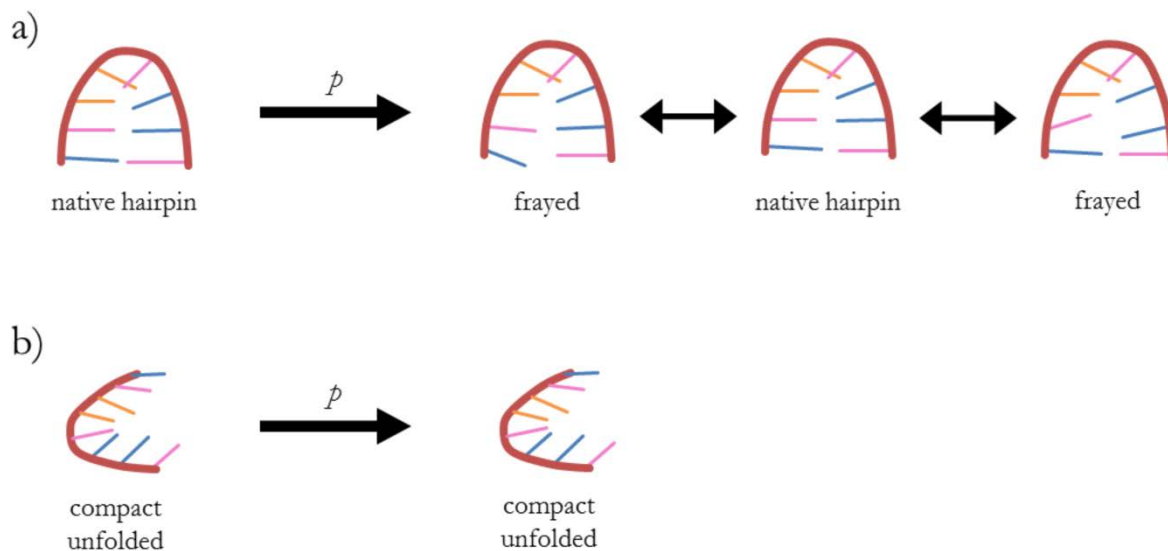


**Figure 43. Effect of temperature and pressure on the structure of the small RNA hairpin.** a) Effect of pressure on the small RNA hairpin structure at 20 °C. The native hairpin structure is slightly destabilized by pressure, inducing variations between native and native-like structures. b) Effect of pressure on the small RNA hairpin structure at 70 °C. The denatured hairpin structure is not affected by high hydrostatic pressure until 400 MPa.

Taken together, the temperature- and pressure-dependent FTIR results show that the small RNA hairpin is a highly stable secondary structure element, with a large free energy landscape and a wide variety of intermediate structures. However, high hydrostatic pressure was not able to promote compact conformations, or any new native stem connections, in disagreement with earlier theoretically proposed elliptical  $p, T$ -stability phase diagram. The thermodynamic stability presented by the small RNA hairpin brought by this study is an important information and it helps to understand the stability of biological systems living under extreme conditions.

---

## 5. Pressure modulation of the hairpin ribozyme structure and self-cleavage reaction



## **5.1. Background**

Ribozymes are catalytically active RNA molecules that can perform enzymatic reactions. Many ribozymes have been identified in the literature and they are responsible to perform different functions such as catalyzing peptide bond formation in the ribosome during protein synthesis, RNA splicing (self-cleaving RNA at groups I and II introns), conversion of transfer RNA from its precursor into transfer RNA by ribonuclease P, and also viral replication. The discovery of ribozymes contributed to the “RNA World” hypothesis, which suggests that early life arose from simple organisms, and RNA molecules were responsible for the storage of genetic information and metabolism. Those organisms would have developed under extreme conditions of temperature and pressure such as the deep-sea volcanic environment.

The hairpin ribozyme is one of the major naturally occurring ribozymes. It is derived from the minus strand of the satellite RNA from tobacco ringspot virus and it was the first autocatalytic RNA characterized. These satellite RNAs are single-stranded RNA molecules that replicate via a rolling circle mechanism. This mechanism is important for processing the produced RNA that was replicated from a circular positive-strand template. Discovery of such catalytically active RNAs, which simultaneously can store genetic information and act as biocatalysts, greatly supported the "RNA world" hypothesis.

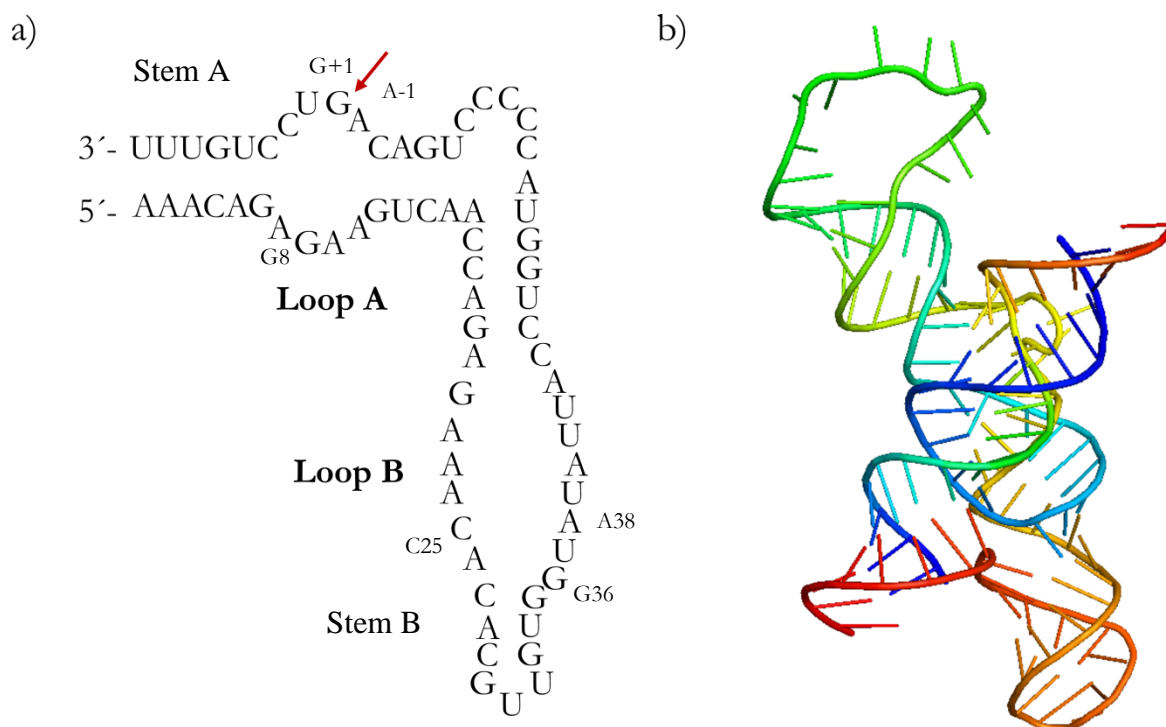


**Figure 44. Hairpin ribozyme secondary and tertiary structures.** a) Secondary structure of the hairpin ribozyme showing the conserved sequence of loop A and loop B, which are essential for catalysis. The cleavage site is indicated by a red arrow. b) Tertiary structure of the hairpin ribozyme in its active or docked state (Image of PDB: 1M5K [65] created using Pymol Molecular Graphic System, Version 1.8 Schrödinger, LLC).

The hairpin ribozyme is capable of catalyzing site-specific self-cleavage transesterification reactions at the RNA backbone (Figure 44a). The self-cleavage reaction involves the nucleophilic attack of the 2'-hydroxy group on the adjacent phosphorus atom, resulting in a 2', 3'-cyclic phosphate and a 5'-hydroxyl terminus (Figure 49) [56, 58, 59]. The reaction is supposed to follow a  $S_N2$  mechanism, in which the reverse reaction (ligation) can also be catalyzed. In this case, a 5'-hydroxyl attacks a cyclic 2', 3'-cyclic phosphate leading to ligation [60]. The hairpin ribozyme has about 50 conserved nucleotides in the RNA sequence necessary for it to be catalytically active. The conserved nucleotides are found in loop A and loop B (Figure 44a), and the helix nucleotides can be substituted to favor synthesis or crystallization [62, 64, 65]. The hairpin ribozyme was widely studied and represents an ideal system to study the structure and behavior of catalytic RNAs [27 - 30, 60 - 66]. The minimal two-way junction hairpin ribozyme structure, derived from the four-way junction structure, can be separated into two stems, stem A and stem B (Figure

44a). The correct folding and interaction between these two domains of the ribozyme are essential to promote catalysis (Figure 44b). In the satellite RNA, the stems A and B are part of a four-helix junction ribozyme, but most experiments in the literature were carried out with the minimal two-helix RNA structure, yet catalytically active. The interaction between these loops, also called docking, is responsible to generate the active conformation of the hairpin ribozyme (Figure 45). Catalysis happens at loop A, between nucleotides A<sub>5</sub> and G<sub>6</sub>. It is known that the correct folding of nucleic acids is facilitated by the presence of cations, and also the docking is facilitated by the cooperativity of cations such as Mg<sup>2+</sup>, excess of Na<sup>+</sup> or the inert cobalt(III) hexammine, which is isosteric with Mg(H<sub>2</sub>O)<sub>6</sub><sup>2+</sup>, but it cannot directly coordinate with water or RNA ligands. However, it has been shown in the literature that the hairpin ribozyme does not use cations to perform the self-cleavage reaction [60, 63, 65, 66].

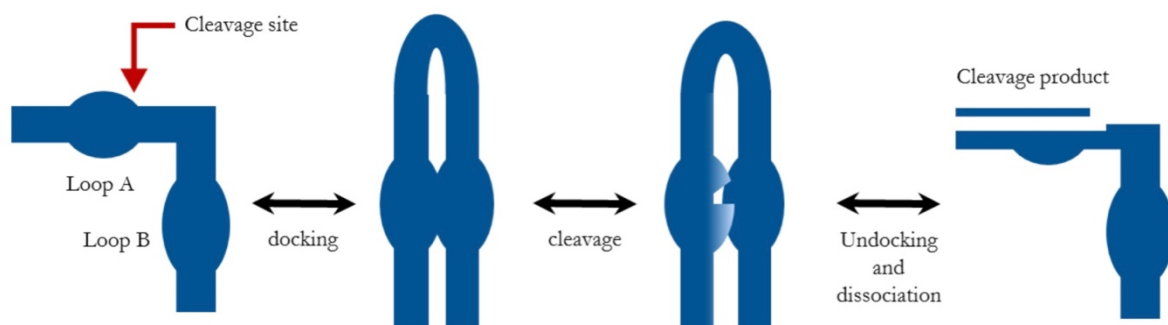


**Figure 45. Hairpin ribozyme docking and cleavage process.** Schematic representation of the hairpin ribozyme's self-cleavage process, which involves correct folding and docking of loop A upon loop B and further correct alignment of the nucleotides inside the cleavage pocket to favor the S<sub>N</sub>2-type transesterification reaction. After cleavage of the backbone and undocking of the loops, a small single strand product is released.

The hairpin ribozyme's structure is rearranged during the docking process, where stem A and B interact. Mutagenesis studies showed that the purine bases G8, A9, A10 and A 38 have an active function during catalysis. Analysis of the hairpin ribozyme crystal structure have shown that the scissile phosphate, G+1 (5'-hydroxyl product), actually adopts the proposed syn conformation and an in line arrangement with A-1 (2'-OH product) which enables the transition state of the S<sub>N</sub>2 transesterification reaction. Docking enables G+1

to make a Watson-Crick pair with C25, a hydrogen bond with G36 and A38, which highly stabilizes the cleavage pocket (Figure 46). It has been shown that mutations of G+1, C25 and A38 to any other nucleotides abolishes the hairpin ribozyme's activity [27, 28, 65].

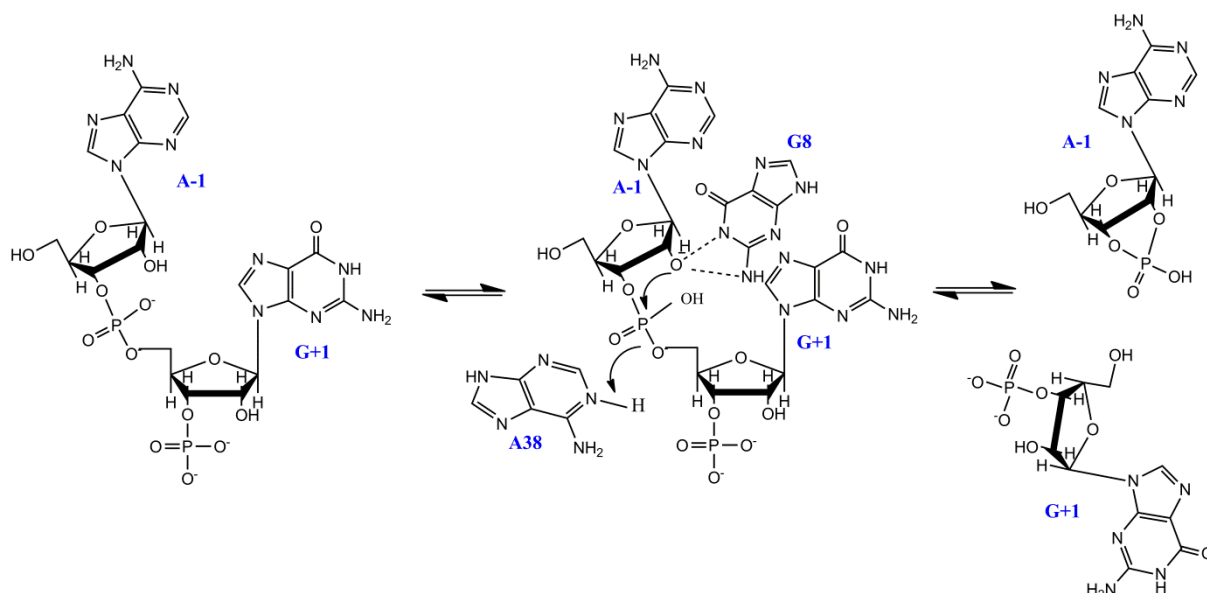


**Figure 46. Hairpin ribozyme nucleotides interaction in the cleavage pocket (ribozyme zipper/docked or active state).** Nucleotides directly involved in the  $S_N2$ -type transesterification reaction resulting in a 2', 3'-cyclic phosphate (A-1) and a 5'-hydroxyl terminus (G+1).

The application of high hydrostatic pressure to modulate the enzymatic activity of the hairpin ribozyme would help to characterize the structure, thermodynamics as well as kinetic parameters of its reaction [67, 68, 70 – 75]. There are a few studies in the literature about the effect of pressure on the catalytic reaction of the hairpin ribozyme. Kinetics studies using the wild type RNA sequence and modified RNA sequence of the hairpin ribozyme were performed under high hydrostatic pressure conditions. A positive activation volume ( $\Delta V^\ddagger$ ) of  $34 \pm 5 \text{ mL mol}^{-1}$  was determined, which was associated with a compaction of the ribozyme structure during docking, which must be accompanied by a consequent release/movement of water molecules and dehydration of the molecule. Osmotic shock experiments also showed that  $78 \pm 4$  water molecules were released per RNA molecule during the docking process [104 – 106].



Many organisms experience environmental stress such as extreme temperature and/or pressure, as found in the deep sea, hydrothermal vents and volcanic environments. In these places, up to kbar pressures are encountered. Moreover, such harsh environment was proposed to be the birthplace of life on Earth, or at least a similar one. High hydrostatic pressure studies are of particular interest to investigate ribozyme's conformational modifications necessary for catalysis.

## **5.2. Experimental details**

### **5.2.1. RNA molecules**

The different hairpin ribozyme molecules, non-labeled wild-type hairpin ribozyme, fluorescent labeled wild-type hairpin ribozyme and fluorescent labeled modified hairpin ribozyme, were synthesized by IBA Life Solutions for Life Science GmbH (Goettingen, Germany), and were received as lyophilized powder. The ribozymes were suspended in a 0.1 nmol  $\mu\text{L}^{-1}$  nuclease free water solution, and stored at - 80 °C.

Fluorescent labeled wild-type hairpin ribozyme molecules, with cyanine 3 and cyanine 5, were used in the Förster resonance energy transfer (FRET) measurements, performed in parallel studies by Dr. Salomé Pataraiá. The fluorescent labeled modified hairpin ribozyme molecules were used in order to compare with molecular dynamics simulations performed in collaboration with Prof. Dr. Dominik Marx's group. The analysis for the modified hairpin ribozyme can be found in the Appendix 8.2.

#### **5.2.1.1. Wild type hairpin ribozyme sequence**

**5'-AAACAGAGAAGUCAACCAGAGAAACACACGUUGUGGUAUAUUAACCGG  
UACCCCUGACAGUCCUGUUU-3'**

The wild type hairpin ribozyme (wtHpRz) creates a two-way junction hairpin ribozyme that independently folds in a helical domain, which is a simple model system of the original four-way junction tobacco ringspot virus satellite RNA.

### 5.2.1.1. FRET-labeled modified hairpin ribozyme sequence

**5'-cyanine 5-ACGGUGAGAAGGGAGGCAGAGAAACACAC-cyanine 3-GUCGU  
GGUACAUUACCUGCCACCCCUCCCAGUCCACCGU-3'**

The labeled modified hairpin ribozyme sequence (modHpRz) sequence is based on the well resolved crystal structure (resolution 2.05 Å) from Salter *et al.* (PDB ID: 2OUE) [108]. The experimental data was used to complement molecular dynamics simulations done in collaboration with Prof. Dr. Dominik Marx (Ruhr-Universität Bochum). It is a well resolved structure in its precatalytic form and suits the simulation purpose. Since only essential nucleobases are required for proper activity, the self-cleavage process is identical in wtHpRz, FRET-wtHpRz and FRET-modHpRz [59].

### 5.2.2. Sample preparation

Different HpRz concentrations were lyophilized to remove H<sub>2</sub>O, and were then suspended in pure 50 mM TRIS- HCl buffer + 0.1 mM EDTA, pH 7.5, to half of the final reaction volume. Samples were subjected to denaturation and renaturation steps (heated to 90 °C for 1 min and slowly cooled till 25 °C in 3 °C min<sup>-1</sup> steps) to ensure proper folding of the RNA loops. The cleavage reaction started by addition of the last half volume to the mixture, a 2X buffer solution of 50 mM TRIS- HCl + 0.1 mM EDTA + 12 mM MgCl<sub>2</sub> or 24 mM Cobalt (III) hexamine + 200 mM NaCl, pH 7.5. Final salt concentrations in the reaction medium were 6 mM MgCl<sub>2</sub> or 12 mM Cobalt (III) hexamine + 100 mM NaCl. The experiments were carried out multiple times, and different lots of RNA were used.

### 5.2.3. Fourier transform infrared spectroscopy

**5.2.3.1. Time dependent kinetics at ambient pressure:** The wtHpRz samples were lyophilized overnight and then diluted in 50 mM Tris-HCl buffer + 0.1 mM EDTA with 6 mM MgCl<sub>2</sub> or 12 mM [Co(NH<sub>3</sub>)<sub>6</sub>]Cl<sub>3</sub> + 100 mM NaCl, to a final concentration of 0.5 wt % in 50 µL volume. The duration of each measurement was 12 hours. The temperature was maintained at 25 °C in the

FTIR cell. The sample temperatures were equilibrated for 20 minutes before the acquisition of a new IR spectrum. The dead time between cell assembly and first spectrum collection should be as little as possible, and was about 10 minutes.

**5.2.3.2. Time dependent kinetics at high pressure:** The wtHpRz samples were lyophilized overnight and then diluted in 50 mM Tris-HCl buffer + 0.1 mM EDTA with 6 mM MgCl<sub>2</sub> or 12 mM [Co(NH<sub>3</sub>)<sub>6</sub>]Cl<sub>3</sub> + 100 mM NaCl, to a final concentration of 4.5 wt % in 6  $\mu$ L volume. The duration of each measurement was 12 hours. Three pressures were selected for this study and they are 50 MPa, 100 MPa and 150 MPa. The temperature was maintained at 25 °C in the FTIR cell. The dead time between cell assembling and first spectrum collection should be as little as possible, and was about 30 minutes.

#### **5.2.4. PAGE analysis of the reaction of hairpin ribozyme kinetics**

**5.2.4.1. Time dependent hairpin ribozyme reaction at ambient pressure:** The ambient pressure reactions were carried out in a thermoshaker (cooling thermal shake touch, VWR) with an accuracy of  $\pm$  2%. The lyophilized wtHpRz and the labeled-modHpRz samples were then dissolved in 50 mM Tris-HCl buffer, pH 7.5, with 0.1 mM EDTA, at a final concentration of 28.7  $\mu$ M. These samples were subjected to denaturation and renaturation. The self-cleavage reaction started by mixing the RNA solution 1:1 with 12 mM MgCl<sub>2</sub> or 24 mM [Co(NH<sub>3</sub>)<sub>6</sub>]Cl<sub>3</sub> + 200 mM NaCl buffer solution. All reactions were conducted at 25 °C, and the time varied from 0 to 360 min. The ribozyme's self-cleavage reaction was stopped by adding 1:1 stopping buffer (7 M urea + 50 mM EDTA, pH 7.5), with further addition of RNA loading buffer 2X (AMRESCO®), and stored in ice. Final aliquots of 10  $\mu$ L were stored at -80 °C.

**5.2.4.2. Time dependent hairpin ribozyme reaction at high pressure:** The high hydrostatic pressure reactions were carried out in a home-built high-pressure

vessel connected to a manual hydraulic pump, using water as pressure-transmitting medium. The temperature was controlled by an external water bath. The lyophilized wtHpRz and the labeled-modHpRz samples were then dissolved in 50 mM Tris-HCl buffer, pH 7.5, with 0.1 mM EDTA, at a final concentration of 28.7  $\mu$ M. These samples were subjected to denaturation and renaturation. The self-cleavage reaction started by mixing the RNA solution 1:1 with 12 mM MgCl<sub>2</sub> or 24 mM [Co(NH<sub>3</sub>)<sub>6</sub>]Cl<sub>3</sub> + 200 mM NaCl buffer solution in the home-built high pressure Teflon bottles. All reactions were conducted at 25 °C. The HpRz samples were maintained at different pressures, 1000 bar, 2000 bar and 3000 bar, from 0 to 360 min. Each data point, at each different time, was measured with a freshly prepared sample. The ribozyme's self-cleavage reaction was stopped by adding 1:1 stopping buffer (7 M urea + 50 mM EDTA, pH 7.5), with further addition of RNA loading buffer 2X (AMRESCO®), and stored in ice. Final aliquots of 10  $\mu$ L were stored at -80 °C.

#### **5.2.4.3. PAGE analysis**

The reaction products of the hairpin ribozyme were analyzed by denaturing Urea Polyacrylamide Gel Electrophoresis (Urea PAGE) using the XCell SureLock® Mini-Cell system (ThermoFisher) with Novex® 15% TBE-Urea gels (ThermoFisher) and TBE running buffer (Ambion®). Cleavage reaction's aliquots of 10  $\mu$ L containing 3.6  $\mu$ M of RNA were applied to the gels. After electrophoresis, the gels were directly stained with SYBR® Gold (Molecular Probes™), and the bands were analyzed by an ultraviolet (UV) transilluminator (AlphaImager Mini, ProteinSimple). The light intensity of each RNA fragment band was then quantified using ImageJ software (N.I.H., USA) [125], and the reaction product is presented by the percentage of cleaved RNA over the total RNA amount (cleaved RNA + native RNA).

## 5.3. Results and discussion

The pressure-induced effect on the self-cleavage reaction of the hairpin ribozyme was analyzed by PAGE and FTIR techniques. These combined techniques enable overall self-cleavage and structural analysis, respectively.

### 5.3.1. PAGE analysis of the hairpin ribozyme self-cleavage reaction

Several self-cleavage reactions were carried out at ambient and high hydrostatic pressure, and analyzed by PAGE as described in section 5.2. The PAGE results were analyzed by the ImageJ® software [125], and the intensity of each band was quantified as percentage of the fraction cleaved and plotted against time. Two different bands can be observed in the PAGE image of wild type hairpin ribozyme (Figure 47). The first one, close to the 70 base marker, is the native/non cleaved ribozyme (fraction native), and the second band is smaller, of around 60 bases size, is related to the large reaction product (fraction cleaved). The smallest reaction product was not efficiently detected. The fraction cleaved observed at the very beginning, denoted time 0' of the reaction, was considered the background of the self-cleavage reaction.

In Figure 50, the TBE-Urea PAGE image of the wild type hairpin ribozyme reaction at different pressure and ionic conditions is shown. It can be observed that, in the presence of MgCl<sub>2</sub> and at atmospheric pressure, there is an increase in the cleaved fraction band compared to the native fraction until 6 hours of measurement. The analysis of the hairpin ribozyme's catalysis without cations clearly shows that, until 6 hours of reaction, there is no change of the band representing the cleaved fraction. However, the hairpin ribozyme already has cleaved molecules even in the absence of cations. This observation is in agreement with the literature saying that the hairpin ribozyme does not require cations for its activity [66, 104 – 108], and that the inert [Co(NH<sub>3</sub>)<sub>6</sub>]<sup>3+</sup> is also capable to promote the hairpin ribozyme reaction without site interaction [108]. However, the PAGE image shows that cations favor the correct active conformation, hence favoring the self-cleavage reaction.

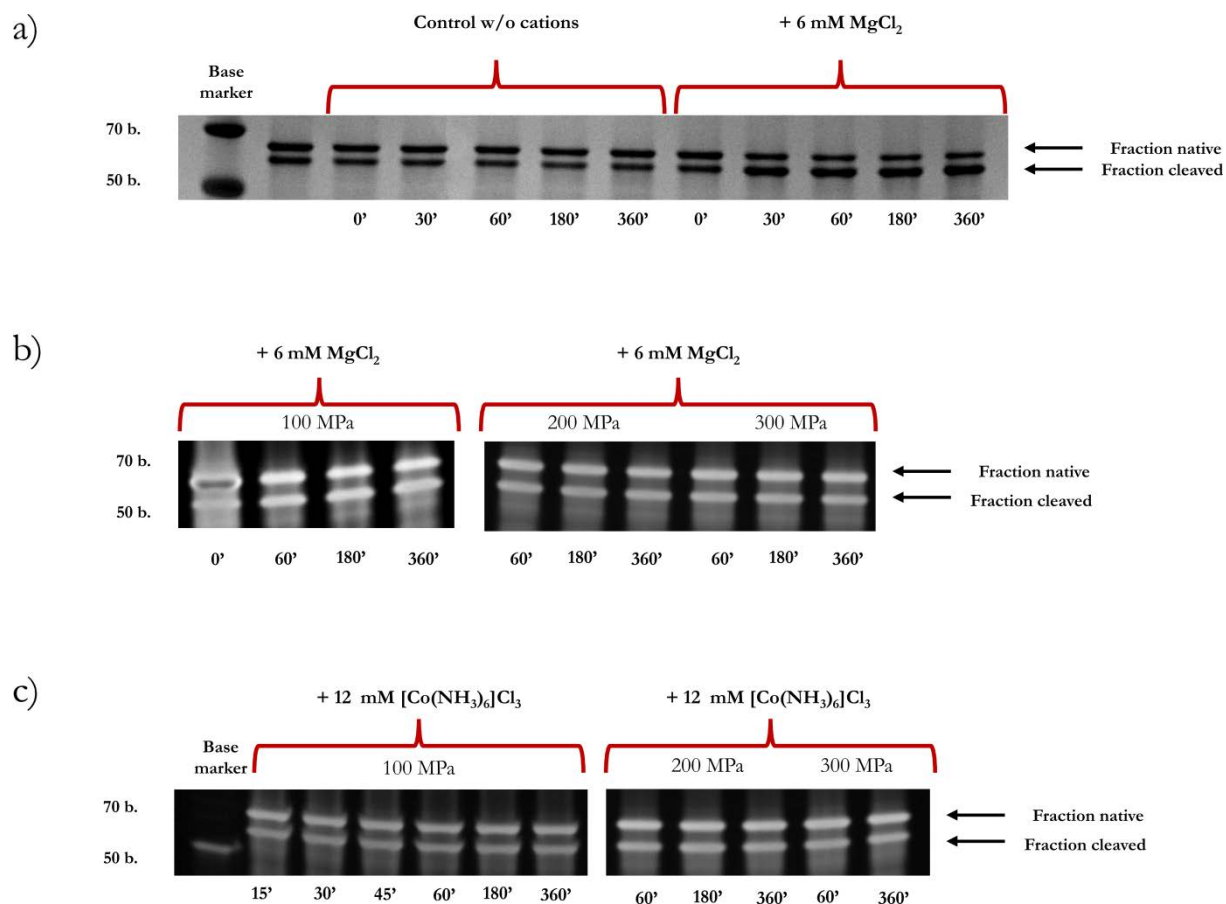


**Figure 47. TBE-Urea PAGE of the hairpin ribozyme's self-cleavage reaction.** a) The wtHpRz control reaction in pure Tris-HCl buffer + 0.1 mM EDTA pH 7.5 and in Tris-HCl buffer + 0.1 mM EDTA + 6 mM MgCl<sub>2</sub> pH 7.5, during 6 hours at 25 °C. b) The wtHpRz reaction in Tris-HCl buffer + 0.1 mM EDTA + 6 mM MgCl<sub>2</sub> pH 7.5, during 6 hours, from 100 to 300 MPa, at 25 °C. c) The wtHpRz reaction in pure Tris-HCl buffer + 0.1 mM EDTA pH 7.5 and in Tris-HCl buffer + 0.1 mM EDTA + 12 mM [Co(NH<sub>3</sub>)<sub>6</sub>]Cl<sub>3</sub> + 100 mM NaCl pH 7.5, during 6 hours, from 100 to 300 MPa, at 25 °C. (Selected data)

The RNA fragment bands were quantitatively analyzed by ImageJ [125], and the reaction product could be plotted against time for better interpretation of the data.

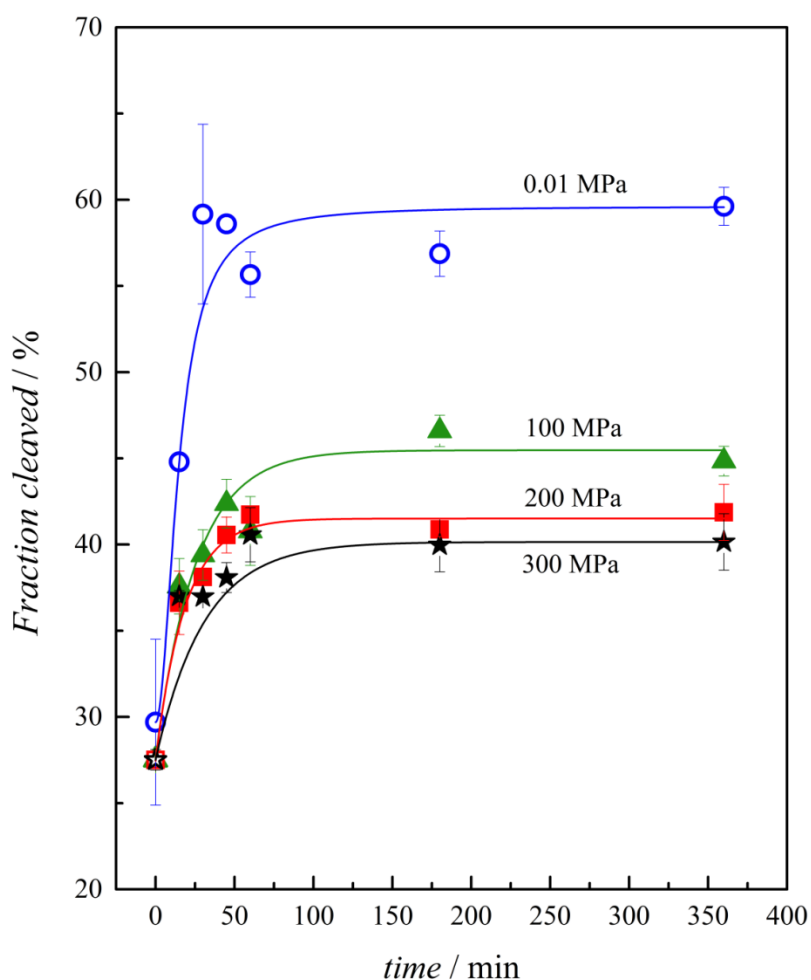


**Figure 48. Time evolution of the hairpin ribozyme's self-cleavage reaction with  $\text{MgCl}_2$  at different pressures.** Fraction of cleaved wtHpRz after addition of 6 mM  $\text{MgCl}_2$ . Self-cleavage reaction conditions were: 50 mM Tris-HCl buffer + 0.1 mM EDTA + 6 mM  $\text{MgCl}_2$ , pH 7.5, 25 °C at 0.1 MPa (blue), 100 MPa (green), 200 MPa (red) and 300 MPa (black). RNA final reaction aliquots, with 3.6  $\mu\text{M}$ , were analyzed by TBE-Urea PAGE and quantified by ImageJ [125].

It can be seen in Figure 48 and Figure 49 that the self-cleavage reaction rapidly reaches an equilibrium, which is achieved after 60 minutes of reaction for both  $\text{MgCl}_2$  and  $[\text{Co}(\text{NH}_3)_6]\text{Cl}_3$ . The percentage of fraction cleaved decreases for both  $\text{MgCl}_2$  and  $[\text{Co}(\text{NH}_3)_6]\text{Cl}_3$  conditions at pressures up to 300 MPa, hence the overall self-cleavage activity of the hairpin ribozyme is decelerated upon pressurization. However, a small

activity can still be observed in the first hour of reaction until equilibrium is reached. In addition, the maximum activity of the hairpin ribozyme at 1 bar in the presence of  $[\text{Co}(\text{NH}_3)_6]\text{Cl}_3$ , around 45% of the fraction cleaved, is smaller than the fraction cleaved in the presence of  $\text{MgCl}_2$ , which amount to  $\sim 60\%$  (Figure 48 and 49). The wtHpRz was less efficient in the presence of the  $[\text{Co}(\text{NH}_3)_6]\text{Cl}_3$  than in the presence of fully hydrated magnesium ions. In order to analyze which structure rearrangements affect the wtHpRz active state under high hydrostatic pressure, FTIR studies were performed.

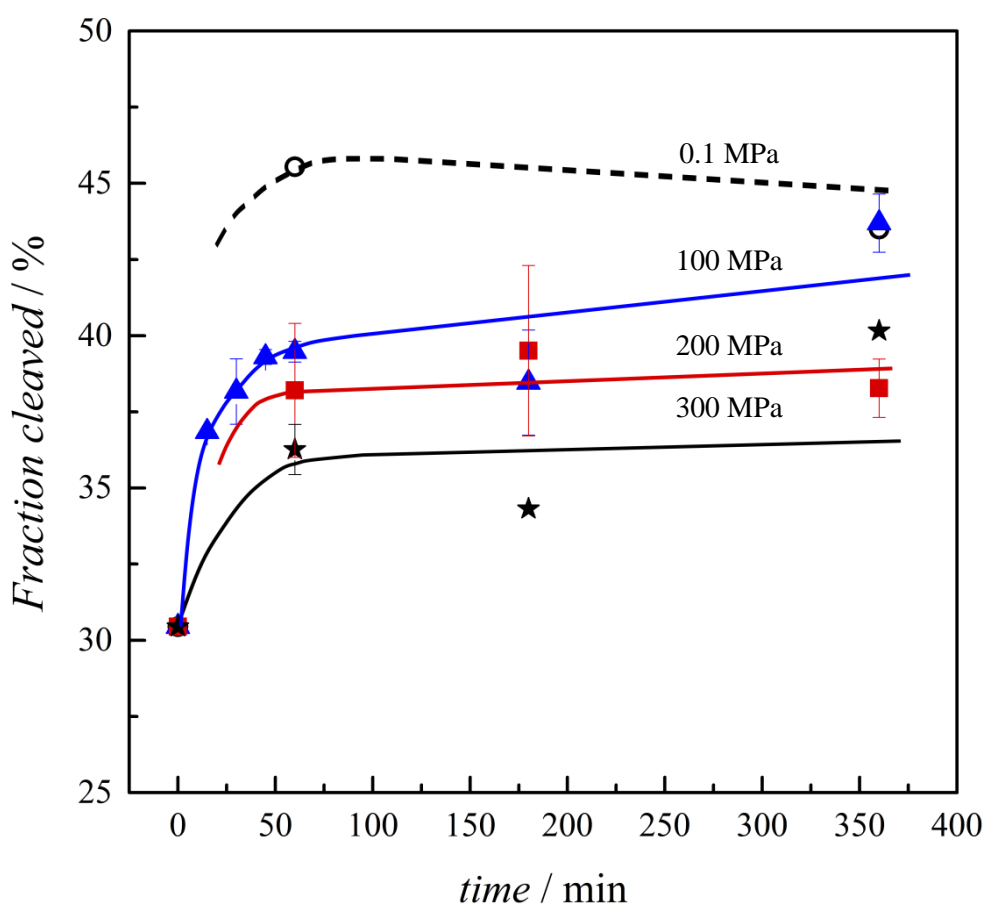


**Figure 49.** Time evolution of the hairpin ribozyme's self-cleavage reaction with  $[\text{Co}(\text{NH}_3)_6]\text{Cl}_3$  at different pressures. Fraction of cleaved wtHpRz after addition of 12 mM  $[\text{Co}(\text{NH}_3)_6]\text{Cl}_3$  + 100 mM NaCl. Self-cleavage reaction conditions were: 50 mM Tris-HCl buffer + 0.1 mM EDTA + 12 mM  $[\text{Co}(\text{NH}_3)_6]\text{Cl}_3$  + 100 mM NaCl, pH 7.5, 25 °C at 0.1 MPa (dotted line), 100 MPa (blue), 200 MPa (red) and 300 MPa (black). RNA final reaction aliquots, with 3.6  $\mu\text{M}$ , were analyzed by TBE-Urea PAGE and quantified by ImageJ [125].



### **5.3.2. FTIR analysis of the hairpin ribozyme's self-cleavage reaction**

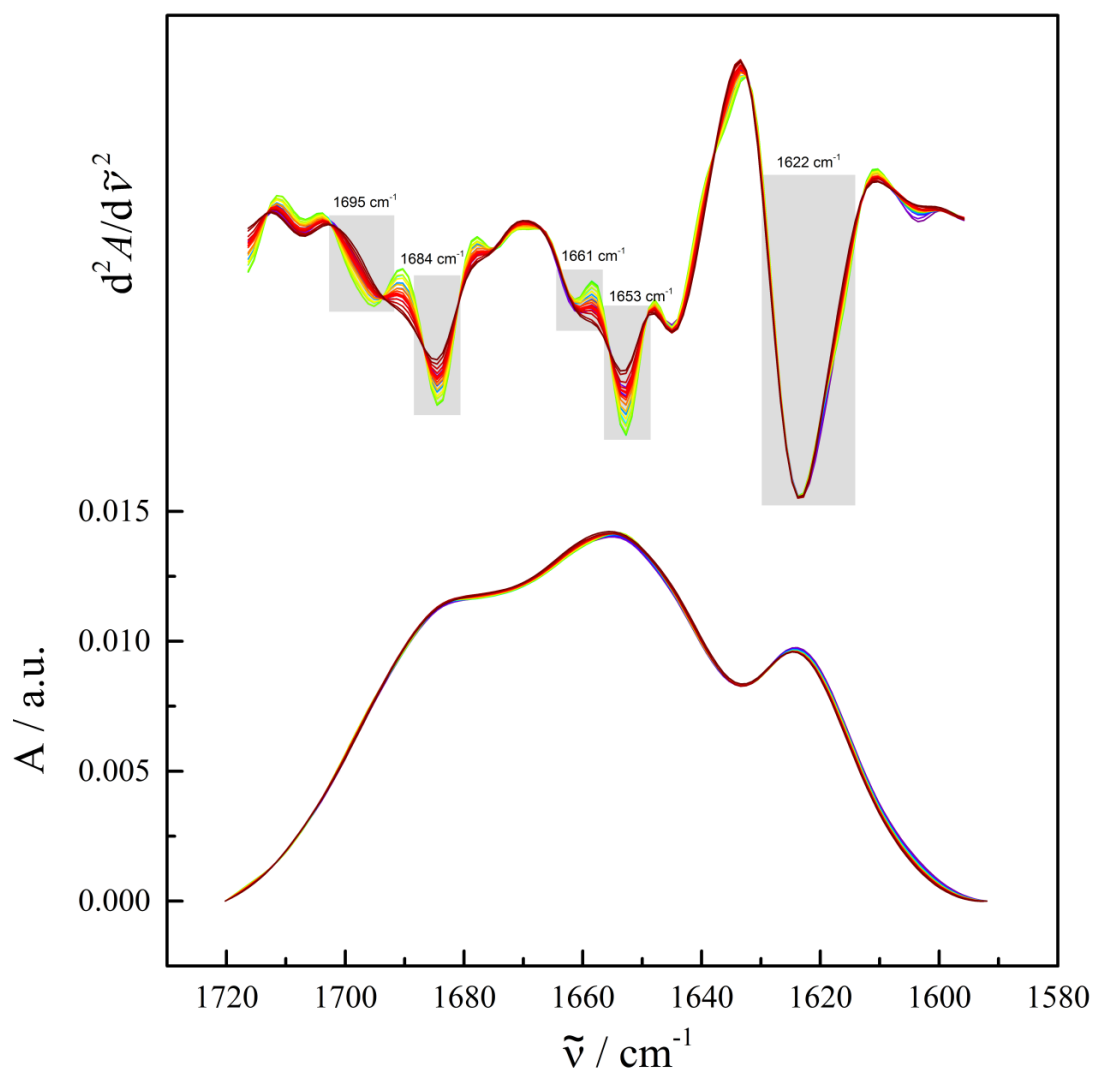
Conformational transitions of RNA molecules can be followed by FTIR spectroscopy under varied conditions. The RNA infrared signal can be divided into two main regions, from 1800 to 1500  $\text{cm}^{-1}$  (related to base pairing and base stacking interaction signals) and from 1500 to 1250  $\text{cm}^{-1}$  (related to glycosidic bond rotation, backbone conformation and sugar pucker). Detailed IR band assignment can be found in Table 1 in section 2.2.1.5.

#### **5.3.2.1. Time-dependent analysis of the structure and reaction of the hairpin ribozyme at ambient pressure**

##### **5.3.2.1.1. Hairpin ribozyme in-plane base vibrations sensitive to effects of base pairing followed by FTIR spectroscopy**

In the 1800 to 1500  $\text{cm}^{-1}$  wavenumber region, the IR bands are originating from nucleobase vibrations, which are sensitive to base stacking and base-pairing interactions. The IR bands are related to double or single strand vibrations, which include C=C, C=N, and C=O stretching of free and/or bonded nucleotides. A double strand to single strand transition results in a decrease in the intensity of the IR band at around 1696 to 1684  $\text{cm}^{-1}$  with a concomitant increase in the band at around 1677 to 1653  $\text{cm}^{-1}$ . The former arises from the C6=O6 stretch of base-paired guanine plus the C2=O2 stretch of uracil. The latter band arises mainly from the stretching vibrations of C6=O6 of free (i.e., non-base paired) guanine, the C2=O2 stretch of free cytosine, and the C4=O4 stretch of free uracil [114, 136]. For better analysis of the IR bands the 1800 to 1500  $\text{cm}^{-1}$  region can be divided into two areas: from 1720 to 1600  $\text{cm}^{-1}$ , and from 1600 – 1550  $\text{cm}^{-1}$ .

## A. Hairpin ribozyme in the absence of cations

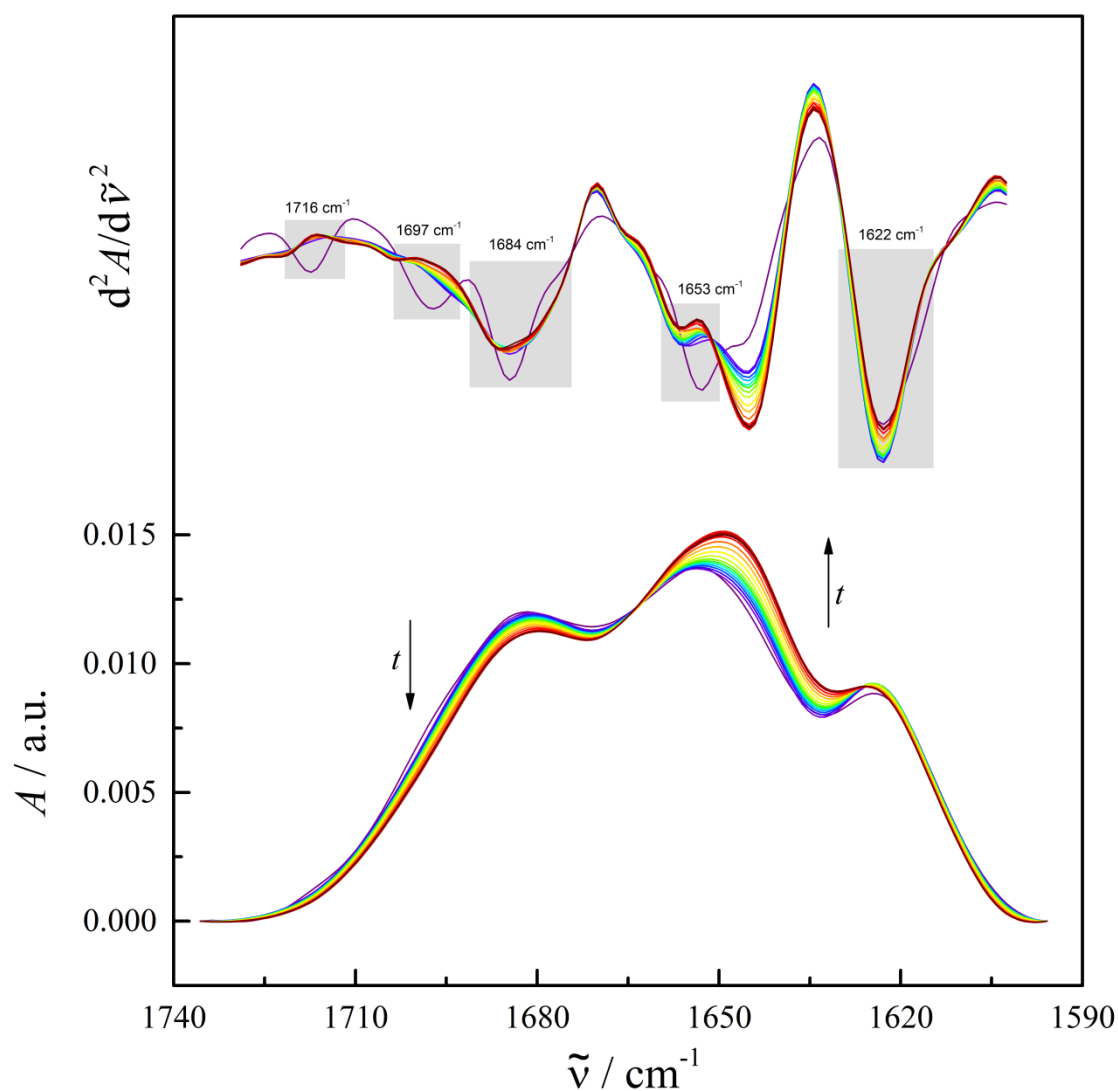


**Figure 50. Time-dependent normalized and second derivative FTIR spectra of the hairpin ribozyme without cations at atmospheric pressure, in the wavenumber region from 1720 to 1580  $\text{cm}^{-1}$ .** Second derivative and normalized spectra of 45  $\text{mg mL}^{-1}$  wtHpRz in 50  $\text{mM}$  Tris-HCl buffer + 0.1  $\text{mM}$  EDTA from 10 to 600 minutes at 25  $^{\circ}\text{C}$  and 0.1 MPa. In the normalized spectra, the IR band from 1696 to 1684  $\text{cm}^{-1}$  is related to base paired nucleotides and does not change with time, and the IR band from 1677 to 1653  $\text{cm}^{-1}$  is related to free nucleotides and also does not change with time. The most important bands are indicated by the grey rectangle at the second derivative spectra. The highlighted bands are: 1695  $\text{cm}^{-1}$ , 1684  $\text{cm}^{-1}$ , 1661  $\text{cm}^{-1}$ , 1653  $\text{cm}^{-1}$ , 1622  $\text{cm}^{-1}$ . (Selected data)

Figure 50 shows the time-dependent FTIR spectra of the wtHpRz in 50  $\text{mM}$  Tris-HCl buffer pH 7.5 + 0.1  $\text{mM}$  EDTA at 25  $^{\circ}\text{C}$ , during 600 minutes, in the wavenumber region

from 1720 to 1600  $\text{cm}^{-1}$ . Structural changes of the ribozyme due to its self-cleavage activity can be followed by changes in the IR band around 1683  $\text{cm}^{-1}$  and 1655  $\text{cm}^{-1}$ . The self-cleavage activity is detected by a decrease in absorbance ( $A$ ) of the IR band at 1684  $\text{cm}^{-1}$ , which is characteristic of base paired G-C vibrations, and the concomitant increase in IR intensity of unpaired nucleic acids at around 1654  $\text{cm}^{-1}$ , which is a combination of free base vibrations of guanine and uracil. There is not any significant change at these bands without cations, as seen in the normalized spectra. The second derivative spectra show that there are small variations at the IR band intensities only. Most of the IR bands intensity fluctuates between higher and lower values during the entire 10 hours of measurement.

The IR bands observed are described as follows. The IR band at 1696  $\text{cm}^{-1}$  is related to the C2=O2 stretch of uracil. The IR band at 1684  $\text{cm}^{-1}$ , related to C6=O6 base paired vibrations of guanine, can be related to the formation of single stranded product and/or undocking. The IR at 1661  $\text{cm}^{-1}$  is assigned to C6=O6 free base vibrations of guanine. The IR band at 1653  $\text{cm}^{-1}$  is related to free base vibrations of uracil (C4=O4 stretch), which can also be related to product formation. A concomitant IR band at 1645  $\text{cm}^{-1}$  is related to C2=O2 stretch of cytosine, and it can also be related to undocking/release of the product, since this band decrease when cytosine is base paired, however no changes are observed in this wavenumber region. The IR band at 1623  $\text{cm}^{-1}$ , related to C=N and C=C ring vibrations of adenine and/or in-plane vibrations of cytosine, does also shows no change during the 10 hours of measurement.

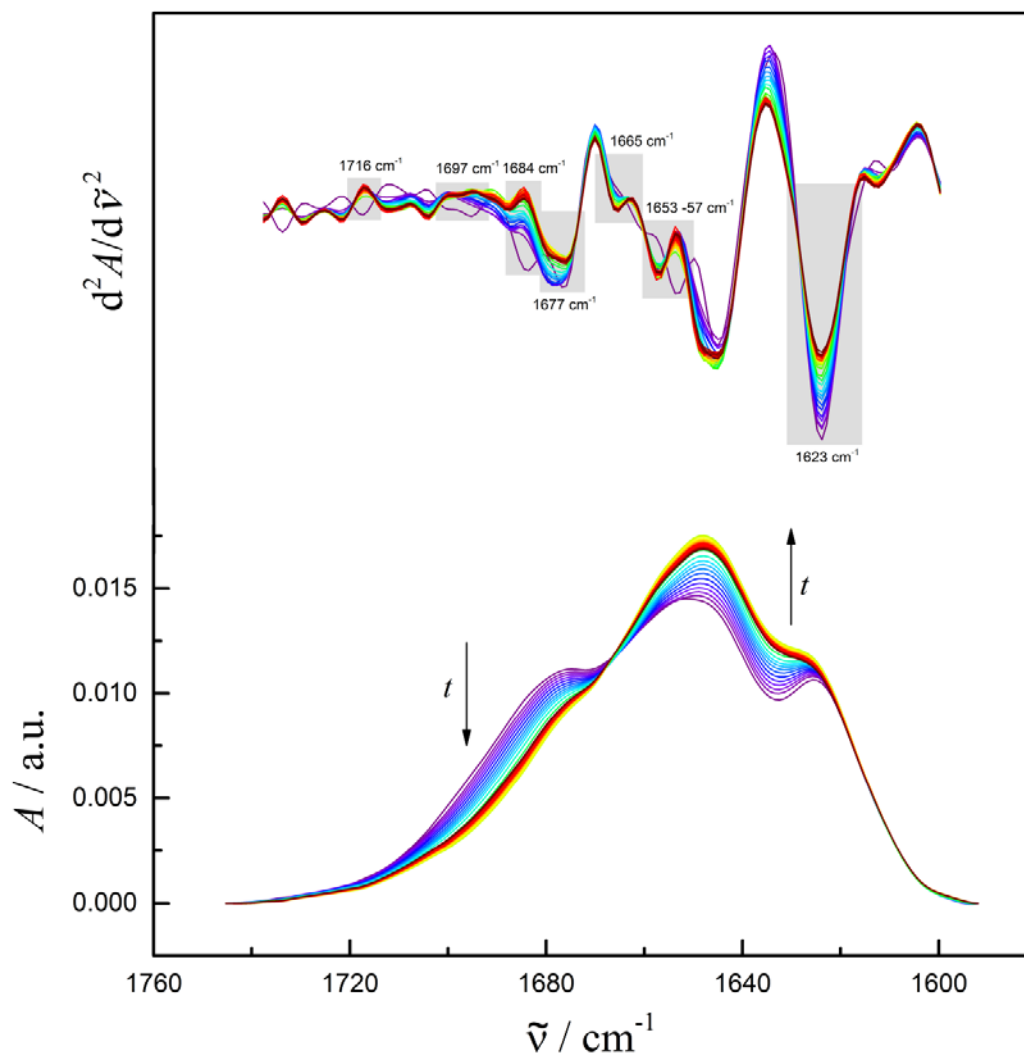
B. Hairpin ribozyme in the presence of  $\text{MgCl}_2$ 

**Figure 51.** Time-dependent normalized and second derivative FTIR spectra of the hairpin ribozyme with  $\text{MgCl}_2$  at atmospheric pressure, in the wavenumber region from 1740 to 1590  $\text{cm}^{-1}$ . Second derivative and normalized spectra of 45  $\text{mg mL}^{-1}$  wtHpRz in 50 mM Tris-HCl buffer + 0.1 mM EDTA + 6 mM  $\text{MgCl}_2$  from 10 to 600 minutes at 25  $^\circ\text{C}$  (0.1 MPa). In the normalized spectra, the IR band from 1696 to 1684  $\text{cm}^{-1}$  is related to base paired nucleotides and decreases in intensity with time (indicated by the arrow). The IR band from 1677 to 1653  $\text{cm}^{-1}$  is related to free nucleotides and increases in intensity with time (indicated by the arrow). The most important bands are indicated by the grey rectangle at the second derivative spectra. The highlighted bands are: 1716  $\text{cm}^{-1}$ , 1697  $\text{cm}^{-1}$ , 1684  $\text{cm}^{-1}$ , 1653  $\text{cm}^{-1}$ , 1622  $\text{cm}^{-1}$ . (Selected data)

The normalized and second derivative time-dependent FTIR spectra of the wtHpRz in 50 mM Tris-HCl buffer pH 7.5 + 0.1 mM EDTA + 6 mM MgCl<sub>2</sub> at 25 °C are shown, during 660 minutes in the wavenumber region from 1720 to 1600 cm<sup>-1</sup> in Figure 51. Ribozyme's self-cleavage reaction includes creation of new base pairs during docking (at ≈ 1682 cm<sup>-1</sup>), and further increase of free bases (at ≈ 1654 cm<sup>-1</sup>) after undocking and release of the product. Some specific bands related to the ribozyme's conformational change are highlighted in the second derivative spectra. The IR band at 1717 cm<sup>-1</sup>, involved in Hoogsteen third strand binding (G\*C-C), decreases over the first hour of the reaction. This IR band can be related to the third strand binding of G36\*G+1.C25 found in the crystal structure of a hairpin ribozyme docked conformation [65]. The band disappears after one hour of measurement, when the ribozyme achieves the reaction equilibrium as observed in the PAGE results (Figure 48). In addition, this IR band is not observed in the spectra of wtHpRz without cations (Figure 50).

The IR band at 1696 cm<sup>-1</sup> is related to C2=O2 stretch of uracil and disappears until the reaction equilibrium is reached. The IR band at 1684 cm<sup>-1</sup>, characteristic of base paired G-C vibrations, shows a decrease in intensity and a small shift to higher wavenumbers, which can be related to the formation of single stranded product and/or undocking. It can be observed, in the second derivative spectra, that the IR band at 1684 cm<sup>-1</sup> shows a pronounced decrease during the first hour of the reaction. In addition, it splits into two different IR bands, with lower and higher wavenumbers, indicating that the wtHpRz consist of different non-active structural components after achieving reaction equilibrium. The IR band at 1653 cm<sup>-1</sup>, related to free base vibrations of uracil (C4=O4 stretch), decreases with time and shifts to higher wavenumbers, which can be related to product formation. The IR band at 1623 cm<sup>-1</sup>, related to C=N and C=C ring vibrations of adenine and/or in-plane vibrations of cytosine, also decreases during the self-cleavage reaction.

The changes observed in the IR bands (1696 cm<sup>-1</sup>, 1684 cm<sup>-1</sup> and 1653 cm<sup>-1</sup>) in the hairpin ribozyme's spectra without and with MgCl<sub>2</sub>, in the wavenumber region from 1720 – 1600 cm<sup>-1</sup>, revealed that cations are responsible for the stabilization of the active state of the ribozyme and favors the self-cleavage reaction.

C. Hairpin ribozyme in the presence of  $[\text{Co}(\text{NH}_3)_6]\text{Cl}_3$ 

**Figure 52.** Time-dependent normalized and second derivative FTIR spectra of the hairpin ribozyme with  $[\text{Co}(\text{NH}_3)_6]\text{Cl}_3$  at atmospheric pressure, in the wavenumber region from 1760 to 1600  $\text{cm}^{-1}$ . Second derivative and normalized spectra of 45  $\text{mg mL}^{-1}$  wtHpRz in 50 mM Tris-HCl buffer + 0.1 mM EDTA + 12 mM  $[\text{Co}(\text{NH}_3)_6]\text{Cl}_3$  + 100 mM NaCl from 10 to 600 minutes at 25  $^\circ\text{C}$ , 0.1 MPa. In the normalized spectra, the IR band from 1696 to 1684  $\text{cm}^{-1}$  is related to base paired nucleotides and decreases in intensity with time (indicated by the arrow). The IR band from 1677 to 1653  $\text{cm}^{-1}$  is related to free nucleotides and exhibits a small increase in intensity with time (indicated by the arrow). The most important bands are indicated by the grey rectangle in the second derivative spectra. The highlighted bands are: 1716  $\text{cm}^{-1}$ , 1697  $\text{cm}^{-1}$ , 1688  $\text{cm}^{-1}$ , 1677  $\text{cm}^{-1}$ , 1665  $\text{cm}^{-1}$ , 1657 - 53  $\text{cm}^{-1}$ , 1623  $\text{cm}^{-1}$ . (Selected data)

Figure 52 shows the normalized and second derivative time-dependent FTIR spectra of the wtHpRz in 50 mM Tris-HCl buffer pH 7.5 + 0.1 mM EDTA + 12 mM  $[\text{Co}(\text{NH}_3)_6]\text{Cl}_3$  + 100 mM NaCl at 25 °C, 0.1 MPa, during 660 minutes, in the wavenumber region from 1720 to 1600  $\text{cm}^{-1}$ . It can be observed in the normalized spectra that there is a decrease in intensity of the IR band at 1684  $\text{cm}^{-1}$ , which is related to the C6 = O6 stretch vibrations of base paired guanine and C4 = O4 stretch vibrations of base paired uracil, with a concomitant increase of the IR band at 1654  $\text{cm}^{-1}$ , assigned to the C6 = O6 stretch of free guanine and C4 = O4 stretch of free uracil. The intensity changes during 3 hours of the reaction and it reaches an equilibrium. However, the PAGE result (Figure 52) shows that, at atmospheric pressure, the reaction reaches equilibrium in one hour. This indicates that many of the structural rearrangements observed by FTIR result from these variations of base paired and free base vibrations, but they are not directly related to cleavage and product formation during the entire 6 hours of measurement.

It is indicated in Figure 52, in the second derivative spectra, that some specific IR bands are related to the ribozyme's conformational changes. The IR band at 1717  $\text{cm}^{-1}$ , involved in Hoogsteen third strand binding ( $\text{G}^*\text{C}-\text{C} \rightarrow \text{G36}^*\text{G}+1.\text{C25}$ ) [65], rapidly decreases in the first 30 minutes of the reaction. This band disappears after 30 minutes of measurement as observed for  $\text{MgCl}_2$  (Figure 51). However, the ribozyme achieves equilibrium after one hour of reaction, only (Figure 52). The IR bands at 1700  $\text{cm}^{-1}$  and 1696  $\text{cm}^{-1}$  are related to the C2=O2 stretch of uracil and they also disappear after 30 minutes of the reaction. The IR band at 1684  $\text{cm}^{-1}$ , characteristic of base paired vibrations of guanine, displays also a rapid decrease in 30 minutes of reaction. It does not show the same behavior as with  $\text{MgCl}_2$ , indicating that different conformations and interactions are promoted, depending on the ion present. The IR band at 1676  $\text{cm}^{-1}$  is related to C4=O4 stretch vibrations of uracil and gradually decreases during 3 hours of reaction. This IR band is not observed in the wtHpRz FTIR spectra in the presence of  $\text{MgCl}_2$ , while a strong signal is detected in the presence of  $[\text{Co}(\text{NH}_3)_6]\text{Cl}_3$ . This clearly indicates that, in the presence of the  $[\text{Co}(\text{NH}_3)_6]\text{Cl}_3$  complex, the wtHpRz adopts different conformations when compared with the ones found in the presence of  $\text{MgCl}_2$ .

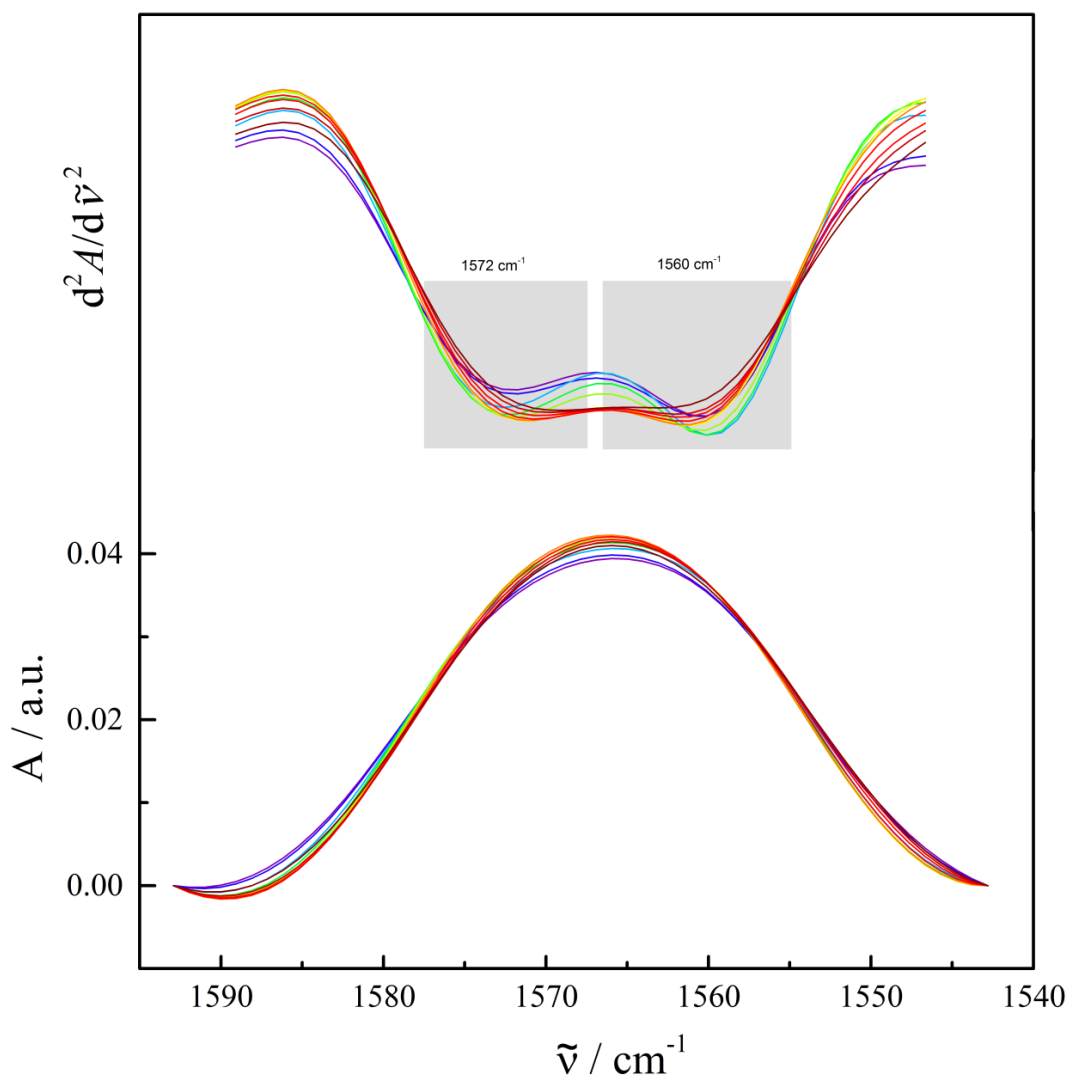
The IR band at  $1665\text{ cm}^{-1}$  appears during the reaction time and increases until 3 hours of the reaction. It is assigned to C6=O6 stretch vibrations of free guanine. The IR band at  $1653\text{ cm}^{-1}$ , related to free base vibrations of uracil (C4=O4 stretch), decreases in 30 minutes of the reaction and shifts to  $1657\text{ cm}^{-1}$ , indicating that different populations are favored with time. A concomitant IR band at  $1645\text{ cm}^{-1}$  related to C2=O2 stretch of cytosine, increases during 3 hours of reaction. These IR bands,  $1665\text{ cm}^{-1}$  and  $1657\text{ cm}^{-1}$  can be related to undocking/release of the single stranded product. The IR band at  $1623\text{ cm}^{-1}$ , related to C=N and C=C ring vibrations of adenine and/or in-plane vibrations of cytosine, increases in intensity during 3 hours of the self-cleavage reaction.

It has been shown in the work of D. Lambert *et al.* (2006) [162], through photo crosslink studies of the active residues U+2 and C+3, that they adopt different conformations in the presence of  $[\text{Co}(\text{NH}_3)_6]\text{Cl}_3$  when compared to the crystal structure in the presence of  $\text{MgCl}_2$ .  $[\text{Co}(\text{NH}_3)_6]\text{Cl}_3$  is able to induce covalent interaction between U+2.G36. The FTIR spectra (Figure 52) clearly show that several IR bands exhibits a different behavior in the presence of  $[\text{Co}(\text{NH}_3)_6]\text{Cl}_3$ , and new IR bands appear, such as of  $1700\text{ cm}^{-1}$  and  $1665\text{ cm}^{-1}$ , indicating that the reaction in the presence of  $[\text{Co}(\text{NH}_3)_6]\text{Cl}_3$  promotes different conformations and interactions between the nucleotides. However, these conformational changes do not result in more product formation (Figure 52), but probably in different non-active conformational states.



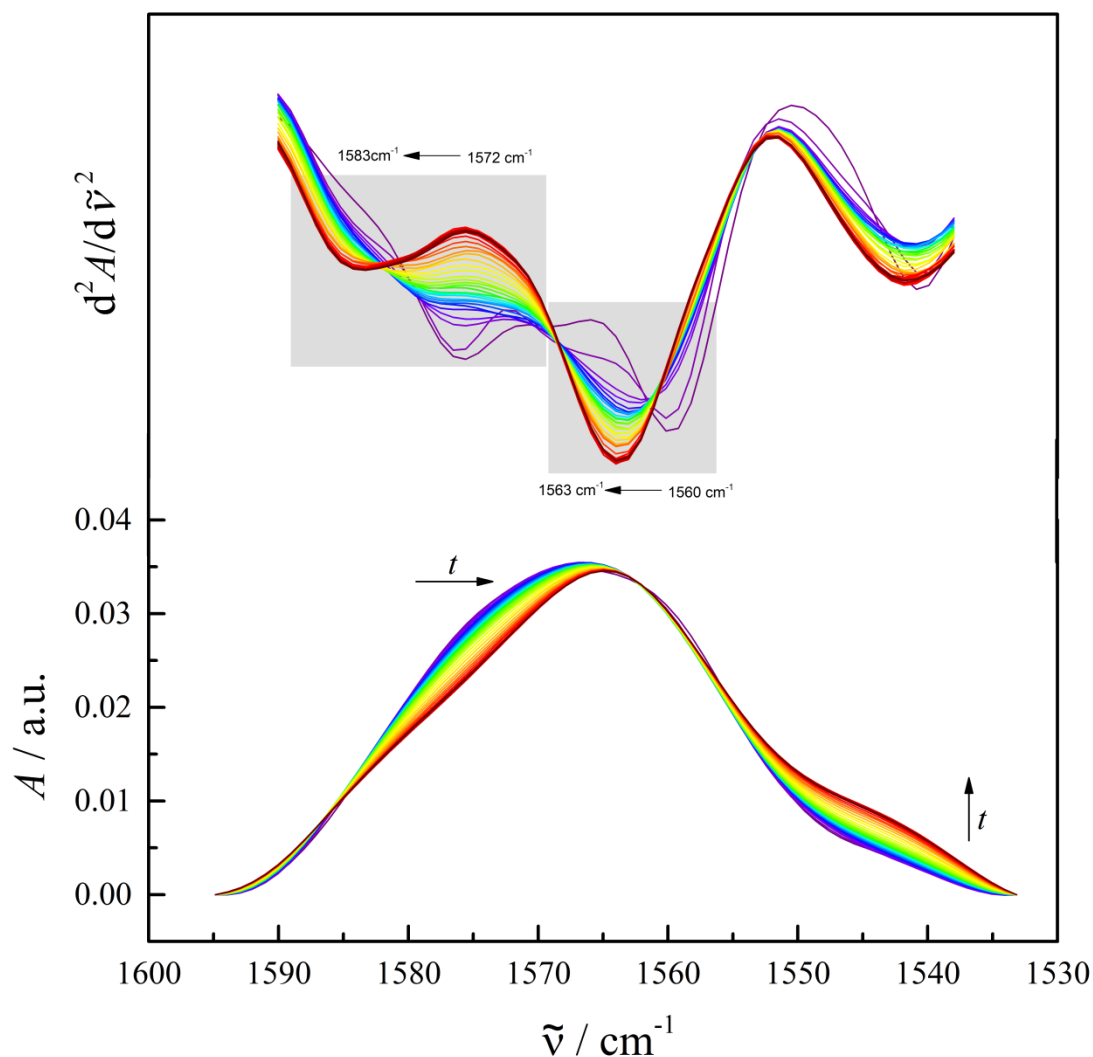
### 5.3.2.1.2. Hairpin ribozyme in-plane base vibrations sensitive to effects of base stacking followed by FTIR spectroscopy

#### A. Hairpin ribozyme in the absence of cations



**Figure 53.** Time-dependent normalized and second derivative FTIR spectra of the hairpin ribozyme without cations at atmospheric pressure, in the wavenumber region from 1600 to 1540  $\text{cm}^{-1}$ . Second derivative and normalized spectra of 45  $\text{mg mL}^{-1}$  wtHpRz in 50 mM Tris-HCl buffer + 0.1 mM EDTA from 10 to 600 minutes at 25  $^{\circ}\text{C}$  and 0.1 MPa. In the normalized spectra, the IR band has its maximum at 1565  $\text{cm}^{-1}$  and its intensity increases slightly with time. In the second derivative spectra, two distinct IR band are highlighted: the IR band at 1590 to 1575  $\text{cm}^{-1}$  is related to ring vibrations of C4 = C5 and C5 – C6 of free and base paired guanine and has small variations in intensity, and the IR band at 1568 to 1564  $\text{cm}^{-1}$ , related to ring vibrations of C6 = O6, C5 – C6 and C4 = C5 of free and base paired guanine, also shows small variations in intensity. These bands are indicated by the grey rectangle in the second derivative spectra. The highlighted bands are: 1572  $\text{cm}^{-1}$ , 1560  $\text{cm}^{-1}$ . (Selected data)

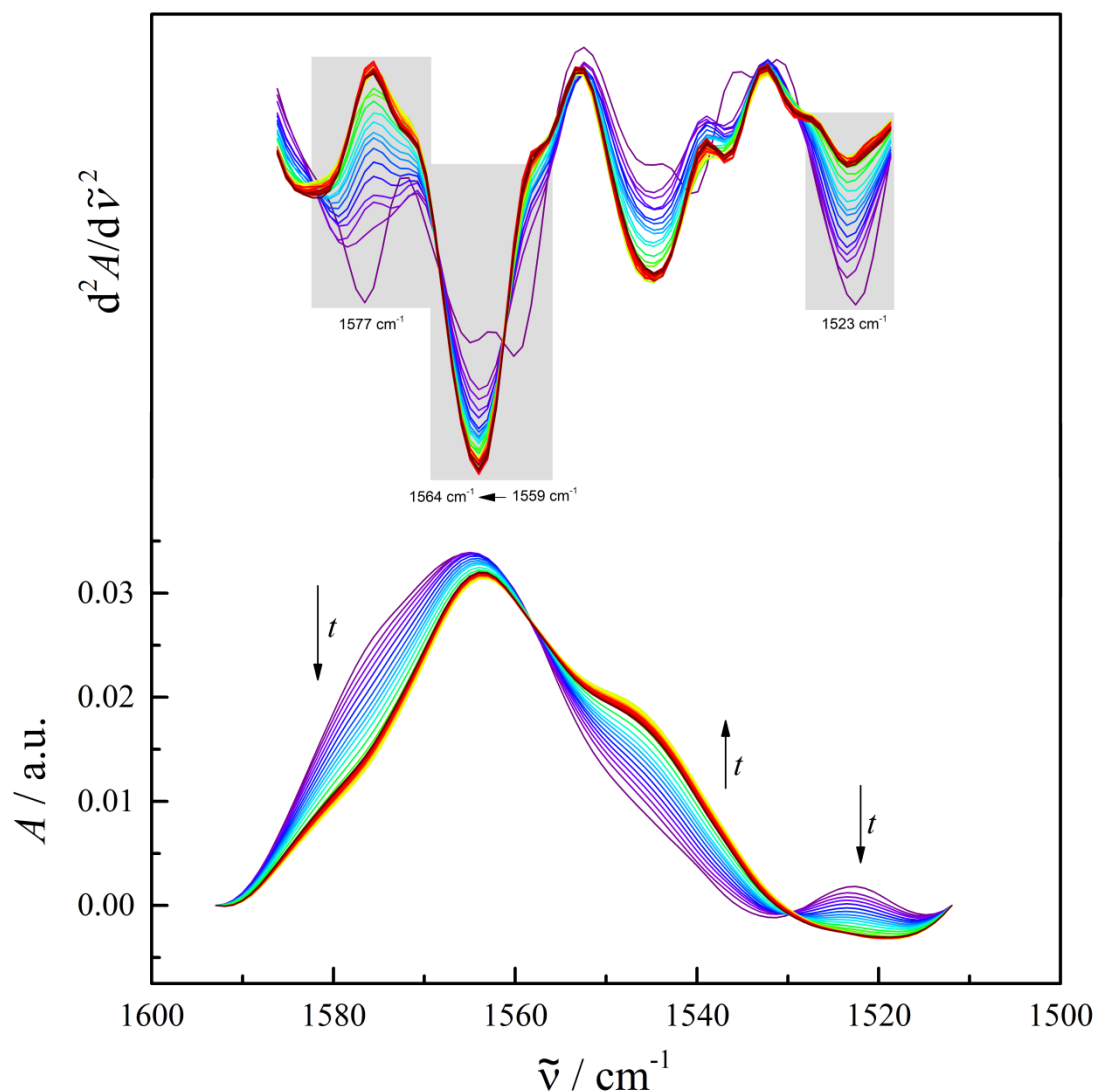
Figure 53 shows the normalized and second derivative time-dependent FTIR spectra of the wtHpRz in 50 mM Tris-HCl buffer pH 7.5 + 0.1 mM EDTA at 25 °C (0.1 MPa), during 600 minutes, in the wavenumber region from 1600 to 1540  $\text{cm}^{-1}$ . In general, in this region of the RNA spectra, two IR bands can be observed: one IR band around 1590 to 1575  $\text{cm}^{-1}$  and another IR band around 1568 - 1564  $\text{cm}^{-1}$ . These former band arises from ring vibrations of C6 = O6, C5 – C6 and C4 = C5 of free and base paired guanine. The latter band arises from ring vibrations of C4 = C5 and C5 – C6 of free and base paired guanine. The intensity of these IR bands decreases when guanine forms base pairs. The intensity of the IR band at 1576  $\text{cm}^{-1}$  exhibits small variations during the entire 10 hours of measurements, only. Additionally, the IR band at 1560  $\text{cm}^{-1}$  also shows small variations of intensity. These bands are assigned in order to follow the behavior of free and base paired guanine of guanine rich regions. Changes in the position of the guanine doublet bands between 1590 – 1564  $\text{cm}^{-1}$  is also related to changes in the environment of the guanine nucleotides [114]. Both bands do not show significant changes in wavenumber, indicating that there are not significant changes in the environment of guanines. Apparently, without the presence of cations, the wtHpRz structure fluctuates between different undocked populations that have difficulties to overcome the repulsion between the negatively charged backbones. This might be a signature of the complexity conformational changes occurring during the self-cleavage reaction.

B. Hairpin ribozyme in the presence of  $\text{MgCl}_2$ 

**Figure 54.** Time-dependent normalized and second derivative FTIR spectra of the hairpin ribozyme with  $\text{MgCl}_2$  at atmospheric pressure, in the wavenumber region from 1600 to 1530  $\text{cm}^{-1}$ . Second derivative and normalized spectra of 45  $\text{mg mL}^{-1}$  wtHpRz in 50 mM Tris-HCl buffer + 0.1 mM EDTA + 6 mM  $\text{MgCl}_2$  from 10 to 600 minutes at 25 °C (0.1 MPa). In the normalized spectra, the IR band at 1590 to 1575  $\text{cm}^{-1}$  is related to ring vibrations of  $\text{C4} = \text{C5}$  and  $\text{C5} - \text{C6}$  of free and base paired guanine and shifts to lower wavenumber (indicated by the arrow), while the IR band at 1568 to 1564  $\text{cm}^{-1}$  is related to ring vibrations of  $\text{C6} = \text{O6}$ ,  $\text{C5} - \text{C6}$  and  $\text{C4} = \text{C5}$  of free and base paired guanine and shows small changes, only. The most important bands are indicated by the grey rectangle in the second derivative spectra. The highlighted bands are: 1583 - 72  $\text{cm}^{-1}$ , 1563 - 60  $\text{cm}^{-1}$ . (Selected data)

The normalized and second derivative time-dependent FTIR spectra of the wtHpRz in 50 mM Tris-HCl buffer pH 7.5 + 0.1 mM EDTA + 6 mM MgCl<sub>2</sub> at 25 °C, during 660 minutes, in the wavenumber region from 1600 to 1530 cm<sup>-1</sup>, is shown at Figure 54. The intensity of the IR band at 1576 cm<sup>-1</sup> decreases with time, and a new band at 1582 cm<sup>-1</sup> appears. Additionally, the IR band at 1560 cm<sup>-1</sup> shifts to higher wavenumber, around 1564 cm<sup>-1</sup>, while the intensity does not change. These bands are assigned to ring vibrations of free and base paired guanine of guanine rich regions. Changes in the position of both guanine bands between 1590 – 1564 cm<sup>-1</sup> are related to changes in the environment of the guanine [114].

It can be observed in the second derivative spectra that, in the presence Mg<sup>2+</sup>, both IR bands show pronounced changes in wavenumber. This indicates significant changes in the environment of guanine, which is due to docking/undocking and formation of intermediate active/non active populations of conformers. These changes were not observed in the absence of cations (Figure 53). It can be noticed, in the second derivative spectra, that an intermediate band appears at 1568 cm<sup>-1</sup> and disappears after one hour of reaction. In addition, a band at 1540 cm<sup>-1</sup> is present and exhibits small changes during the reaction, but there is no literature data regarding the nature of this vibrational band. These details demonstrate the complexity involved in the conformational dynamics occurring during the self-cleavage reaction, where different active and non-active structure conformers are encountered.

C. Hairpin ribozyme in the presence of  $[\text{Co}(\text{NH}_3)_6]\text{Cl}_3$ 

**Figure 55.** Time-dependent normalized and second derivative FTIR spectra of the hairpin ribozyme with  $[\text{Co}(\text{NH}_3)_6]\text{Cl}_3$  at atmospheric pressure, in the wavenumber region from 1600 to  $1510\text{ cm}^{-1}$ . Second derivative and normalized spectra of  $45\text{ mg mL}^{-1}$  wtHpRz in  $50\text{ mM}$  Tris-HCl buffer +  $0.1\text{ mM}$  EDTA +  $12\text{ mM}$   $[\text{Co}(\text{NH}_3)_6]\text{Cl}_3$  +  $100\text{ mM}$  NaCl from 10 to 600 minutes at  $25\text{ }^\circ\text{C}$ ,  $0.1\text{ MPa}$ . In the normalized spectra, the IR band at  $1590$  to  $1575\text{ cm}^{-1}$  is related to ring vibrations of  $\text{C}_4 = \text{C}_5$  and  $\text{C}_5 - \text{C}_6$  of free and base paired guanine and shows an intensity decrease and a small shift to lower wavenumbers (indicated by the arrow), while the IR band at  $1568$  to  $1564\text{ cm}^{-1}$ , related to ring vibrations of  $\text{C}_6 = \text{O}_6$ ,  $\text{C}_5 - \text{C}_6$  and  $\text{C}_4 = \text{C}_5$  of free and base paired guanine, increases in intensity (indicated by the arrow). The most important bands are indicated by the grey rectangle at the second derivative spectra. The highlighted bands are:  $1577\text{ cm}^{-1}$ ,  $1564 - 59\text{ cm}^{-1}$ ,  $1523\text{ cm}^{-1}$ . (Selected data)

Figure 55 shows the normalized and second derivative time-dependent FTIR spectra of the wtHpRz in 50 mM Tris-HCl buffer pH 7.5 + 0.1 mM EDTA + 12 mM  $[\text{Co}(\text{NH}_3)_6]\text{Cl}_3$  + 100 mM NaCl at 25 °C, 0.1 MPa, during 660 minutes, in the wavenumber region from 1600 to 1510  $\text{cm}^{-1}$ . In this region of the RNA normalized spectra, two different IR bands related to ring vibrations of free and base paired guanine can be observed: from 1590 to 1575  $\text{cm}^{-1}$  (C4 = C5 and C5 – C6), and from 1560 to 1530  $\text{cm}^{-1}$  (C4 = C5 and C5 – C6). There appears also a third IR band from 1530 to 1510  $\text{cm}^{-1}$ , which is related to ring vibrations of free and base paired cytosine. The intensity of these bands drastically decreases upon duplexation. The intensity of the IR band around 1576  $\text{cm}^{-1}$  and 1522  $\text{cm}^{-1}$  decreases with time (for more detailed RNA IR band assignment, see Table 1 in section 2.2.1.5).

It can be observed, in the second derivative spectra, that the IR band at 1576  $\text{cm}^{-1}$  rapidly decreases with time. However, the new IR band at higher wavenumber (1582  $\text{cm}^{-1}$ ), observed with  $\text{MgCl}_2$ , is not observed. This shows that different conformations are formed depending on the ion, which is expected to have a direct effect on the efficiency of the self-cleavage reaction. The IR band at 1559  $\text{cm}^{-1}$  also shows a rapid intensity decrease after a few minutes of the reaction. The IR band at 1522  $\text{cm}^{-1}$  drastically decreases with time, indicating base pair formation. However, the PAGE result (Figure 52) shows that in one hour of reaction the equilibrium was reached.

These IR bands present pronounced changes in intensity and less pronounced changes in wavenumbers. However, more subbands can be observed in the second derivative, when compared to the spectra with  $\text{MgCl}_2$  (Figure 57). Apparently,  $[\text{Co}(\text{NH}_3)_6]\text{Cl}_3$  promotes the formation of different conformational states within the active/non active ensemble. These results show that in the presence of  $[\text{Co}(\text{NH}_3)_6]\text{Cl}_3$ , even after one hour of reaction, docked states can be formed, but they do not result in product formation. Also, the  $[\text{Co}(\text{NH}_3)_6]\text{Cl}_3$  interaction with the wtHpRz did not result in drastic environmental changes for the guanine nucleotides as observed with  $\text{MgCl}_2$ , which could be related to the lack of hydration regarding the  $[\text{Co}(\text{NH}_3)_6]\text{Cl}_3$  complex. It has been proposed in literature that water molecules would play an essential role in the catalytic activity of the wtHpRz [28, 29, 58, 108].

### 5.3.2.1.3. Hairpin ribozyme base-sugar vibrations followed by FTIR spectroscopy

The base sugar vibrations were also followed by FTIR spectroscopy, the wavenumber area ranges from 1500 to 1250  $\text{cm}^{-1}$  (for more detailed RNA IR band assignment, see Table 1 in section 2.2.1.5). In the 1500 to 1250  $\text{cm}^{-1}$  wavenumber region, the IR bands originate from base-sugar vibrations that are sensitive to glycosidic bond rotation, backbone conformation and sugar pucker. The IR bands are related to backbone vibrations in A-, B- and Z-forms, sugar pucker in N- or S-type conformations and N7 site vibrations of purines. It is a spectral region where a wide variety of subbands can appear.

The sugar pucker conformation is directly related to the backbone conformation. When the RNA molecule takes A- and/or Z-forms, *i. e.* a right-handed more compact helix and a left-handed helix conformation, respectively, the ribose sugar adopts a C3'-endo conformation. This means that the C3 atom of the sugar pucker is above the plane in comparison to the nucleoside. This conformation brings the nucleotides closer, which in turns makes the helix more compact than the B-form helix. The Z-form has the guanine sugar pucker in C3'-endo conformation, but its cytosine stays in C2'-endo conformation (C2 atom of sugar pucker is above the plane), and this makes the Z-form adopt a left-handed helix conformation. The Z-form is an intermediate and less stable backbone conformation, and can be found in RNA and DNA. C2'-endo sugar puckers are characteristic of a B-form helix, a less compact right-handed helix typical for DNA backbone conformations. However, the position of these bands are very sensitive to the RNA sequence. Reference literature regarding these interactions are mostly available on simple RNA sequences, only, therefore any deeper structural analysis is not possible at this point.

## A. Hairpin ribozyme in the absence of cations

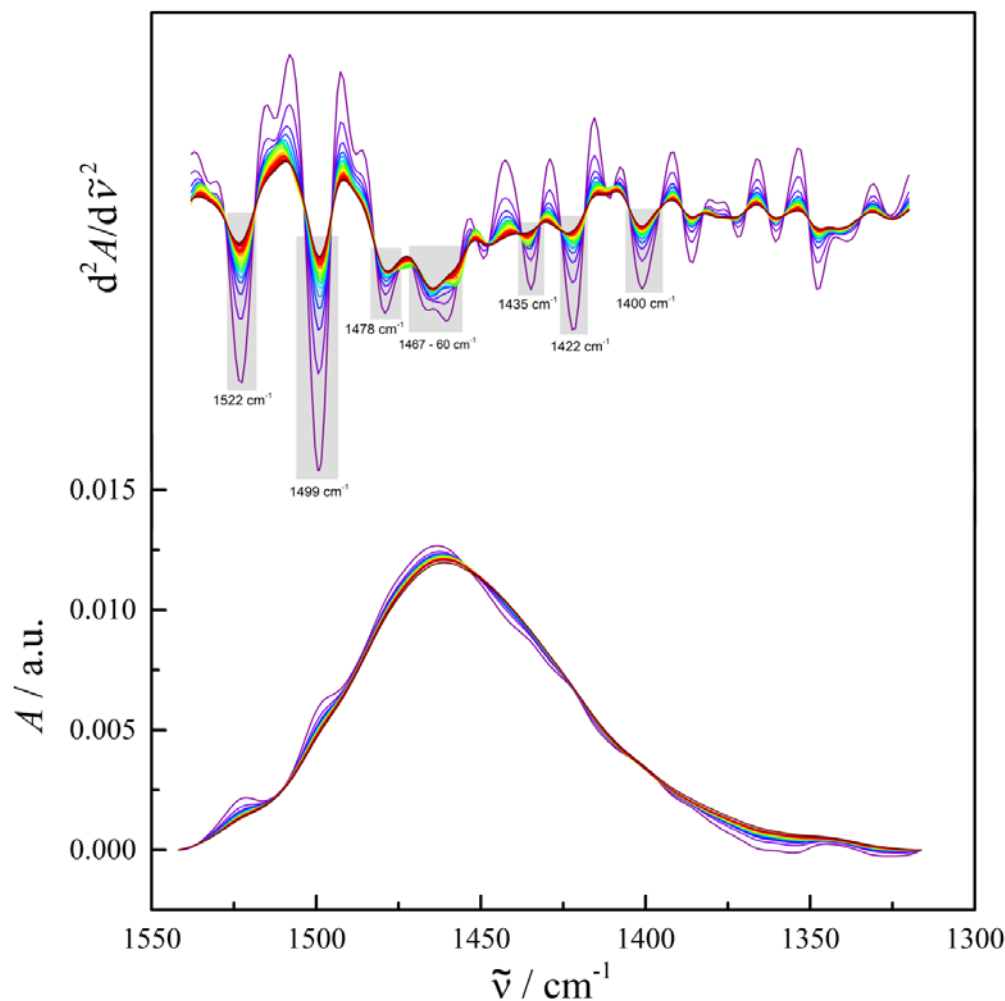


**Figure 56.** Time-dependent normalized and second derivative FTIR spectra of the hairpin ribozyme without cations at atmospheric pressure, in the wavenumber region from 1550 to 1300  $\text{cm}^{-1}$ . Second derivative and normalized spectra of 45  $\text{mg mL}^{-1}$  wtHpRz in 50 mM Tris-HCl buffer + 0.1 mM EDTA from 10 to 600 minutes at 25 °C and 0.1 MPa. IR bands originate from base-sugar vibrations that are sensitive to glycosidic bond rotation, backbone and sugar pucker conformations. These IR bands are related to backbone vibrations in A-, B- and Z-forms, sugar pucker in N- or S-type conformations and N7 site vibrations of purines. The most important bands are indicated by the grey rectangle in the second derivative spectra. The highlighted bands are: 1522  $\text{cm}^{-1}$ , 1499  $\text{cm}^{-1}$ , 1478  $\text{cm}^{-1}$ , 1467 - 60  $\text{cm}^{-1}$ , 1435  $\text{cm}^{-1}$ , 1422  $\text{cm}^{-1}$ , 1400  $\text{cm}^{-1}$ . (Selected data)

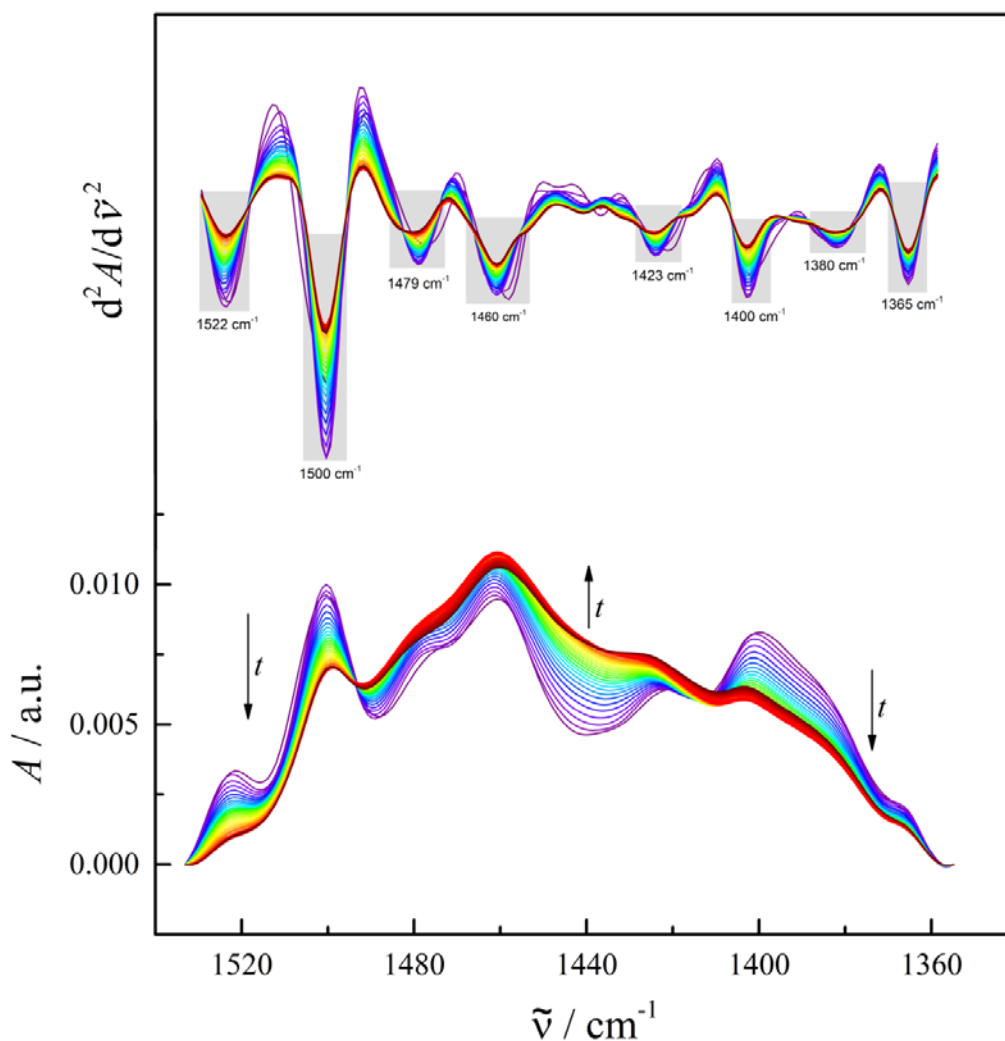
Figure 56 depicts the normalized and second derivative time-dependent FTIR spectra of the wtHpRz in 50 mM Tris-HCl buffer pH 7.5 + 0.1 mM EDTA at 25 °C (0.1 MPa), during 600 minutes, in the wavenumber region from 1550 to 1300  $\text{cm}^{-1}$ . In the normalized spectra, the IR band at 1522  $\text{cm}^{-1}$  is assigned to in-plane vibrations of



cytosine, and its intensity decreases when cytosine is paired. This band shows a small decrease in intensity during the first 30 minutes of the measurement. The IR band at 1497  $\text{cm}^{-1}$ , which is assigned to in-plane vibration of cytosine, also shows a small intensity decrease. The decrease of both bands is assigned to cytosine, and indicates that only small structural rearrangements occur in the overall secondary structure of the ribozyme.

In the second derivative spectra, it can be observed that the IR band at 1478  $\text{cm}^{-1}$ , which is assigned to ring vibrations of adenine and guanine at its N7 site, decreases slightly in intensity. Changes in the position or intensity of this band are related to interactions at N7 sites or changes in hydration in the major groove of the helix. It has been shown in the literature that G+1 receives a hydrogen bond at its N7 site from 2'-OH of A38 at the cleavage pocket. However, it was observed through PAGE (Figure 47), that there is no marked increase in product formation during 6 hours of reaction without cations besides the same initial amount. This indicates that at these “no cations” condition the wtHpRz undergoes several structural rearrangements, i.e. experiences different non-active populations. The IR bands at 1466  $\text{cm}^{-1}$  and 1460  $\text{cm}^{-1}$  are not assigned in the literature, but also reinforce the presence of strong variations of intermediate structures.

The IR band at 1434  $\text{cm}^{-1}$  shows very small variation of intensity only; it is assigned to adenine vibrations in Z-form backbone conformation. A small IR band at 1421  $\text{cm}^{-1}$  can be observed in the second derivative spectra, which is assigned to purine vibrations (adenine and guanine) in B-form helices with C2'-endo ribose pucker. The IR band observed at 1400  $\text{cm}^{-1}$  does not vary in intensity, and is assigned as RNA vibrations of an in-plane C – O – H deformation mode at the 2' position of the ribose ring [160]. A small IR band at 1386  $\text{cm}^{-1}$  and 1347  $\text{cm}^{-1}$  can be observed, but there are not assignments in the literature for these vibrations (see section 5.3.2.1.3 for more information on sugar pucker and backbone conformations). These small variations in backbone and sugar pucker vibrations indicate that very few conformational rearrangements occur in the absence of cations.

B. Hairpin ribozyme in the presence of MgCl<sub>2</sub>

**Figure 57. Time-dependent normalized and second derivative FTIR spectra of the hairpin ribozyme with MgCl<sub>2</sub> at atmospheric pressure, in the wavenumber region from 1530 to 1360 cm<sup>-1</sup>.** Second derivative and normalized spectra, of 45 mg mL<sup>-1</sup> wtHpRz in 50 mM Tris-HCl buffer + 0.1 mM EDTA + 6 mM MgCl<sub>2</sub> from 10 to 600 minutes at 25 °C (0.1 MPa). IR bands originate from base-sugar vibrations that are sensitive to glycosidic bond rotation, backbone and sugar pucker conformations. These IR bands are related to backbone vibrations in A-, B- and Z-forms, sugar pucker in N- or S-type conformations and N7 site vibrations of purines. The most important bands are indicated by the grey rectangle in the second derivative spectra. The highlighted bands are: 1522 cm<sup>-1</sup>, 1500 cm<sup>-1</sup>, 1479 cm<sup>-1</sup>, 1460 cm<sup>-1</sup>, 1423 cm<sup>-1</sup>, 1400 cm<sup>-1</sup>, 1380 cm<sup>-1</sup>, 1365 cm<sup>-1</sup>. (Selected data)

Figure 57 shows the normalized and second derivative time-dependent FTIR spectra of the wtHpRz in 50 mM Tris-HCl buffer pH 7.5 + 0.1 mM EDTA + 6 mM MgCl<sub>2</sub> at 25 °C, during 660 minutes, in the wavenumber region from 1530 to 1360 cm<sup>-1</sup>. It can be

clearly observed that  $Mg^{2+}$  induces pronounced structural rearrangements at the ribozyme backbone, when compared to Figure 56, and these changes are probably directly related to the increased catalytic activity. The IR band at  $1522\text{ cm}^{-1}$  is assigned to in-plane vibrations of cytosine, and its intensity decreases when cytosine is paired. This band shows a significant decrease in intensity until the reaction achieves equilibrium. The IR band at  $1500\text{ cm}^{-1}$ , which is assigned to in-plane vibrations of cytosine, appears only in the presence of  $Mg^{2+}$ , also shows a significant intensity decrease. The decrease of both bands assigned to cytosine indicates that several structural rearrangements occur in the ribozyme's secondary structure.

The IR band at  $1477\text{ cm}^{-1}$ , which is assigned to ring vibrations of adenine and guanine at its N7 site, reveals an increase in intensity, the opposite behavior when in the absence of cation (Figure 56). Changes in the position or intensity of this band are related to interactions at N7 sites or changes in hydration in the major groove of the helix. Changes at this band position are expected since it was shown in the literature that G+1 receives a hydrogen bond at its N7 site from 2'-OH of A38 at the cleavage pocket [65]. The IR band at  $1460\text{ cm}^{-1}$  increases with time until 6 hours of the reaction. It is assigned to adenine vibrations of B/A-form backbone. The IR band observed at  $1422\text{ cm}^{-1}$ , which is assigned to N-type or C3'-endo sugar pucker conformations in A-form helices, increases in intensity until 6 hours of the reaction. The IR band observed at  $1400\text{ cm}^{-1}$  decreases in intensity until 6 hours of the reaction. It is assigned to RNA vibrations of the in-plane C – O – H deformation mode at the 2' position of the ribose ring [160].

A small IR band at  $1380\text{ cm}^{-1}$  is related to purine (guanine) sugar in anti conformation (sugars at C2' / C3' – endo sugar pucker conformation of guanine in B/A-form) and can also be observed. This band shows a decrease in intensity, indicating that there occur environmental changes in the A-form backbone of the wtHpRz. This IR band can also be related to structural changes upon docking. A-1 and G+1 are twisted out of the helical stack, leading the ribose to form C2'-endo puckers, B-form like twists. These structural rearrangements result in alignments of the two nucleotides, and consequently alignment of the nucleophile 2'-OH of A-1 and the leaving group 5'-oxo of G+1 [65]. The IR band at  $1365\text{ cm}^{-1}$  is related to cytosine in anti-conformation, sugar pucker at C2'/C3'-endo.

This band shows a small decrease in intensity during 3 hours of reaction time. These variations in backbone and sugar pucker vibrations indicate that many conformational rearrangements occur during the reaction.

### C. Hairpin ribozyme in the presence of $[\text{Co}(\text{NH}_3)_6]\text{Cl}_3$

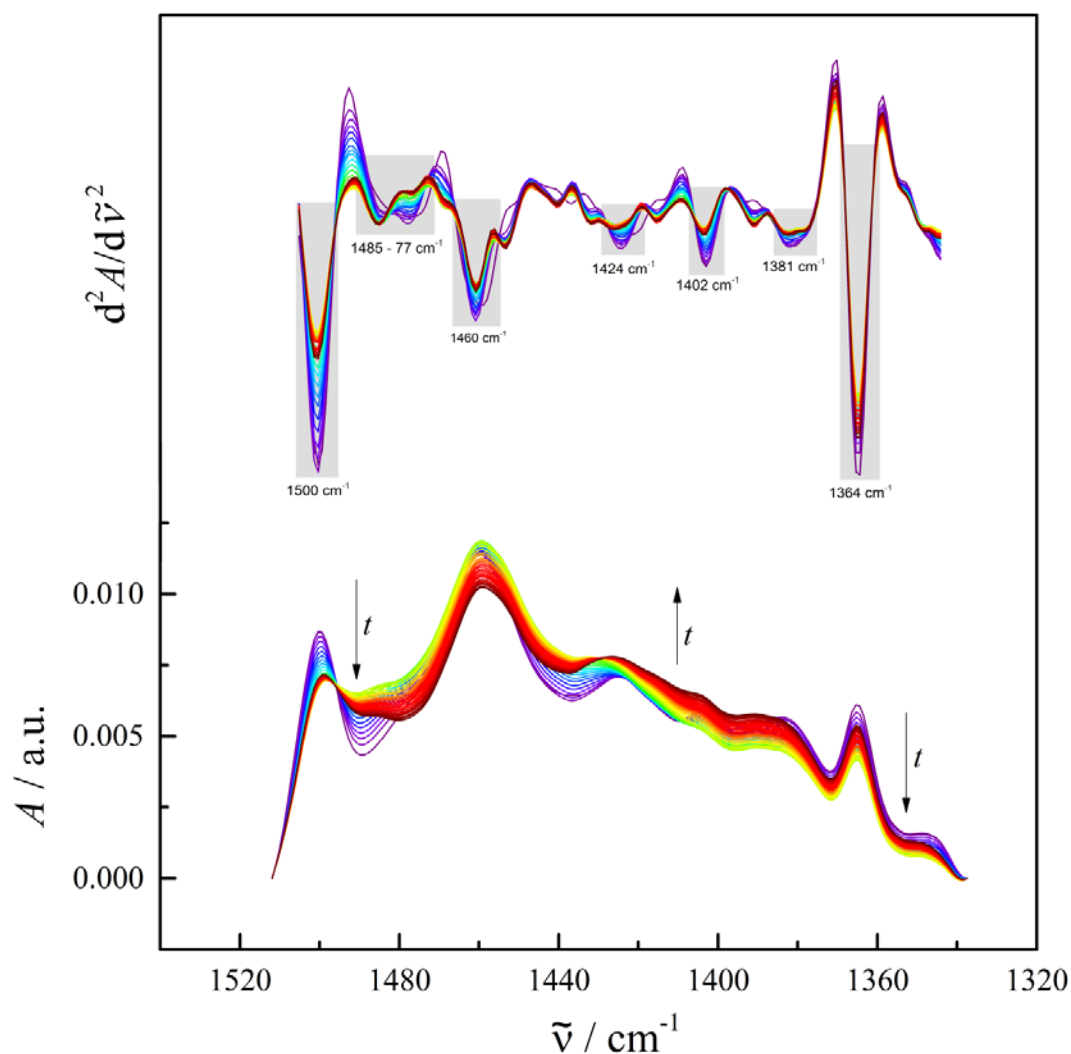


**Figure 58.** Time-dependent normalized and second derivative FTIR spectra of the hairpin ribozyme with  $[\text{Co}(\text{NH}_3)_6]\text{Cl}_3$  at atmospheric pressure, in the wavenumber region from 1520 to 1320  $\text{cm}^{-1}$ . Second derivative and normalized spectra of 45  $\text{mg mL}^{-1}$  wtHpRz in 50 mM Tris-HCl buffer + 0.1 mM EDTA + 12 mM  $[\text{Co}(\text{NH}_3)_6]\text{Cl}_3$  + 100 mM NaCl from 10 to 600 minutes at 25 °C, 0.1 MPa. IR bands originate from base-sugar vibrations that are sensitive to glycosidic bond rotation, backbone and sugar pucker conformations. These IR bands are related to backbone vibrations in A-, B- and Z-forms, sugar pucker in N- or S-type conformations and N7 site vibrations of purines. The most important bands are indicated by the grey rectangle in the second derivative spectra. The highlighted bands are: 1523  $\text{cm}^{-1}$ , 1500  $\text{cm}^{-1}$ , 1485 - 77  $\text{cm}^{-1}$ , 1460  $\text{cm}^{-1}$ , 1424  $\text{cm}^{-1}$ , 1402  $\text{cm}^{-1}$ , 1381  $\text{cm}^{-1}$ , 1364  $\text{cm}^{-1}$ . (Selected data)

Figure 58 shows the normalized and second derivative time-dependent FTIR spectra of the wtHpRz in 50 mM Tris-HCl buffer pH 7.5 + 0.1 mM EDTA + 12 mM  $[\text{Co}(\text{NH}_3)_6]\text{Cl}_3$  + 100 mM NaCl at 25 °C, during 600 minutes, in the wavenumber region from 1520 to 1320  $\text{cm}^{-1}$ . The IR band at 1500  $\text{cm}^{-1}$ , which is assigned to in-plane vibrations of cytosine, shows a significant intensity decrease. This information complements the decrease of intensity observed for the band at 1522  $\text{cm}^{-1}$  (Figure 55), indicating that the RNA structure undergoes many structural rearrangements. The IR band at 1477  $\text{cm}^{-1}$ , which is assigned to ring vibrations of adenine and guanine at its N7 site, has a very small signal that decreases with time, and the band shifts to higher wavenumbers. This IR band has a different behavior in the presence of  $\text{Mg}^{2+}$ . However, changes of this band are expected, since G+1 receives a hydrogen bond at its N7 site from 2'-OH of A38 in the cleavage pocket [65]. It has been shown in the literature that this interaction, considered essential for catalysis, is maintained at the ribozyme zipper (which is formed by the interactions between the nucleotides in the loop A and B during docking) in the presence of  $[\text{Co}(\text{NH}_3)_6]\text{Cl}_3$  [162].

The IR band at 1460  $\text{cm}^{-1}$  increases with time until 6 hours of the reaction, and is assigned to adenine vibrations of the B/A-form backbone. There is no IR band related to vibrations in Z-form helices, as observed in the presence of  $\text{MgCl}_2$ . The IR band observed at 1422  $\text{cm}^{-1}$ , which is assigned to S-type or C2'-endo sugar pucker conformation in B-form helices, decreases in intensity until 3 hours of the reaction. The IR band observed at 1400  $\text{cm}^{-1}$ , assigned to RNA vibrations [161], decreases in intensity until 3 hours of the reaction. A small IR band at 1380  $\text{cm}^{-1}$ , related to purine (guanine) sugar in anti conformation (sugars at C2' / C3' – endo sugar pucker conformation of guanine in B/A-form), can also be observed. This band shows a decrease in intensity, indicating that there are environmental changes in the B/A-form backbone variations during the self-cleavage reaction of the wtHpRz in the presence of  $[\text{Co}(\text{NH}_3)_6]\text{Cl}_3$ , as observed for  $\text{Mg}^{2+}$  (Figure 57). The IR band at 1365  $\text{cm}^{-1}$ , related to cytosine in anti-conformation, sugar pucker at C2'/C3'-endo, displays a significant decrease in intensity during the measurement time (6 hours). These variations at the backbone and sugar pucker vibrations indicate that many conformational rearrangements are involved during the reaction at this ionic conditions.

The backbone rearrangement and sugar pucker formation are not the same when comparing the  $\text{MgCl}_2$  and  $[\text{Co}(\text{NH}_3)_6]\text{Cl}_3$  conditions. The signal of the IR band at  $1477\text{ cm}^{-1}$  related to the N7 site interaction is more pronounced in the presence of  $\text{MgCl}_2$ , which might explain the higher cleavage efficiency (product formation) observed in the PAGE result (Figures 48 and 49). The presence of  $[\text{Co}(\text{NH}_3)_6]\text{Cl}_3$  induced significant changes in the behavior of guanine and cytosine related bands, which can be explained by changes in C+3, C8+, G36 and G8 position and pairing upon this ionic condition. These changes also affect the environment and pairing/stacking interaction of U+2 and G+1 [162]. These interactions are all important for formation of the active docked complex, and these changes explain the lower efficiency of the wtHpRz in the presence of  $[\text{Co}(\text{NH}_3)_6]\text{Cl}_3$  compared to the biologically relevant  $\text{MgCl}_2$ .

### 5.3.2.2. Time-dependent analysis of the structure and reaction of the hairpin ribozyme at high hydrostatic pressure

The same analysis was carried out for the FTIR measurement under high hydrostatic pressure conditions. Two different pressures, 50 and 100 MPa, were chosen for analysis of the  $\text{Mg}^{2+}$  condition. One pressure value was chosen for analysis of the  $[\text{Co}(\text{NH}_3)_6]\text{Cl}_3$  condition. In the  $1800$  to  $1500\text{ cm}^{-1}$  wavenumber region, the IR bands are originated from nucleobase vibrations, which are sensitive to base stacking and base-pairing interactions. The IR bands are related to double or single strand vibrations, which include C=C, C=N, and C=O stretching of free and/or bonded nucleotides. A double strand to single strand transition results in a decrease in the intensity of the IR band at around  $1696$  to  $1684\text{ cm}^{-1}$  with a concomitant increase in the band at around  $1677$  to  $1653\text{ cm}^{-1}$ . The former arises from the C6=O6 stretch of base-paired guanine plus the C2=O2 stretch of uracil. The latter band arises mainly from the stretching vibrations of C6=O6 of free (i.e., non-base paired) guanine, the C2=O2 stretch of free cytosine, and the C4=O4 stretch of free uracil [114, 136]. For better analysis of the IR bands the  $1800$  to  $1500\text{ cm}^{-1}$  region can be divided into two regions: from  $1720$  to  $1600\text{ cm}^{-1}$ , and from  $1600$  –  $1550\text{ cm}^{-1}$  (for more detailed RNA IR band assignment, see Table 1 in section 2.2.1.5).

### 5.3.2.2.1. Hairpin ribozyme in-plane base vibrations sensitive to effects of base pairing followed by FTIR spectroscopy

#### D. Hairpin ribozyme in the presence of MgCl<sub>2</sub> at 50 MPa

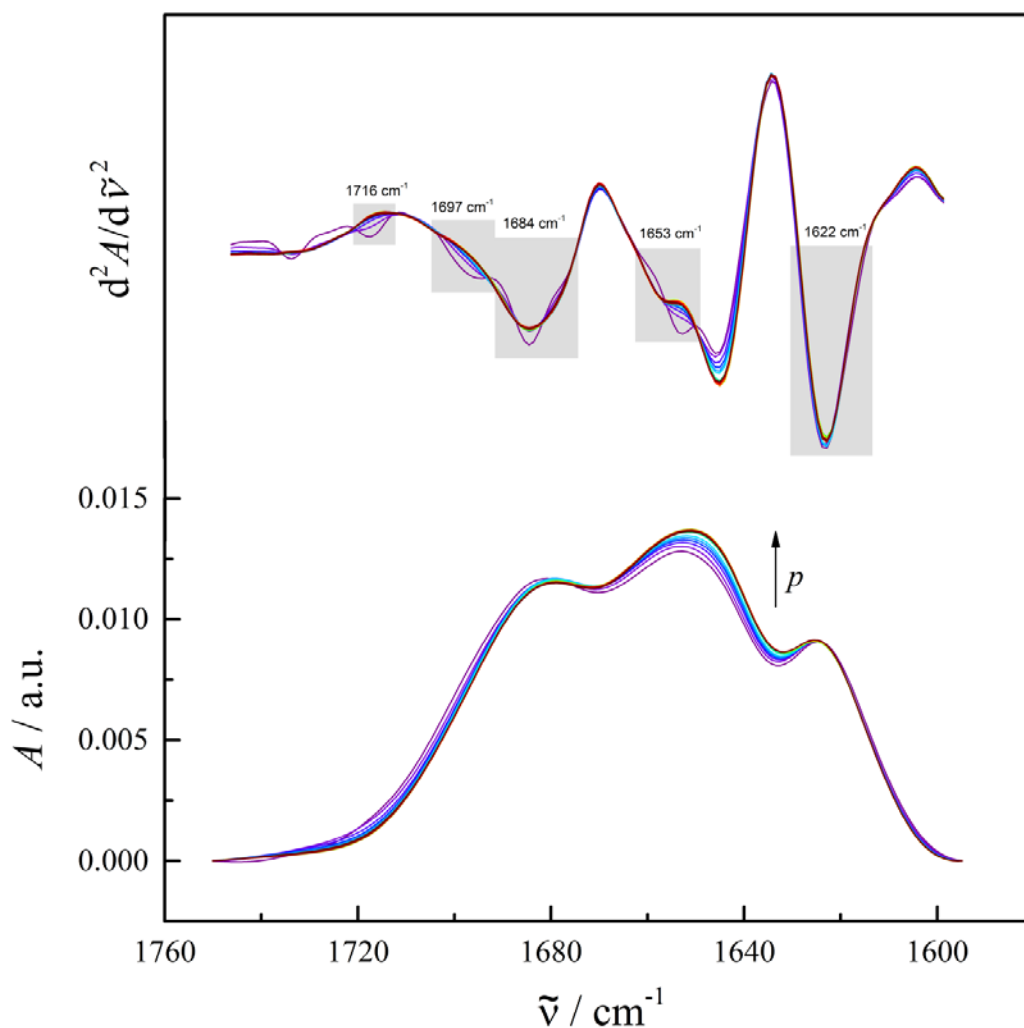


**Figure 59.** Time-dependent normalized and second derivative FTIR spectra of the hairpin ribozyme with MgCl<sub>2</sub> at 50 MPa, in the wavenumber region from 1760 to 1600 cm<sup>-1</sup>. Second derivative and normalized spectra of 45 mg mL<sup>-1</sup> wtHpRz in 50 mM Tris-HCl buffer + 0.1 mM EDTA + 6 mM MgCl<sub>2</sub> from 30 to 600 minutes at 25 °C, 50 MPa. In the normalized spectra, the IR band from 1696 to 1684 cm<sup>-1</sup> is related to base paired nucleotides and shows only very small variations with time. The IR band from 1677 to 1653 cm<sup>-1</sup> is related to free nucleotides and increases slightly in intensity with time (indicated by the arrow). The most important bands are indicated by the grey rectangle in the second derivative spectra. The highlighted bands are: 1716 cm<sup>-1</sup>, 1697 cm<sup>-1</sup>, 1684 cm<sup>-1</sup>, 1653 cm<sup>-1</sup>, 1622 cm<sup>-1</sup>. (Selected data)

The normalized and second derivative time-dependent FTIR spectra of the wtHpRz in 50 mM Tris-HCl buffer pH 7.5 + 0.1 mM EDTA + 6 mM MgCl<sub>2</sub> at 25 °C, 50 MPa, during 600 minutes, in the wavenumber region from 1720 to 1600 cm<sup>-1</sup>, are presented in Figure 59. In Figure 59, in the second derivative spectra, some specific bands related to the ribozyme's conformational change can be found. The IR band at 1716 cm<sup>-1</sup>, involved in Hoogsteen third strand binding (G\*C-C), disappear just after 30 minutes of pressurization. This IR band can be related to the third strand binding of G36\*G+1.C25 found in the crystal structure of a hairpin ribozyme docked conformation [65]. Apparently, pressure destabilizes the third strand interaction found in the active pocket during docked states, which agrees with the reduction in product formation observed in the PAGE results (Figure 49).

The IR band at 1696 cm<sup>-1</sup> is related to the C2=O2 stretch of uracil and disappears in 30 minutes after pressurization. The IR band at 1684 cm<sup>-1</sup>, characteristic of base paired G-C vibrations, shows only small variations in intensity, as seen in the normalized spectra. This can be related to minor changes in product formation and/or undocking. It can be observed, in the second derivative spectra, that this IR band decreases after pressurization without further changes in intensity. In addition, it splits into different IR bands with lower and higher wavenumbers after one hour of the reaction. This indicates that the wtHpRz at 50 MPa achieved the reaction equilibrium faster, but there is less product formation, indicating that there are different non-active docked conformations.

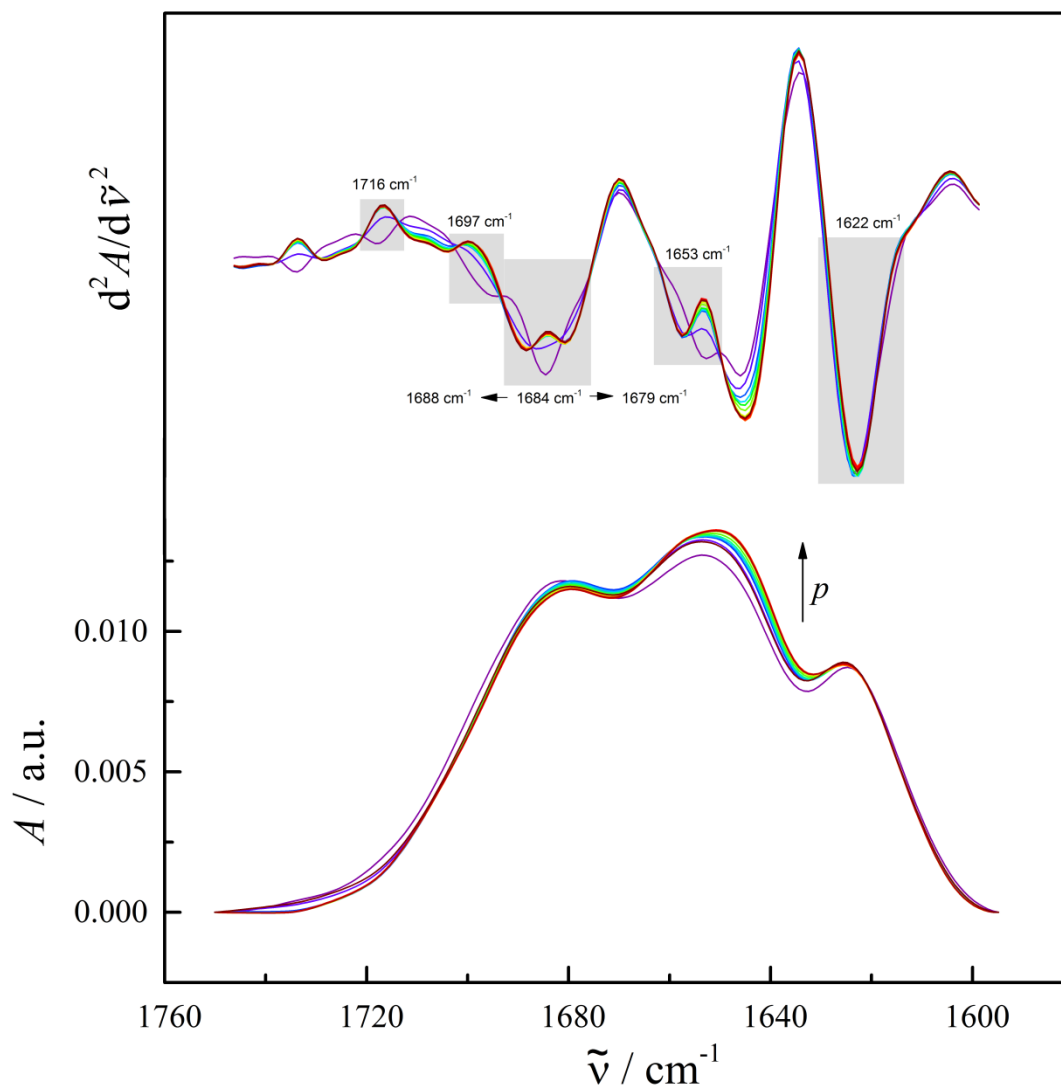
The IR band at 1653 cm<sup>-1</sup>, assigned to free base vibrations of uracil (C4=O4 stretch), can be related to product formation. It displays a less pronounced intensity decrease with time, compared to ambient pressure (Figure 54), and shifts to higher wavenumbers upon pressurization. The IR band at 1623 cm<sup>-1</sup>, related to C=N and C=C ring vibrations of adenine and/or in-plane vibrations of cytosine, also decreases after pressurization without further changes.

Small differences can be observed between the FTIR spectra of the wtHpRz at 0.1 MPa and 50 MPa. These changes indicate that pressure did not induce the formation of new



interactions or destabilization of the docked states while favoring undocked states. But pressure favors the docked state, and accelerates its formation.

### E. Hairpin ribozyme in the presence of $\text{MgCl}_2$ at 100 MPa

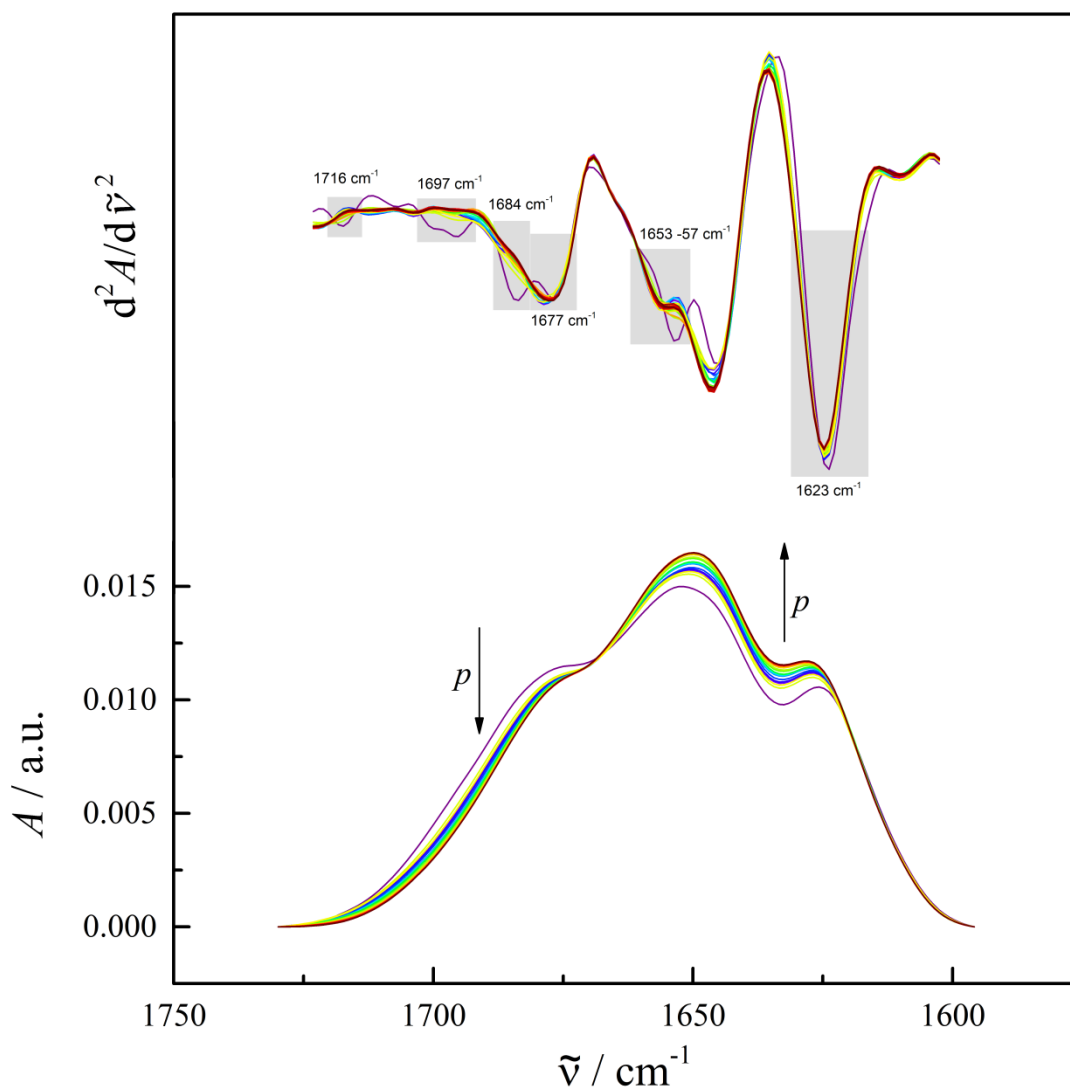


**Figure 60.** Time-dependent normalized and second derivative FTIR spectra of the hairpin ribozyme with  $\text{MgCl}_2$  at 100 MPa, in the wavenumber region from 1760 to 1600  $\text{cm}^{-1}$ . Second derivative and normalized spectra of 45  $\text{mg mL}^{-1}$  wtHpRz in 50 mM Tris-HCl buffer + 0.1 mM EDTA + 6 mM  $\text{MgCl}_2$  from 30 to 600 minutes at 25  $^{\circ}\text{C}$ , 100 MPa. In the normalized spectra, the IR band from 1696 to 1684  $\text{cm}^{-1}$  is related to base paired nucleotides and shows only very small variations with time. The IR band from 1677 to 1653  $\text{cm}^{-1}$  is related to free nucleotides and shows a small increase in intensity with time (indicated by the arrow). The most important bands are indicated by the grey rectangle in the second derivative spectra. The highlighted bands are: 1716  $\text{cm}^{-1}$ , 1697  $\text{cm}^{-1}$ , 1688  $\text{cm}^{-1}$  - 1684  $\text{cm}^{-1}$  - 1679  $\text{cm}^{-1}$ , 1653  $\text{cm}^{-1}$ , 1622  $\text{cm}^{-1}$ . (Selected data)

Figure 60 shows the normalized and second derivative time-dependent FTIR spectra of the wtHpRz in 50 mM Tris-HCl buffer pH 7.5 + 0.1 mM EDTA + 6 mM MgCl<sub>2</sub> at 25 °C, 100 MPa, during 600 minutes, in the wavenumber region from 1760 to 1600 cm<sup>-1</sup>. The second derivative spectra show some specific bands related to the ribozyme's conformational changes. The IR band at 1717 cm<sup>-1</sup>, involved in Hoogsteen third strand binding (G\*C-C), disappears just after pressurization at 100 MPa. This IR band can be related to the third strand binding of G36\*G+1.C25 found in the active pocket of the crystal structure of the hairpin ribozyme's docked conformation [65]. As observed for the 50 MPa data, pressure destabilizes the third strand interaction found in the active pocket during docking, leading to the formation of non-active docked conformations, which is in agreement with the reduced amount of reaction product found in the PAGE results (Figure 51).

The IR band at 1696 cm<sup>-1</sup> is related to the C=O<sub>2</sub> stretch of uracil and disappears after pressurization. The IR band at 1684 cm<sup>-1</sup>, characteristic of base paired G-C vibrations, displays a small decrease in intensity, as seen in the normalized spectra, which can be related to a small formation of product and/or undocking. It can be observed, in the second derivative spectra, that this IR band decreases after pressurization, and it splits into two different IR bands with lower and higher wavenumbers after 30 minutes of the reaction at 100 MPa. This indicates that 100 MPa, just as 50 MPa, promotes the formation of docked states found only after a few hours of the reaction at 0.1 MPa. The IR band at 1653 cm<sup>-1</sup>, assigned to free base vibrations of uracil, which can be related to product formation, reveals an intensity decrease after pressurization at 100 MPa. It also shifts to 1657 cm<sup>-1</sup>, as seen in the second derivative spectra. The IR band at 1623 cm<sup>-1</sup>, related to C=N and C=C ring vibrations of adenine and/or in-plane vibrations of cytosine, shows a small increase after pressurization without further changes, when compared to the 0.1 MPa spectra (Figure 51).

This FTIR result at 100 MPa confirms that pressure does not induce new interactions, as seen in the FTIR at 50 MPa (Figure 59). Pressure also did not favor destabilized undocked states. On the other hand, pressure favored the formation of docked states. However, the majority of these docked states were not active (Figure 51).

F. Hairpin ribozyme in the presence of  $[\text{Co}(\text{NH}_3)_6]\text{Cl}_3$  at 100 MPa

**Figure 61.** Time-dependent normalized and second derivative FTIR spectra of the hairpin ribozyme with  $[\text{Co}(\text{NH}_3)_6]\text{Cl}_3$  at 100 MPa, in the wavenumber region from 1750 to 1600  $\text{cm}^{-1}$ . Second derivative and normalized spectra of 45  $\text{mg mL}^{-1}$  wtHpRz in 50 mM Tris-HCl buffer + 0.1 mM EDTA + 12 mM  $[\text{Co}(\text{NH}_3)_6]\text{Cl}_3$  + 100 mM NaCl from 30 to 600 minutes at 25  $^\circ\text{C}$ , 100 MPa. In the normalized spectra, the IR band from 1696 to 1684  $\text{cm}^{-1}$  is related to base paired nucleotides and decreases in intensity with time (indicated by the arrow). The IR band from 1677 to 1653  $\text{cm}^{-1}$  is related to free nucleotides and increases in intensity with time (indicated by the arrow). The most important bands are indicated by the grey rectangle in the second derivative spectra. The highlighted bands are: 1716  $\text{cm}^{-1}$ , 1697  $\text{cm}^{-1}$ , 1688  $\text{cm}^{-1}$ , 1677  $\text{cm}^{-1}$ , 1665  $\text{cm}^{-1}$ , 1657 - 53  $\text{cm}^{-1}$ , 1623  $\text{cm}^{-1}$ . (Selected data)

Figure 61 shows the normalized and second derivative time-dependent FTIR spectra of the wtHpRz in 50 mM Tris-HCl buffer pH 7.5 + 0.1 mM EDTA + 12 mM  $[\text{Co}(\text{NH}_3)_6]\text{Cl}_3$  + 100 mM NaCl, 100 MPa, at 25 °C, during 660 minutes, in the wavenumber region from 1750 to 1600  $\text{cm}^{-1}$ . It can be observed, in the normalized spectra, that there is a small decrease in intensity of the IR band at 1682  $\text{cm}^{-1}$ , which is related to base paired guanine and base paired uracil, with a concomitant increase of the IR band at 1654  $\text{cm}^{-1}$ , which is assigned to C free guanine and free uracil vibrations. The intensity changes are observed during the first 3 hours of the reaction, and then it reaches an equilibrium. The IR band related to free base vibrations shows a more significant increase compared to the small intensity decrease of the base paired band. The PAGE result (Figure 49) showed that under 100 MPa the product formation is decreased until one hour compared to the 0.1 MPa reaction. However, until 6 hours of reaction at 100 MPa and in the presence of  $[\text{Co}(\text{NH}_3)_6]\text{Cl}_3$ , the wtHPRz still undergoes conformational changes, which are not observed at higher pressures or in the presence of  $\text{MgCl}_2$  at 100 MPa (Figure 63). This indicates that  $[\text{Co}(\text{NH}_3)_6]\text{Cl}_3$  favors different structural rearrangements, resulting in alternative docked states. However, some of these states were still active under 100 MPa.

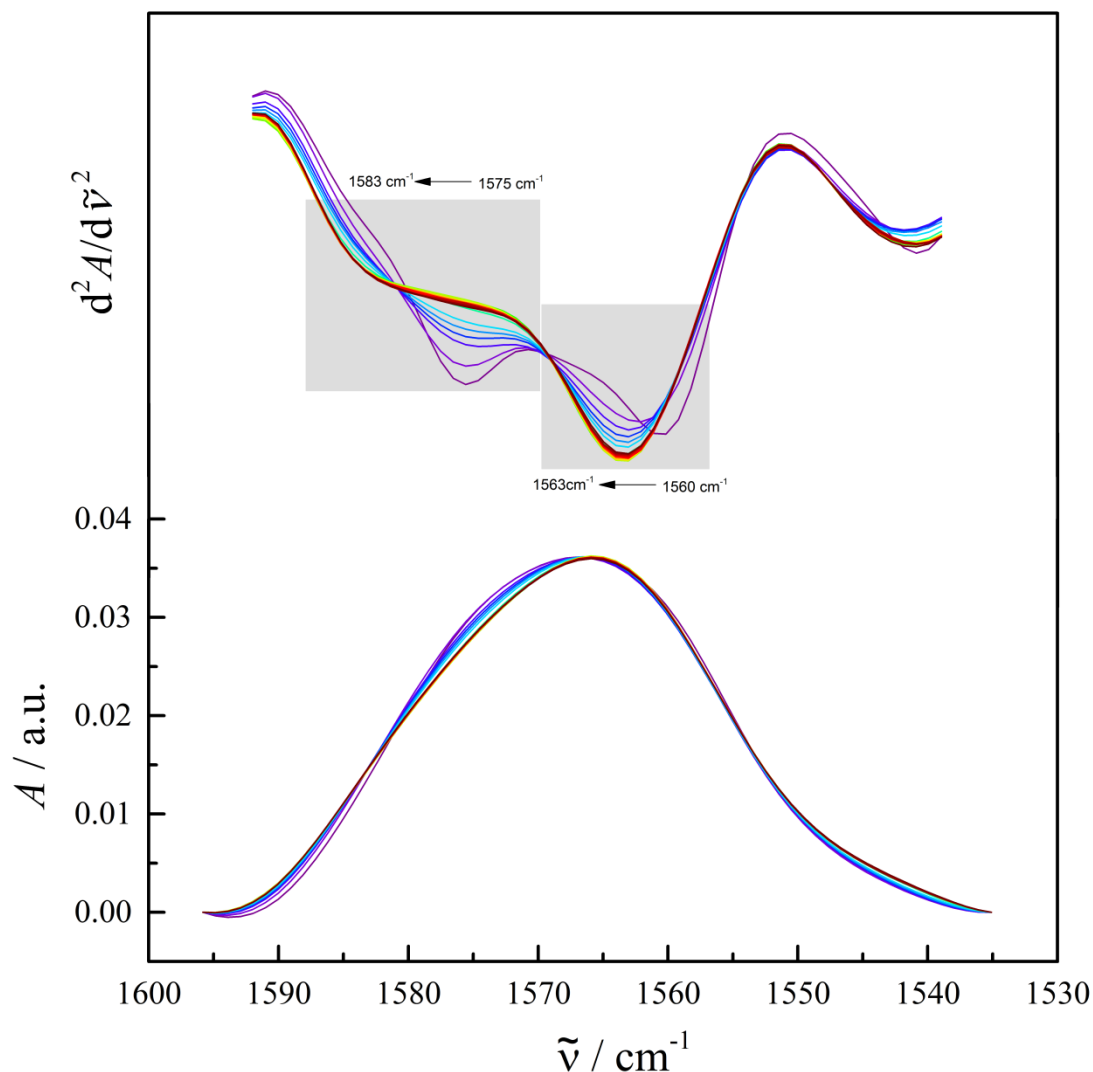
It can be observed in the second derivative spectra, that some specific bands are related to the ribozyme's conformational changes. The IR band at 1717  $\text{cm}^{-1}$ , involved in Hoogsteen third strand binding ( $\text{G}^*\text{C}-\text{C} \rightarrow \text{G36}^*\text{G}+1.\text{C25}$ ), rapidly decreases after pressurization. This interaction is found in the crystal structure of the hairpin ribozyme docked conformation, and this interaction is maintained by  $[\text{Co}(\text{NH}_3)_6]\text{Cl}_3$  [65, 162]. This IR band disappears after pressurization of the system. However, the ribozyme achieves equilibrium after one hour of reaction (Figure 52). The IR band at 1696  $\text{cm}^{-1}$  is related to free and base paired uracil and disappears after pressurization of the system. The IR band at 1684  $\text{cm}^{-1}$ , characteristic of base paired vibrations of guanine, shows also a rapid decrease after pressurization at 100 MPa and disappears after one hour of reaction.

The wtHpRz does not have the same behavior as with  $\text{MgCl}_2$  at 100 MPa, as the IR band at 1684  $\text{cm}^{-1}$  reveals a small intensity decrease and splits into two different bands with higher and lower wavenumbers. This indicates that  $[\text{Co}(\text{NH}_3)_6]\text{Cl}_3$  stabilizes different

ribozyme conformations with different cleavage efficiency. The IR band at 1677  $\text{cm}^{-1}$ , related to C4=O4 stretch vibrations of uracil, shows small intensity variations, only. This IR band is not observed in the wtHpRz FTIR spectra in the presence of  $\text{MgCl}_2$  at both atmospheric and high hydrostatic pressure. However, a strong signal is detected in the presence of  $[\text{Co}(\text{NH}_3)_6]\text{Cl}_3$ . It has been shown in the literature that the residues U+2 and C+3, in the active core, adopt different conformations in the presence of  $[\text{Co}(\text{NH}_3)_6]\text{Cl}_3$  when compared to the crystal structure in the presence of  $\text{MgCl}_2$  [162]. The small change of this IR band indicates that pressure has a smaller effect on these new interactions formed at the ribozyme zipper by  $[\text{Co}(\text{NH}_3)_6]\text{Cl}_3$ . The IR band at 1665  $\text{cm}^{-1}$ , assigned to vibrations of free guanine and observed during the reaction at 0.1 MPa, is not observed during the reaction at 100 MPa. The IR band at 1653  $\text{cm}^{-1}$ , related to free base vibrations of uracil, decreases in 30 minutes of the reaction and shifts to 1657  $\text{cm}^{-1}$ , indicating that different populations are favored with time. The IR band at 1623  $\text{cm}^{-1}$  is related to ring vibrations of adenine and/or in-plane vibrations of cytosine, and the intensity varies during the entire measurement (for more detailed RNA IR band assignment, see Table 1 in section 2.2.1.5).

### 5.3.2.2.2. Hairpin ribozyme in-plane base vibrations sensitive to effects of base stacking followed by FTIR

#### D. Hairpin ribozyme in the presence of $\text{MgCl}_2$ at 50 MPa

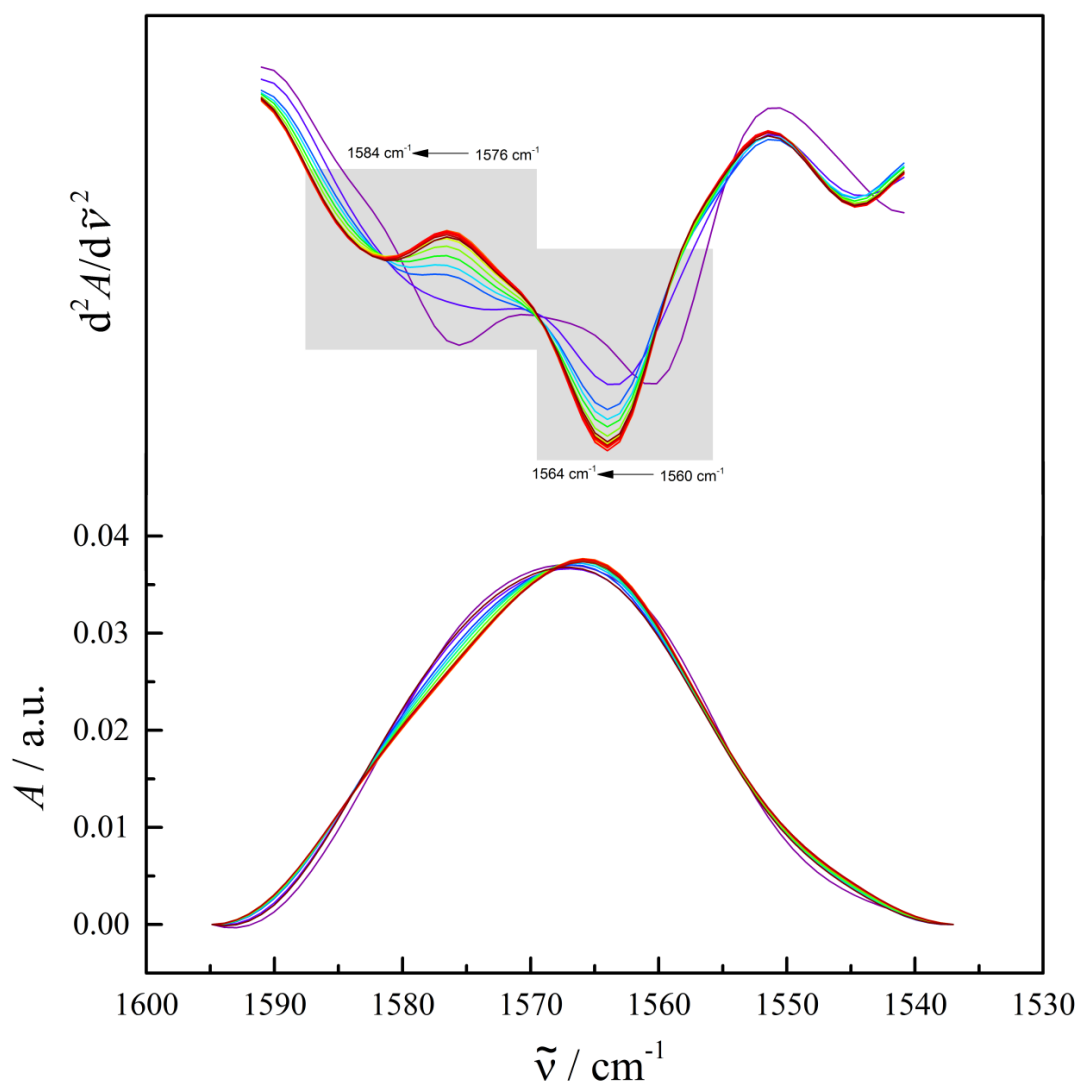


**Figure 62.** Time-dependent normalized and second derivative FTIR spectra of the hairpin ribozyme with  $\text{MgCl}_2$  at 50 MPa, in the wavenumber region from 1600 to 1530  $\text{cm}^{-1}$ . Second derivative and normalized spectra of 45  $\text{mg mL}^{-1}$  wtHpRz in 50 mM Tris-HCl buffer + 0.1 mM EDTA + 6 mM  $\text{MgCl}_2$  from 30 to 600 minutes at 25  $^{\circ}\text{C}$ , 50 MPa. In the normalized spectra, the IR band at 1590 to 1575  $\text{cm}^{-1}$  is related to ring vibrations of  $\text{C4} = \text{C5}$  and  $\text{C5} - \text{C6}$  of free and base paired guanine and has a small shift to lower wavenumber, while the IR band at 1568 to 1564  $\text{cm}^{-1}$  is related to ring vibrations of  $\text{C6} = \text{O6}$ ,  $\text{C5} - \text{C6}$  and  $\text{C4} = \text{C5}$  of free and base paired guanine and shows very small changes, only. The most important bands are indicated by the grey rectangle in the second derivative spectra. The highlighted bands are: 1583 - 75  $\text{cm}^{-1}$ , 1563 - 60  $\text{cm}^{-1}$ . (Selected data)

Figure 62 shows the normalized and second derivative time-dependent FTIR spectra of the wtHpRz in 50 mM Tris-HCl buffer pH 7.5 + 0.1 mM EDTA + 6 mM MgCl<sub>2</sub> at 25 °C, 50 MPa, during 600 minutes, in the wavenumber region from 1600 to 1530 cm<sup>-1</sup>. In general, in this region of the RNA spectra two IR bands can be observed: one IR band around 1590 to 1575 cm<sup>-1</sup> and another IR band around 1568 - 1564 cm<sup>-1</sup>. Both IR bands are related to ring vibrations of free and base paired guanine, and the intensity of these IR bands decreases when guanine forms base pairs.

There are only small changes observable in the normalized spectra, and the most prominent is a change in wavenumber of the IR band at 1576 cm<sup>-1</sup>. It can be observed, in the second derivative spectra, that the intensity of the IR band at 1576 cm<sup>-1</sup> decreases when pressurized. In addition, after 30 minutes of reaction, under 50 MPa, the IR band at 1576 cm<sup>-1</sup> disappears with a concomitant increase of the band at 1584 cm<sup>-1</sup>. The IR band at 1560 cm<sup>-1</sup> shifts to higher wavenumbers, to around 1564 cm<sup>-1</sup>, with a small increase in intensity. These IR bands present the same behavior at 0.1 MPa and 50 MPa. However, pressure rapidly induced the wavenumber shift observed only after one hour of reaction at 0.1 MPa.

These bands are also assigned in order to follow the behavior of free and base paired guanine of guanine rich regions. Changes in the position of the guanine doublet bands between 1590 – 1564 cm<sup>-1</sup> are also related to changes in the environment of the guanine nucleotides [114]. Both bands present pronounced changes in wavenumber, indicating that there are significant changes in the environment of guanine due to docking/undocking and formation of intermediate active/non active conformers. These results suggest that pressure induces conformational changes achieved only at reaction equilibrium.

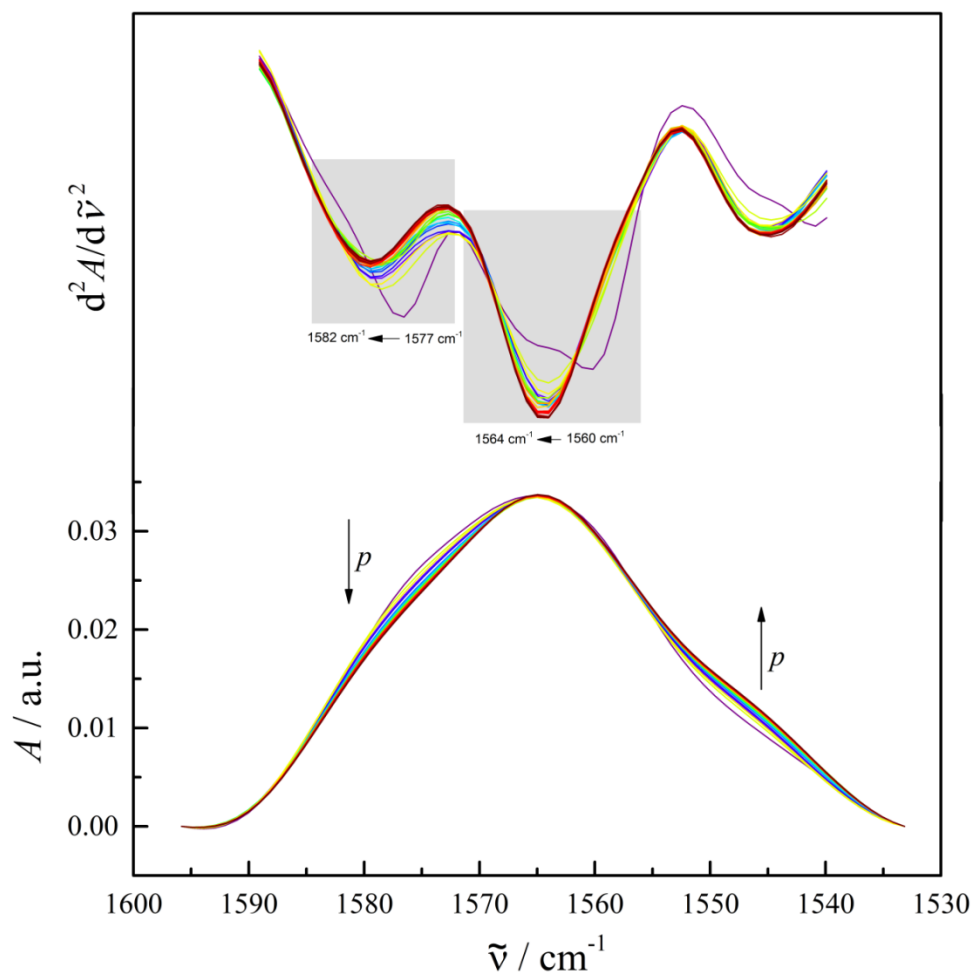
E. Hairpin ribozyme in the presence of  $\text{MgCl}_2$  at 100 MPa

**Figure 63.** Time-dependent normalized and second derivative FTIR spectra of the hairpin ribozyme with  $\text{MgCl}_2$  at 100 MPa, in the wavenumber region from 1600 to 1530  $\text{cm}^{-1}$ . Second derivative and normalized spectra of 45  $\text{mg mL}^{-1}$  wtHpRz in 50 mM Tris-HCl buffer + 0.1 mM EDTA + 6 mM  $\text{MgCl}_2$  from 30 to 600 minutes at 25  $^\circ\text{C}$ , 100 MPa. In the normalized spectra, the IR band at 1590 to 1575  $\text{cm}^{-1}$  is related to ring vibrations of  $\text{C4} = \text{C5}$  and  $\text{C5} - \text{C6}$  of free and base paired guanine and shows a small shift to lower wavenumber, while the IR band at 1568 to 1564  $\text{cm}^{-1}$  related to ring vibrations of  $\text{C6} = \text{O6}$ ,  $\text{C5} - \text{C6}$  and  $\text{C4} = \text{C5}$  of free and base paired guanine, displays very small changes, only. The most important bands are indicated by the grey rectangle in the second derivative spectra. The highlighted bands are: 1584 - 76  $\text{cm}^{-1}$ , 1564 - 60  $\text{cm}^{-1}$ . (Selected data)



Figure 63 shows the normalized and second derivative time-dependent FTIR spectra of the wtHpRz in 50 mM Tris-HCl buffer pH 7.5 + 0.1 mM EDTA + 6 mM MgCl<sub>2</sub> at 25 °C, 100 MPa, during 600 minutes, in the wavenumber region from 1600 to 1530 cm<sup>-1</sup>. In general, this region of the RNA spectrum shows two IR bands: one IR band around 1590 to 1575 cm<sup>-1</sup> and another IR band around 1568 - 1564 cm<sup>-1</sup>. These bands arise from ring vibrations of free and base paired guanines. The intensity of these IR bands decreases when guanine forms base pairs.

There are only small changes observable in the normalized spectra, and the most prominent is a change in wavenumber of the IR band at 1576 cm<sup>-1</sup>, as observed at 50 MPa (Figure 65). The second derivative spectra show that the intensity of the IR band at 1576 cm<sup>-1</sup> decreases when the sample is pressurized. After 30 minutes of reaction under 100 MPa, the IR band at 1576 cm<sup>-1</sup> disappears with a concomitant increase of the band at 1584 cm<sup>-1</sup>. Additionally, the IR band at 1560 cm<sup>-1</sup> shifts to higher wavenumbers, around 1564 cm<sup>-1</sup>, with a small increase in intensity. These IR bands present the same behavior at 0.1 MPa and 50 MPa. As observed at 50 MPa, both IR bands present pronounced changes in wavenumber at 100 MPa, but the changes are more prominent at 100 MPa than at 50 MPa. This indicates that there are changes in the environment of guanine during docking/undocking, and that pressure favors conformational changes achieved only after hours of reaction at 0.1 MPa. However, as mentioned before, these changes do not favor cleavage, and an increase of product formation is not observed (figure 48).

F. Hairpin ribozyme in the presence of  $[\text{Co}(\text{NH}_3)_6]\text{Cl}_3$  at 100 MPa

**Figure 64.** Time-dependent normalized and second derivative FTIR spectra of the hairpin ribozyme with  $[\text{Co}(\text{NH}_3)_6]\text{Cl}_3$  at 100 MPa, in the wavenumber region from 1600 to 1530  $\text{cm}^{-1}$ . Second derivative and normalized spectra of 45  $\text{mg mL}^{-1}$  wtHpRz in 50 mM Tris-HCl buffer + 0.1 mM EDTA + 12 mM  $[\text{Co}(\text{NH}_3)_6]\text{Cl}_3$  + 100 mM NaCl from 30 to 600 minutes at 25  $^\circ\text{C}$ , 100 MPa. In the normalized spectra, the IR band at 1590 to 1575  $\text{cm}^{-1}$  is related to ring vibrations of C4 = C5 and C5 – C6 of free and base paired guanine and decreases in intensity (indicated by the arrow), while the IR band at 1568 to 1564  $\text{cm}^{-1}$  is related to ring vibrations of C6 = O6, C5 – C6 and C4 = C5 of free and base paired guanine, and displays no significant change. The most important bands are indicated by the grey rectangle in the second derivative spectra. The highlighted bands are: 1582 - 77  $\text{cm}^{-1}$ , 1564 - 60  $\text{cm}^{-1}$ , 1523  $\text{cm}^{-1}$ . (Selected data)

The normalized and second derivative time-dependent FTIR spectra of the wtHpRz in 50 mM Tris-HCl buffer pH 7.5 + 0.1 mM EDTA + 12 mM  $[\text{Co}(\text{NH}_3)_6]\text{Cl}_3$  + 100 mM NaCl,

100 MPa, at 25 °C, during 600 minutes, in the wavenumber region from 1600 to 1540  $\text{cm}^{-1}$ , are presented at Figure 64. In this region of the RNA normalized spectra, two IR bands can be observed: a first IR band from 1590 to 1570  $\text{cm}^{-1}$ , and a second IR band from 1560 to 1530  $\text{cm}^{-1}$ . Both bands arise from ring vibrations of free and base paired guanine and the intensity of these IR bands decreases when guanine forms base pairs.

It can be observed in the normalized spectra that pressure causes a decrease in intensity of the IR band at  $\approx 1580 \text{ cm}^{-1}$ , until it reaches constant intensity values after 3 hours of the reaction. The second IR band, at  $\approx 1564 \text{ cm}^{-1}$ , shows no significant modification under 100 MPa during 6 hours. It can be observed, in the second derivative spectra, that the intensity of the IR band at  $\approx 1576 \text{ cm}^{-1}$ , decrease rapidly upon pressurization at 100 MPa, and shifts to higher wavenumbers ( $1582 \text{ cm}^{-1}$ ), as observed in the presence of  $\text{MgCl}_2$  conditions (Figure 63). The IR bands at  $1567 \text{ cm}^{-1}$  and  $1560 \text{ cm}^{-1}$ , also observed at 0.1 MPa, reveal a small increase in intensity. In addition, pressure accelerates the shift of this IR band to  $1564 \text{ cm}^{-1}$ . These bands are also assigned in order to follow the behavior of free and base paired guanine of guanine rich regions.

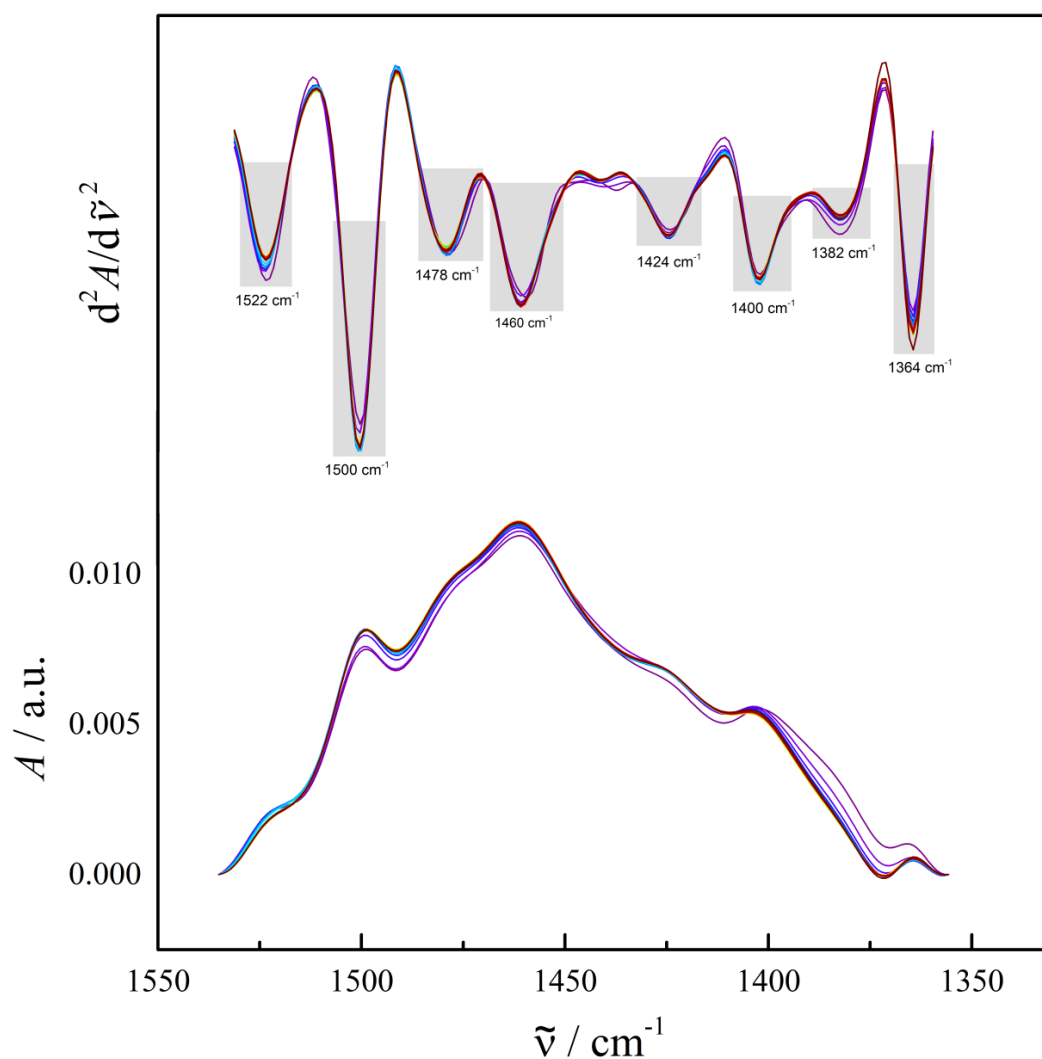
There are small differences between the spectra at 100 MPa in the presence of  $\text{MgCl}_2$  or  $[\text{Co}(\text{NH}_3)_6]\text{Cl}_3$ . This can be related to the formation of different conformational states induced by  $[\text{Co}(\text{NH}_3)_6]\text{Cl}_3$ , which were not observed in the presence of  $\text{MgCl}_2$ . This may include population of alternative active/non active intermediate states.

#### **5.3.2.2.3. Hairpin ribozyme base-sugar vibrations followed by FTIR spectroscopy**

The base sugar vibrations were also followed by FTIR spectroscopy under high hydrostatic pressure, in the wavenumber region from 1500 to 1250  $\text{cm}^{-1}$ . In the 1500 to 1250  $\text{cm}^{-1}$  wavenumber region, the IR bands originate from base-sugar vibrations that are sensitive to glycosidic bond rotation, backbone conformation and sugar pucker. The IR bands are related to backbone vibrations in A-, B- and Z-forms, sugar pucker in N- or S-type conformations and N7 site vibrations of purines. It is a spectral region where a wide variety of subbands can appear. Detailed information on IR band assignment can be found in section 5.3.2.1.3 and/or Table 1 in section 2.2.1.5. The position of these bands

are very sensitive to the RNA sequence and reference literature of these interactions describes mostly simple RNA sequences, therefore any deeper structural analysis is not possible.

#### D. Hairpin ribozyme in the presence of MgCl<sub>2</sub> at 50 MPa



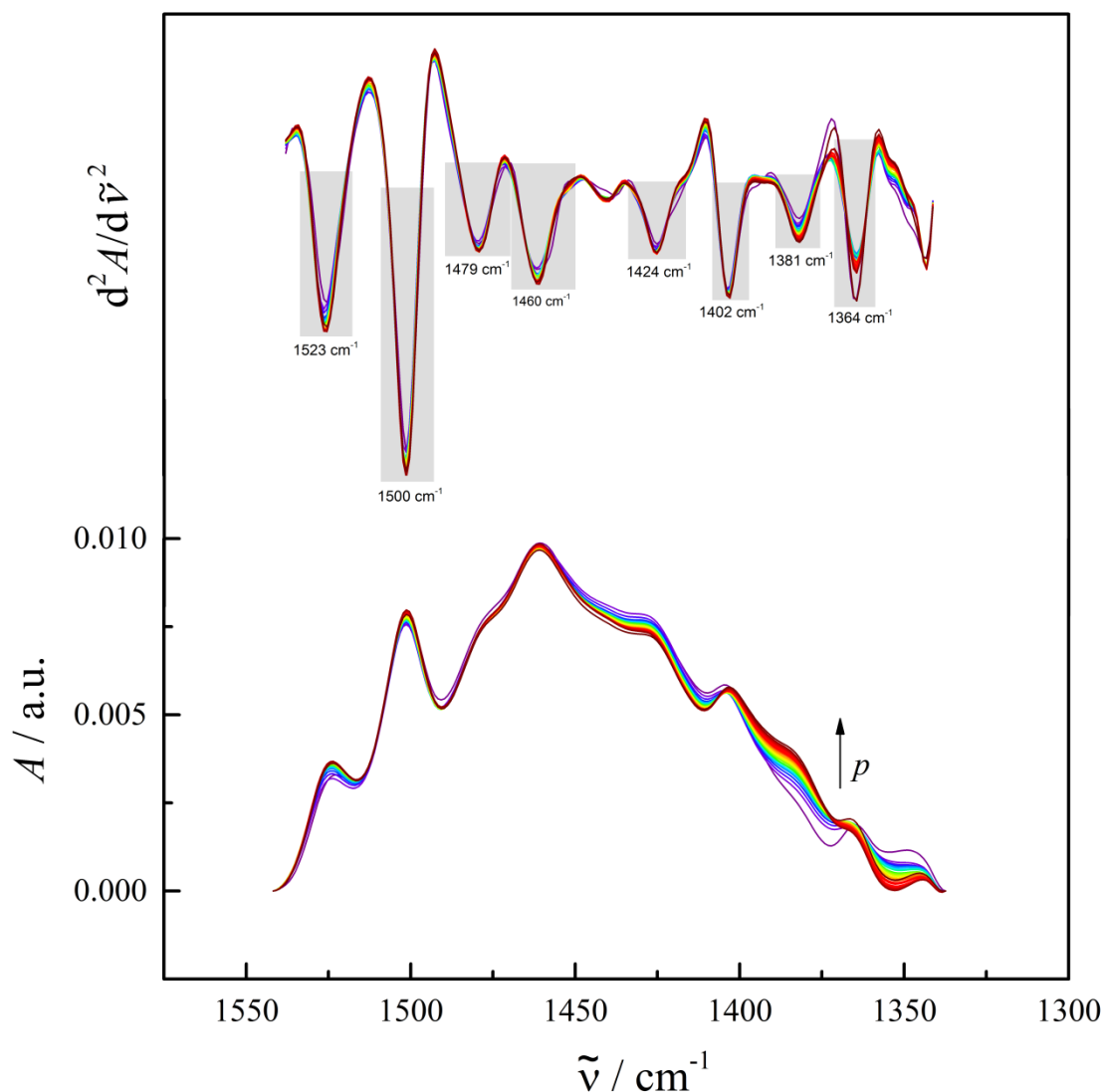
**Figure 65.** Time-dependent normalized and second derivative FTIR spectra of the hairpin ribozyme with MgCl<sub>2</sub> at 50 MPa, in the wavenumber region from 1550 to 1350 cm<sup>-1</sup>. Second derivative and normalized spectra of 45 mg mL<sup>-1</sup> wtHpRz in 50 mM Tris-HCl buffer + 0.1 mM EDTA + 6 mM MgCl<sub>2</sub> from 30 to 600 minutes at 25 °C, 50 MPa. IR bands originate from base-sugar vibrations which are sensitive to glycosidic bond rotation, backbone and sugar pucker conformations. These IR bands are related to backbone vibrations in A-, B- and Z-forms, sugar pucker in N- or S-type conformations and N7 site vibrations of purines. The most important bands are indicated by the grey rectangle in the second derivative spectra. The highlighted bands are: 1522 cm<sup>-1</sup>, 1500 cm<sup>-1</sup>, 1478 cm<sup>-1</sup>, 1460 cm<sup>-1</sup>, 1424 cm<sup>-1</sup>, 1400 cm<sup>-1</sup>, 1382 cm<sup>-1</sup>, 1364 cm<sup>-1</sup>. (Selected data)

Figure 65 shows the normalized and second derivative time-dependent FTIR spectra of the wtHpRz in 50 mM Tris-HCl buffer pH 7.5 + 0.1 mM EDTA + 6 mM MgCl<sub>2</sub> at 25 °C, 50 MPa, during 600 minutes, in the wavenumber region from 1550 to 1350 cm<sup>-1</sup>. The IR band at 1522 cm<sup>-1</sup> is assigned to in-plane vibrations of cytosine, and its intensity decreases when cytosine is paired. This band shows a small variation in intensity under 50 MPa, only. The IR band at 1500 cm<sup>-1</sup>, which is assigned to in-plane vibrations of cytosine, displays a significant intensity decrease. However, pressure has a small influence on the behavior of this particular band. The decrease of both bands assigned to cytosine indicates that several structural rearrangements occur in the ribozyme's secondary structure during the reaction and pressure seems to promote and accelerate these rearrangements. The IR band at 1478 cm<sup>-1</sup>, which is assigned to ring vibrations of adenine and guanine at its N7 site, shows small changes in intensity. Changes in the position or intensity of this band are related to interactions at N7 sites or changes in hydration in the major groove of the helix. It was shown in the literature that G+1 receives a hydrogen bond at its N7 site from the 2'-OH group of A38 in the cleavage pocket [65]. It can be observed, in the second derivative spectra, that pressure seems to stabilize the N7 site interactions of purines, and there is no change in intensity or wavenumber upon pressurization.

The IR band at 1460 cm<sup>-1</sup> displays a small increase upon pressurization, only. It is assigned to adenine vibrations in B/A-form of backbone. There are no adenine vibrations in Z-form helices at 50 MPa. The IR band observed at 1423 cm<sup>-1</sup>, which is assigned as S-type or C2'-endo sugar pucker conformation in B-form helices, increases slightly after pressurization without further changes during the 6 hours of the reaction. The IR band observed at 1400 cm<sup>-1</sup> shows a small decrease in intensity. It is assigned to RNA vibrations of the ribose ring [160]. The small IR band at 1380 cm<sup>-1</sup> is related to purine (guanine) sugar in anti conformation (sugars at C2' / C3' – endo sugar pucker conformation of guanine in B/A-form) and can also be observed. This band displays a small decrease in intensity after pressurization with no further changes. This indicates that the changes occurring in the A-form backbone of the wtHpRz during the reaction at 0.1 MPa cannot be observed at 50 MPa after 30 minutes of reaction.

The presence of both IR bands, at 1423  $\text{cm}^{-1}$  and 1380  $\text{cm}^{-1}$ , can also be related to structural changes during docking. A-1 and G+1 are twisted out of the helical stack, leading the ribose into C2'-endo puckers, B-form like twists. These structural rearrangements result in alignment of the two nucleotides, and consequent alignment of the nucleophile 2'-OH of A-1 and the leaving group, 5'-oxo of G+1. The IR band at 1365  $\text{cm}^{-1}$  is related to cytosine in anti-conformation, sugar pucker at C2'/C3'-endo, and it displays a minor decrease in intensity after pressurization. These changes in backbone and sugar pucker vibrations indicate that many conformational rearrangements occur in the course of the reaction.

Small changes can be observed between the FTIR spectra of the wtHpRz at 0.1 MPa and 50 MPa. Pressure did not induce the formation of new interactions or destabilization of the docked states while favoring undocked states. The FTIR results indicate that pressure favors the docked state, and accelerates its formation. Pressure induces the ribozyme molecules to achieve docked state conformations, but does not increase product formation, as observed by PAGE (Figure 48 and 49). Therefore, pressure accelerates the formation of docked states but these conformational states do not seem to be active, thereby reducing the overall self-cleavage activity and product formation.

E. Hairpin ribozyme in the presence  $\text{MgCl}_2$  at 100 MPa

**Figure 66.** Time-dependent normalized and second derivative FTIR spectra of the hairpin ribozyme with  $\text{MgCl}_2$  at 100 MPa, in the wavenumber region from 1550 to 1300  $\text{cm}^{-1}$ . Second derivative and normalized spectra of 45  $\text{mg mL}^{-1}$  wtHpRz in 50 mM Tris-HCl buffer + 0.1 mM EDTA + 6 mM  $\text{MgCl}_2$  from 30 to 600 minutes at 25 °C, 100 MPa. IR bands originate from base-sugar vibrations which are sensitive to glycosidic bond rotation, backbone and sugar pucker conformations. These IR bands are related to backbone vibrations in A-, B- and Z-forms, sugar pucker in N- or S-type conformations and N7 site vibrations of purines. The most important bands are indicated by the grey rectangle in the second derivative spectra. The highlighted bands are: 1523  $\text{cm}^{-1}$ , 1500  $\text{cm}^{-1}$ , 1479  $\text{cm}^{-1}$ , 1460  $\text{cm}^{-1}$ , 1424  $\text{cm}^{-1}$ , 1402  $\text{cm}^{-1}$ , 1381  $\text{cm}^{-1}$ , 1364  $\text{cm}^{-1}$ . (Selected data)

The normalized and second derivative time-dependent FTIR spectra of the wtHpRz in 50 mM Tris-HCl buffer pH 7.5 + 0.1 mM EDTA + 6 mM MgCl<sub>2</sub> at 25 °C, 100 MPa, during 600 minutes, in the wavenumber region from 1550 to 1300 cm<sup>-1</sup> are shown at Figure 69. The IR band at 1523 cm<sup>-1</sup> is assigned to in-plane vibrations of cytosine, and its intensity decreases when cytosine is paired. This band shows a small increase in intensity during the first one hour after pressurization, then stays constant. The IR band at 1500 cm<sup>-1</sup>, which is assigned as in-plane vibrations of cytosine, reveal a very small increase in intensity during the reaction at 100 MPa. However, at 0.1 MPa, this IR band displays a significant intensity change, indicating that pressure has a significant influence on the behavior of the in/plane interactions of cytosine. The small decrease of both bands assigned to cytosine, when compared to the 0.1 MPa measurements, indicates that pressure inhibits structural rearrangements that occur in the wtHpRz's secondary structure during the self-cleavage reaction.

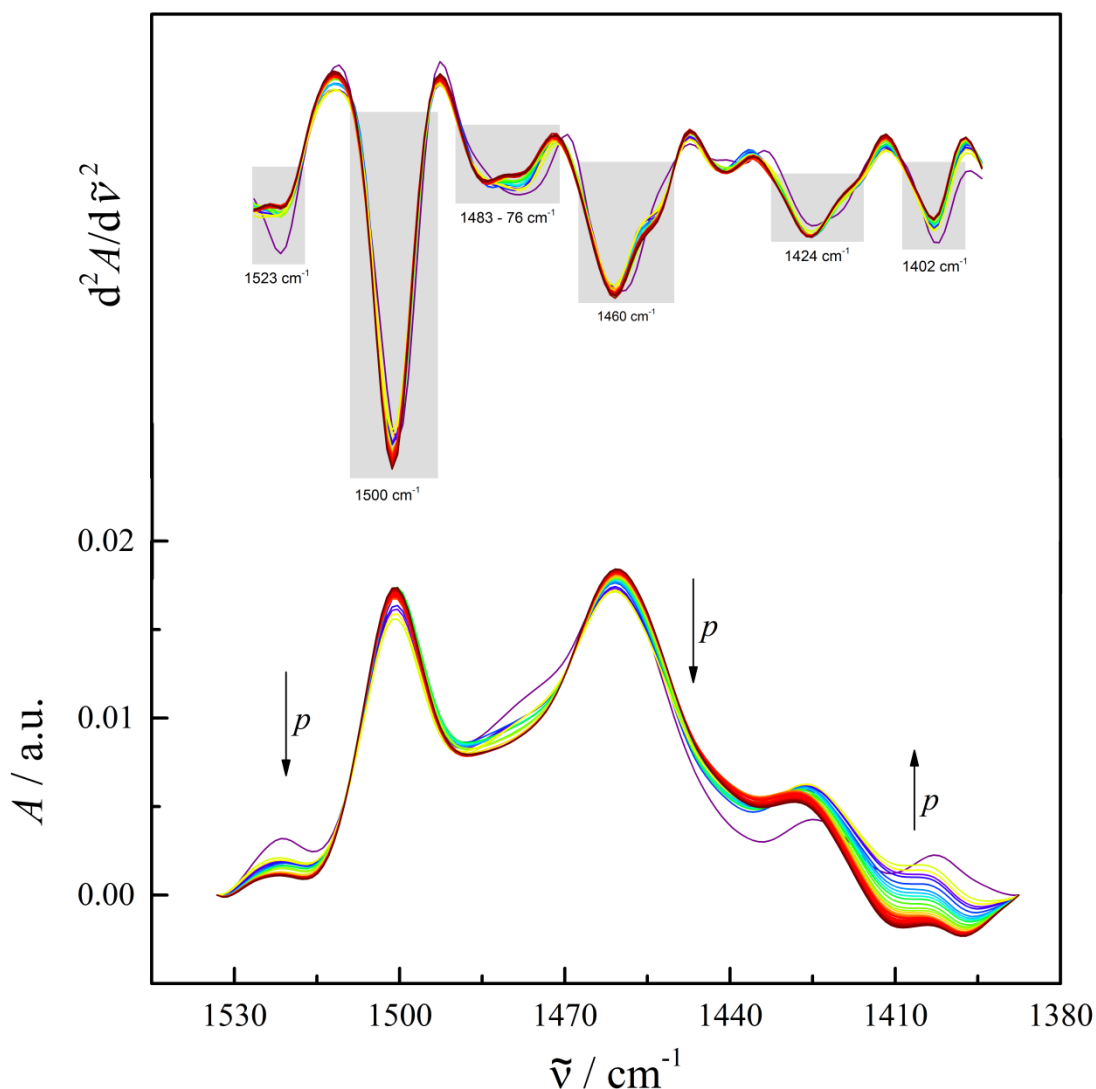
The IR band at 1478 cm<sup>-1</sup> is assigned to ring vibrations of adenine and guanine at its N7 site. Changes in the position or intensity of this band are related to interactions at N7 sites (G+1 receives a hydrogen bond at its N7 site from 2'-OH of A38 in the cleavage pocket [65]) or to changes in hydration in the major groove of the helix. It can be observed, in the normalized and second derivative spectra, that pressure seems to stabilize the N7 site interactions of purines, and there is no significant change in intensity or wavenumber after pressurization. The IR band at 1460 cm<sup>-1</sup>, assigned to adenine vibrations in B/A-form backbone, shows a small decrease after pressurization, only.

The IR band observed at 1424 cm<sup>-1</sup>, which is assigned to S-type or C2'-endo sugar pucker conformation of adenine and guanine in B-form helices, shows very small variations in intensity during the 6 hours of reaction. The IR band observed at 1402 cm<sup>-1</sup>, assigned to RNA vibrations of the ribose ring [160], also shows small variations in intensity after pressurization only. The small IR band at 1381 cm<sup>-1</sup> is related to purine (guanine) sugar in anti conformation (sugars at C2' / C3' – endo sugar pucker conformation of guanine in B/A-form), and it displays a small increase in intensity after pressurization at 100 MPa. This indicates that there are some environmental changes occurring in the B/A-form backbone of the active wtHpRz upon pressurization. This IR band can also be related to



structural changes that take place during docking, as mentioned before, due to formation of B-form like twists (C2'-endo puckers) during docking. These structural rearrangements result in alignment of the two nucleotides, and consequently alignment of the nucleophile 2'-OH of A-1 and the leaving group, 5'-oxo of G+1. The IR band at 1365 cm<sup>-1</sup>, which is related to cytosine in anti-conformation, sugar pucker at C2'/C3'-endo, displays a small decrease in intensity after pressurization.

Small variations can be observed between the spectra of the wtHpRz at 0.1 MPa, 50 MPa and 100 MPa. Pressure did not induce the formation of new interactions or destabilize the docked states while favoring undocked states. The pressure-dependent FTIR measurements started after 30 minutes of the reaction, due to the time needed to assemble the high pressure system (for more details, see section 2.2.1) and to reach a stable background recording. During this time, the wtHpRz had already half of the product cleaved (according to the PAGE data from Figures 48 and 49). These combined results indicate that pressure promotes the formation of docked states, but these states are non-active docked (folded) states, leading to stagnation of the self-cleavage, probably since some structural interactions and rearrangements cannot take place under high hydrostatic pressure. Pressure also seems to induce the purine B-form sugar pucker at the active core, while purine vibrations in A-form (more compact conformation) were favored. Therefore, high pressure seems to modulate the structural rearrangement and the kinetics of the wtHpRz by favoring folded/docked states, but non-productive states, and the overall self-cleavage activity and product formation is reduced upon pressurization, as observed in the PAGE data shown in Figure 48.

F. Hairpin ribozyme in the presence of  $[\text{Co}(\text{NH}_3)_6]\text{Cl}_3$  at 100 MPa

**Figure 67.** Time-dependent normalized and second derivative FTIR spectra of the hairpin ribozyme with  $[\text{Co}(\text{NH}_3)_6]\text{Cl}_3$  at 100 MPa, in the wavenumber region from 1530 to 1380  $\text{cm}^{-1}$ . Second derivative and normalized spectra of 45  $\text{mg mL}^{-1}$  wtHpRz in 50 mM Tris-HCl buffer + 0.1 mM EDTA + 12 mM  $[\text{Co}(\text{NH}_3)_6]\text{Cl}_3$  + 100 mM NaCl from 30 to 600 minutes at 25  $^\circ\text{C}$ , 100 MPa. IR bands originate from base-sugar vibrations which are sensitive to glycosidic bond rotation, backbone and sugar pucker conformations. These IR bands are related to backbone vibrations in A-, B- and Z-forms, sugar pucker in N- or S-type conformations and N7 site vibrations of purines. The most important bands are indicated by the grey rectangle in the second derivative spectra. The highlighted bands are: 1523  $\text{cm}^{-1}$ , 1500  $\text{cm}^{-1}$ , 1483 - 76  $\text{cm}^{-1}$ , 1460  $\text{cm}^{-1}$ , 1424  $\text{cm}^{-1}$ , 1402  $\text{cm}^{-1}$ . (Selected data)

Figure 67 shows the normalized and second derivative time-dependent FTIR spectra of the wtHpRz in 50 mM Tris-HCl buffer pH 7.5 + 0.1 mM EDTA + 12 mM  $[\text{Co}(\text{NH}_3)_6]\text{Cl}_3$  + 100 mM NaCl, 100 MPa, at 25 °C, during 600 minutes, in the wavenumber region from 1530 to 1380  $\text{cm}^{-1}$ . The IR band at 1520  $\text{cm}^{-1}$ , assigned to in-plane vibrations of cytosine, drastically decreases upon pressurization and there are small variations in intensity observable during the reaction time, indicating base pair formation. The PAGE result (Figure 49) showed that, in one hour of reaction, the maximum of product formation should be achieved. However, there is still some conformational change occurring until 6 hours of measurement under 100 MPa. These results show that in the presence of  $[\text{Co}(\text{NH}_3)_6]\text{Cl}_3$ , even after one hour of reaction, docked/folded states can be formed, but they do not result in product formation. The IR band at 1500  $\text{cm}^{-1}$ , which is assigned to in-plane vibrations of cytosine, shows a significant intensity increase instead of the decrease observed at 0.1 MPa.

The IR band at 1477  $\text{cm}^{-1}$ , which is assigned as ring vibrations of adenine and guanine at its N7 site, shows an intensity decrease with time and the band shifts to higher wavenumber. These changes are more pronounced at 100 MPa than with  $[\text{Co}(\text{NH}_3)_6]\text{Cl}_3$  at 0.1 MPa or with  $\text{MgCl}_2$  at 100 MPa. It has been shown in the literature that the N7 site interaction from the 2'-OH group of A38 at the cleavage pocket with G+1, which is considered essential for catalysis, is maintained in the presence of  $[\text{Co}(\text{NH}_3)_6]\text{Cl}_3$  [162]. The intensity of the IR band at 1460  $\text{cm}^{-1}$ , which is assigned to adenine vibrations in B/A-form backbone, increases during the first hour of the reaction. The IR band observed at 1426  $\text{cm}^{-1}$ , which is assigned to S-type or C2'-endo sugar pucker conformation in B-form helices, decreases in intensity upon pressurization, but then its intensity increases during the first hour of reaction. When the ribozyme is docked the nucleotides in the active pocket are twisted out of the helical stack, resulting in B-form like twists [65]. The intensity of this IR band decreases at 0.1 MPa. The IR band observed at 1400  $\text{cm}^{-1}$  that is assigned to RNA vibration, decreases in intensity until 3 hours of reaction.

Small differences can be observed between the spectra of the wtHpRz at 0.1 MPa and 100 MPa and in the presence of 12 mM  $[\text{Co}(\text{NH}_3)_6]\text{Cl}_3$  + 100 mM NaCl. The wtHpRz

had already 30 minutes of reaction at atmospheric pressure when the pressure-dependent FTIR measurements started (for more details, see section 2.2.1). This is half of the time until reaction equilibrium is reached (Figure 49). The high pressure FTIR result indicates that  $[\text{Co}(\text{NH}_3)_6]\text{Cl}_3$  favors different conformations of the wtHpRz, as shown in the literature [162]. The wtHpRz showed to be less efficient in the presence of  $[\text{Co}(\text{NH}_3)_6]\text{Cl}_3$  and this may be related to the formation of different intramolecular interactions at the active pocket of the ribozyme. The wtHpRz backbone and sugar pucker conformations showed to be more pressure sensitive in the presence of  $[\text{Co}(\text{NH}_3)_6]\text{Cl}_3$  if compared with the  $\text{MgCl}_2$  data (Figures 66 and 67). These results indicate that pressure favors docked states, but the majority of conformers is composed of non-active states. Therefore, the overall self-cleavage activity and product formation is reduced upon pressurization.

The backbone rearrangement and sugar pucker formation are not the same when comparing the  $\text{MgCl}_2$  (Figure 69) and  $[\text{Co}(\text{NH}_3)_6]\text{Cl}_3$  data (Figure 67). The signal of the IR band at  $1477\text{ cm}^{-1}$ , related to N7 site interaction, is more pronounced in the presence of  $\text{MgCl}_2$ , which might explain the higher cleavage efficiency (product formation) observed in the PAGE result (Figures 48 and 49). The presence of  $[\text{Co}(\text{NH}_3)_6]\text{Cl}_3$  induced significant changes in the behavior of guanine and cytosine related bands, which can be explained by changes in C+3, C8+, G36 and G8 position and pairing depending on the conditions. These changes also affect the environment and pairing/stacking interaction of U+2 and G+1 [162]. Pressure induced the formation of more compact docked states at both  $\text{MgCl}_2$  and  $[\text{Co}(\text{NH}_3)_6]\text{Cl}_3$  conditions, but these conditions favors different conformational states and intramolecular interactions. Therefore, these states might have different compressibility and hence behave differently under high hydrostatic pressure, which explains different amounts of product formation after 6 hours of reaction. These interactions are important for formation of different active docked complexes, and might also explain the lower efficiency of the wtHpRz in the presence of  $[\text{Co}(\text{NH}_3)_6]\text{Cl}_3$  compared to the biologically relevant  $\text{MgCl}_2$ .

### 5.3.2.3. $I_{\text{ratio}}$ analysis of unpaired to paired nucleotides of the hairpin ribozyme self-cleavage reaction

The overall conformational changes in the structure of the wtHpRz during the self-cleavage reaction have been determined in terms of the  $I_{\text{ratio}}$  of unpaired to paired guanine and uracil nucleotides ( $I_{\text{free}}/I_{\text{duplex}}$ ), as seen in Figure 68, using band intensity at 1660 and 1686  $\text{cm}^{-1}$ , respectively.

#### 5.3.2.3.1. $I_{\text{ratio}}$ analysis of the ambient and high hydrostatic pressure conditions in the presence of $\text{MgCl}_2$

Data were obtained from the IR bands of different recorded spectra in the presence of  $\text{MgCl}_2$  at 0.1 MPa, 50 MPa and 100 MPa.

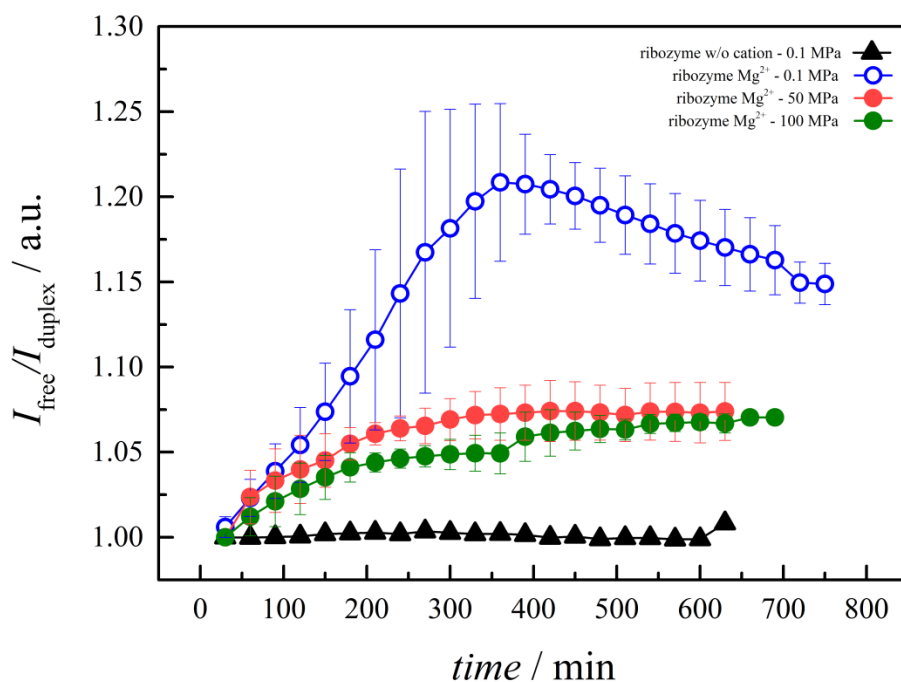


**Figure 68.**  $I_{\text{free}}/I_{\text{duplex}}$  analysis of the time-dependent FTIR data of the hairpin ribozyme with  $\text{MgCl}_2$  from 0.1 to 100 MPa. Temperature-dependence of the ratio of unpaired (free) to duplexed GC pairs ( $I_{\text{free}}/I_{\text{duplex}}$ ) as obtained from the infrared spectra recorded at  $\approx 1658 \text{ cm}^{-1}$  and  $\approx 1686 \text{ cm}^{-1}$ , respectively, for  $45 \text{ mg mL}^{-1}$  wild type hairpin ribozyme in  $50 \text{ mM}$  Tris-HCl buffer +  $0.1 \text{ mM}$  EDTA +  $6 \text{ mM}$   $\text{MgCl}_2$  at  $25 \text{ }^\circ\text{C}$ . Pressures analyzed were 0.1 MPa, 50 MPa and 100 MPa. The error bars cover the scattering of three independent measurements.

It can be observed, at Figure 68, that at 0.1 MPa the structural rearrangements between free and base paired nucleotides take place until 6 hours of the reaction, when a plateau is achieved. However, PAGE analysis shows that the reaction equilibrium is reached in one hour. This indicates that these conformational states are mainly non-active. In addition, the  $I_{\text{ratio}}$  is greatly reduced at high pressures, but there is only a small difference between 50 MPa and 100 MPa. It can be observed that pressure reduces the ribozyme's structural rearrangements, and the plateau is achieved after 3 hours of the reaction. The  $I_{\text{ratio}}$  and IR band analysis combined indicate that docked states may be favored by pressure, where mainly non-active conformers are encountered (Figure 48).

### 5.3.2.3.2. $I_{\text{ratio}}$ analysis of the ambient and high hydrostatic pressure conditions with the presence of $[\text{Co}(\text{NH}_3)_6]\text{Cl}_3$

Data were obtained from the IR bands of different recorded spectra in the presence of  $[\text{Co}(\text{NH}_3)_6]\text{Cl}_3$  and NaCl at 0.1 MPa and 100 MPa.

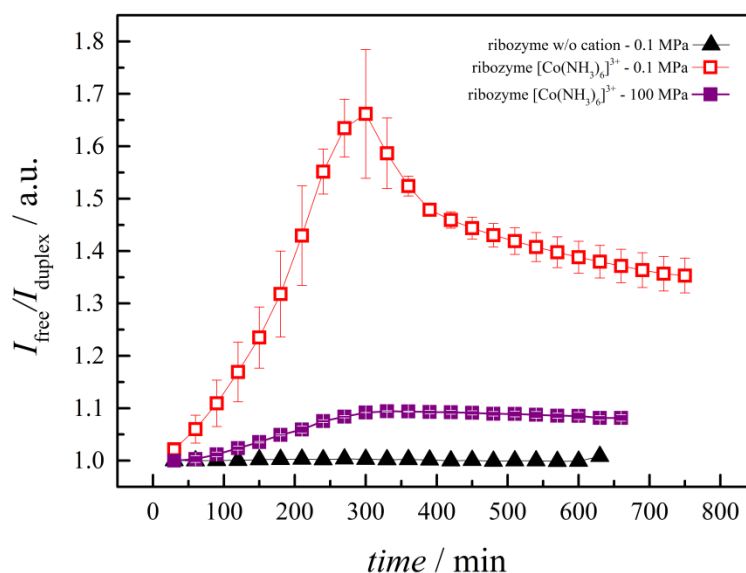


**Figure 69.**  $I_{\text{free}}/I_{\text{duplex}}$  analysis of the time-dependent FTIR data of the hairpin ribozyme with  $[\text{Co}(\text{NH}_3)_6]\text{Cl}_3$  from 0.1 to 100 MPa. Temperature-dependence of the ratio of unpaired (free) to duplexed GC pairs ( $I_{\text{free}}/I_{\text{duplex}}$ ) as obtained from the infrared spectra recorded at  $\approx 1658 \text{ cm}^{-1}$  and  $\approx 1686 \text{ cm}^{-1}$ , respectively, for  $45 \text{ mg mL}^{-1}$  wild type hairpin ribozyme in  $50 \text{ mM}$  Tris-HCl buffer +  $0.1 \text{ mM}$  EDTA +  $12 \text{ mM}$   $[\text{Co}(\text{NH}_3)_6]\text{Cl}_3$  +  $100 \text{ mM}$  NaCl at  $25 \text{ }^\circ\text{C}$ . Pressures analyzed were 0.1 MPa and 100 MPa. The error bars cover the scattering of three independent measurements.

Figure 69 shows the pressure-dependent  $I_{\text{free}}/I_{\text{duplex}}$  analysis of the IR bands around  $1654\text{ cm}^{-1}$  and  $1686\text{ cm}^{-1}$  in the presence of  $[\text{Co}(\text{NH}_3)_6]\text{Cl}_3$ . There are significant structural rearrangements between free and base paired nucleotides until 6 hours of the reaction, when a plateau is achieved. However, these conformers are not prone to cleavage (Figure 49). In addition, the  $I_{\text{ratio}}$  is greatly reduced at high pressure, as observed for the  $\text{MgCl}_2$  data (Figure 68). This indicates that docked states may be favored by pressure, where mainly non-active conformers are encountered, as seen at the PAGE data (Figure 49).

### 5.3.2.3.3. $I_{\text{ratio}}$ analysis of the ambient and high hydrostatic pressure conditions in the presence of $\text{MgCl}_2$ or $[\text{Co}(\text{NH}_3)_6]\text{Cl}_3$

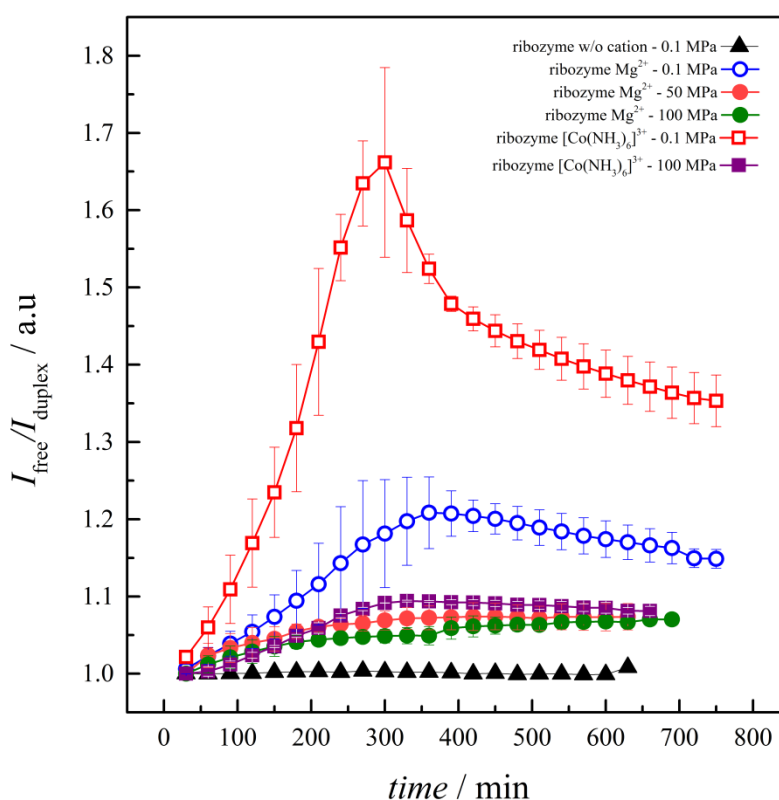


**Figure 70.**  $I_{\text{free}}/I_{\text{duplex}}$  analysis of the time-dependent FTIR data of the hairpin ribozyme with  $\text{MgCl}_2$  or  $[\text{Co}(\text{NH}_3)_6]\text{Cl}_3$  from 0.1 to 100 MPa. Temperature-dependence of the ratio of unpaired (free) to duplexed GC pairs ( $I_{\text{free}}/I_{\text{duplex}}$ ) as obtained from the infrared spectra recorded at  $\approx 1658\text{ cm}^{-1}$  and  $\approx 1686\text{ cm}^{-1}$ , respectively, for  $45\text{ mg mL}^{-1}$  wild type hairpin ribozyme in  $50\text{ mM}$  Tris-HCl buffer +  $0.1\text{ mM}$  EDTA +  $6\text{ mM}$   $\text{MgCl}_2$  or  $12\text{ mM}$   $[\text{Co}(\text{NH}_3)_6]\text{Cl}_3$  +  $100\text{ mM}$  NaCl at  $25\text{ }^\circ\text{C}$ . Pressures analyzed were 0.1 MPa and 100 MPa. The error bars cover the scattering of three independent measurements.

Figure 70 presents the combination of the  $I_{\text{ratio}}$  results for wtHpRz in the presence of 6 mM  $\text{MgCl}_2$  and 12 mM  $[\text{Co}(\text{NH}_3)_6]\text{Cl}_3$ . It can be observed that the  $I_{\text{ratio}}$  is greatly reduced at high pressures for both conditions. However,  $[\text{Co}(\text{NH}_3)_6]\text{Cl}_3$  shows a greater increase of  $I_{\text{ratio}}$  if compared to  $\text{MgCl}_2$  at 0.1 MPa, which is mostly related to a significant increase of free base vibrations. This indicates that the wtHpRz structure varies in many different conformers, but the self-cleavage reaction is less efficient when compared to the reaction in the presence of  $\text{MgCl}_2$  (Figure 48 and 49), suggesting that different undocked states not prone for cleavage can be formed. These results also confirmed that pressure indeed shifts the population of different structures toward docked/folded states, but those are mostly non-active docked states.

#### 5.4. Summary and conclusion

A combined PAGE and FTIR spectroscopy study was performed using the minimal model of the wild-type hairpin ribozyme, derived from the minus strand of the tobacco ringspot virus, under atmospheric and high hydrostatic pressure. The FTIR results showed that there are only small differences between the IR spectra of the wtHpRz secondary structure at 0.1 MPa, 50 MPa and 100 MPa in the presence of  $\text{MgCl}_2$ . Some interactions characteristic of the active state are destabilized by pressure, such as the triple strand Hoogsteen binding and B-form backbone and S-type (C2''-endo) sugar pucker, while pressure stabilizes the A-form (compact) backbone. Thereby, high hydrostatic pressure leads to a stagnation of the self-cleavage reaction by shifting the conformational ensembles toward folded/docked states that are not prone to cleavage, with consequent reduction of the overall product formation.

The effect of high hydrostatic pressure on the activity and structure of the wild-type hairpin ribozyme was also analyzed in the presence of 12 mM  $[\text{Co}(\text{NH}_3)_6]\text{Cl}_3$  and 100 mM NaCl at atmospheric and high hydrostatic pressure (100 MPa).  $[\text{Co}(\text{NH}_3)_6]\text{Cl}_3$  is an inert complex that mimics the hexahydrate magnesium. The FTIR results indicate that  $[\text{Co}(\text{NH}_3)_6]\text{Cl}_3$  favors different conformations of the wtHpRz, in accordance to the literature data [162]. These different conformations are less catalytically active than the conformations favored in the presence of  $\text{MgCl}_2$ . The wild-type hairpin ribozyme



achieved a maximum of cleaved product of 60% and 45% in the presence of  $\text{MgCl}_2$  and  $[\text{Co}(\text{NH}_3)_6]\text{Cl}_3$ , respectively. This difference may be related to the formation of different intramolecular interactions in the active pocket of the ribozyme, and destabilization of the backbone and sugar pucker conformations. These wtHpRz showed to be more pressure sensitive in the presence of  $[\text{Co}(\text{NH}_3)_6]\text{Cl}_3$  than  $\text{MgCl}_2$ . However, pressure shifts the ribozyme's conformational equilibrium from undocked/native toward docked states, in the presence of  $[\text{Co}(\text{NH}_3)_6]\text{Cl}_3$ , and this population is composed of undocked and docked/folded states not prone to cleavage.

The intensity ratio ( $I_{\text{ratio}}$ ) analysis showed that the structural equilibrium is shifted by pressure to the docked state for both  $\text{MgCl}_2$  and  $[\text{Co}(\text{NH}_3)_6]\text{Cl}_3$  conditions, where populations of active docked and non-active docked states are encountered. Some cleavage reaction can still take place at these conditions, as confirmed by the PAGE results. Higher hydrostatic pressures, such as 100 MPa, favor mostly non-active docked population, and the most significant decay of cleavage activity occurs from 0.1 to 100 MPa. However,  $[\text{Co}(\text{NH}_3)_6]\text{Cl}_3$  shows a marked increase of  $I_{\text{ratio}}$  when compared to  $\text{MgCl}_2$  at 0.1 MPa. This is indicated by the significant increase of free base vibrations, suggesting that different undocked states not prone for cleavage (docking) were formed. Despite the structural changes being more pronounced in the presence of  $[\text{Co}(\text{NH}_3)_6]\text{Cl}_3$ , the overall cleavage reaction was less efficient.

The formation of the docked state, a folded/compact pre-catalytic conformational state where the two helices come close in contact, is necessary for the self-cleavage reaction [27 – 29, 58 – 66].  $[\text{Co}(\text{NH}_3)_6]\text{Cl}_3$  can support the folding and activity of the hairpin ribozyme as analog of hexahydrate magnesium, but it cannot make the inner-sphere interactions with the RNA structure [161]. The presence of  $[\text{Co}(\text{NH}_3)_6]\text{Cl}_3$  induces different conformational states through different intramolecular interactions. The hairpin ribozyme showed to be less active in the presence of  $[\text{Co}(\text{NH}_3)_6]\text{Cl}_3$  when compared to  $\text{MgCl}_2$ . One can say that increased pressure favors the self-cleavage reaction, since pressure favors the formation of more compact conformational states. However, the combined study of the wild-type hairpin ribozyme self-cleavage activity, and the structural features related to it under high hydrostatic pressure showed that the overall equilibrium between undocked,

docked and cleaved state is shifted to the docked state by pressure in the presence of  $\text{MgCl}_2$  and  $[\text{Co}(\text{NH}_3)_6]\text{Cl}_3$ . These docked states were less prone to cleavage at both ionic conditions, despite having greater catalytic efficiency at high hydrostatic pressure in the presence of  $\text{MgCl}_2$  than  $[\text{Co}(\text{NH}_3)_6]\text{Cl}_3$ . Therefore, high hydrostatic pressure can modulate the structural rearrangement and the kinetics of the wild-type hairpin ribozyme by shifting the conformational equilibrium toward the folded/docked state, but these states are mainly not prone to cleavage, and the product formation is reduced upon pressurization.

---

## 6. Global summary



The “RNA World” is a 50-year-old conceptual idea, which states that, in the early history of life on Earth, RNA, or RNA-like molecules were precursors and carried out most of information processing and metabolic transformations for living organisms [76]. Studies have demonstrated the evolutionary capabilities of RNA to perform different tasks as carrier of genetic information, essential participation during protein expression and catalysis of enzymatic reaction, which emphasize the possibility that life started with RNA. It has also been shown that catalytic RNA molecules vary from riboswitches to autocatalytic ribozymes. However, in the modern world, most ribozymes require protein for efficient catalysis *in vivo*, and the majority of ribozyme destitute of protein interaction have been found only in a few virus-like forms [77].

Little is known about the effect that temperature and pressure have on the structure stability of nucleic acids. The tertiary structure of biomolecules is stabilized by inter- and intramolecular interactions, which comprise covalent and non-covalent interactions. The non-covalent interactions are weaker and easily perturbed by temperature, but pressure can also perturb molecular interactions, mainly due to the overall system’s volume change. Therefore, properties that depend on hydration and degree of packing, such as volume, compressibility and expansibility, will set how pressure can affect the structure, and also how it can shift the equilibrium between denatured and native states. The general high-pressure approaches for studies on biomolecules range from 0.1 MPa to 1000 MPa, where the non-covalent bonds in the tertiary structure are essentially affected, only [82-84]. It has been shown in the literature that structural changes in DNA are very small, and that major changes take place in the hydration layer, which will influence and alter the way DNA interacts with proteins and the overall transcriptional process [83]. In addition, the binding of proteins and drugs to DNA is weakened under pressure [85], and the RNA polymerase activity is reduced as well [86, 87]. Therefore, the study of biomolecules under extreme conditions, including high hydrostatic pressure, is of fundamental biological and biotechnological importance. Elucidation of the mechanistic details involved in the stability of biomolecules under extreme conditions, such as the deep sea, hydrothermal vents and volcanic environment, also proposed to be the likely birthplace of life, is important to understand how piezophiles could adapt and survive where high pressures are easily encountered [88].

To this end, the goal of this work was to combine temperature- and pressure-dependent studies, using different techniques in order to reveal the conformational and free energy landscape of different RNA molecules: the transfer RNA<sup>Phe</sup>, a small RNA hairpin and hairpin ribozymes.

*Exploring the free energy and conformational landscape of tRNA at high temperature and pressure conditions*

A combined temperature- and pressure-dependent study was carried out to explore the conformational and free energy landscape of yeast tRNA<sup>Phe</sup>, a well-known model for RNA function studies. To this end, FTIR and fluorescence spectroscopy, SAXS, and calorimetric methods were applied. The temperature and pressure stability of the tRNA<sup>Phe</sup> structure is highly dependent on the presence of Mg<sup>2+</sup>. This ion is responsible for screening the negatively charged phosphate-sugar backbone and stabilizes the tRNA structure against temperature increases the melting transition and the cooperativity of the melting transition. According to the FTIR data, the tertiary structure stabilized by Mg<sup>2+</sup> melts following a two-state model transition, in agreement with the literature [144]. Na<sup>+</sup> ions have a smaller effect on screening the negative charges of the tRNA backbone, as seen in the literature [145]. According to the SAXS data, the structural changes that take place upon melting seem to involve essentially internal structural rearrangements of the tRNA molecule, rather than a complete disruption of the tertiary structure. The pressure-dependent changes in the secondary structure of the tRNA<sup>Phe</sup> are rather small compared to the temperature dependent effect. A maximum increase of only about 15% unpaired bases is observed upon pressurization up to 1000 MPa. The tRNA<sup>Phe</sup> presents a different behavior in Mg<sup>2+</sup>-free and Mg<sup>2+</sup>-complexed states, which indicates that different regions of the tRNA possess different pressure stabilities. The stability is slightly decreased at high pressure in the Mg<sup>2+</sup>-complexed state, probably owing to the creation of small voids in the compact native structure of tRNA. The fluorescence data of the Y-base, which is located in the anticodon loop of tRNA<sup>Phe</sup>, show that the Mg<sup>2+</sup>-complexed state is highly stable under high pressure, which indicates that pressure-induced melting of the base pairs takes place in other regions of the tRNA structure first. Structural changes in the hydrating solvent, water, may also contribute to the pressure-induced changes observed

[146]. The spectroscopic data indicate that upon compression, the overall volume change of tRNA<sup>Phe</sup> is very small and slightly negative. It is confirmed by PPC data, which do not reveal significant changes in the temperature-dependent expansivity at  $T_m$  that would indicate a significant volume change upon RNA melting. Conversely, an overall volume change upon DNA duplex melting ( $\Delta V$ ) is small and positive [109, 147]. The pressure stability of tRNA<sup>Phe</sup> seems to be similar to that of non-canonical DNA structures (negative  $\Delta V$ ) [89]. The different pressure stabilities of DNA and tRNA might be due to a significant void volume contribution to  $\Delta V$  in the case of the less efficiently packed tRNA.

These findings have biological implications regarding organisms living under high-pressure conditions, such as in the deep sea, where pressures up to the 100 MPa (1 kbar) level are encountered [126, 127]. In this pressure range, the tRNA is highly stable and only minor conformational changes are observable. Therefore, tRNA molecules would hardly be affected up to this pressure range in living organisms.

### *Exploring temperature and pressure effects on the structure and stability of a small RNA hairpin*

In a second project, the temperature- and pressure-dependent stability of a small RNA hairpin, having the sequence gcUUCGgc, was explored. It is known as the smallest RNA entity that serves as nucleation site for RNA folding, ligand binding and tertiary folding initiation. It is also present in different RNA molecules such as the tRNA and ribozymes. Due to their importance, simplicity and size, small RNA hairpins serve as a prototype for folding dynamics and structure stability studies. An early MD simulation study proposed an elliptical  $p, T$ -stability diagram, where the structure of the small RNA hairpin (gcUUCGgc) could be denatured at high hydrostatic pressure and low temperature, and high hydrostatic pressure could promote refolding to its native or near-native structure at high temperatures [55]. To this end, FTIR and UV-vis spectroscopy methods were applied. The temperature-dependent FTIR data show that the small RNA hairpin structure might not be fully unfolded at high temperatures, forming extended chain ensembles, but rather to population of still compact unfolded or coil like structures. In

these compact unfolded structures, the double helical bonds of the native structure are lost, but apparently, some loop interactions remain. In the literature, molecular dynamics calculation showed that the small RNA molecule is highly stable and can populate numerous transition states, which is in accord with the broad melting transition observed for the small RNA hairpin. These states can vary between native structure (all native stem connections are present), frayed structure (conformations that lack one of the native stem connections), compact unfolded/coil like structure (conformations that lack both native stem connections, but retain the loop interaction), and extended/fully unfolded structures (neither stem nor loop connections are retained). However, the fully extended conformation is an unpopulated state, which is likely be achieved under forced melting conditions, only [47]. The pressure-dependent FTIR data reveal that pressure has a small destabilizing effect on the native structure of the small RNA hairpin at temperatures below thermal denaturation. Moreover, high-pressure does not promote formation of new native stem connections in denatured states, as proposed by the molecular dynamics study. This clearly indicates that pressure can perturb the small RNA hairpin structure and favor a large number of near-native intermediate structures, but high-pressure is not able to promote unfolding or refolding of the structure. Further, the FTIR data indicate that pressure has a small effect on the sugar pucker conformation of the small RNA hairpin structure at low and high temperatures. These small changes indicate that pressure causes small rearrangements of A-form RNA type, pressure does not induce Z-form RNA type conformations. This is consistent with a recent MD simulation study showing that high hydrostatic pressure has a stabilizing effect on the A-form helix, and destabilizes the Z-form helix of the RNA tetraloop backbone (gcGCAAgc) [103].

Overall, these findings indicate that the small RNA hairpin is a highly stable secondary structure element, with a rough free energy landscape and a wide variety of intermediate structures. These intermediates can be populated by pressure perturbation of the RNA structure, thereby increasing the population of near native structures. However, high hydrostatic pressure is not able to favor compact conformers or new native stem connections in the denatured ensemble. The earliest theoretically proposed elliptical  $p, T$ -stability phase diagram could not be proven experimentally.



---

***Pressure modulation of the hairpin ribozyme's structure and self-cleavage reaction***

In a last project, the structure and self-cleavage reaction of the [-]TRSV hairpin ribozyme was examined under atmospheric and high hydrostatic pressure conditions using PAGE and FTIR spectroscopy. The hairpin ribozyme features a four-way junction and is capable of catalyzing a site-specific self-cleavage transesterification reaction at the RNA backbone. The self-cleavage reaction follows a  $S_N2$ -type mechanism, in which the reverse reaction (ligation) can also be catalyzed under specific conditions [56-60].

The ribozyme's negatively charged structure is stabilized by cations, favoring folding of the RNA to the docked state, where the two helices come into close contact, forming new specific interactions that favor the cleavage reaction. The hairpin ribozyme was the first naturally occurring ribozyme to be characterized. It was widely studied and is a great model to study catalytic reactions of ribozymes [27, 29, 58-66, 106]. In this work, it could be shown that pressure favors the formation of the docked state for the  $Mg^{2+}$ -complexed state. However, some intramolecular interactions characteristic of the ribozyme's active state are probably destabilized by pressure, such as the triple strand, B-form backbone and S-type (C2'-endo) sugar pucker, while it stabilizes the more compact A-form backbone. Therefore, high hydrostatic pressure is responsible for the overall observed stagnation of the self-cleavage reaction by shifting the conformational equilibrium of substates structure populations toward folded/docked states that are not prone to cleavage, finally leading to a with consequent reduction of the overall self-cleavage reaction and product formation.

Further, the effect of high hydrostatic on the activity and structure of the hairpin ribozyme was also analyzed in the presence of  $[Co(NH_3)_6]Cl_3$  and NaCl at atmospheric and high hydrostatic pressure.  $[Co(NH_3)_6]^{3+}$  is an inert complex and is often used in theoretical work to mimic  $Mg^{2+}$ -hexahydrate. In this work, it could be shown that  $[Co(NH_3)_6]^{3+}$  favors different conformations of the hairpin ribozyme in agreement with the literature [163], and these conformations are more pressure sensitive. In the presence of  $[Co(NH_3)_6]^{3+}$  and at ambient pressure, the hairpin ribozyme features increased free base vibrations, suggesting that different undocked states not prone for docking/cleavage

were formed. Despite the structural changes being more pronounced in the presence of  $[\text{Co}(\text{NH}_3)_6]^{3+}$ , the overall cleavage reaction is less efficient. Also, pressure shifts the  $[\text{Co}(\text{NH}_3)_6]^{3+}$ -complexed ribozyme's conformational ensemble from undocked/native toward docked states that are not prone to cleavage. The  $[\text{Co}(\text{NH}_3)_6]^{3+}$ -complexed states are also less catalytically active than the  $\text{Mg}^{2+}$ -complexed states.

In addition, a modified hairpin ribozyme, featuring no junction, was studied in the presence of  $[\text{Co}(\text{NH}_3)_6]^{3+}$  and  $\text{Mg}^{2+}$ . Complementary MD simulations have been performed by collaborators. The modified hairpin ribozyme's self-cleavage activity is more efficient compared to the wild-type hairpin ribozyme. The  $[\text{Co}(\text{NH}_3)_6]^{3+}$ -complexed state is more reactive at atmospheric and high pressure than the  $\text{Mg}^{2+}$ -complexed state. Hence, modified sequence has a significant positive effect on the activity and stability of the ribozyme, which is in agreement with the literature that showed that  $[\text{Co}(\text{NH}_3)_6]^{3+}$  favors the stabilization of catalytically prone conformations of the hairpin ribozyme mutant. The overall self-cleavage reaction decelerated under pressure, but the  $[\text{Co}(\text{NH}_3)_6]^{3+}$ -complexed state retained the same amount of product formation up to 300 MPa as the  $\text{Mg}^{2+}$ -complexed state at atmospheric pressure.

In summary, the comparison of the wild type and the mutant ribozyme at different ionic conditions shows that high hydrostatic pressure can modulate the structural conformations and the kinetics of the hairpin ribozyme, by shifting the conformational ensemble toward the folded/docked state. However, these states are mainly not prone to cleavage and the overall self-cleavage activity and product formation is reduced upon pressurization. The effect of pressure on the self-cleavage step itself could not be evaluated.

In conclusion, the pressure studies on  $\text{tRNA}^{\text{Phe}}$ , the small RNA hairpin and the hairpin ribozyme show that pressure hardly affects secondary structure elements, but minor changes of tertiary structures can lead to significant effects on the function and activity of the RNA. Therefore, the results of the here presented work underline the importance of the structure-function relationships for RNA molecules. Nevertheless, under natural high-pressure conditions, such as the deep sea, where pressures up to 100 MPa are

encountered [126, 127], the RNA molecules studied were not affected drastically by pressure.



---

## 7. Zusammenfassung



Die RNA-Welt Theorie ist eine 50 Jahre alte konzeptionelle Idee, die besagt, dass in der frühen Geschichte des Erdenlebens RNA oder RNA-ähnliche Moleküle als Bausteine zur Informationsspeicherung und zur metabolischen Umwandlung in lebenden Organismen dienten und somit Vorläufermoleküle der heutigen Biomoleküle darstellen [76]. Studien haben bereits die evolutionären Fähigkeiten der RNA gezeigt. Sie besitzen vielfältige Funktionen. Dazu gehören die Speicherung von genetischen Informationen, die essentielle Beteiligung an der Proteinexpression und die Katalyse von enzymatischen Reaktionen. Dies bekräftigt die Hypothese, dass die RNA ein wichtiger Baustein für die Entstehung des Lebens darstellt. Zusätzlich wurde gezeigt, dass katalytische RNA Moleküle eine große strukturelle Vielfalt aufweisen; sie reicht von Riboswitches bis zu Ribozymen. In der modernen Welt benötigen Ribozyme allerdings Proteine um eine effiziente Katalyse *in vivo* zu gewährleisten. Ribozyme, die ohne Protein-Bindungspartner auskommen, wurden bisher nur in wenigen Viren-ähnlichen Formen gefunden [77].

Wenig ist bekannt über den Einfluss von Temperatur und Druck auf die Strukturstabilität von Nukleinsäuren. Die Tertiärstruktur von Biomolekülen wird durch inter- und intramolekulare Wechselwirkungen, die aus kovalenten und nicht-kovalenten Interaktionen bestehen, stabilisiert. Die nicht-kovalenten Wechselwirkungen sind dabei wesentlich schwächer und können leicht durch Temperatur beeinflusst werden. Druckänderungen dagegen führen zu Perturbationen von Wechselwirkungen, die ausschließlich mit Änderungen des Volumens einhergehen. Deshalb können Eigenschaften wie Volumen, Kompressibilität und Expansibilität, die von der Hydratation und dem Packungsgrad abhängen, bestimmen, wie sich Druck auf die Struktur und insbesondere auf die Verschiebung des Gleichgewichtes zwischen denaturierten und nativen Zuständen auswirkt. In der Regel werden Druckuntersuchungen an Biomolekülen zwischen 0,1 und 1000 MPa durchgeführt, sodass im Wesentlichen nicht-kovalente Wechselwirkungen in Tertiärstrukturen beeinflusst werden [82-82]. Aus der Literatur ist bekannt, dass druckinduzierte Strukturänderungen von DNA-Doppelsträngen sehr klein sind, sodass die wesentlichen Änderungen in der Hydrathülle zu erwarten sind. Diese können Interaktionen von DNA mit Proteinen und gar dadurch den Transkriptionsprozess beeinflussen und verändern [83]. Bei erhöhtem Druck werden Bindungen von Proteinen und Arzneimitteln an die

DNA geschwächt [85] und die Aktivität der RNA Polymerase reduziert [86, 87]. Deshalb ist die Untersuchung von Biomolekülen unter Extrembedingungen wie hoher hydrostatischer Druck von fundamentaler Bedeutung für die Biologie und Biotechnologie. Eine mechanistische Aufklärung der Stabilitäten von Biomolekülen unter extremen Umweltbedingungen wie Tiefsee, hydrothermalen Quellen und vulkanischen Umgebungen gibt Hinweise auf die Adaptationsstrategie der druckliebenden Organismen (Piezophile). Die Entstehung des Lebens fand wahrscheinlich ebenfalls unter solchen extremen Umweltbedingungen statt [88].

Das Ziel dieser Arbeit war es, mit Hilfe von verschiedenen Messmethoden die Konformations- und Energielandschaft verschiedener RNA Moleküle temperatur- und druckabhängig zu untersuchen. Dazu gehörten die Transfer-RNA tRNA<sup>Phe</sup>, eine kleine RNA Haarnadel und ein Haarnadel-Ribozym.

### ***Untersuchung der Energie- und Konformationslandschaft einer tRNA unter dem Einfluss von hohen Temperaturen und Drücken***

Als Modell für temperatur- und druckabhängige Studien wurde die bereits gut untersuchte tRNA<sup>Phe</sup> aus Hefe gewählt, um deren Energie- und Konformationslandschaft zu untersuchen. Als Messmethoden dienten FTIR- und Fluoreszenz-Spektroskopie sowie SAXS und Kalorimetrie. Es wurde gezeigt, dass die Anwesenheit von Mg<sup>2+</sup>-Ionen für die Temperatur- und Druckstabilität der tRNA<sup>Phe</sup> von entscheidender Bedeutung ist. Sowohl eine thermische Stabilisierung als auch ein Anstieg der Kooperativität während der Entfaltung konnten beobachtet werden. Dies ist durch die Abschirmung des negativ geladenen Zucker-Phosphat-Rückgrats durch Mg<sup>2+</sup>-Ionen zu erklären. Im Einklang mit Literaturdaten bestätigten FTIR Untersuchungen die Annahme eines Zweizustand-Modells für die Entfaltung [144]. Na<sup>+</sup>-Ionen hingegen sind weniger effizient in der Abschirmung der Phosphatgruppen [145]. Ferner zeigten SAXS Untersuchungen, dass die Strukturänderung der tRNA während des Schmelzens im Wesentlichen durch eine interne strukturelle Umorientierung des Moleküls hervorgerufen wurde, wobei die Tertiärstruktur nicht vollständig zerstört wurde. Die druckinduzierten Änderungen in der Sekundärstruktur der tRNA<sup>Phe</sup> sind im Vergleich dazu geringer. Nur 15% der



Basenpaarungen wurden durch Druckapplikation bis zu 1000 MPa aufgebrochen. Die tRNA<sup>Phe</sup> wies unterschiedliches Verhalten in der Mg<sup>2+</sup>-freien und Mg<sup>2+</sup>-gebundenen Form auf, was darauf hindeutet, dass verschiedene Regionen der tRNA unterschiedliche Druckstabilitäten besitzen. In der Mg<sup>2+</sup>-gebundenen Form nahm die Druckstabilität der tRNA geringfügig ab. Dies kann durch die Bildung von kleinen Hohlräumen in der kompakten und nativen Struktur der tRNA erklärt werden. Fluoreszenz-Untersuchungen an der Anticodon-Schleife der tRNA ergaben, dass diese in der Mg<sup>2+</sup>-stabilisierten Form sehr druckresistent war. Daraus kann geschlossen werden, dass die druckinduzierten Konformationsänderungen der tRNA von anderen Regionen des Moleküls ausgehen. Druck kann ebenfalls die Hydrathülle der tRNA beeinflussen und somit indirekt die beobachteten Strukturänderungen der tRNA induzieren [146]. Spektroskopische Daten zeigten, dass das Gesamtvolumen der tRNA während des Schmelzvorgangs nur geringfügig abnahm. In der Druck-Perturbations-Kalorimetrie (PPC) wurde ebenfalls keine signifikante Änderung des thermischen Expansionskoeffizienten am Entfaltungsübergang beobachtet. Volumenänderungen von DNA Doppelsträngen ( $\Delta V$ ), die mit dem Schmelzvorgang einhergehen, sind zumeist klein und positiv [109, 147]. Das Druckverhalten der tRNA ist vergleichbar mit der von nicht-kanonischen DNA Strukturen wie G-Quadruplexen (negatives  $\Delta V$ ) [89]. Die unterschiedlichen Druckstabilitäten der Nukleinsäuren fußen auf der Packungseffizienz und somit der Bildung von Hohlräumen, die einen signifikanten  $\Delta V$ -Beitrag aufweisen.

Die Ergebnisse dieser Studie liefern somit wichtige Erkenntnisse für das Verständnis des Lebens bei Hochdruckbedingungen wie in der Tiefsee (bis zu 100 MPa) [126, 127]. In diesem Druckbereich ist die tRNA stabil und nur sehr geringe Konformationsänderungen sind zu beobachten, sodass eine signifikante Beeinträchtigung der tRNA-Funktion durch Druck *in vivo* nicht zu erwarten ist.

### ***Untersuchung der Struktur und der Stabilität einer kleinen RNA-Haarnadel unter dem Einfluss von hohen Temperaturen und Drücken***

In einer zweiten Studie wurde die kleine RNA-Haarnadel mit der Sequenz gcUUCGgc im Hinblick auf ihre Temperatur- und Druckstabilität untersucht. Diese RNA-Haarnadel

stellt die kleinste RNA-Einheit dar, die Faltung von Sekundär- und Tertiärstrukturen sowie Ligandenbindung ermöglicht, und ist als Strukturmotiv in vielen verschiedenen RNA-Molekülen wie tRNAs und Ribozymen verankert. Aufgrund ihrer Größe, Einfachheit und Wichtigkeit dienen solche kleinen RNA-Haarnadeln oft als Modelle für Faltungsdynamik- und Strukturstabilitätsstudien. Eine frühe MD Simulationsstudie postulierte ein ellipsenförmiges Druck-Temperatur-Stabilitätsdiagramm für die gcUUCGgc RNA-Haarnadel; entsprechend sind Entfaltungsprozesse bei hohen Drücken und niedrigen Temperaturen sowie Faltung bei hohen Drücken und hohen Temperaturen zu erwarten [55]. Mittels FTIR und UV/Vis Spektroskopie konnte im Rahmen dieser Arbeit gezeigt werden, dass sich die RNA-Haarnadel in dem untersuchten Temperaturbereich nicht vollständig entfalten konnte, sondern ein Ensemble intermediär kompakter oder Coil-ähnlicher Strukturen formte. In diesen kompakten und entfaltenen Konformationen waren die Doppelhelix-Wechselwirkungen der gefalteten Struktur aufgehoben, während einige Interaktionen in der Schleife höchstwahrscheinlich bestehen blieben. Ferner wurde ein sehr breiter Schmelzübergang beobachtet. Diese Ergebnisse sind im Einklang mit einer weiteren MD Simulation, die zeigt, dass die RNA-Haarnadel sehr stabil ist und zahlreiche Übergangszustände besitzt. Diese Zustände können zwischen der nativen Struktur (beide Basenpaarungen sind intakt), einer „*frayed*“ (zerfasert) Struktur (mit einer Basenpaarung), einer kompakten und entfaltenen/Coil-ähnlichen Struktur (nur Schleifen-Interaktionen) und schließlich einer ausgedehnten und vollständig entfaltenen Konformation variieren. Allerdings ist die vollständig ausgedehnte Konformation kein besetzter Zustand und dieser kann nur unter erzwungenen Schmelzbedingungen erreicht werden [47]. Bei tiefen Temperaturen wurden im Gegensatz nur sehr geringe Druckeffekte, die sich destabilisierend auf die Haarnadelstruktur auswirkten, gefunden. Auch eine druckinduzierte Rückfaltung der denaturierten RNA konnte nicht beobachtet werden. Bei hohen Drücken wurde zwar das Einnehmen von quasi nativen Intermediatstrukturen bevorzugt, aber keine Entfaltung oder Faltung der Haarnadel induziert. Der Druckeinfluss auf die Konformation des Zuckers in der A-Form der RNA Helix war ebenfalls gering. Analoge Beobachtungen wurden in einer aktuellen MD Simulation gemacht: Hoher hydrostatischer Druck wirkt sich stabilisierend auf die A-Helix und destabilisierend auf die Z-Helix der Haarnadel aus [103].

Insgesamt haben die Ergebnisse dieser Studie gezeigt, dass die kleine RNA-Haarnadel ein sehr stabiles Sekundärstrukturelement darstellt. Es weist eine raue Energielandschaft und eine Vielzahl von Intermediatstrukturen auf. Diese werden bei hohen Drücken favorisiert, sodass die Population der quasi nativen Strukturen zunimmt. Das früher theoretisch postulierte Druck-Temperatur-Stabilitätsdiagramm der RNA-Haarnadel konnte allerdings nicht experimentell bestätigt werden; denn eine druckinduzierte Entfaltung (bei tiefen Temperaturen) oder Faltung (bei hohen Temperaturen) konnte nicht beobachtet werden.

### ***Druckmodulation der Struktur und der Selbstspaltungsreaktion von einem Haarnadel-Ribozym***

In einem letzten Projekt wurden die Struktur und die Selbstspaltungsreaktion des [-]TRSV Haarnadel-Ribozyms bei verschiedenen Drücken untersucht. Das Haarnadel-Ribozym weist in seiner Tertiärstruktur eine „4-way junction“ auf und katalysiert eine seitenspezifische Selbstspaltung durch eine Umesterung des RNA-Rückgrats. Diese Reaktion kann durch einen S<sub>N</sub>2-Mechanismus beschrieben werden, so dass unter spezifischen Bedingungen die Rückreaktion (Ligation) ebenfalls katalysiert werden kann [56-60]. In Anwesenheit von Ionen wird das Ribozym in einen angedockten Zustand gefaltet. In dieser Konformation treten zwei Helices in Kontakt und bilden neue spezifische Interaktionen, sodass die Selbstspaltungsreaktion bevorzugt wird. Das Haarnadel-Ribozym gehört zu den ersten untersuchten natürlich vorkommenden Ribozymen und stellt ein gutes Modellsystem für die Untersuchung von ribozymkatalysierten Reaktionen dar [27, 29, 58-66, 106]. Im Rahmen dieser Arbeit konnte gezeigt werden, dass in Anwesenheit von Mg<sup>2+</sup>-Ionen und bei hohen Drücken die Ausbildung der „*docked*“-Konformation bevorzugt wurde. Allerdings wurden einige intramolekulare Interaktionen, die für den aktiven Zustand des Ribozyms charakteristisch sind, durch Druckapplikation destabilisiert. Dazu gehörten der Dreifachstrang, ein RNA Rückgrat in der B-Form und die C2'-endo-Konformation des Zuckers (S-Typ). Unter hohen Drücken wurde das Ribozym in der kompakten A-Form stabilisiert. Als Folge wurde insgesamt eine Reduktion der Selbstspaltungsaktivität beobachtet. Druckapplikation führte somit zu einer Verschiebung des Gleichgewichtes in Richtung

gefalteter „*docked*“-Zustände, die die Katalyse der Selbstspaltungsreaktion nicht begünstigten und eine Stagnation der Reaktion verursachten.

Ferner wurde die Struktur und die Enzymaktivität des Haarnadel-Ribozyms in Anwesenheit von  $[\text{Co}(\text{NH}_3)_6]\text{Cl}_3$  und  $\text{NaCl}$  untersucht.  $[\text{Co}(\text{NH}_3)_6]^{3+}$  ist ein inerte Komplex und wird in theoretischen Arbeiten oft als  $\text{Mg}^{2+}$ -Hexahydrat-Analogon verwendet. Im Einklang mit der Literatur konnte gezeigt werden, dass in Anwesenheit von  $[\text{Co}(\text{NH}_3)_6]^{3+}$  verschiedene Konformationen des Haarnadel-Ribozyms bevorzugt wurden [163]. Diese wiesen eine erhöhte Anzahl an freien Basen auf, was auf eine strukturelle Vielfalt hindeutet. Dies korrelierte jedoch nicht mit der katalytischen Effizienz des Haarnadel-Ribozyms. Eine deutlich erniedrigte Reaktionsrate der Selbstspaltung wurde beobachtet. Bei Druckapplikationen wurde eine erhöhte Drucksensitivität des Haarnadel-Ribozyms festgestellt. Auch hier wurde eine druckinduzierte Verschiebung des Gleichgewichts in Richtung „*docked*“-Zustände gemessen. Allerdings waren diese Konformationszustände weniger katalytisch aktiv als die der  $\text{Mg}^{2+}$ -komplexierten.

Weiterhin wurde ein modifiziertes Haarnadel-Ribozym, das keine Kreuzungstellen aufweist, im Hinblick auf die Komplexierung durch  $\text{Mg}^{2+}$  und  $[\text{Co}(\text{NH}_3)_6]^{3+}$  untersucht. Ergänzende MD Simulationen wurden in Kollaboration durchgeführt. Im Vergleich zu dem Wildtyp zeigte das modifizierte Ribozym eine deutlich erhöhte Selbstspaltungsaktivität. Sowohl bei atmosphärischem als auch bei hohem Druck wurde für die  $[\text{Co}(\text{NH}_3)_6]^{3+}$ -gebundene Form eine höhere katalytische Effizienz gefunden. Die modifizierte Sequenz wirkte sich somit positiv auf die Aktivität und Stabilität des Ribozyms aus. Literaturdaten zeigen ebenfalls, dass in Anwesenheit von  $[\text{Co}(\text{NH}_3)_6]^{3+}$  Katalyse-freundliche Konformationen der Ribozym-Mutante stabilisiert und bevorzugt werden. Bei hohen Drücken wurde die Selbstspaltungsreaktion insgesamt verlangsamt, aber bei 300 MPa besaß die  $[\text{Co}(\text{NH}_3)_6]^{3+}$ -gebundene Mutante immer noch die gleiche Umsatzrate wie die  $\text{Mg}^{2+}$ -gebundene Variante bei atmosphärischem Druck. Informationen über dem Einfluss von Druck auf den alleinigen Schritt der Selbstspaltung konnten nicht erhalten werden.

Insgesamt hat der Vergleich des Wildtyp Ribozyms und dessen Mutante in verschiedenen ionischen Umgebungen gezeigt, dass hoher hydrostatischer Druck die Konformationen und als Folge die Enzymkinetik des Haarnadel-Ribozyms modulieren kann. Dabei werden kompakte Strukturesembles bevorzugt, die die Katalyse der Selbstspaltungsreaktion insgesamt erschweren.

Druckstudien an tRNA<sup>Phe</sup>, eine kleine RNA-Haarnadel und das Haarnadel-Ribozym haben insgesamt gezeigt, dass Sekundärstrukturelemente von Nukleinsäuren durch Druck kaum moduliert werden, während geringfügige Veränderungen in der Tertiärstruktur signifikante Auswirkung auf die Funktion und Aktivität von RNA haben können. Die Ergebnisse der vorliegenden Arbeit unterstreichen somit die Wichtigkeit der Struktur-Funktionsbeziehung für RNA Moleküle. Ferner wurde gezeigt, dass die hier untersuchten RNA Moleküle im Druckbereich, die in der Tiefsee zu finden sind (bis zu 100 MPa), weitgehend stabil und funktional sind [126, 127].



---

## 8. Appendix





## 8.1. Labeled-small RNA hairpin

Temperature- and pressure-dependent measurement were carried out on the fluorescent labeled-small RNA hairpin (labeled-sRNAH), sequence 5' - cyanine 3 -GCUUCGGC - cyanine 5 - 3'. To this end, UV-vis and FTIR spectroscopy techniques were applied. These results were used for comparison with the results obtained by Förster (fluorescence) resonance energy transfer (FRET) measurements, which were performed in parallel work by Dr. Salomé Pataráia. The experimental details can be found in section 4.2.

### 8.1.1. Temperature-dependent analysis of the labeled-small RNA hairpin

#### 8.1.1.1. Labeled-small RNA hairpin in-plane base vibrations sensitive to effects of base pairing followed by FTIR spectroscopy

Conformational transitions of RNA molecules can be followed by FTIR spectroscopy under varied conditions, such as different temperatures and high hydrostatic pressures. The RNA infrared signal can be divided into two main regions, from 1800 to 1500  $\text{cm}^{-1}$  (related to base pairing and base stacking interaction signals) and from 1500 to 1250  $\text{cm}^{-1}$  (related to glycosidic bond rotation, backbone conformation and sugar pucker). For detailed information on RNA IR band assignment, see Table 1 in section 2.2.1.5. In the 1800 to 1500  $\text{cm}^{-1}$  wavenumber region, the IR bands are originating from nucleobase vibrations, which are sensitive to base stacking and base-pairing interactions. The IR bands are related to double or single strand vibrations, which include C=C, C=N, and C=O stretching of free and/or bonded nucleotides. A double strand to single strand transition results in a decrease in the intensity of the IR band at around 1696 to 1684  $\text{cm}^{-1}$  with a concomitant increase in the band at around 1677 to 1653  $\text{cm}^{-1}$ . The former arises due to the C6=O6 stretch of base-paired guanine plus the C2=O2 stretch of uracil. The latter band arises mainly from the stretching vibrations of C6=O6 of free (i.e., non-base paired) guanine, the C2=O2 stretch of free cytosine, and the C4=O4 stretch of free uracil [114, 136]. For better analysis of the IR bands the 1800 to 1500  $\text{cm}^{-1}$  region can be divided into two areas, from 1720 to 1600  $\text{cm}^{-1}$ , and from 1600 – 1550  $\text{cm}^{-1}$ .

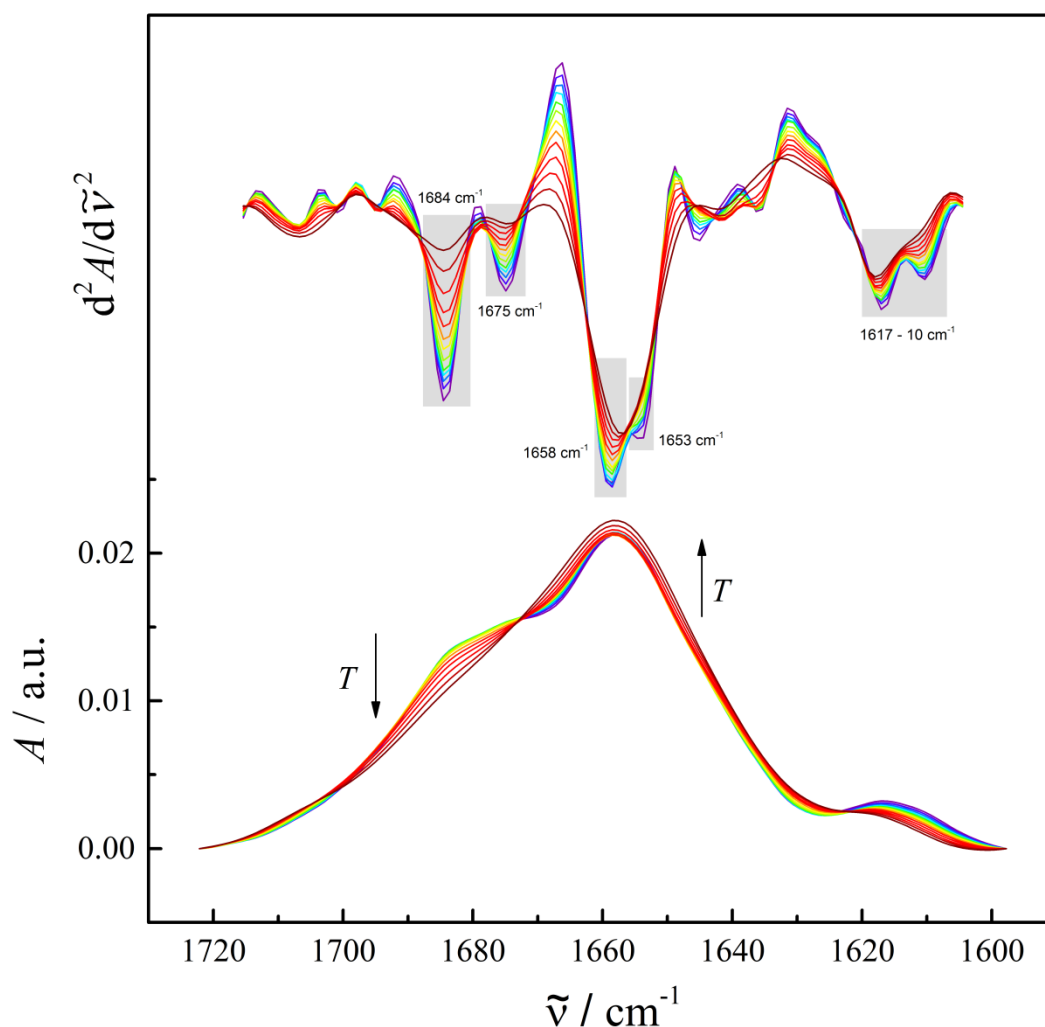


**Figure A1. Temperature-dependent normalized and second derivative spectra of the labeled -small RNA hairpin in the wavenumber region from 1740 to 1600  $\text{cm}^{-1}$ .** Second derivative and normalized spectra of 5  $\text{mg mL}^{-1}$  small RNA hairpin in 50  $\text{mM}$  Tris-HCl buffer + 0.1  $\text{mM}$  EDTA from 10 to 80  $^{\circ}\text{C}$ . In the normalized spectra the IR band from 1696 to 1684  $\text{cm}^{-1}$  is related to base paired nucleotides and decreases with temperature (indicated by the arrow), while the IR band from 1677 to 1653  $\text{cm}^{-1}$  is related to free nucleotides and increases with temperature (indicated by the arrow). The most important bands are indicated by the grey rectangles in the second derivative spectra. The highlighted bands are: 1684  $\text{cm}^{-1}$ , 1675  $\text{cm}^{-1}$ , 1581  $\text{cm}^{-1}$ , 1653  $\text{cm}^{-1}$ , 1617-10  $\text{cm}^{-1}$ . (Selected data)

Figure A1 shows the temperature-dependent FTIR spectra of the labeled -sRNAH in 50  $\text{mM}$  Tris-HCl buffer pH 7.5 + 0.1  $\text{mM}$  EDTA, from 10 to 80  $^{\circ}\text{C}$ , in the wavenumber region from 1720 to 1600  $\text{cm}^{-1}$ . Thermal unfolding was easily detected by the decrease in absorbance ( $A$ ) of the IR band at 1686  $\text{cm}^{-1}$ , which is characteristic of base paired G-C

vibrations, and the concomitant increase in IR intensity of unpaired nucleic acids at around  $1660\text{ cm}^{-1}$ . The conformational changes observed in the labeled-sRNAH have been also determined in terms of the ratio of intensity ( $I_{\text{ratio}}$ ) of unpaired to paired G-C nucleotides pairs ( $I_{\text{free}}/I_{\text{duplex}}$ ) (Figure A2). These data were obtained from the IR bands of different recorded spectra (Figure A1), at  $1660$  and  $1686\text{ cm}^{-1}$ , respectively. The labeled -sRNAH does not show a “two state model” like denaturation melting profile, and the melting transition temperature stays around  $50\text{ }^{\circ}\text{C}$ . The labeled-sRNAH molecule presents an inverse melting profile when compared to the sRNAH. The intensity ratio ( $I_{\text{free}}/I_{\text{duplex}}$ ) increases only after  $50\text{ }^{\circ}\text{C}$  and does not reach an equilibrium or a plateau, whereas the  $I_{\text{ratio}}$  of the sRNAH increases until achieving a plateau at  $60\text{ }^{\circ}\text{C}$ , as seen at figures A2 and 30, respectively. The labeled-sRNAH melting transition is very broad and hence of low cooperativity. In both sRNAH cases, non-labeled and labeled, the distribution of conformational ensembles seems to be very broad during thermal denaturation. However, in comparison with the sRNAH, the melting transition of the labeled-sRNAH seems to be delayed by the presence of the fluorescent dyes.

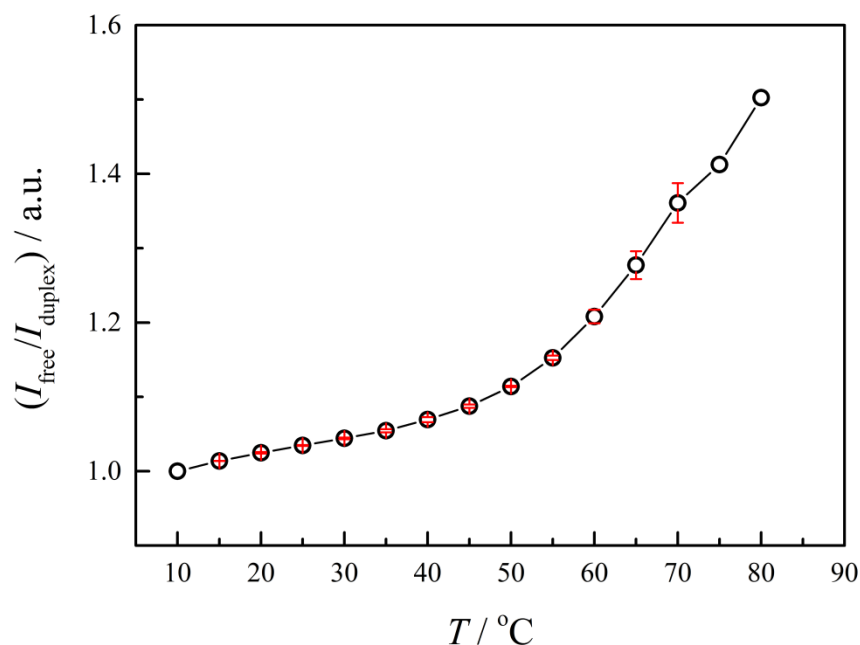


**Figure A2.**  $I_{\text{free}}/I_{\text{duplex}}$  analysis of the temperature-dependent FTIR data of the labeled-small RNA hairpin. Temperature-dependence of the ratio of unpaired to duplexed (GC pairs) ratio ( $I_{\text{free}}/I_{\text{duplex}}$ ) as obtained from the infrared spectra recorded at  $\approx 1660\text{ cm}^{-1}$  and  $\approx 1686\text{ cm}^{-1}$ , respectively, for  $5\text{ mg mL}^{-1}$  labeled-small RNA hairpin in  $50\text{ mM}$  Tris-HCl buffer +  $0.1\text{ mM}$  EDTA from  $10$  to  $80\text{ }^{\circ}\text{C}$ . The error bars cover the scattering of three independent measurements.

### 8.1.1.2. UV-vis spectroscopy of the labeled-small RNA hairpin

UV-vis spectroscopy measurements were also carried out for the labeled-sRNAH, in order to confirm the melting profile observed by temperature-dependent FTIR spectroscopy results.

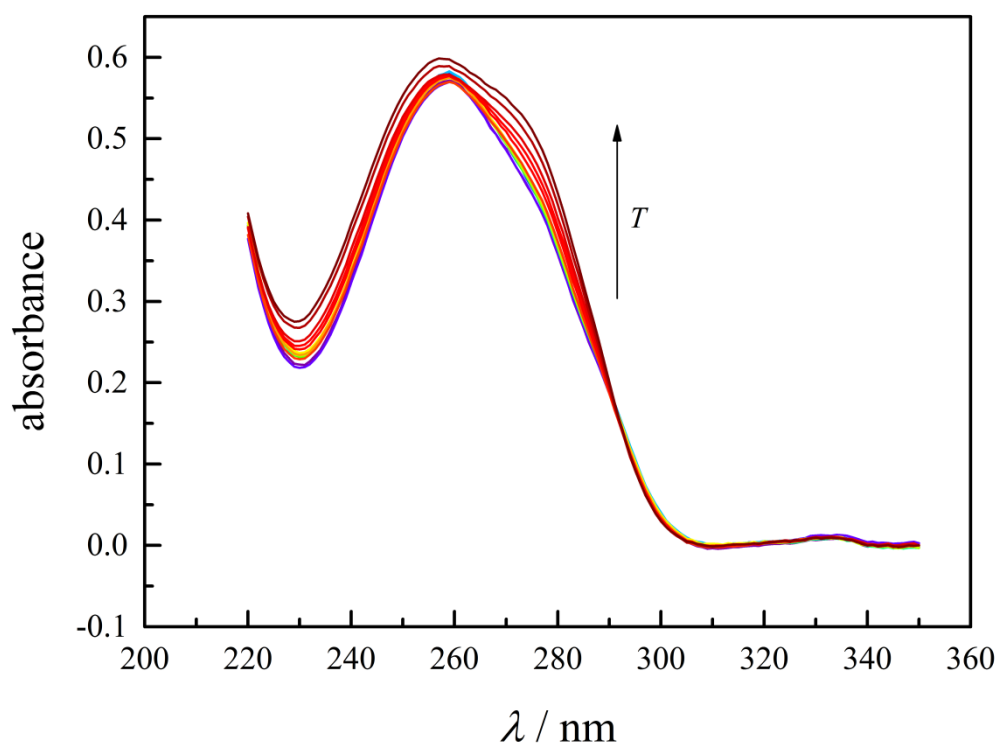


**Figure A3. Temperature-dependent UV-vis spectra of the labeled-small RNA hairpin.** UV-vis spectra of 40  $\mu\text{M}$  labeled-small RNA hairpin in 50 mM Tris-HCl buffer + 0.1 mM EDTA from 10 to 80  $^{\circ}\text{C}$ . The UV-vis absorbance increases with increasing temperature (indicated by the arrow). (Selected data)

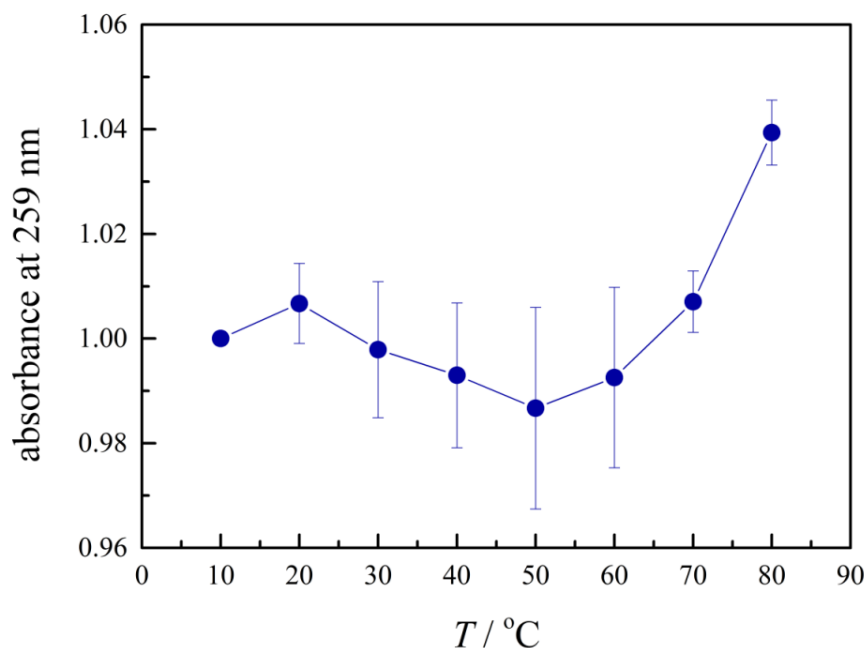


**Figure A4. Temperature-dependent UV-vis maximum absorbance at 259 nm of the labeled-small RNA hairpin.** Maximum absorbance at 259 nm, standard marker of polymeric RNA at UV-vis, of 40  $\mu\text{M}$  labeled-small RNA hairpin in 50 mM Tris-HCl buffer + 0.1 mM EDTA from 10 to 80  $^{\circ}\text{C}$ . The error bars cover the scattering of three independent measurements.

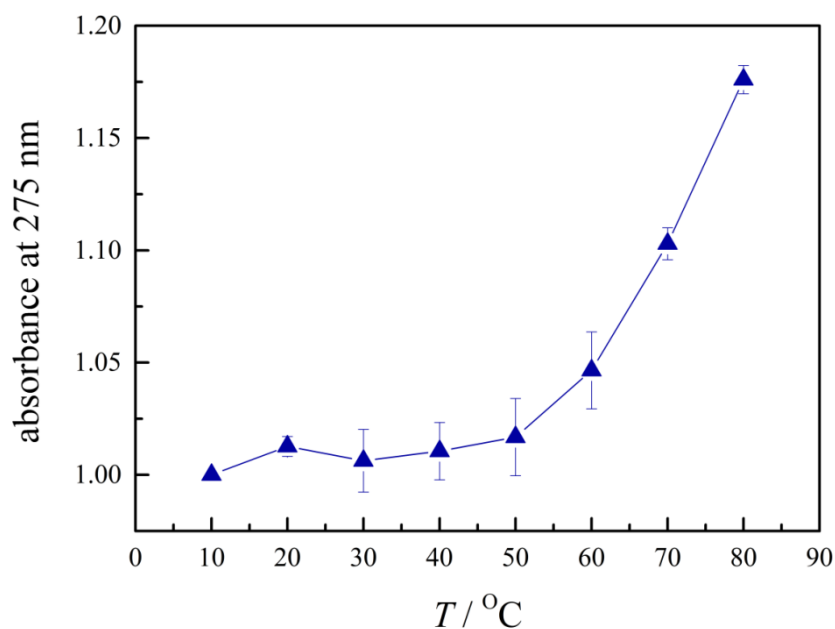


**Figure A5. Temperature-dependent UV-vis maximum absorbance at 275 nm of the labeled-small RNA hairpin.** Maximum absorbance at 275 nm, UV absorption maxima for guanine, of 40  $\mu\text{M}$  labeled-small RNA hairpin in 50 mM Tris-HCl buffer + 0.1 mM EDTA from 10 to 80  $^{\circ}\text{C}$ . The error bars cover the scattering of three independent measurements.

The UV-vis spectroscopy result, at Figure A4 is in good agreement with FTIR data. The UV-vis data show a denaturation that starts only after 50 °C. The UV-vis spectroscopy data suggest the same denaturation profile observed with FTIR, in which the denaturation starts only after 50 °C (Figure A1-A5). The UV-vis signal at 275 nm, related to the absorbance of free guanines, can be observed in the UV-vis spectra from 60 to 80 °C, only (Figure A3). This is in good agreement with the FTIR data (Figure A2), indicating that the helix interactions are not fully denatured until 80 °C, and that the fluorescent dyes, Cy3' and Cy5', can be interfering on the structure dynamics of the labeled-sRNAH. The denaturation profile following the signal at 275 nm (Figure A5) has the same trend observed for the main UV signal at 259 nm (Figure A4).

### 8.1.1.3. Labeled-small RNA hairpin in-plane base vibrations sensitive to effects of base stacking followed by FTIR spectroscopy

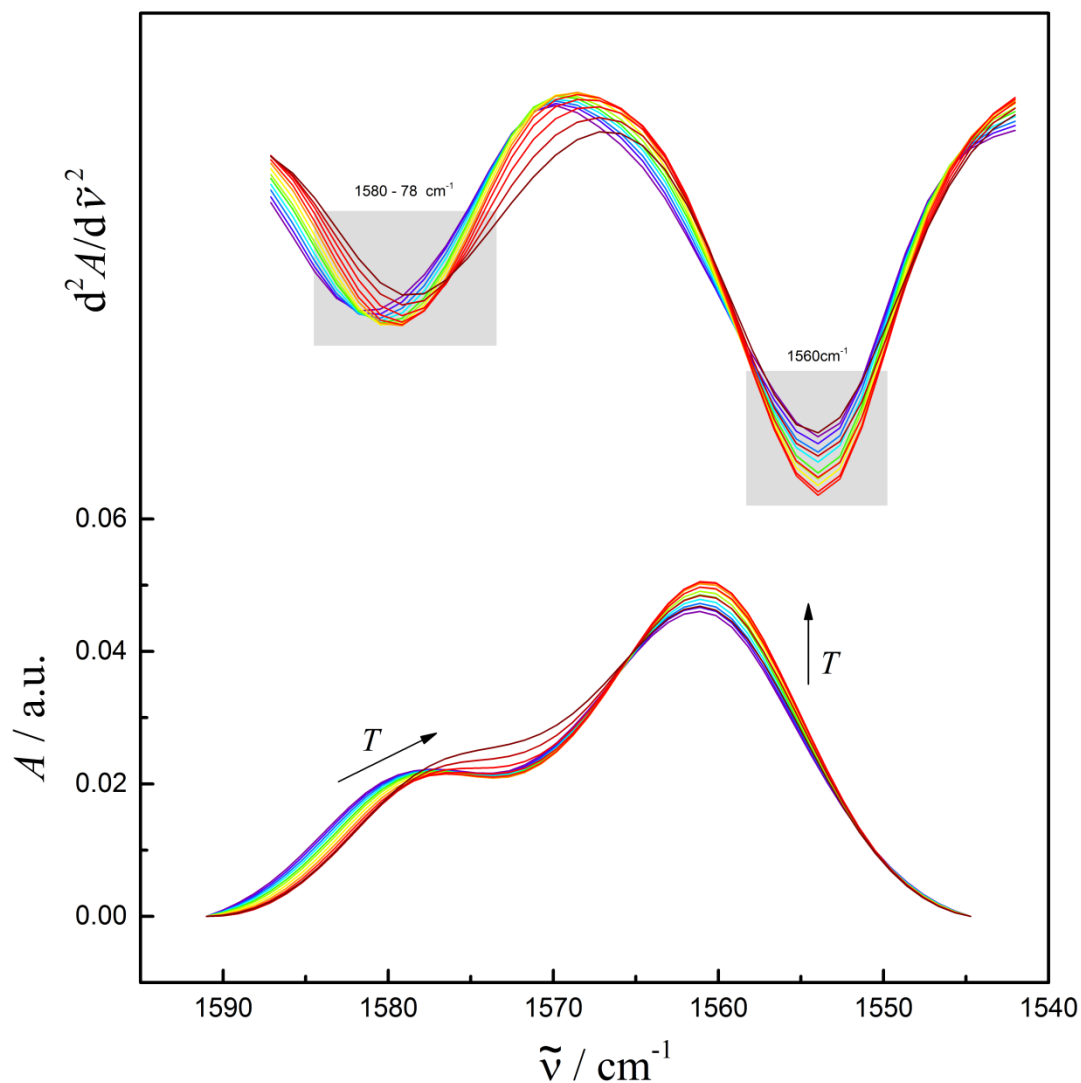


**Figure A6.** Temperature-dependent normalized and second derivative spectra of the labeled-small RNA hairpin in the wavenumber region from 1600 to 1540  $\text{cm}^{-1}$ . Second derivative and normalized spectra of 5  $\text{mg mL}^{-1}$  labeled-small RNA hairpin in 50  $\text{mM}$  Tris-HCl buffer + 0.1  $\text{mM}$  EDTA from 10 to 80  $^{\circ}\text{C}$ . In the normalized spectra, the IR band at 1590 to 1575  $\text{cm}^{-1}$ , related to ring vibrations of C4 = C5 and C5 – C6 of free and base paired guanine, shifts to lower wavenumbers (indicated by the arrow). The intensity of the IR band at 1568 to 1564  $\text{cm}^{-1}$ , related to ring vibrations of C6 = O6, C5 – C6 and C4 = C5 of free and base paired guanine, increases with temperature (indicated by the arrow). The most important bands are indicated by the grey rectangle in the second derivative spectra. The highlighted bands are: 1580 - 78  $\text{cm}^{-1}$ , 1560  $\text{cm}^{-1}$ . (Selected data)

---

Figure A6 shows the temperature-dependent FTIR spectra of the labeled-sRNAH in 50 mM Tris-HCl buffer pH 7.5 + 0.1 mM EDTA, from 10 to 80 °C, in the wavenumber region from 1600 to 1550  $\text{cm}^{-1}$ . The two characteristic IR bands of this region are the bands from 1590 to 1575  $\text{cm}^{-1}$ , and from 1568 to 1564  $\text{cm}^{-1}$ . These bands arise from ring vibrations of C6 = O6, C5 – C6 and C4 = C5 of free and base paired guanine and are used to follow the behavior of guanine rich regions, complementing the information obtained with the IR bands that are related to base pairing. It can be observed that the labeled-sRNAH displays an inverse profile when compared with the sRNAH. The intensity of the IR band at 1575  $\text{cm}^{-1}$  decreases during denaturation, which indicates formation of base pairs, and the IR band shifts to higher wavenumbers. The IR band at 1560  $\text{cm}^{-1}$  increases in intensity during denaturation, but no shift in wavenumber can be observed. The changes in intensity and wavenumber observed in the FTIR spectra of the labeled-sRNAH are less pronounced than the changes observed in the spectra of the sRNAH, which suggests that the fluorescent dyes can influence the environment of guanine-rich areas and can stabilize the sRNAH structure upon melting.



#### 8.1.1.4. Labeled-small RNA hairpin base-sugar vibrations followed by FTIR spectroscopy

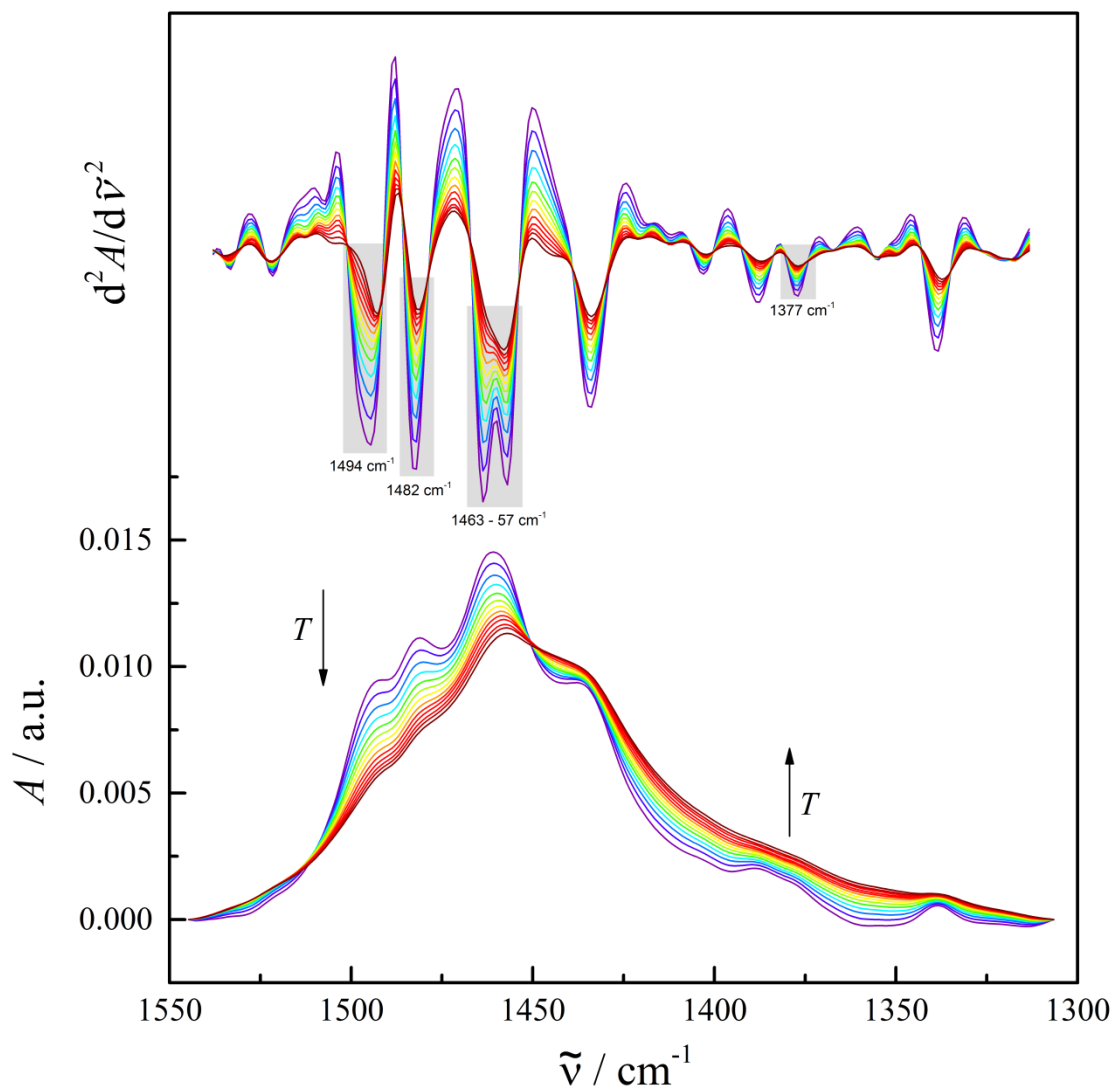


**Figure A7.** Temperature-dependent normalized and second derivative spectra of the labeled-small RNA hairpin in the wavenumber region from 1550 to 1300  $\text{cm}^{-1}$ . Second derivative and normalized spectra of 5  $\text{mg mL}^{-1}$  labeled-small RNA hairpin in 50  $\text{mM}$  Tris-HCl buffer + 0.1  $\text{mM}$  EDTA from 10 to 80  $^{\circ}\text{C}$ . IR bands are originating from base-sugar vibrations that are sensitive to glycosidic bond rotation, backbone and sugar pucker conformations. These IR bands are related to backbone vibrations in A-, B- and Z-forms, sugar pucker in N- or S-type conformations and N7 site vibrations of purines. The most important bands are indicated by the grey rectangle in the second derivative spectra. The highlighted bands are: 1594  $\text{cm}^{-1}$ , 1482  $\text{cm}^{-1}$ , 1463 – 57  $\text{cm}^{-1}$ , 1421  $\text{cm}^{-1}$ , 1377  $\text{cm}^{-1}$ . (Selected data)

Figure A7 shows the temperature-dependent FTIR spectra of the labeled-sRNAH in 50 mM Tris-HCl buffer pH 7.5 + 0.1 mM EDTA, from 10 to 80 °C, in the wavenumber region from 1550 to 1300  $\text{cm}^{-1}$ . The IR bands are originating from base-sugar vibrations which are sensitive to glycosidic bond rotation, backbone and sugar pucker conformation (for a more detailed RNA IR band assignment, see Table 1 in section 2.2.1.5). The IR bands at 1493  $\text{cm}^{-1}$  and at 1483  $\text{cm}^{-1}$ , which are assigned to ring vibrations of guanine at its N7 site, show a significant decrease in intensity. Changes in the position or intensity of these IR bands are related to interactions at N7 sites or to changes in hydration in the major groove of the double helix. These two IR bands appear in labeled-sRNAH FTIR spectra, which suggest that the fluorescent dyes could be interacting with the N7 site of guanines. The N7 site of the  $G_{L4}$  is exposed to the solvent when compared to other guanine residues (Figure 26), and could act as a binding site, for example. Both IR bands at 1460  $\text{cm}^{-1}$  and 1436  $\text{cm}^{-1}$  are related to backbone vibrations of adenine, which is not present in the sRNAH structure, therefore these two bands will not be discussed.

A small IR band can be observed at 1403  $\text{cm}^{-1}$ , which is assigned to RNA vibrations of in-plane C – O – H deformation mode at the 2' position of the ribose ring [160]. A small IR band at 1377  $\text{cm}^{-1}$  related to purine (guanine) sugar in anti conformation (sugars at C2' / C3' – endo sugar pucker conformation) can also be observed. The ribose sugar adopts a C3'-endo conformation when the RNA structure is in A- or Z-form. This conformation brings the nucleotides closer, which in turn renders the helix more compact. The Z-form has its cytosine in C2'-endo conformation, which makes the Z-form adopt a left-handed helical conformation. This band indicates that the backbone of the labeled-sRNAH vary in its guanine C3-endo sugar pucker, between the A- and B-helix.

The sRNAH and the labeled-sRNAH show distinct characteristics during thermal denaturation. The changes of secondary structure features observed in the FTIR data of the labeled-sRNAH showed that the fluorescent dyes, Cy3' and Cy5', have a large influence on the melting profile. The double helical bonds of the native structure, of the labeled-sRNAH, are not entirely broken until 80 °C. On the other hand, the sRNAH would be denatured by 50 °C (Figure 30). The changes observed in the intensity of the base pair and ring stacking vibrations for the labeled-sRNAH are small when compared to the

changes observed during melting transition for the sRNAH. Moreover, the IR bands related to interactions with the N7 sites of purines were observed for the labeled-sRNAH, only. The temperature-dependent FTIR and UV-vis spectroscopy results suggest that, until 80 °C, the labeled-sRNAH did not achieved the compact unfolded state. The labeled-sRNAH structure may still vary between near native conformations due to stabilization of its duplex stem, as suggested in the study of B. G. Moreira *et al.* (2015) [161]. In this particular study, it was suggested that the attachment of Cy3 and Cy5 dyes was responsible to stabilize DNA duplex and to enhance duplex formation, due to stacking interaction between the fluorescent dye and the purine of the complimentary strand. To this end, the interference of the dyes on the sRNAH definitely should be taken in account when analyzing fluorescence data.

## 8.1.2. Pressure-dependent FTIR analysis of the labeled-small RNA hairpin

### 8.1.2.1. Labeled-small RNA hairpin in-plane base vibrations sensitive to effects of base pairing followed by FTIR spectroscopy

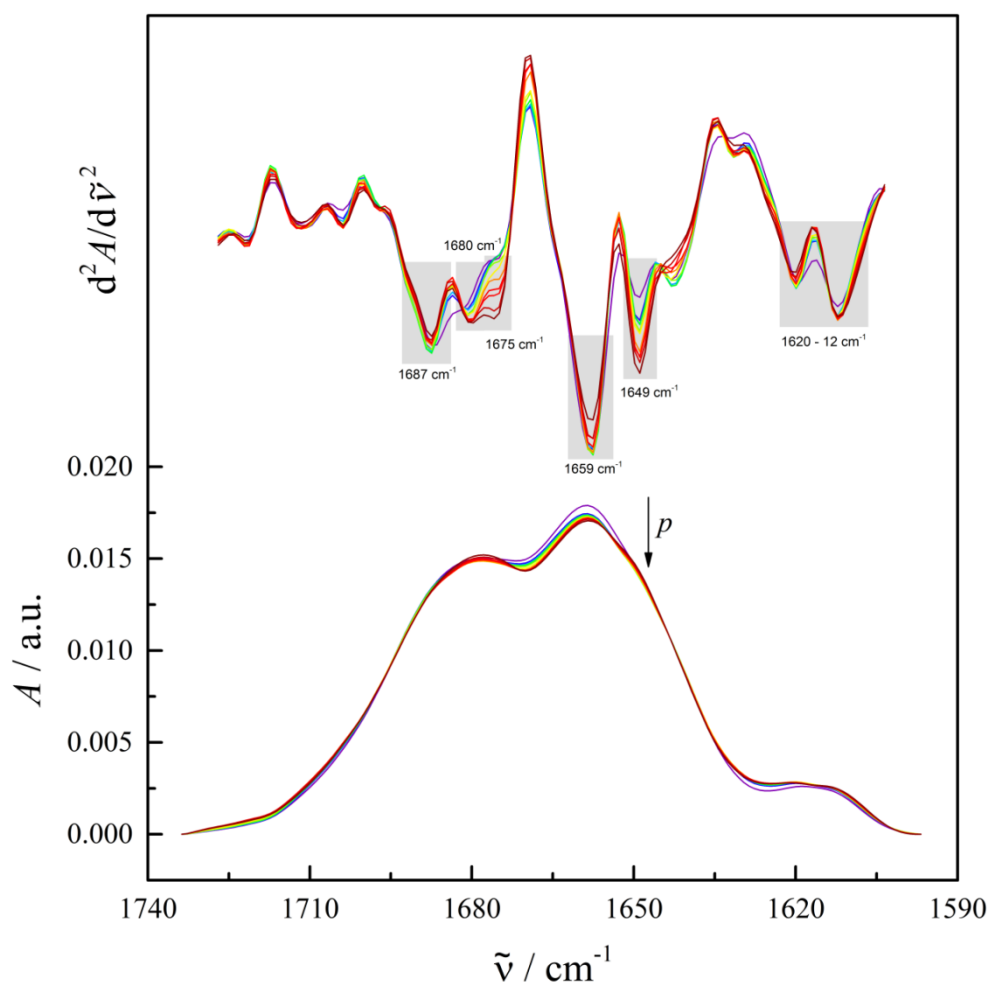


**Figure A8. Pressure-dependent normalized and second derivative spectra of the labeled-small RNA hairpin in the wavenumber region from 1740 to 1590  $\text{cm}^{-1}$  at 20 °C.** Second derivative and normalized spectra of 5  $\text{mg mL}^{-1}$  labeled-small RNA hairpin in 50  $\text{mM}$  Tris-HCl buffer + 0.1  $\text{mM}$  EDTA from 0.1 to 400 MPa at 20 °C. In the normalized spectra, the IR band from 1696 to 1684  $\text{cm}^{-1}$ , related to base paired nucleotides, does not change with pressure. The IR band from 1677 to 1653  $\text{cm}^{-1}$ , related to free nucleotides, decreases with pressure (indicated by the arrow). The most important bands are indicated by the grey rectangle in the second derivative spectra. The highlighted bands are: 1687  $\text{cm}^{-1}$ , 1675  $\text{cm}^{-1}$ , 1659  $\text{cm}^{-1}$ , 1649  $\text{cm}^{-1}$ , 1620 - 12  $\text{cm}^{-1}$ . (Selected data)

Figure A8 shows the pressure-dependent FTIR spectra of the labeled – sRNAH in 50  $\text{mM}$  Tris-HCl buffer pH 7.5 + 0.1  $\text{mM}$  EDTA, from 0.1 to 400 MPa at 20 °C, in the

wavenumber region from 1740 to 1590  $\text{cm}^{-1}$ . Pressure does not change the absorbance ( $A$ ) of the IR band at 1686  $\text{cm}^{-1}$ , which is characteristic of base paired G-C vibrations. In addition, there is a small intensity decrease in IR intensity of unpaired nucleic acids at 1660  $\text{cm}^{-1}$ . Pressure, apparently, induces only small structural rearrangement of the native folded ensembles, which can be related to the presence of the fluorescent dyes, changes in volume and hydration of the molecule.

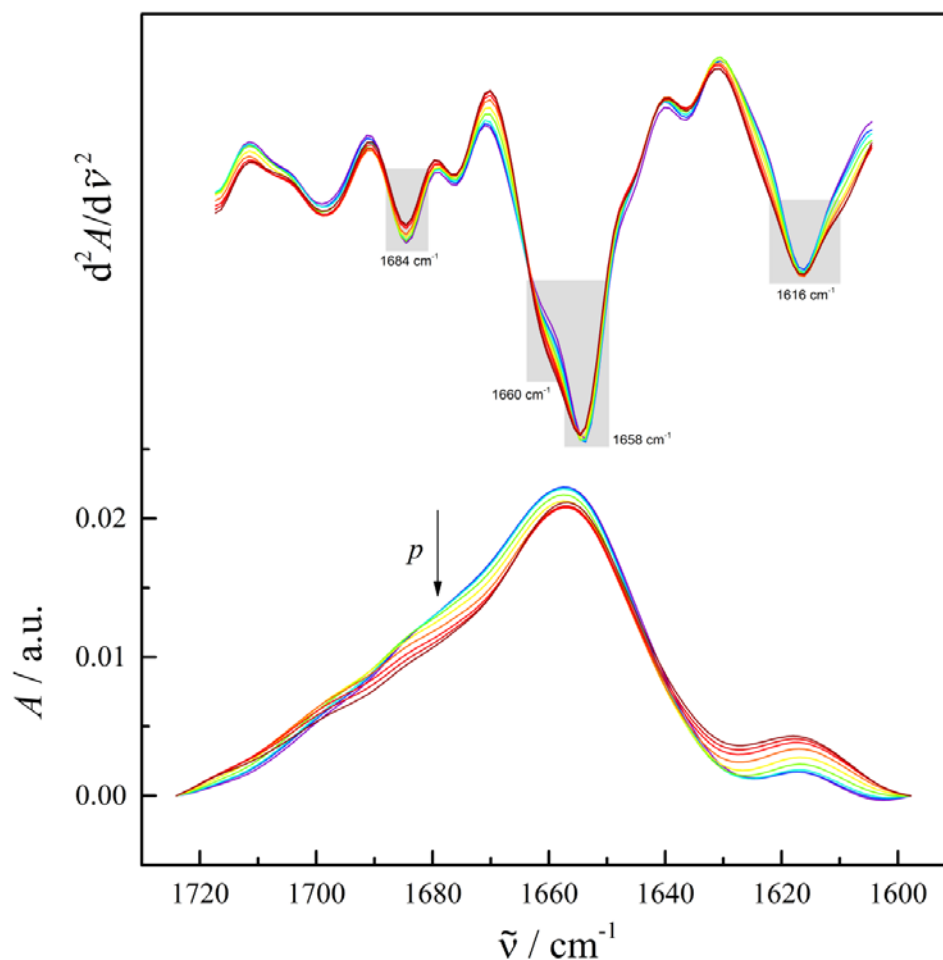


**Figure A9. Pressure-dependent normalized and second derivative spectra of the labeled-small RNA hairpin in the wavenumber region from 1720 to 1590  $\text{cm}^{-1}$  at 70 °C.** Second derivative and normalized spectra of 5  $\text{mg mL}^{-1}$  labeled-small RNA hairpin in 50  $\text{mM}$  Tris-HCl buffer + 0.1  $\text{mM}$  EDTA from 0.1 to 400  $\text{MPa}$  at 70 °C. At the normalized spectra, the IR band from 1696 to 1684  $\text{cm}^{-1}$  is related to base paired nucleotides and cannot be observed due to denaturation, while the IR band from 1677 to 1653  $\text{cm}^{-1}$  is related to free nucleotides and decreases with pressure (indicated by the arrow). The most important bands are indicated by the grey rectangle at the second derivative spectra. The highlighted bands are: 1684  $\text{cm}^{-1}$ , 1660  $\text{cm}^{-1}$ , 1658  $\text{cm}^{-1}$ , 1616  $\text{cm}^{-1}$ . (Selected data)

Figure A9 shows the pressure-dependent FTIR spectra of the labeled-sRNAH in 50 mM Tris-HCl buffer pH 7.5 + 0.1 mM EDTA, from 0.1 to 400 MPa at 70 °C, in the wavenumber region from 1720 to 1600  $\text{cm}^{-1}$ . Pressure causes a small decrease in absorbance ( $A$ ) of the IR band at 1662  $\text{cm}^{-1}$ , which is characteristic of unpaired guanine bases. There is only a small IR signal for the IR band at 1686  $\text{cm}^{-1}$ , which is characteristic of base paired G-C vibrations, due to thermal denaturation of sRNAH molecule. Comparison between the IR band intensity at 1600  $\text{cm}^{-1}$  of the pressure dependent FTIR measurements at 20 °C and 70 °C is shown in Figure A10.

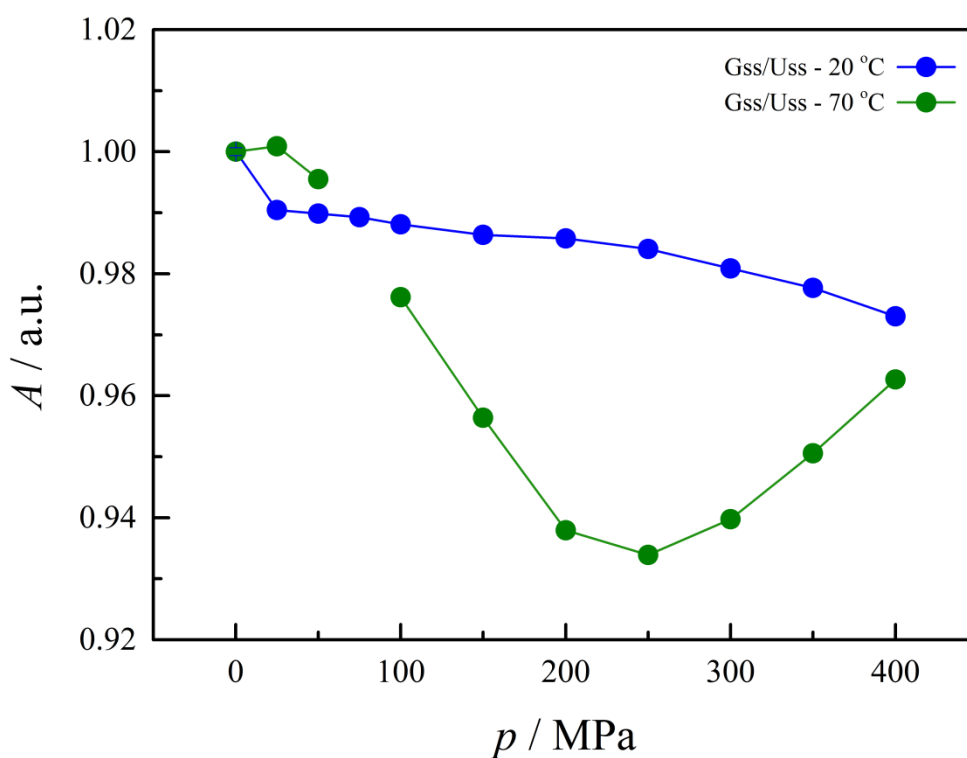


**Figure A10. Pressure-dependent changes of the labeled-small RNA hairpin free base vibrations of guanine and uracil followed by FTIR spectroscopy.** Pressure-dependence change of the intensity of unpaired GC pairs obtained from the infrared spectra recorded at  $\approx 1658 \text{ cm}^{-1}$  for  $5 \text{ mg mL}^{-1}$  labeled-small RNA hairpin in 50 mM Tris-HCl buffer + 0.1 mM EDTA from 0.1 to 400 MPa, at 20 °C and 70 °C.

It can be seen at Figure A10 that the labeled-sRNAH structure seems to be slightly stabilized by pressure, due to the small decrease of single strand vibrations of guanines ( $1660 \text{ cm}^{-1}$ ). The pressure-induced decrease of single strand intensity is larger at 70 °C

than at 20 °C. It has been shown by temperature-dependent FTIR and UV-vis spectroscopy, that the labeled-sRNAH displays a different melting profile than the sRNAH (Figures A2 and 30). The labeled-sRNAH started to melt at 50 °C, and it did not achieve the plateau until 80 °C. On the other hand, the sRNAH achieved the plateau at 50 °C. These results indicate that the labeled-sRNAH structure is stabilized by the fluorescent dyes, Cy3 and Cy5, against extreme temperature and pressure conditions, as observed in the literature [161]. Therefore, the structure of the labeled-sRNAH is not fully denatured at 70 °C. In addition, pressure can be responsible for stabilizing the helix stem, and may promote the re-bond of G-C interactions until 250 MPa. Overall, sRNAH and labeled-sRNAH are highly stable molecules, which are not denatured by pressure at lower temperatures.

### 8.1.2.2. Labeled-small RNA hairpin in-plane base vibrations sensitive to effects of base stacking followed by FTIR spectroscopy

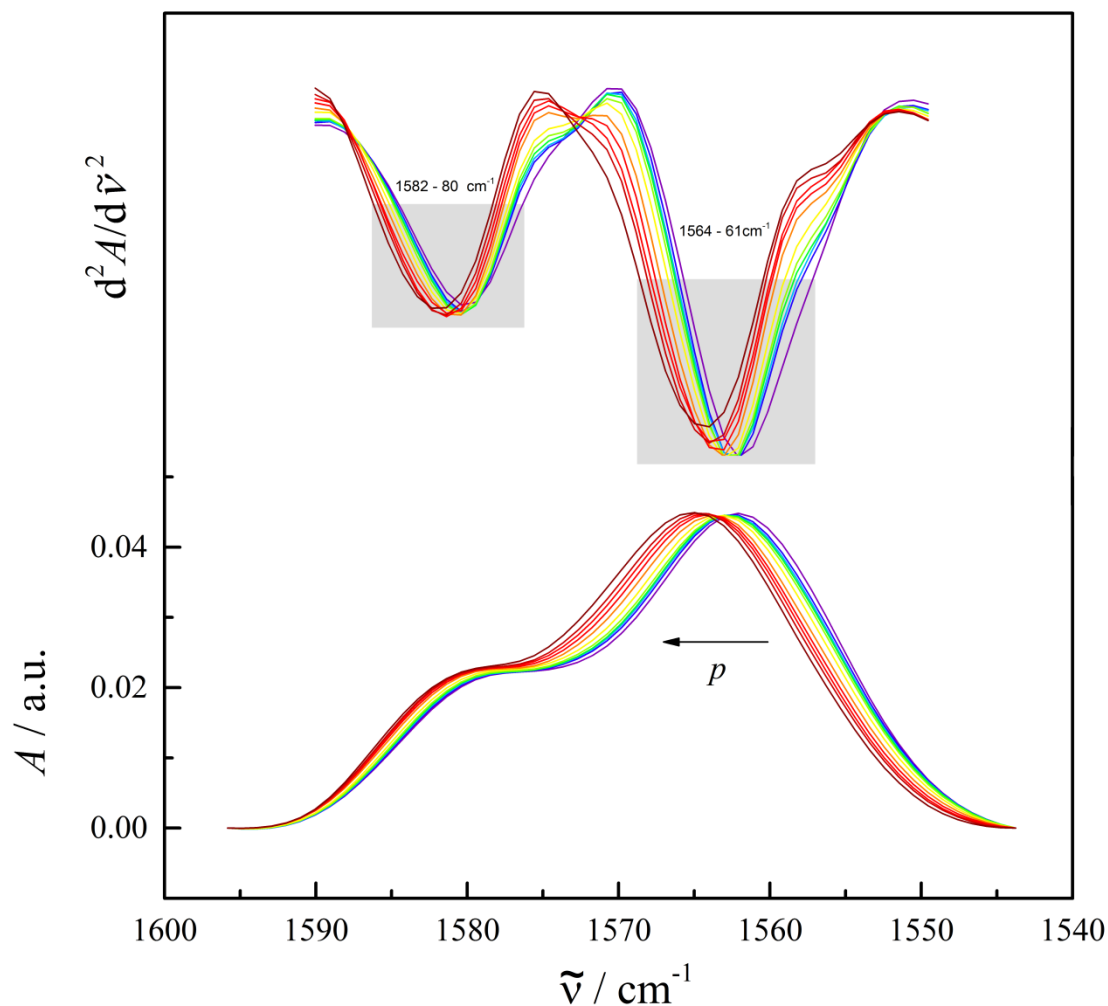


**Figure A11.** Pressure-dependent normalized and second derivative spectra of the labeled-small RNA hairpin in the wavenumber region from 1600 to 1540  $\text{cm}^{-1}$  at 20  $^{\circ}\text{C}$ . Second derivative and normalized spectra of 5  $\text{mg mL}^{-1}$  labeled-small RNA hairpin in 50  $\text{mM}$  Tris-HCl buffer + 0.1  $\text{mM}$  EDTA from 0.1 to 400  $\text{MPa}$  at 20  $^{\circ}\text{C}$ . In the normalized spectra, the IR band at 1590 to 1575  $\text{cm}^{-1}$ , related to ring vibrations of  $\text{C4} = \text{C5}$  and  $\text{C5} - \text{C6}$  of free and base paired guanine, does not show significant change. The the IR band at 1568 to 1564  $\text{cm}^{-1}$ , related to ring vibrations of  $\text{C6} = \text{O6}$ ,  $\text{C5} - \text{C6}$  and  $\text{C4} = \text{C5}$  of free and base paired guanine, shifts to higher wavenumbers (indicated by the arrow). The most important bands are indicated by the grey rectangle in the second derivative spectra. The highlighted bands are: 1582 - 80  $\text{cm}^{-1}$ , 1564 - 61  $\text{cm}^{-1}$ . (Selected data)



---

Figure A11 shows the pressure-dependent FTIR spectra of the labeled-sRNAH in 50 mM Tris-HCl buffer pH 7.5 + 0.1 mM EDTA, from 0.1 to 400 MPa at 20 °C, in the wavenumber region from 1600 to 1540  $\text{cm}^{-1}$ . The two characteristic IR bands in this region are the bands around 1590 to 1575  $\text{cm}^{-1}$ , and 1568 to 1564  $\text{cm}^{-1}$ . Both of these bands arise due to ring vibrations of  $\text{C6} = \text{O6}$ ,  $\text{C5} - \text{C6}$  and  $\text{C4} = \text{C5}$  of free and base paired guanine. It can be observed that the IR band at 1579  $\text{cm}^{-1}$  shows a small shift in wavenumber, only. The IR band at 1562  $\text{cm}^{-1}$  shows a large shift to higher wavenumbers. Apparently, the fluorescent dyes have high influence on the stacking interactions of guanines and its environment conditions at 20 °C in the labeled-sRNAH structure when compared to the sRNAH. Furthermore, the effect of high hydrostatic pressure on the sRNAH native structure is rather small (Figure 39).

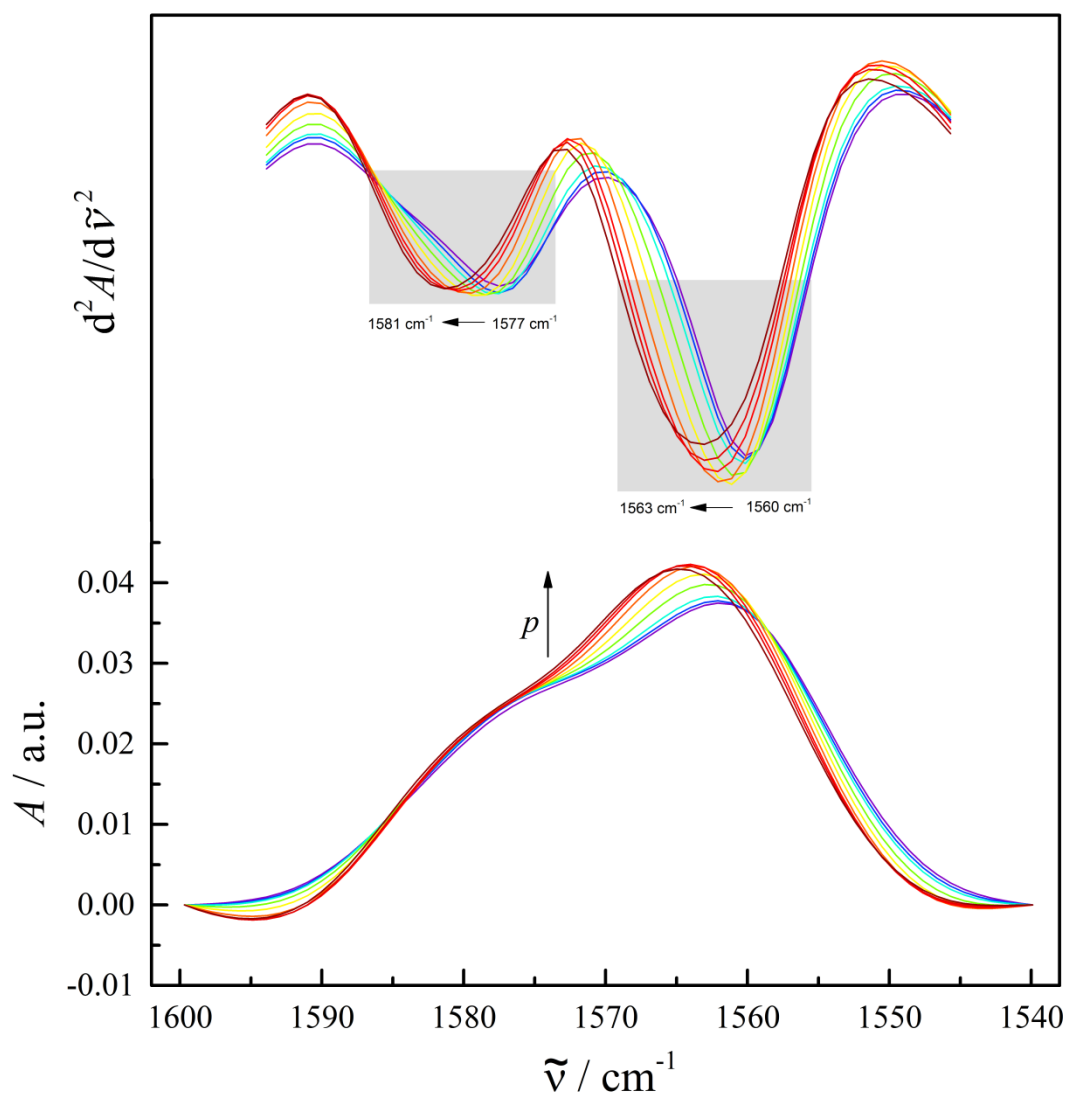


**Figure A12. Pressure-dependent normalized and second derivative spectra of the labeled-small RNA hairpin in the wavenumber region from 1600 to 1550  $\text{cm}^{-1}$  at 70 °C.** Second derivative and normalized spectra of 5  $\text{mg mL}^{-1}$  labeled-small RNA hairpin in 50  $\text{mM}$  Tris-HCl buffer + 0.1  $\text{mM}$  EDTA from 0.1 to 400 MPa at 70 °C. In the normalized spectra, the IR band at 1590 to 1575  $\text{cm}^{-1}$ , related to ring vibrations of  $\text{C4} = \text{C5}$  and  $\text{C5} - \text{C6}$  of free and base paired guanine, does not show significant change. The IR band at 1568 to 1564  $\text{cm}^{-1}$ , related to ring vibrations of  $\text{C6} = \text{O6}$ ,  $\text{C5} - \text{C6}$  and  $\text{C4} = \text{C5}$  of free and base paired guanine, shows a small increase in intensity with pressure (indicated by the arrow). The most important bands are indicated by the grey rectangle in the second derivative spectra. The highlighted bands are: 1581 - 77  $\text{cm}^{-1}$ , 1563 - 60  $\text{cm}^{-1}$ . (Selected data)

---

Figure A12 shows the pressure-dependent FTIR spectra of the labeled – sRNAH in 50 mM Tris-HCl buffer pH 7.5 + 0.1 mM EDTA, from 0.1 to 400 MPa at 70 °C, in the wavenumber region from 1600 to 1550  $\text{cm}^{-1}$ . It can be observed, in the normalized spectra, that the IR band around 1580  $\text{cm}^{-1}$  does not change in intensity. In the second derivative spectra, this IR band displays a small shift in wavenumber. The IR band at 1561  $\text{cm}^{-1}$  increase in intensity within increasing pressure, as well as it shifts to higher wavenumbers. When compared to the sRNAH spectra (Figure 40), the fluorescent dyes display high influence on the ring vibrations (stacking interactions) of the guanine bases, resulting in an inverse profile when compared to the sRNAH. High hydrostatic pressure shows larger influence on the labeled-sRNAH structure than the sRNAH structure.

### 8.1.2.3. Labeled-small RNA hairpin base-sugar vibrations followed by FTIR spectroscopy

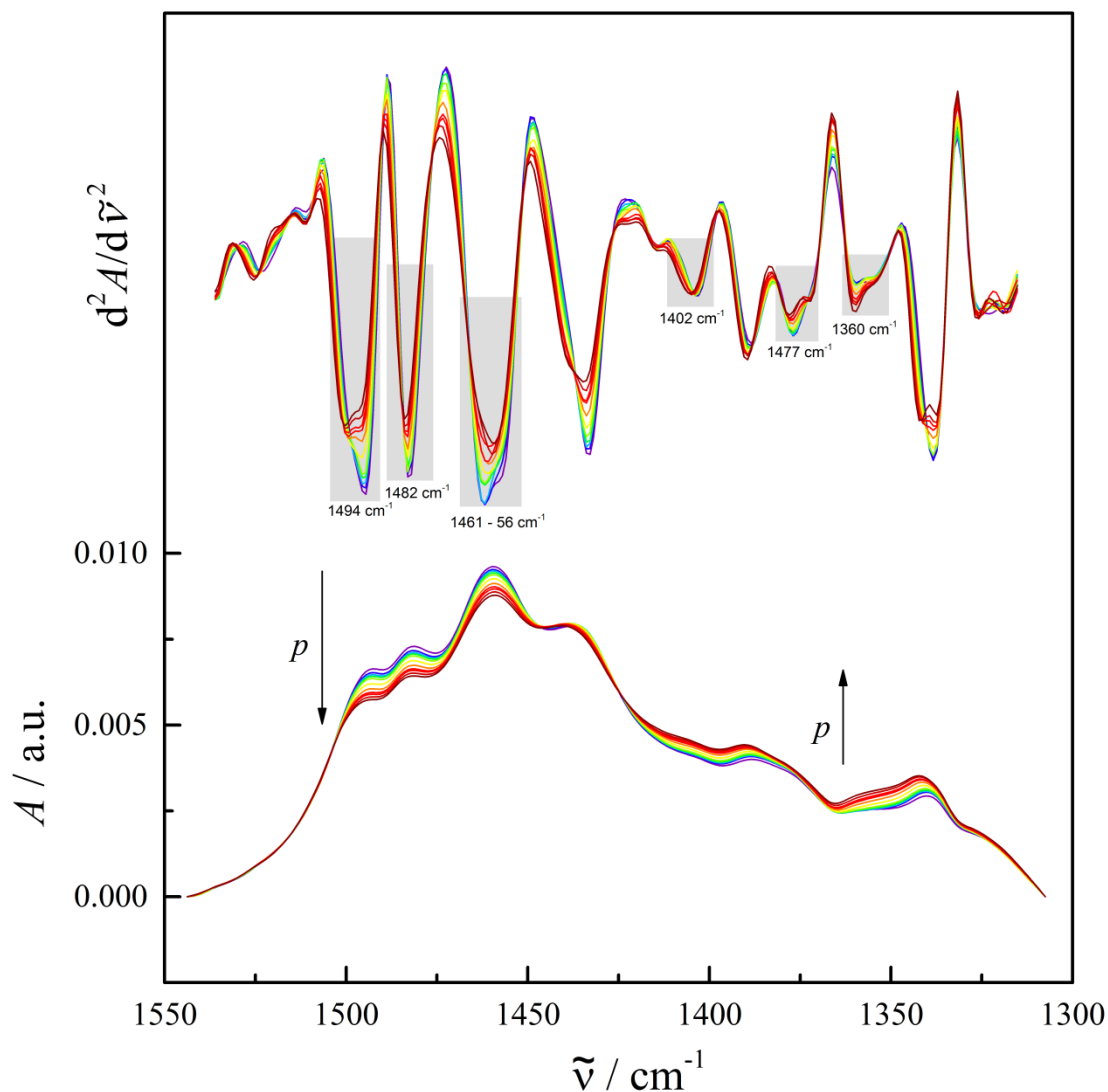


**Figure A13.** Pressure-dependent normalized and second derivative spectra of the labeled-small RNA hairpin in the wavenumber region from 1550 to 1300  $\text{cm}^{-1}$  at 20 °C. Second derivative and normalized spectra of 5  $\text{mg mL}^{-1}$  labeled - small RNA hairpin in 50 mM Tris-HCl buffer + 0.1 mM EDTA from 0.1 to 400 MPa at 20 °C. IR bands originating from base-sugar vibrations which are sensitive to glycosidic bond rotation, backbone and sugar pucker conformations. These IR bands are related to backbone vibrations in A-, B- and Z-forms, sugar pucker in N- or S-type conformations and N7 site vibrations of purines. The most important bands are indicated by the grey rectangle at the second derivative spectra. The highlighted bands are: 1494  $\text{cm}^{-1}$ , 1482  $\text{cm}^{-1}$ , 1461 - 56  $\text{cm}^{-1}$ , 1402  $\text{cm}^{-1}$ , 1377  $\text{cm}^{-1}$ , 1380  $\text{cm}^{-1}$ . (Selected data)

Figure A13 shows the pressure-dependent FTIR spectra of labeled-sRNAH in 50 mM Tris-HCl buffer pH 7.5 + 0.1 mM EDTA, from 0.1 to 400 MPa at 20 °C, in the wavenumber region from 1550 to 1300  $\text{cm}^{-1}$ . The IR band at 1522  $\text{cm}^{-1}$ , which is characteristic of in-plane vibrations of cytosine (for a more detailed RNA IR band assignment, see Table 1 in section 2.2.1.5) shows a small shift to slightly higher wavenumber, only. The IR bands at 1494  $\text{cm}^{-1}$  and at 1482  $\text{cm}^{-1}$ , which are assigned as ring vibrations of guanine at its N7 site, have a significant decrease. Changes in the position or intensity of these bands are related to interactions at N7 sites, or changes in hydration of the major groove of the helix. In the temperature-dependent FTIR spectra of the labeled-sRNAH, these IR bands are show large changes under high temperature and pressure. This indicates that the fluorescent dyes are interacting with the guanine nucleotides, and are changing the dynamics of the sRNAH structure, as observed in the literature [161]. The IR bands observed from 1490 to 1420  $\text{cm}^{-1}$  are related to adenine backbone vibrations, and cannot be related to sRNAH structure. An IR band can be observed at 1403  $\text{cm}^{-1}$ , which is assigned as RNA vibrations of the ribose ring [160].

A broad band between 1392 to 1368  $\text{cm}^{-1}$ , related to purine (guanine) sugar in anti conformation (sugars at C2' / C3' – endo sugar pucker conformation), can also be observed. This band vary inside its IR range, 1381 – 1369  $\text{cm}^{-1}$ , which is in agreement with the small variations pressure caused at IR bands related to A-form helix. The intensity of this band increases under high hydrostatic pressure. There is a concomitant increase in the intensity of the IR band at 1355  $\text{cm}^{-1}$ , which is assigned to the purine glycosil angle in syn conformation related to Z-form backbone. These IR bands indicate that pressure can promote the rearrangement of the RNA backbone, favoring the Z-helix, which is less stable and commonly an intermediate conformation. The Z-helix is unfavorable to form, but some conditions such as high salt concentration can promote its formation. Molecular dynamics studies by Miner *et al.* (2016) [103] showed that high hydrostatic pressure has a stabilizing effect on the A-form, and a destabilizing effect on the Z-form of the RNA tetraloop (gcGCAAgc).

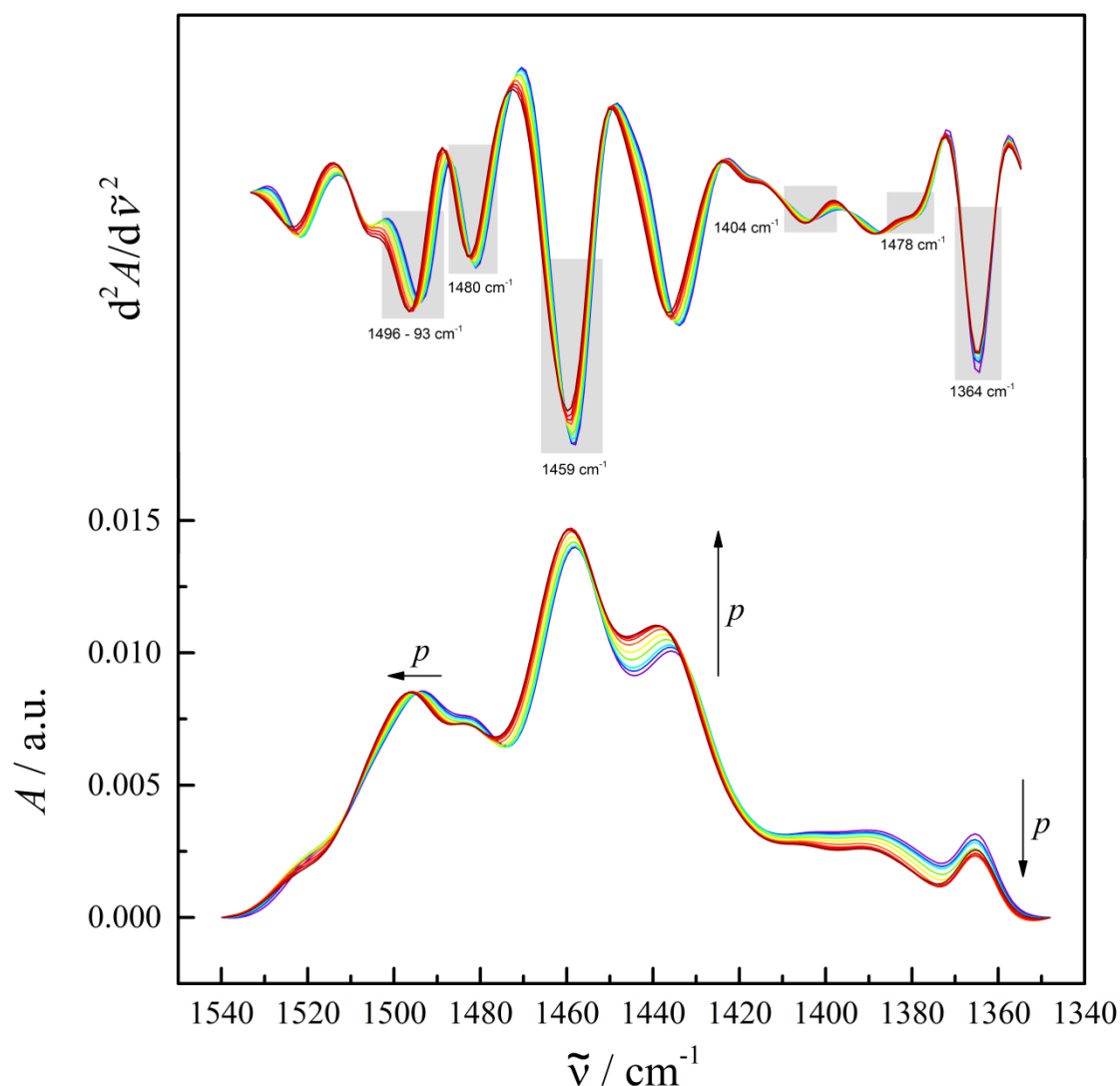


**Figure A14. Pressure-dependent normalized and second derivative spectra of the labeled-small RNA hairpin in the wavenumber region from 1540 to 1340  $\text{cm}^{-1}$  at 70  $^{\circ}\text{C}$ .** Second derivative and normalized spectra of 5  $\text{mg mL}^{-1}$  labeled-small RNA hairpin in 50  $\text{mM}$  Tris-HCl buffer + 0.1  $\text{mM}$  EDTA from 0.1 to 400 MPa at 70  $^{\circ}\text{C}$ . IR bands originating from base-sugar vibrations that are sensitive to glycosidic bond rotation, backbone and sugar pucker conformations. These IR bands are related to backbone vibrations in A-, B- and Z-forms, sugar pucker in N- or S-type conformations and N7 site vibrations of purines. The most important bands are indicated by the grey rectangle in the second derivative spectra. The highlighted bands are: 1496  $\text{cm}^{-1}$ , 1480  $\text{cm}^{-1}$ , 1459  $\text{cm}^{-1}$ , 1404  $\text{cm}^{-1}$ , 1378  $\text{cm}^{-1}$ , 1364  $\text{cm}^{-1}$ . (Selected data)

Figure A14 shows the pressure-dependent FTIR spectra of labeled-sRNAH in 50  $\text{mM}$  Tris-HCl buffer pH 7.5 + 0.1  $\text{mM}$  EDTA, from 0.1 to 400 Mpa at 70  $^{\circ}\text{C}$ , in the wavenumber region from 1540 to 1380  $\text{cm}^{-1}$ . The IR band at 1522  $\text{cm}^{-1}$ , which is

characteristic of in-plane vibrations of cytosine, shows a small shift to higher wavenumber, only. The IR bands at  $1494\text{ cm}^{-1}$  and at  $1482\text{ cm}^{-1}$ , related to ring vibrations of guanine at its N7 site, have small changes only. The IR band at  $1494\text{ cm}^{-1}$  shifts to higher wavenumbers, while the IR band at  $1482\text{ cm}^{-1}$  shows a small intensity decrease. It can be observed that changes in the IR spectra at  $70\text{ }^{\circ}\text{C}$  are less pronounced than the changes observed at  $20\text{ }^{\circ}\text{C}$ . However, changes in intensity and/or wavenumber can be observed in this region, which suggests that the fluorescent dyes display a large influence on the dynamics of the sRNAH structure through interaction with the guanine bases. The IR band at  $1403\text{ cm}^{-1}$  is assigned to RNA vibrations of the ribose ring [160].

A small IR band at around  $1386\text{ cm}^{-1}$  related to purine (guanine) sugar in anti conformation (sugars at C2' / C3' – endo sugar pucker conformation – A-form) can also be observed. The band is related to guanine in A-form RNA, A-form has sugar at C3'-endo in anti conformation. The intensity of this band decreases with increasing pressure. The intensity of the IR band at  $1365\text{ cm}^{-1}$ , assigned to cytidine in anti conformation (sugars at C2' / C3' – endo sugar pucker conformation), also decrease with pressure. Cytidine at A-form helix has the glycosil angles in anti conformation, with the sugar pucker at C3'-endo conformation. While the RNA at Z-form helix, the glycosil angles adopts the anti conformation, with the sugar pucker at C2'-endo conformation. It seems that pressure induces the fluctuation between Z- and A-helix, and that only small alterations occur at backbone of the not fully unfolded labeled-sRNAH. According to Miner *et al.* (2016) [103] pressure favors A-form and destabilizes Z-form. However, pressure did not favor A-helix in the labeled-sRNAH structure, which can be related to structure stabilization induced by the dyes.

### 8.1.2. Summary and conclusions:

In order to compare with the results obtained with the sRNAH and with FRET results, which are not discussed here, the fluorescent labeled-small RNA hairpin was submitted to the same experimental analysis. To this end, UV-vis and FTIR spectroscopy measurements were carried out. The small RNA hairpin and the labeled- small RNA hairpin showed distinct profiles. The changes in the secondary structure features observed

in the temperature- and pressure-dependent FTIR of the labeled-sRNAH show that the fluorescent dyes, Cyanine 3 and Cyanine 5, can significantly interfere on the RNA structural dynamics. The fluorescent dyes were responsible for increasing the thermal and pressure stability of sRNAH. The temperature-dependent FTIR and UV-vis spectroscopy results suggest that, until 80 °C, the labeled- small RNA hairpin did not achieve the compact unfolded state, and it would still maintain some native stem connections (Figure A15). Pressure-dependent FTIR results show that the labeled-sRNAH structure is slightly stabilized by pressure at lower and high temperatures. The labeled-sRNAH was influenced by temperature and pressure in an inverse way than observed for the sRNAH. These results are in agreement with a study of B. G. Moreira *et al.* (2015) [161]. They showed that the attachment of Cy3 and Cy5 dyes was responsible to stabilize DNA duplex and to enhance duplex formation, due to stacking interaction between the dye and the purine of the complimentary strand. Thereby, the interference of the fluorescent dyes, Cy3 and Cy5, should be taken in account when analyzing fluorescence data.

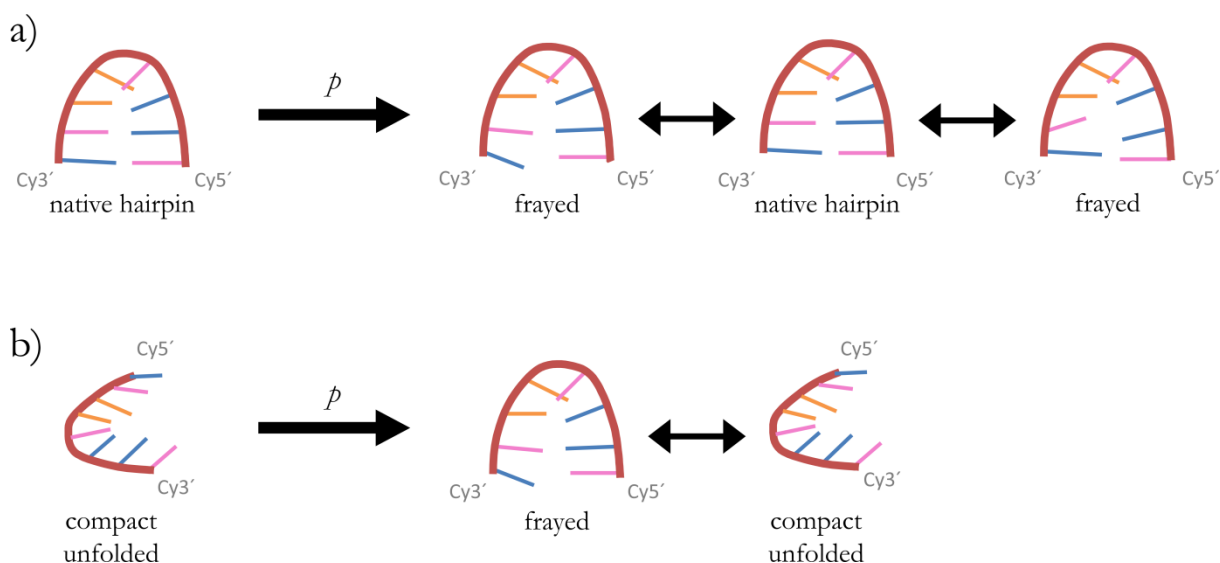


**Figure A15.** Effect of temperature and pressure on the structure of the labeled-small RNA hairpin. a) Effect of pressure on the labeled-small RNA hairpin structure at 20 °C. The native hairpin structure is slightly destabilized by pressure, inducing variation between native and native-like structures. b) Effect of pressure on the labeled-small RNA hairpin structure at 70 °C. The denatured hairpin structure is slightly stabilized by high hydrostatic pressure.



## 8.2. Modified hairpin ribozyme

PAGE measurements were also carried out using another hairpin ribozyme model, in order to compare with molecular dynamics measurements performed in collaboration (as details at section 2.1.2). The model used in this work was named as modified hairpin ribozyme (modHpRz), and is based on the crystal structure of the hairpin ribozyme in the docked state [108]. This crystal structure contains four dissociated chains which comes together and they interact as a junctionless hairpin ribozyme.

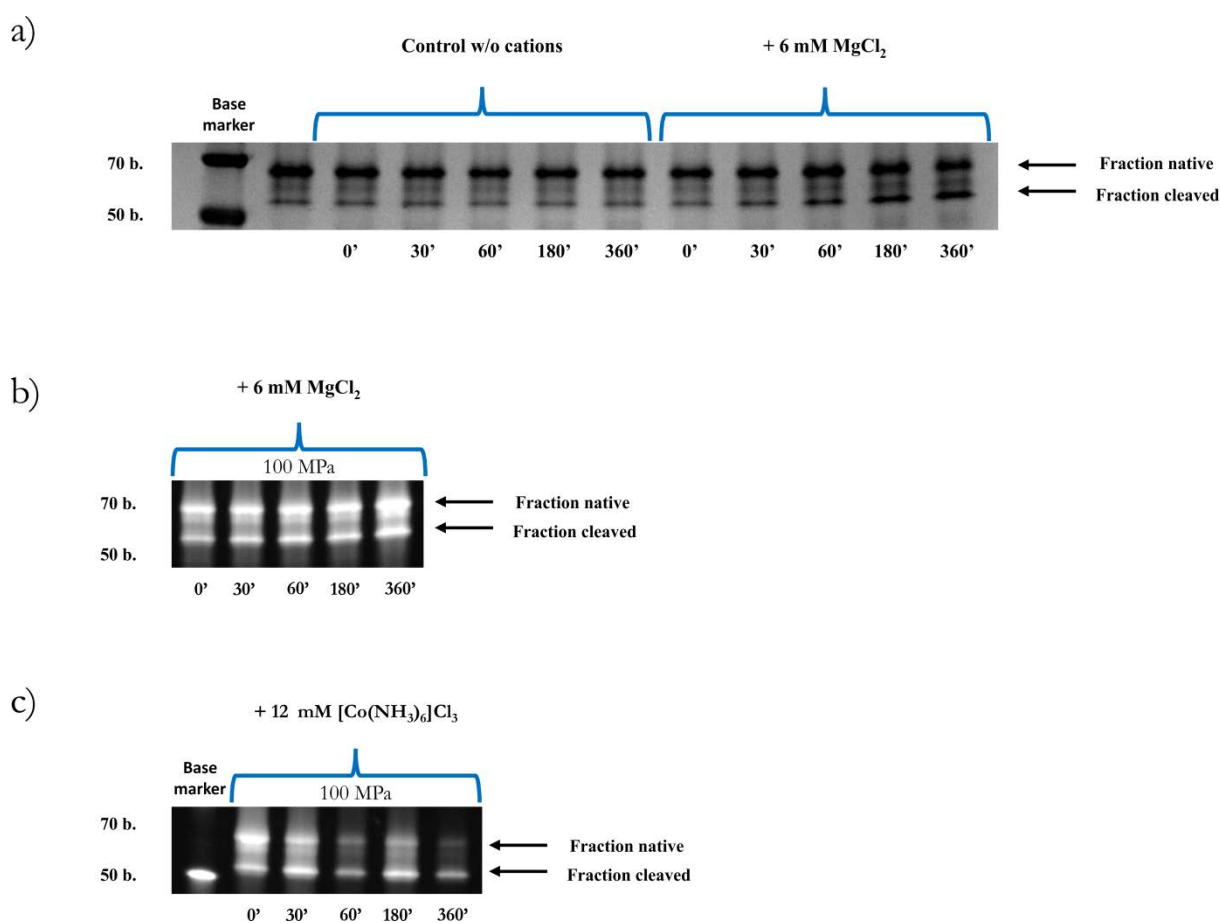


**Figure A16. TBE-urea PAGE of the modified hairpin ribozyme's self-cleavage reaction.** a) The modHpRz control reaction in pure Tris-HCl buffer + 0.1 mM EDTA pH 7.5 and in Tris-HCl buffer + 0.1 mM EDTA + 6 mM MgCl<sub>2</sub> pH 7.5, during 6 hours at 25 °C. b) The modHpRz reaction in Tris-HCl buffer + 0.1 mM EDTA + 6 mM MgCl<sub>2</sub> pH 7.5, during 6 hours, at 100 MPa, at 25 °C. c) The modHpRz reaction in pure Tris-HCl buffer + 0.1 mM EDTA pH 7.5 and in Tris-HCl buffer + 0.1 mM EDTA + 12 mM [Co(NH<sub>3</sub>)<sub>6</sub>]Cl<sub>3</sub> + 100 mM NaCl pH 7.5, during 6 hours, at 100 MPa, at 25 °C. (Selected data)

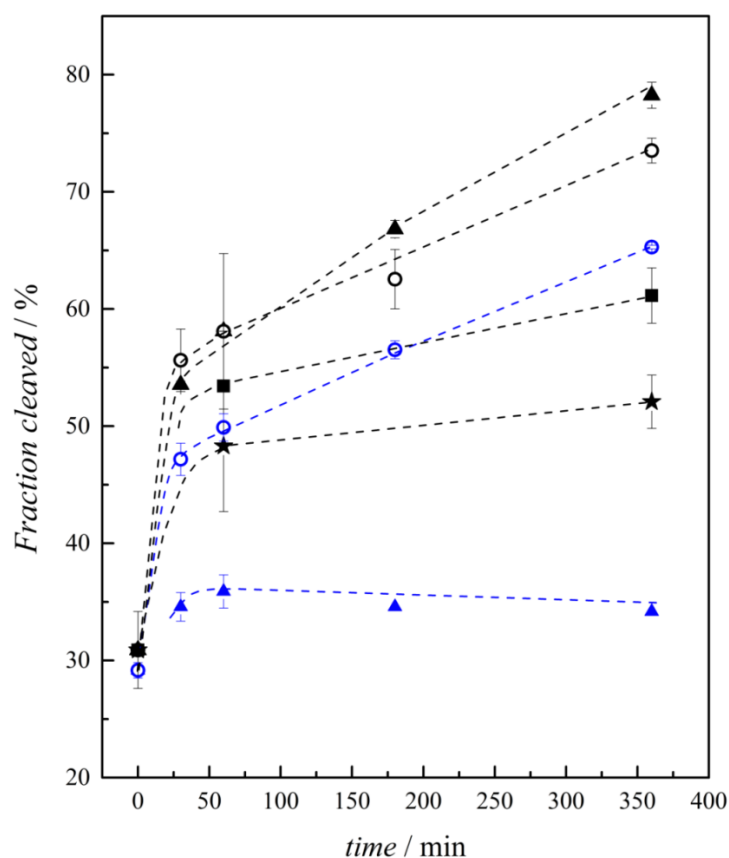


**Figure A17.** Time evolution of the modified hairpin ribozyme self-cleavage reaction with  $[\text{Co}(\text{NH}_3)_6]\text{Cl}_3$  and  $\text{MgCl}_2$  at different pressures. Fraction of cleaved wtHpRz after addition of 6 mM  $\text{MgCl}_2$  (blue) or 12 mM  $[\text{Co}(\text{NH}_3)_6]\text{Cl}_3$  + 100 mM NaCl (black). Self-cleavage reaction conditions were: 50 mM Tris-HCl buffer + 0.1 mM EDTA + 6 mM  $\text{MgCl}_2$  or 12 mM  $[\text{Co}(\text{NH}_3)_6]\text{Cl}_3$  + 100 mM NaCl, pH 7.5, 25 °C at 0.1 MPa (open circles), 100 MPa (closed triangles), 200 MPa (closed square) and 300 MPa (closed star). RNA final reaction aliquot, with 3.6  $\mu\text{M}$ , was analyzed by TBE-Urea PAGE and quantified by ImageJ [125].

It can be seen at Figure A16 that there is a significant difference in the self-cleavage reaction between  $\text{MgCl}_2$  and  $[\text{Co}(\text{NH}_3)_6]\text{Cl}_3$ .  $[\text{Co}(\text{NH}_3)_6]^{3+}$  promotes efficient cleavage of modHpRz structure as the percentage of fraction cleaved reaches almost 80% at 0.1 MPa and slightly increase by pressurization at 100 MPa. The modHpRz cleavage reaction was less efficient with  $\text{MgCl}_2$ , reaching around 60% of fraction cleaved after 6 hours of reaction. This behavior is similar as with the wtHpRz (Figure 71). The

---

modHpRz+[Co(NH<sub>3</sub>)<sub>6</sub>]Cl<sub>3</sub> achieved the same amount of reaction product at 200 MPa as 0.1 MPa with MgCl<sub>2</sub>. The modHpRz + [Co(NH<sub>3</sub>)<sub>6</sub>]Cl<sub>3</sub> did not achieve an equilibrium state, as did the wtHpRz, until 6 hours of measurements and it also showed to be highly efficient until 300 MPa. On the other hand, the modHpRz activity was significantly affected by 100 MPa pressure when in the presence of MgCl<sub>2</sub>. The junctionless condition and changes on the nucleotide sequence of the helices had a significant effect on the ribozyme activity when compared to the wild-type hairpin ribozyme. This result is in good agreement with the literature, when a crystal structure analysis of this mutant hairpin ribozyme showed that the binding of [Co(NH<sub>3</sub>)<sub>6</sub>]Cl<sub>3</sub> at the ribozyme zipper favors the stabilization of the catalytically prone conformations [163]. The overall self-cleavage activity of the hairpin ribozyme is decelerated upon pressurization. However, the modHpRz stabilized by [Co(NH<sub>3</sub>)<sub>6</sub>]Cl<sub>3</sub> retains high catalytic activity until 300 MPa when compared to reactions at 0.1 MPa in the presence of MgCl<sub>2</sub>.



---

# 9. Bibliography

•



- 
- [1]. B. Alberts, A. Johnson, J. Lewis, M. Raff, K. Roberts & P. Walter, *Molecular Biology of the Cell* (2002) New York, NY: Garland Science.
- [2]. T. Casperson, Studien uber den Eiweissumsatz der Zelle *Naturwissenschaft* (1941) 29, 33-43.
- [3]. J. Brachet & H. Chantrenne, The function of the nucleus in the synthesis of cytoplasmic proteins *Symp. Quant. Biol.* (1956) 21, 329-337.
- [4]. F. H. C. Crick, On protein synthesis *Symp. Soc. Exp. Biol.* (1958) 12, 138-163.
- [5]. M. B. Hoagland, M. L. Stephenson, J. F. Scott, L. I. Hecht & P. C. Zamecnik, A soluble ribonucleic acid intermediate in protein synthesis *J. Biol. Chem.* (1958) 231, 241-257.
- [6]. R. W. Holley, G. A. Everett, T. J. Madison & A. Zamir, Nucleotide sequence in the yeast alanine transfer ribonucleic acid *J. Biol. Chem.* (1965) 240, 2122-2128.
- [7]. F. H. C. Crick, The origin of the genetic code *J. Mol. Biol.* (1968) 38, 367-379.
- [8]. L. E. Orgel, Evolution of the genetic apparatus *J. Mol. Biol.* (1968) 38, 381-393.
- [9]. C. R. Woese, *The genetic code: the molecular basis for genetic expression* (1967) p.186 harper & Row.
- [10]. W. Gilbert, Origin of life: The RNA world *Nature* (1986) 319, 618.
- [11]. K. Hall, P. Cruz, I. Tinoco, Jr., T. M. Jovin, & J.H. van de Sande, 'Z-RNA'--a left-handed RNA double helix *Nature* (1984) 311, 584-586.
- [12]. D. A. Zarling, C. J. Calhoun, C. C. Hardin & A. H. Zarling, Cytoplasmic Z-RNA *Proc Natl Acad Sci U S A* (1987) 84, 6117-6121.
- [13]. B. A. Brown, 2nd, K. Lowenhaupt, C. M. Wilbert, E. B. Hanlon & A. Rich, The zalpha domain of the editing enzyme dsRNA adenosine deaminase binds left-handed Z-RNA as well as Z-DNA. *Proc Natl Acad Sci U S A* (2000) 97, 13532-13536.

- 
- [14]. M. Popena, J. Milecki & R.W. Adamiak, High salt solution structure of a left-handed RNA double helix. *Nucleic Acids Res.* (2004) 32, 4044-4054.
- [15]. S. R. Eddy, Non-coding RNA genes and the modern RNA world *Nat. Rev. Genet* (2001) 2, 919-929.
- [16]. M. Illangasekare, G. Sanchez, T. Nickels & M. Yarus, Aminoacyl-RNA synthesis catalyzed by an RNA *Science* (1995) 267, 643-647.
- [17]. D. M. Shechner, R. A. Grant, S. C. Bagby, Y. Koldobskaya, J. A. Piccirilli, & D. P. Bartel, Crystal structure of the catalytic core of an RNA-polymerase ribozyme *Philos Trans R Soc Lond B Biol Sci.* (2009) 326, 1271-1275.
- [18]. P. B. Moore, Structural motifs in RNA *Annu. Rev. Biochem.* (1999) 68, 287-300.
- [19]. A. R. Ferré-D'Amaré & J. A. Doudna, RNA folds: insights from recent crystal structures. *Annu. Rev. Biophys. Biomol. Struct.* (1999) 28, 57-73.
- [20]. V. K. Misra & D. E. Draper, On the role of magnesium ions in RNA stability. *Biopolymers* (1998) 48, 113-135.
- [21]. V. K. Misra & D. E. Draper, A thermodynamic framework for Mg<sup>2+</sup> binding to RNA *Proc. Natl Acad. Sci. USA* (2011) 98, 12456-12461.
- [22]. V. K. Misra & D. E. Draper, The linkage between magnesium binding and RNA folding *J. Mol. Biol.* (2002) 317, 507-521.
- [23]. D. E. Draper, A guide to ions and RNA structure *RNA* (2004) 10, 335-343.
- [24]. M. Menger, T. Tuschl, F. Eckstein & D. Porschke, Mg<sup>2+</sup>-dependent conformational changes in the hammerhead ribozyme *Biochemistry* (1996) 35, 14710-14716.
- [25]. A. Khvorova, A. Lescoute, E. Westhof & S. D. Jayasena, Sequence elements outside the hammerhead ribozyme catalytic core enable intracellular activity *Nat. Struct. Biol.* (2003) 9, 708-872.



- 
- [26]. J. C. Penedo, T. J. Wilson, S. D. Jayasena, A. Khvorova & D. M. J. Lilley, Folding of the natural hammerhead ribozyme is enhanced by interaction of auxiliary elements *RNA* (2004) 10, 880-888.
- [27]. A. R. Ferré-D'Amaré, The hairpin ribozyme *Biopolymers* (2004) 73, 71-78.
- [28]. A. R. Ferré-D'Amaré & W. G. Scott, Small self-cleaving ribozymes *Cold Spring Harb Perspect Biol* (2010) 2:a003574.
- [29]. N. G. Walter, J. M. Burke & D.P. Millar, Stability of hairpin ribozyme tertiary structure is governed by the interdomain junction *Nat. Struct. Biol.* (1999) 6, 544-549.
- [30]. V. K. Misra, & D. E. Draper, Mg(2+) binding to tRNA revisited: The nonlinear Poisson-Boltzmann model. *J. Mol. Biol.* (2000) 299, 813–825.
- [31]. H. Shi & P. B. Moore, The crystal structure of yeast phenylalanine tRNA at 1.93 Å resolution: A classic structure revisited *RNA* (2000) 6, 1091-1105.
- [32]. R. Ehrlich, J. F. Lefevre & P. Remy, Fluorimetric study of the complex between yeast phenylalanyl-tRNA synthetase and tRNA<sup>Phe</sup> *Eur. J. Biochem.* (1980) 103, 145-153.
- [33]. B. D. Wells, The conformation of tRNA<sup>Phe</sup> anticodon monitored by fluorescence *Nucleic acid Res.* (1984) 12, 2157-2170.
- [34]. M. Giel-Pietraszuk & J. Barciszewski, A nature of conformational changes of yeast tRNA<sup>Phe</sup> high hydrostatic pressure effects *Int. J. Biol. Macromol.* (2005) 37, 109-114.
- [35]. Nucleic Acids: Structures, Properties, and Functions (Eds.:V. A. Bloomfield, D. M. Crothers, I. Tinoco, Jr.) (2000) University Science Books, Sausalito, CA.
- [36]. D. M. Thompson & R. Parker, Stressing Out Over tRNA Cleavage *Cell* (2009) 24, 215-219.

- 
- [37]. S. Kichner & Z. Ignatove, Emerging roles of tRNA in adaptive translation, signalling dynamics and disease *Nature Rev. Genet.* (2015) 16, 98-112.
- [38]. I. Tinoco Jr., J. R. Puglisi, J. R. Wyatt, RNA folding *Nucleic Acid Mol. Biol.* (1990) 4, 206-226.
- [39]. C. R. Woese, S. Winker, R. R. Guttell, Architecture of ribosomal RNA: constraints on the sequence of "tetraloops." *Proc. Natl. Acad. Sci. USA* (1990) 87, 8467-8471.
- [40]. G. Varani, Exceptionally stable nucleic acid hairpins *Annu. Rev. Biophys. Biomol. Struct.* (1995) 24, 379-404.
- [41]. H. Ma, D. J. Proctor, E. Kierzek, R. Kierzek, P. C. Bevilacqua & M. Gruebele, Exploring the Energy Landscape of a Small RNA Hairpin *J. Am. Chem. Soc.* (2006) 128, 1523-1530.
- [42]. I. Tinoco Jr., C. Bustamante, How RNA folds *J. Mol. Biol.* (1999), 293, 271-281.
- [43]. J. P. Marino, J. Gregorian, G. Csankovszki, D. M. Crothers, Bent helix formation between RNA hairpins with complementary loops *Science* (1995) 268, 1448-1454.
- [44]. S. Chauhan, S. A. Woodson, Tertiary interactions determine the accuracy of RNA folding *J. Am. Chem. Soc.* (2008) 130, 1296-1303.
- [45]. R. Thapar, A. P. Denmon, E. P. Nikonowicz, Recognition modes of RNA tetraloops and tetraloop-like motifs by RNA-binding proteins *Wiley Interdiscip. Rev. RNA* (2014), 5, 49-67.
- [46]. J. P. Sheehy, A. R. Davis, B. M. Znosko, Thermodynamic characterization of naturally occurring RNA tetraloops *RNA* (2010) 16, 417-429.
- [47]. D. Chakraborty, R. Collepardo-Guevara & D. J. Wales, Energy Landscapes, Folding Mechanisms, and Kinetics of RNA Tetraloop Hairpins *J. Am. Chem. Soc.* (2014) 136, 18052-18061.

- 
- [48]. E. Ennifar, A. Nikulin, S. Tishchenko, A. Serganov, N. Nevskaya, M. Garber, B. Ehresmann, C. Ehresmann, S. Nikonov & P. Dumas, The crystal structure of UUCG tetraloop *J. Mol. Biol.* (2000) 304, 35–42.
- [49]. F. H. Allain & G. Varani, Structure of the P1 helix from group I self-splicing introns. *J. Mol. Biol.* (1995) 250, 333–353.
- [50]. S.-J. Chen & K. A. Dill, RNA folding energy landscape *Proc. Natl. Acad. Sci. U. S. A.* (2000) 97, 646–651.
- [51]. W. B. Zhang & S. J. Chen, RNA hairpin-folding kinetics *Proc. Natl. Acad. Sci. U. S. A.* (2002) 99, 1931–1936.
- [52]. J. Jung & A. Van Orden, A three-state mechanism for DNA hairpin folding characterized by multiparameter fluorescence fluctuation spectroscopy. *J. Am. Chem. Soc.* (2006) 128, 1240–1249.
- [53]. H. Ma, C. Wan, A. Wu & A. H. Zewail, DNA folding and melting observed in real time redefine the energy landscape *Proc. Natl. Acad. Sci. U. S. A.* (2007) 104, 712–716.
- [54]. K. Sarkar, D. A. Nguyen, M. Gruebele, Loop and stem dynamics during RNA hairpin folding and unfolding *RNA* (2010) 16, 2427–2434.
- [55]. A. E. Garcia & D. Paschek, Simulation of the pressure and temperature folding/unfolding equilibrium of a small RNA hairpin *J. Am. Chem. Soc.* (2008) 130, 815–817.
- [56]. J. M. Buzayan, A. Hampel, G. Bruening, Nucleotide sequence and newly formed phosphodiester bond of spontaneously ligated satellite tobacco ringspot virus RNA *Nucleic Acids Res.* (1986) 14, 9729–9743.
- [57]. J. M. Buzayan, P. A. Feldstein, C. Segrelles & G. Bruening, G. Autolytic processing of a phosphorothioate diester bond *Nucleic Acids Res.* (1988) 16, 4009–4023.

- 
- [58]. M. DeYoung, A. M. Siwkowski, Y. Lian & A. Hampel, Catalytic properties of hairpin ribozymes derived from Chicory yellow mottle virus and arabis mosaic virus satellite RNAs. *Biochemistry* (1995) 34, 15785-15791.
- [59]. N. G. Walter & J. M. Burke The hairpin ribozyme: structure, assembly and catalysis *Curr. Opin. Struct. Biol.* (1998) 2, 24-30.
- [60]. D. M. J. Lilley, Origins of RNA catalysis in the hairpin ribozyme *ChemBioChem* (2001) 2, 729-733.
- [61]. C. Shin, J. N. Choi, S. I. Song, J. T. Song, J. H. Ahn, J. S. Lee & Y. Do Choi, The loop B domain is physically separable from the loop A domain in the hairpin ribozyme *Nucleic acids Res.* (1996) 14, 2685-2689.
- [62]. Z. Cai & I. Tinoco Jr., Solution structure of loop A from the hairpin ribozyme from tobacco ringspot virus satellite *Biochemistry* (1996) 35, 6026-6036.
- [63]. R. Shippy, R. Lockner, M. Farnsworth & A. Hampel The hairpin ribozyme: discovery, mechanism and development for gene therapy *Mol. Biotechnol.* (1999) 12, 117-129.
- [64]. S. E. Butcher, F. H. T. Allain & J. Feigon, Solution structure of the loop B domain from the hairpin ribozyme *Nat. Struct. Biol.* (1999) 6, 212-216.
- [65]. P. B. Rupert & A. R. Ferré-D'Amaré Crystal structure of a hairpin ribozyme-inhibitor complex with implications for catalysis *Nature* (2001) 410, 780-786.
- [66]. T. J. Wilson & D. M. J. Lilley, Meta ion binding and the folding of the hairpin ribozyme *RNA* (2002) 8, 587-600.
- [67]. K. Heremans & L. Smeller, Protein structure and dynamics at high pressure *Biochim. Biophys. Acta* (1998) 1386, 353-370.
- [68]. J. L. Silva, D. Foguel & C. A. Royer, Pressure provides new insights into protein folding, dynamics and structure *Trends Biochem. Sci.* (2001) 26, 612-618.

- 
- [69]. K. Akasaka, Probing conformational fluctuation of proteins by pressure perturbation *Chem. Rev.* (2006) 106, 1814-1835.
- [70]. R. Mishra & R. Winter, Cold- and pressure-induced dissociation of protein aggregates and amyloid fibrils *Angew. Chem. Int. Ed. Engl.* (2008) 47, 6518-6521.
- [71]. S. Kapoor, G. Triola, I. R. Vetter, M. Erlkamp, H. Waldmann & R. Winter, Revealing conformational substates of lipidated N-Ras protein by pressure modulation *Proc. Natl. Acad. Sci. U. S. A.* (2012) 109, 460-465.
- [72]. M. B. Prigozhin, Y. Liu, A. J. Wirth, S. Kapoor, R. Winter, K. Schulten & M. Gruebele, Misplaced helix slows down ultrafast pressure-jump protein folding *Proc. Natl. Acad. Sci. U. S. A.* (2013) 110, 8087-8092.
- [73]. S. I. Nakano, D. Miyoshi & N. Sugimoto, Effects of molecular crowding on the structures, interactions, and functions of nucleic acids *Chem. Rev.* (2014) 114, 2733-2758.
- [74]. J. L. Silva, A. C. Oliveira, T. C. R. G. Vieira, G. A. P. de Oliveira, M. C. Suarez, D. Foguel, High-pressure chemical biology and biotechnology *Chem. Rev.* (2014) 114, 7239-7267.
- [75]. T. Q. Luong & R. Winter, Combined pressure and cosolvent effects on enzyme activity - a high-pressure stopped-flow kinetic study on  $\alpha$ -chymotrypsin. *Phys. Chem. Chem. Phys.* (2015) 17, 23273-23278.
- [76]. P. G Higgs & N. Lehman, The RNA World: molecular cooperation at the origins of life *Nat. Rev. Genet* (2015) 16, 7-17.
- [77]. A. Serganov & D. J. Patel, Ribozymes, riboswitches and beyond: regulation of gene expression without proteins *Nat. Rev. Genet* (2007) 8, 776-790.
- [78]. L. J. Rothschild & R. L. Mancinelli, Life in extreme environment *Nature* (2001) 22, 1092-1101.

- 
- [79]. D. H. Bartlett, Pressure effects on in vivo microbial processes *Biochim Biophys Acta* (2002) 25, 367-381.
- [80]. E. A. Eloë, F. M. Lauro, R. F. Vogel & D. H. Bartlett, The deep-sea bacterium *Photobacterium profundum* SS9 utilizes separate flagellar system for swimming and swarming under high-pressure conditions *Appl. Environ. Microbiol.* (2008) 74, 6298-6305.
- [81]. P. M. Oger & M. Jebbar, The many ways of coping with pressure *Res. Microbiol.* (2010) 16, 799-809.
- [82]. D. J. Wilton, M. Ghosh, K. V. A. Chary, K. Akasaka & M. P. Williamson, Structural change in a B-DNA helix with hydrostatic pressure *Nucleic acids Res* (2008) 36, 4032-4037.
- [83]. S. Takahashi & N. Sugimoto, Effect of pressure on thermal stability of G-quadruplex DNA and double-stranded DNA structures *Molecules* (2013) 18, 13297-13319.
- [84]. M. C. Lin, P. Eid, P. T. T. Wong & R. B. Macgregor Jr, High pressure fourier transform infrared spectroscopy of poly(dA)poly(dT), poly(dA) and poly(dT) *Biophys. Chem.* (1999) 76, 87-94.
- [85]. R. B. Macgregor Jr., The interactions of nucleic acids at elevated hydrostatic pressure. *Biochim. Biophys. Acta* (2002) 1595, 266–276.
- [86]. C. R. Robinson & S. G. Sligar, Hydrostatic pressure reverses osmotic pressure effects on the specificity of *E. coli* DNA interactions. *Biochemistry* (1994) 33, 3787–3793.
- [87]. C. R. Robinson & S. G. Sligar, Heterogeneity in molecular recognition by restriction endonucleases: osmotic and hydrostatic pressure effects on BamHI, PvuII, and EcoRV specificity *Proc. Natl Acad. Sci. USA* (1995) 92, 3444–3448.

- [88]. D. R. Dixon, A. M. Pruski & L. R. J. Dixon, The effects of hydrostatic pressure change on DNA integrity in the hydrothermal-vent mussel *Bathymodiolus azoricus*: implications for future deep-sea mutagenicity studies. *Mutat. Res.* (2004) 552, 235–246.
- [89]. S. Takahashi & N. Sugimoto Effect of pressure on the stability of G-quadruplex DNA: thermodynamics under crowding conditions *Angew. Chem. Int. Ed.* (2013) 52, 13774-13778.
- [90]. E. Girard, T. Prange, A. –C. Dhaussy, E. Migianu-Griffoni, M. Lecouvey, J. –C. Chervin, M. Mezouar, R. Kahn & R. Fourme, Adaptation of the base-paired double-helix molecular architecture to extreme pressure. *Nucleic Acids Res.* (2007) 35, 4800–4808.
- [91]. A. Krzyżaniak, P. Salański, J. Jurczak, J. Barciszewski, B-Z DNA reversible conformation changes effected by high pressure. *FEBS Lett.* (1991) 279, 1–4.
- [92]. J. Q. Wu & R. B. Macgregor Jr., Pressure dependence of the melting temperature of dA-dT polymers. *Biochemistry* (1993) 32, 12531–12537.
- [93]. J. Q. Wu & R. B. Macgregor, Pressure dependence of the helix-coil transition temperature of poly [d (G-C)]. *Biopolymers* (1995) 35, 369–376.
- [94]. H. Y. Fan, Y. L. Shek, A. Amiri, D. N. Dubins, H. Heerklotz, R. B. Macgregor Jr & T. V. Chalikian, Volumetric characterization of sodium-induced G-quadruplex formation. *J. Am. Chem. Soc.* (2011) 133, 4518–4526.
- [95]. D. H. Zhang, T. Fujimoto, S. Saxena, H. Q. Yu, D. Miyoshi & N. Sugimoto Monomorphic RNA G-quadruplex an dpolyomorphic DNA G-quadruplex structures responding to cellular environmental factors *Biochemistry* (2010) 49, 4554-4563.
- [96]. J. R. Williamson, G-quartet structures in telomeric DNA *Annu. Rev. Biophys. Biomol. Struct.* (1994) 23, 703-730.

- 
- [97]. S. Nakano, H. Karimata, T. Ohmichi, J. Kawakami & N. Sugimoto, The effect of molecular crowding with nucleotide length and cosolute structure on DNA duplex stability *J. Am. Chem. Soc.* (2004) 126, 14330-14331.
- [98]. D. Miyoshi, H. Karimata & N. Sugimoto, Hydration regulates thermodynamics of G-quadruplex formation under molecular crowding conditions *J. Am. Chem. Soc.* (2004) 128, 7957-7963.
- [99]. S. Muhuri, K. Mimura, D. Miyoshi & N. Sugimoto, Stabilization of the three-way junctions of DNA under molecular crowding conditions *J. Am. Chem. Soc.* (2009) 131, 9268-9280.
- [100]. M. Giel-Pietraszuk & J. Barciszewski, Hydrostatic and osmotic pressure study of the RNA hydration *Mol. Biol. Rep.* (2012) 39, 6309-6318.
- [101]. F. Hughes & R. Steiner, Effects of pressure on the helix-coil transitions of the polyA-polyU system *Biopolymers* (1966) 4, 1081-1090.
- [102]. O. C. Uhlenbeck, Tetraloops and RNA folding *Nature* (1990) 346, 613-614.
- [103]. J. C. Miner, A. A. Chen & A. E. Garcia, Free-energy landscape of a hyperstable RNA tetraloop *Proc. Natl Acad. Sci. USA* (2016) 113, 6665-6670.
- [104]. S. Tobé, T. Heams, J. Vergne, G. Hervé & M. -C. Maurel, The catalytic mechanism of hairpin ribozyme studied by hydrostatic pressure *Nucleic Acids Res.* (2005) 33, 2557-2564.
- [105]. G. Hervé, S. Tobé, T. Heams, J. Vergne & M.-C. C. Maurel, Hydrostatic and osmotic pressure study of the hairpin ribozyme *Biochim. Biophys. Acta, Proteins Proteomics* (2006) 1764, 573-577.
- [106]. M. Ztouti, H. Kaddour, F. Miralles, C. Simian, J. Vergne, G. Hervé, M. -C. Maurel, Adenine, a hairpin ribozyme cofactor – high-pressure and competition studies *FEBS J.* (2009) 276, 2574-2588.



- 
- [107]. J.A. Doudna & T.R. Cech, The chemical repertoire of natural ribozymes *Nature* (2002) 418, 222–227.
- [108]. J. Salter, J. Krucinska, S. Alam, V. Grum-Tokars & J. E. Wedekind, Water in the active site of an all-RNA hairpin ribozyme and effects of Gua8 base variants on the geometry of phosphoryl transfer *Biochemistry* (2006) 45, 686–700.
- [109]. D. N. Dubins, A. Lee, R. B. Macgregor & T. V. Chalikian, On the stability of double stranded nucleic acids *J. Am. Chem. Soc.* (2001) 123, 9254–9259.
- [110]. D. J. Wilton, M. Ghosh, K. Chary, K. Akasaka & M. P. Williamson, Structural change in a B-DNA helix with hydrostatic pressure *Nucleic Acids Res.* (2008) 36, 4032–4037.
- [111]. J. L. Silva, D. Foguel, C. A. Royer, Pressure provides new insights into protein folding, dynamics and structure *Trends Biochem. Sci.* (2001) 26, 612–618.
- [112]. D. J. Dunstan & I. L. Spain, The Technology of Diamond Anvil High Pressure Cells .1.Principles, Design and Construction *J. Phys. ESci. Inst.* (1989) 22, 913–923.
- [113]. I. L. Spain & D. J. Dunstan, The Technology of Diamond Anvil High-Pressure Cells .2. Operation and Use *J. Phys. ESci. Inst.* (1989) 22, 923–933.
- [114]. M. Banyay, M. Sarkar & A. Gräslund, A library of IR bands of nucleic acids in solution *Biophys. Chem.* (2003) 104, 477–488.
- [115]. P. R. Griffiths & G. L. Pariente, Introduction to Spectral Deconvolution. *Trends in Anal. Chem.* (1986) 5, 209–215.
- [116]. R. Winter, F. Noll & C. Czeslik, Methoden der Biophysikalischen Chemie (2011) 2<sup>nd</sup> edition, Vieweg+Teubner.
- [117]. J. R. Lakowicz, Principles of fluorescence spectroscopy (2006) 3<sup>rd</sup> edition, Springer.

- 
- [118]. J. Koo, C. Czeslik, Volume changes of proteins adsorbed on silica particles *Soft Matter* (2012) 8, 11670–11676.
- [119]. B. D. Wells, The conformation of the tRNA<sup>Phe</sup> anticodon loop monitored by fluorescence *Nucleic Acids Res.* (1984) 12, 2157–2170.
- [120]. T. V. Chalikian, J. Völker, A. R. Srinivasan, W. K. Olson & K. J. Breslauer, The hydration of nucleic acid duplexes as assessed by a combination of volumetric and structural techniques *Biopolymers* (1999) 50, 459–471.
- [121]. E. Girard, T. Prange, A.-C. Dhaussy, E. Migianu-Griffoni, M. Lecouvey, J.-C. Chervin, M. Mezouar, R. Kahn & R. Fourme, Adaptation of the base-paired double-helix molecular architecture to extreme pressure *Nucleic Acids Res.* (2007) 35, 4800–4808.
- [122]. T. Maniatis, E. F. Fritsch & J. Sambrock, *Molecular Cloning: A Laboratory Manual*, Cold Spring Harbor Laboratory (1982), Cold Spring Harbor, NY.
- [123]. F. X. Schmid, Biological Macromolecules UV-visible spectrophotometry *Encyclopedia of LifeSciences*, (2001) 1-3.
- [124]. T. Takaya, C. Su, C., K. de La Harpe, C. E. Crespo-Hernández & B. Kohler, UV excitation of single DNA and RNA strands produces high yields of exciplex states between two stacked bases *Proc. Natl Acad. Sci. USA* (2008) 105, 10285–10290.
- [125]. C. A. Schneider, W. S. Rasband, & K. W. Eliceiri, "NIH Image to ImageJ: 25 years of image analysis", *Nature methods* (2012) 9, 671-675.
- [126]. F. Meersman, I. Daniel, D. H. Bartlett, R. Hazael, P. F. McMillan & R. Winter, High pressure biophysics and biochemistry *Rev. Mineral. Geochem.* (2013) 75, 607–648.
- [127]. I. Daniel, P. Oger, R. Winter, Origins of life and biochemistry under high-pressure conditions *Chem. Soc. Rev.* (2006) 35, 858–875.

- 
- [128]. T. V. Chalikian, J. Völker, G. E. Plum & K. J. Breslauer, A more unified picture for the thermodynamics of nucleic acid duplex melting: A characterization by calorimetric and volumetric techniques *Proc. Natl. Acad. Sci. U. S. A.* (1999) 96, 7853–7858.
- [129]. L. Smeller, P. Rubens & K. Heremans, Pressure Effect on the Temperature-Induced Unfolding and Tendency to Aggregate of Myoglobin *Biochemistry* (1999) 38, 3816–3820.
- [130]. R. Winter, C. Jeworrek, Effect of pressure on membranes *Soft Matter* (2009) 5, 3157–3173.
- [131]. J. Roche, J. A. Caro, D. R. Norberto, P. Barthe, C. Roumestand, J. L. Schlessman, A. E. Garcia, B. E. Garcia-Moreno & C. A. Royer, Cavities determine the pressure unfolding of proteins *Proc. Natl. Acad. Sci. U. S. A.* (2012) 109, 6945–6950.
- [132]. C. D. Downey, R. L. Crisman, T. W. Randolph & A. Pardi, Influence of hydrostatic pressure and cosolutes on RNA tertiary structure *J. Am. Chem. Soc.* (2007) 129, 9290–9291.
- [133]. H. Kaddour, J. Vergne, G. Hervé & M.-C. Maurel, High-pressure analysis of a hammerhead ribozyme from *Chrysanthemum chlorotic mottle viroid* reveals two different populations of self-cleaving molecule *FEBS J.* (2011) 278, 3739–3747.
- [134]. D. H. Turner, Fundamental interactions in RNA: Questions answered and remaining *Biopolymers* (2013) 99, 1097–1104.
- [135]. M. W. Friederich, E. Vacano & P. J. Hagerman, Global flexibility of tertiary structure in RNA: Yeast tRNA<sup>Phe</sup> as a model system *Proc. Natl. Acad. Sci. U. S. A.* (1998) 95, 3572–3577.
- [136]. E. B. Brauns & B. Dyer, Time-resolved infrared spectroscopy of RNA folding *Biophys. J.* (2005) 89, 3523–3530.

- 
- [137]. G. Panick, R. Malessa, R. Winter, G. Rapp, K. J. Frye & C. A. Royer, Structural characterization of the pressure-denatured state and unfolding/refolding kinetics of staphylococcal nuclease by synchrotron small-angle X-ray scattering and Fourier-transform infrared spectroscopy *J. Mol. Biol.* (1998) 275, 389–402.
- [138]. J. Eisinger, B. Feuer & T. Yamane, Luminescence and Binding Studies on tRNA<sup>Phe</sup> *Proc. Natl. Acad. Sci. U. S. A.* (1970) 65, 638–644.
- [139]. H.-J. Hinz, V. V. Filimonov & P. L. Privalov, Calorimetric studies on melting of tRNA<sup>Phe</sup> (yeast) *Eur. J. Biochem.* (1977) 72, 79–86.
- [140]. K. Beardsley, T. Tao & C. R. Cantor, Conformation of the anticodon loop of phenylalanine transfer ribonucleic acid. Effect of environment on the fluorescence of the Y base *Biochemistry* (1970) 9, 3524–3532.
- [141]. I. Pilz, O. Kratky, F. Cramer, F. von der Haar & E. Schlimme, On the Conformation of Phenylalanine Specific Transfer RNA Studies on Size and Shape of the Molecule by X-Ray Small Angle Scattering *Eur. J. Biochem.* (1970) 15, 401–409.
- [142]. X. Fang, K. Littrell, X. J. Yang, S. J. Henderson, S. Siefert, P. Thiyagarajan, T. Pan & T. R. Sosnick, Mg<sup>2+</sup>-Dependent Compaction and Folding of Yeast tRNA<sup>Phe</sup> and the Catalytic Domain of the *B. subtilis* RNase P RNA Determined by Small-Angle X-ray Scattering *Biochemistry* (2000) 39, 11107–11113.
- [143]. R. Macgregor, Jr., Effect of hydrostatic pressure on nucleic acids *Biopolymers* (1998) 48, 253–263.
- [144]. V. Serebrov, K. Vassilenko, N. Kholod, H. J. Gross, & L. Kisselev, Mg<sup>2+</sup> binding and structural stability of mature and *in vitro* synthesized unmodified *Escherichia coli* tRNA<sup>Phe</sup> *Nucl. Acids Res.* (1998) 26, 2723–2728.
- [145]. Z. J. Tan & S. J. Chen, Salt Contribution to RNA Tertiary Structure Folding Stability *Biophys. J.* (2011) 101, 176–187.

- [146]. Y. Katayama, T. Hattori, H. Saitoh, T. Ikeda, K. Aoki, H. Fukui, K. Funakoshi, Structure of liquid water under high pressure up to 17 GPa *Phys. Rev. B* (2010) 81, 014109.
- [147]. I. Son, Y. L. Shek, D. N. Dubins & T. V. Chalikian, Hydration Changes Accompanying Helix-to-Coil DNA Transitions *J. Am. Chem. Soc.* (2014) 136, 4040-4047.
- [148]. L. Mitra, J.-B. Rouget, B. Garcia-Moreno, C. A. Royer & R. Winter, Towards a Quantitative Understanding of Protein Hydration and Volumetric Properties *ChemPhysChem* (2008) 9, 2715–2721.
- [149]. G. Rayan & R. B. Macgregor Jr., Comparison of the Heat- and Pressure-Induced Helix–Coil Transition of Two DNA Copolymers *J. Phys. Chem. B* (2005) 109, 15558 – 15565.
- [150]. Y. Zhai, L. Okoro, A. Cooper & R. Winter, Applications of pressure perturbation calorimetry in biophysical studies *Biophys. Chem.* (2011) 156, 13–23.
- [151]. R. Ravindra & R. Winter, Pressure Perturbation Calorimetry: A New Technique Provides Surprising Results on the Effects of Co-solvents on Protein Solvation and Unfolding Behaviour *ChemPhysChem* (2004) 5, 566–571.
- [152]. L. Mitra, N. Smolin, R. Ravindra, C. Royer, R. Winter, Pressure perturbation calorimetric studies of the solvation properties and the thermal unfolding of proteins in solution—experiments and theoretical interpretation *Phys. Chem. Chem. Phys.* (2006) 8, 1249–1265.
- [153]. Y. Zhai & R. Winter, Effect of Molecular Crowding on the Temperature–Pressure Stability Diagram of Ribonuclease A *ChemPhysChem* (2013) 14, 386–393.
- [154]. M. Erlkamp, S. Grobelny & R. Winter, Crowding effects on the temperature and pressure dependent structure, stability and folding kinetics of *Staphylococcal Nuclease* *Phys. Chem. Chem. Phys.* (2014) 16, 5965 –5976.

- 
- [155]. D. I. Svergun, Determination of the regularization parameter in indirect-transform methods using perceptual criteria *J. Appl. Crystallogr.* (1992) 25, 495–503.
- [156]. C. R. Woese, R. Gutell, R. Gupta & H. F. Noller, Detailed analysis of the higher-order structure of 16S-like ribosomal ribonucleic acid *Microbiol. Rev.* (1983) 47, 621-669.
- [157]. D. Moazed, S. Stern, H. F. Noller, Rapid chemical probing of conformation in 16 S ribosomal RNA and 30 S ribosomal subunits using primer extension. *J Mol Biol.* (1986) 187, 399–416.
- [158]. J. Jung, A. Van Orden, Folding and unfolding kinetics of DNA hairpins in flowing solution by multiparameter fluorescence correlation spectroscopy *J. Phys. Chem. B* (2005) 109, 3648–3657.
- [159]. A. A. Chen, A. E. Garcia, High-resolution reversible folding of hyperstable RNA tetraloops using molecular dynamics simulations *Proc. Natl. Acad. Sci. U.S.A.* (2013) 110, 16820–16825.
- [160]. M. Tsuboi, Application of infrared spectroscopy to structure studies of nucleic acids *Appl. Spectrosc. Rev.* (1969) 3, 45-90.
- [161]. B. G. Moreira, Y. You & R. Owczarzy, Cy3 and Cy5 dyes attached to oligonucleotide terminus stabilize DNA duplexes: Predictive thermodynamic model *Biophysical Chemistry* (2015) 198, 36 – 44.
- [162]. D. Lambert, J. E. Heckman & J. M. Burke, Cation-specific structural accommodation within a catalytic RNA *Biochemistry* (2006) 45, 829 – 838.
- [163]. S. Alam, V. Grum-Tokars, J. Krucinska, M. L. Kundracik & J. E. Wedekind, Conformational heterogeneity at position U37 of an all RNA hairpin ribozyme with implications for metal binding and the catalytic structure of the S-turn *Biochemistry* (2005) 44, 14396-14408.

- [164]. J. A. Liberman, M. Guo, J. L. Jenkins, J. Krucinska, Y. Chen, Y. Chen, P. R. Carey & J. E. Wedekind, A transition-state interaction shifts nucleobase ionization toward neutrality to facilitate small ribozyme catalysis *J. Am. Chem. Soc.* (2012) 134, 16933-16936.





---

# 10. Publications and presentations



## Results presented in this thesis have contributed to:

### PUBLICATION

- **C. Schuabb**, M. Berghaus, C. Rosin & R. Winter, Exploring the free energy and conformational landscape of tRNA at high temperature and pressure *ChemPhysChem* (2015) 16, 138-146.

### PRESENTATIONS

- **C. Schuabb**, S. Patariaia, R. Winter, “Exploring the effects of temperature and pressure on the structure and stability of a small RNA hairpin”, 60<sup>th</sup> Annual Meeting of Biophysical Society, Los Angeles, USA, 2016 (Poster).
- **C. Schuabb**, S. Patariaia, R. Winter, “The effect of temperature and pressure on the structure, energy landscape and reactivity of RNAs”, 8<sup>th</sup> International Meeting on Biomolecules under High Pressure, Dortmund, Germany, 2016 (Poster).
- **C. Schuabb**, S. Patariaia, M. Berghaus, R. Winter, “Energy Landscape, Conformational Mechanism and Kinetics of RNAs and Ribozymes at High Temperature and Pressure”, 53<sup>th</sup> EHPRG Meeting on High Pressure Science and Technology/25<sup>th</sup> International Conference of the AIRAPT, Madrid, Spain, 2015 (Poster).
- **C. Schuabb**, M. Berghaus, C. Rosin, R. Winter, “Exploring the free Energy and Conformational Landscape of tRNA at High Temperature and Pressure”, 114<sup>th</sup> General Assembly of the German Bunsen Society for Physical Chemistry, Bochum, Germany, 2015 (Poster).

- **C. Schuabb**, S. Pataraiia, R. Winter, “Influence of temperature, pressure, and ionic strength on the structure and stability of tRNA<sup>Phe</sup> and small RNA hairpin”, 8<sup>th</sup>International Conference on High Pressure Bioscience and Biotechnologie, Nantes, France, 2014 (Poster).
  
- **C. Schuabb**, R. Winter, “Influence of temperature, pressure, and ionic strength on the structure and stability of tRNA<sup>Phe</sup>”, 113<sup>th</sup> General Assembly of the German Bunsen Society for Physical Chemistry, Hamburg, Germany, 2014 (Poster).

---

## 11. *Curriculum Vitae*



Caroline Mello Pimentel Schuabb

---

**EDUCATION**

2013 - present

**Technical University of Dortmund** Germany

PhD in NATURAL SCIENCE

Certificate in PHYSICAL CHEMISTRY

2012

**Federal University of Rio de Janeiro** Brazil

Master Degree in BIOLOGICAL CHEMISTRY

Certificate in BIOLOGICAL SCIENCE

2010

**Federal University of Rio de Janeiro** Brazil

Complementary license in PHARMACEUTICAL INDUSTRY

Certificate in INDUSTRIAL PHARMACIST

2009

**Federal University of Rio de Janeiro** Brazil

Bachelor Degree in PHARMACY

Certificate in PHARMACIST

**PROFESSIONAL  
ASSOCIATIONS**

Biophysical Society, USA.